THE PROCEEDINGS OF THE PHYSICAL SOCIETY

VOL. 58, PART 1 1 January 1946 No. 325

CONTENTS

PAGE

H. G. W. HARDING. Colours of total radiators expressed on the C.I.E. trichromatic system for the temperature range 0–1–660 mireds (C_2=14384·8) 1

A. J. C. WILSON. Hysteresis and eddy losses in single crystals of an alloy of iron and silicon 21

H. MOTZ and LAURA KLANFER. Complete computation of electron optical systems . . 30

W. S. STILES. A modified Helmholtz line-element in brightness-colour space . . . 41

E. H. LINFOOT. On decentred aspheric plates 65

R. F. S. HEARMON. The fundamental frequency of vibration of rectangular wood and plywood plates 78

H. H. HOPKINS. The optical sine-condition 92

H. H. HOPKINS. Herschel's condition 100

S. BAXTER. The thermal conductivity of textiles. 105

KERR GRANT. The dependence of pressure-variation, with depth in a liquid, on the vertical acceleration of the liquid. (Demonstration.) 118

The Rev. G. D. YARNOLD. The hysteresis of the angle of contact of mercury . . . 120

Sir STAFFORD CRIPPS. Address delivered at the opening of the thirtieth exhibition of scientific instruments and apparatus 125

Reviews of books 127

Price to non-members 8*s*. 4*d*. net ; 8*s*. 10*d*. inclusive of postage
Annual subscription 42*s*. inclusive of postage, payable in advance

Published by
THE PHYSICAL SOCIETY
1 Lowther Gardens, Exhibition Road, London S.W.7

Printed by
TAYLOR AND FRANCIS, LTD.,
Red Lion Court, Fleet Street, London E.C.4

ADVERTISEMENTS
in the
PROCEEDINGS

Rates for one insertion
Page - £10 0s. 0d. ¼-page - £2 12s. 6d
½-page - £5 2s. 6d. ⅛-page - £1 7s. 6d.

10% and 20% reductions for series of three and six, respectively, in consecutive issues.

Applications for space should be made to

THE PHYSICAL SOCIETY
1 Lowther Gardens, Exhibition Road,
London S.W.7.

BINDING CASES
for the
PROCEEDINGS

Binding Cases for volume 57 (1945) and previous volumes may be obtained for 6s., inclusive of postage. For 9s. the six parts of a volume will be bound in the publisher's binding cases and returned.

THE PHYSICAL SOCIETY
1 Lowther Gardens, Exhibition Road,
London S.W.7

NORTHAMPTON POLYTECHNIC
St. John Street, London, E.C. 1.
(nearest station, ANGEL, Underground Northern Line)

A Course of Lectures on
ELEMENTS *of the* DESIGN
of
AUTOMATIC CONTROL
(SERVO) SYSTEMS

will be conducted at the Polytechnic on
TUESDAY EVENINGS
at 6 p.m. commencing 5th March, 1946.

Lecturers :
Dr. A. Porter, M.Sc., A.M.I.E.E.
(Ministry of Supply) from 5th March to 2nd April.
Mr. M. L. Jofeh, A.M.I.E.E.
(Messrs A. C. Cossor, Ltd.) from 9th April to 14th May.
Prof. K. A. Hayes, O.B.E., B.Sc., M.I.E.E.
(Military College of Science) 21st May.

Fee for the course : 21/-

Admission by ticket, obtainable from the Secretary, Northampton Polytechnic,
St. John Street, London, E.C.1.

SCIENTIFIC BOOKS

Messrs H. K. LEWIS can supply from stock or to order any book on the Physical and Chemical Sciences.

German Technical Books. A twelve-page list together with two eight-page supplements giving details of reproductions of German technical publications issued under the authority of the Alien Property Custodian in Washington has just been prepared ; copies will be sent on application.

SECOND-HAND SCIENTIFIC BOOKS. An extensive stock of books in all branches of Pure and Applied Science may be seen in this department. Large and small collections bought. Back volumes of Scientific Journals. Old and rare Scientific Books. Mention interests when writing.
140 GOWER STREET.

SCIENTIFIC LENDING LIBRARY

Annual subscription from One Guinea. *Details of terms and prospectus free on request.*
THE LIBRARY CATALOGUE revised to December 1943, containing a classified index of authors and subjects : to subscribers 12s. 6d. net., to non-subscribers 25s. net., postage 8d.
Bi-monthly List of Additions, free on application

Telephone : EUSton 4282
Telegrams : "Publicavit, Westcent, London"

H. K. LEWIS & Co. Ltd.
136 GOWER STREET, LONDON, W.C.1

WESTALITE
RECTIFIERS
DOUBLE-VOLTAGE
WESTALITE RECTIFIERS
(Size and weight halved)
MINIATURE
METAL RECTIFIERS
CONSTANT
POTENTIAL A.C.
(THE STABILISTOR)
ATIC PHASE CONVERSION
are a few of the latest
WESTINGHOUSE
DEVELOPMENTS

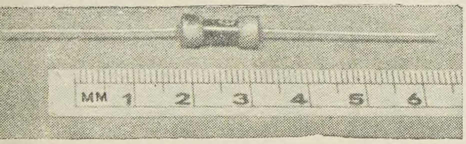

Miniature "Westector"

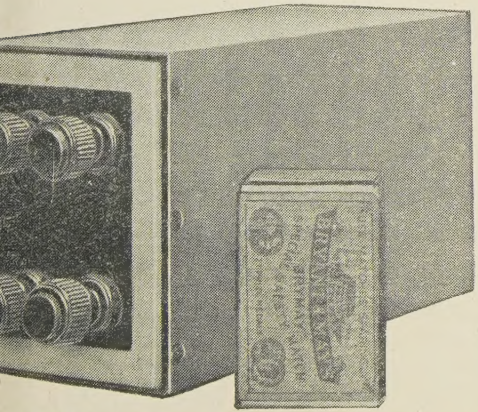

"Stabilistor"
STINGHOUSE BRAKE & SIGNAL Co. Ltd.
Pew Hill House, Chippenham, Wilts.

ANNOUNCEMENT
Megatron Selenium
Photo Cells
are now
in PRODUCTION
Technical Enquiries to
Dr. G. A. VESZI,
at our Laboratories,
115a, FONTHILL ROAD, N.4
Archway 3739
HEAD OFFICE :
MEGATRON LTD.
96/97, CHANDOS HOUSE,
BUCKINGHAM GATE, S.W.1
Abbey 7216

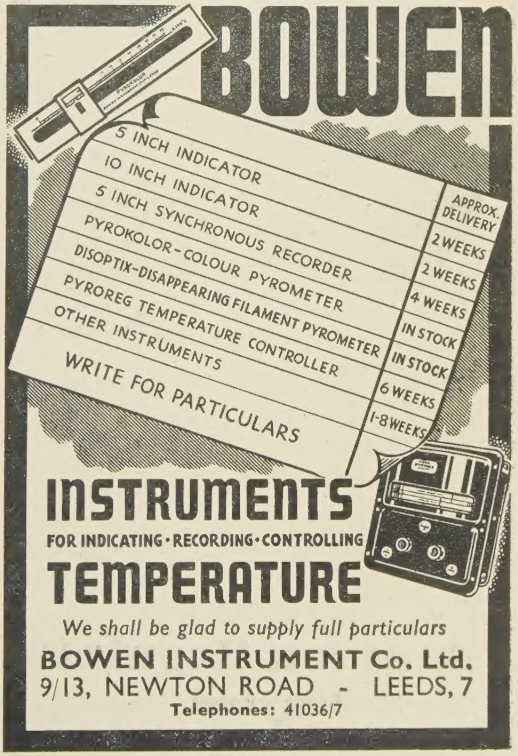

BOWEN

	APPROX. DELIVERY
5 INCH INDICATOR	2 WEEKS
10 INCH INDICATOR	2 WEEKS
5 INCH SYNCHRONOUS RECORDER	4 WEEKS
PYROKOLOR-COLOUR PYROMETER	IN STOCK
DISOPTIX-DISAPPEARING FILAMENT PYROMETER	IN STOCK
PYROREG TEMPERATURE CONTROLLER	6 WEEKS
OTHER INSTRUMENTS	1-8 WEEKS

WRITE FOR PARTICULARS

INSTRUMENTS
FOR INDICATING · RECORDING · CONTROLLING
TEMPERATURE
We shall be glad to supply full particulars
BOWEN INSTRUMENT Co. Ltd.
9/13, NEWTON ROAD - LEEDS, 7
Telephones: 41036/7

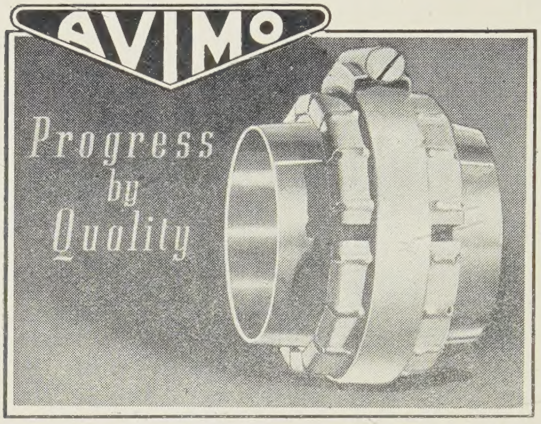

AVIMO HIGH PRESSURE COUPLINGS

The only really efficient pressure-resisting coupling for pipe connections. Approved by the Air Ministry and standarised by leading aircraft manufacturers. For water, oil and glycol, at any temperature. Flexible. Vibration proof. Available in sizes from ½″ o/d to 3¼″ o/d. Avimo facilities are at your disposal.

DESIGN · DEVELOPMENT · MANUFACTURE
of
OPTICAL-MECHANICAL-ELECTRICAL INSTRUMENTS

★ AVIMO LTD · TAUNTON · ENG. ★

8440 C

VITREOSIL APPARATUS

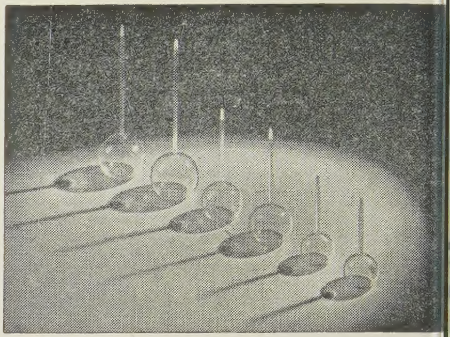

This photograph—by the way, it won International Exhibition in 1939—shows some pre-war apparatus made to specification in VITREOSIL pure fused silica, but you need hardly be reminded that this work can always be done for you.

THE THERMAL SYNDICATE LTD
Head Office: Wallsend, Northumberland.
London Depot: 12-14, Old Pye Street,
Westminster, S.W.1.

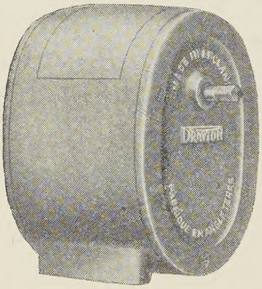

SMALL GEARED MOTOR UNITS

Drayton " RQ " motors are available unidirectional or reversing with or without self-switching for 100 110 or 200 250 Volts A.C.

FIL NASHAFT SPEEDS :
Reversing type. ... Maximum 600 rev./min. ; minimum 27 min./rev.
Unidirectional type Maximum 280 rev./min. ; minimum 60 min./rev.

TORQUE
Reversing ... ... 60 lb. in. maximum.
Unidirectional ... ... 37 lb. in. maximum.

TYPICAL APPLICATIONS :—Operating valves, dampers, or rheostats actuating Geneva movements for drum-type switches, rocking baths, continuous turning, feed of light strip under process, work movement, *e.g.* soldering and welding fixtures.

The
Drayton Regulator & Instrument Co Ltd.
West Drayton : : Middlesex

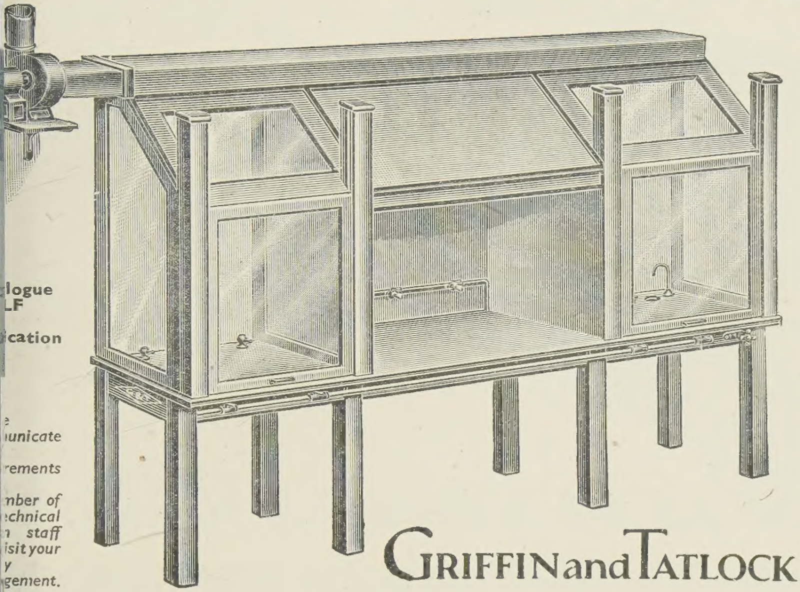

LABORATORY FURNITURE

Functional suitability, technical convenience and personal convenience are three important factors to be observed in designing a laboratory.

It is evident that the successful planning of a laboratory requires the exercise of a degree of technical knowledge which few fully appreciate. It involves the solution of complex design problems (ventilating, fume removal, drainage, layout, disposal of supply services) and a thorough knowledge of structural materials and their suitability for use in various parts of the laboratory.

We are experienced designers of laboratory furniture, manufactured in our own works.

logue
LF
cation

unicate
ements
nber of
chnical
staff
isit your
y
gement.

GRIFFIN and TATLOCK Ltd

Established as Scientific Instrument Makers in 1826

LONDON Kemble Street, W.C.2
MANCHESTER 19, Cheetham Hill Rd., 4
GLASGOW 45, Renfrew Street, C.2
EDINBURGH 7, Teviot Place, 1

BIRMINGHAM : STANLEY BELCHER & MASON LTD., CHURCH STREET, 3

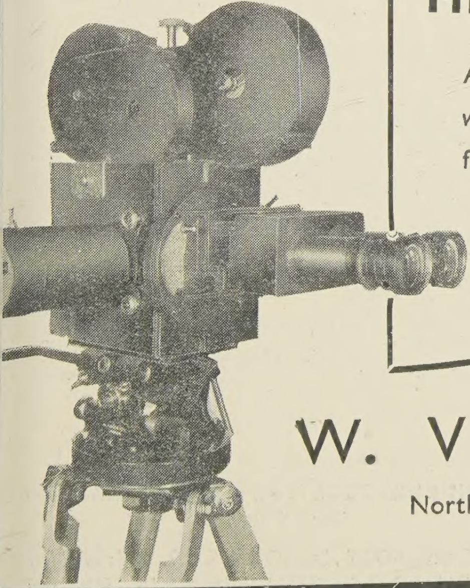

Model H.S. 300 with variable speed shutter giving exposures up to 1/20,000th second

The Model H.S. 300
HIGH SPEED CAMERA

Available on hire for high speed research work requiring accurate observation of fast moving machinery, projectiles, etc.

COST OF HIRE :-
15.15.0 PER DAY *(including operator)*

W. VINTEN LIMITED

North Circular Road, Cricklewood, N.W.2.

Telephone : GLAdstone 6373

EEL

SELENIUM PHOTOCELLS
for use with direct reading instruments or valve amplifiers.

TEST TUBE COLORIMETERS
for Haemoglobin and other determinations.

REFLECTOMETERS
for comparing reflectance from all surfaces.

• • • •

EVANS ELECTROSELENIUM
LIMITED
BISHOP'S STORTFORD, HERTS.

TELCON
T & M LTD. C
METALS

Manufacturers of

SPECIAL ALLOYS FOR THE SCIENTIFIC INSTRUMENT AND RADIO INDUSTRIES

★

MUMETAL
REGD.

MAGNETIC SCREENS

MUMETAL is a renowned TELCON alloy unsurpassed for the shielding of delicate equipment from uni-directional or alternating magnetic fluxes. During wartime MUMETAL has been extensively employed for screens in Radar and other important, equipment. The experience gained from these activities is now available for the solution of your peacetime problems and inquiries are invited.

THE TELEGRAPH CONSTRUCTION & MAINTENANCE CO.
Founded 1864

Head Office: 22 OLD BROAD ST., LONDON, E.C.2. *Tel: LONdon W*
Enquiries to: TELCON WORKS, GREENWICH, S.E.10. *Tel: Greenwi*

WRAY

SCIENTIFIC
LENSES

FOR NEARLY A CENTURY WRAY LENSES HAVE ENJOYED THE CONFIDENCE OF SCIENTISTS

THE LENS HERE ILLUSTRATED HAS BEEN SPECIALLY DESIGNED FOR USE ON CONSTANT SPEED CAMERAS TO RECORD ON 35 mm. FILM FROM A CATHODE RAY TUBE. IT IS AN ANASTIGMAT OF 2″ FOCAL LENGTH, HAS AN APERTURE OF F.I. AND IS CORRECTED FOR AN OBJECT TO IMAGE RATIO OF 4 : I.

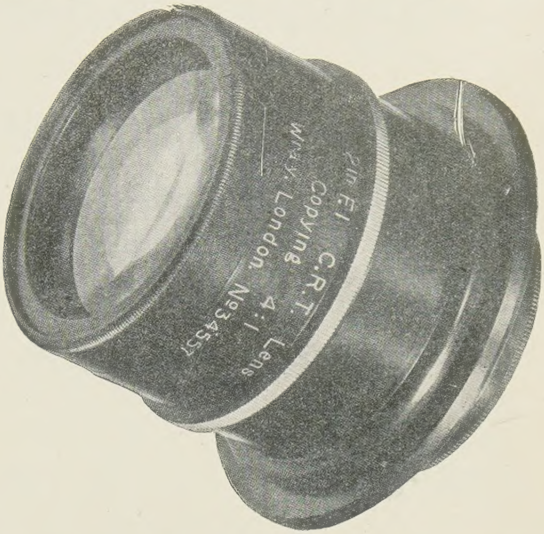

VRAY (OPTICAL WORKS) LTD. BROMLEY, KENT

BALDWIN
INSTRUMENT COMPANY LIMITED

Laboratory methods of determination requiring time and skill can often be replaced by direct-reading instruments that can be successfully used by the non-technical worker. Our development service for industry covers the field of Idea, Prototype and Manufacture. Ask us about it.

SIMPLIFIED
MEASUREMENT
AND
CONTROL

BALDWIN INSTRUMENT COMPANY LIMITED
CUMNOR - OXFORD

riginators and makers of scientific instruments for measurement and control.

TEMPERATURE and HUMIDITY-CONTROL with Adjustable Contact Thermometers

●

AUTOMATIC VACUUM-CONTROL for LABORATORY and ALTITUDE TESTS

●

SUPER-SENSITIVE RELAYS and MERCURY SWITCHES

●

COMPONENTS for HERMETIC SEALING

ELECTRO METHODS Ltd.

112, BRENT ST., N.W.4 Hen. 744
220, THE VALE, N.W.11 - Glad. 661

LABGEAR

MANUFACTURERS OF

Laboratory Apparatus
Scientific Instruments &
Electronic Equipment, etc.

INVITE YOUR INQUIRIES FOR SPECIAL REQUIREMENTS OR CATALOGUES

WRITE OR PHONE **LABGEAR** PHONE: 2494/5
WILLOW PLACE **CAMBRIDGE**

ELECTRONICS

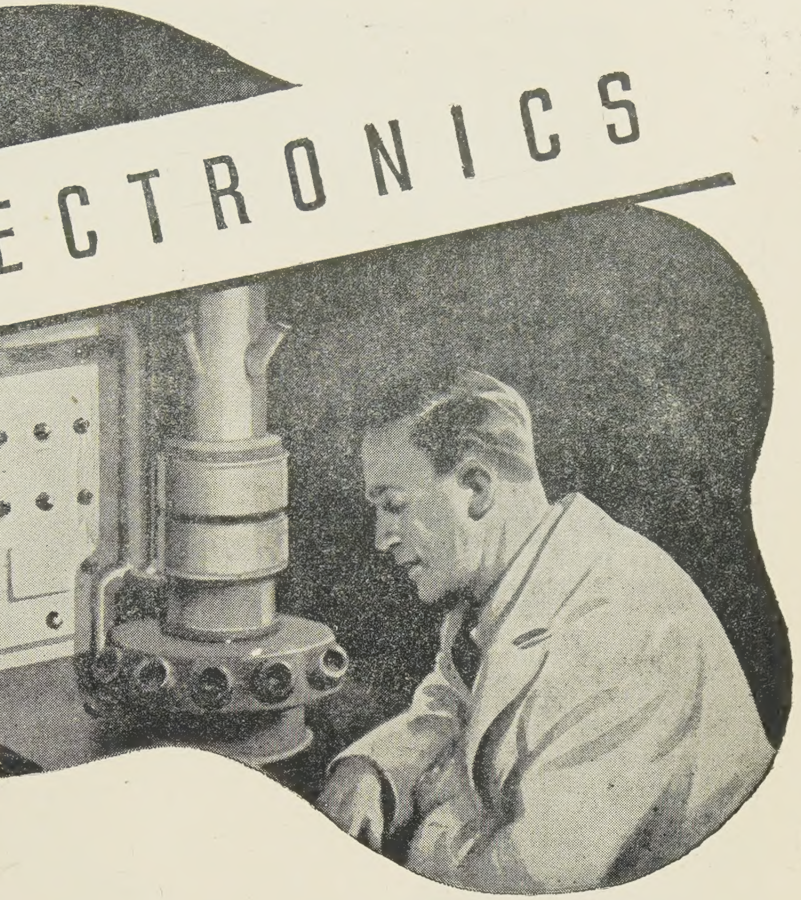

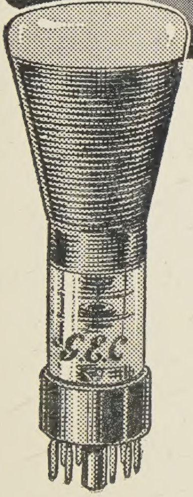

A typical G.E.C. Cathode Ray Tube 4102, with $2\frac{3}{4}''$ screen, widely used in industry during the war, and with many peace-time applications.

made it possible!

On the screen of the Electron Microscope, the scientist examines the characteristics of tiny organisms less than a millionth of an inch long. Electronics have, in fact, brought under scientific examination many germs and bacteria so small that they have never previously been observed in detail by the human eye.

G.E.C. Cathode Ray Tubes and OSRAM Valves cover every electronic application, and will bring to the pursuits of peace many well-tried electronic devices to speed, smooth, and make safer our way of life.

Osram PHOTO CELLS

G.E.C. CATHODE RAY TUBES

Osram Valves

of The General Electric Co. Ltd., Magnet House, Kingsway, London, W.C.2.

ACCURATE
TESTING

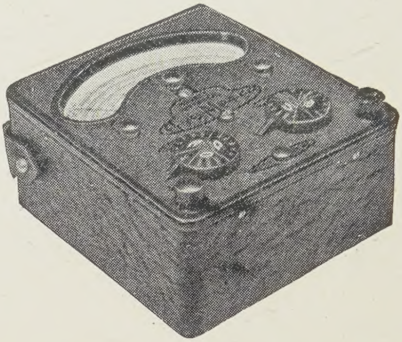

Current, A.C. and D.C. (0 to 10 amps.)
Voltage, A.C. and D.C. (0 to 1000 v.)
Resistance (up to 40 megohms.)
Capacity (0 to 20 mfds.)
Audio-frequency Power Output (0 to 2 watts.)
Decibels (—25 Db. to +16 Db.)

The MODEL 7 *50-Range Universal*

AVOMETER

Electrical Measuring Instrument

The Model 7 Universal AvoMeter is a multi-range A.C./
Measuring Instrument of B.S. 1st grade accuracy, provid
50 ranges of readings on a 5″ hand calibrated scale. Ra
selection is by means of two rotary switches, for A.C. and
respectively. A press button provides an additional range
each value of current and voltage shown on the switch kn
Current consumption is 1 mA. or 2 mA. at full scale deflec
according to whether the press button is used or not.
total resistance of the Meter is 500,000 ohms.
The Meter is protected by an automatic cut-out aga
damage through severe over-load, and compensation is p
vided for variations in ambient temperature.

Size: 8″×7¼″×4½″.

Nett Weight: 6¾ lbs. (including leads).

Various accessories are available for extending the above ran

●

The UNIVERSAL AVOMINOR

Electrical Measuring Instrument

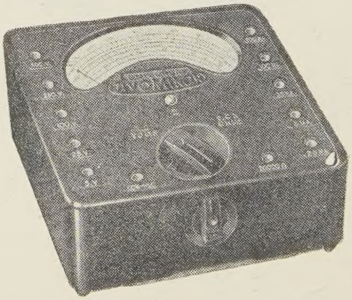

An accurate moving coil meter providing 22 ranges of readings on a 3-inch scale. Total resistance 200,000 ohms. Self-contained for resistance measurements up to 20,000 ohms, and by using an external source of voltage the resistance ranges can be extended to 10 megohms. The ohms compensator for incorrect voltage works on all ranges. Suitable for use as an output meter when the A.C. voltage ranges are being used. Complete with leads, testing prods, crocodile clips, and instruction booklet.

D.C. Voltage : 0—500 volts.
A.C. Voltage : 0—500 volts.
D.C. Current : 0—500 milliamps.
Resistance : 0—10 meghoms.

Size: 4¾″×3¾″×1¾″. *Nett Weight: 18 ozs.*

The MODEL 40 *Universal*

AVOMETER

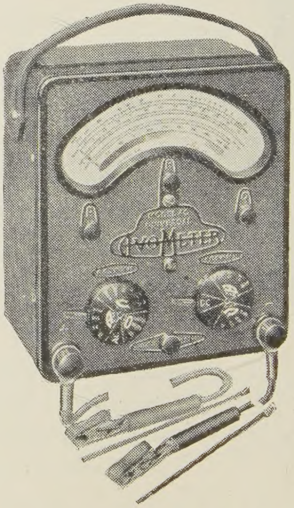

Size : 8″ × 7¼″ × 4½″.

Weight: 6¼ lbs.
(including leads).

A self-contained m
range A.C./D.C. ins
ment providing 40 ra
of readings of curr
voltage and resist
without external shu
transformers or m
pliers. Range selecti
accomplished by m
of A.C. and D.C. sw
knobs, also a press bu
which halves the valu
any current or vol
range.
A 3 mA. movemen
incorporated, full s
deflection on vol
ranges being gene
obtained with the
sumption of 3 or 6
The resistance of
meter on the 600
1,200 volt ranges
200,000 ohms.
5″ hand calibrated sc
with parallax mir
Accuracy within B.S.
grade limits guaran
on both A.C. and
Provided with autom
overload cut-out.

Sole Proprietors and Manufacturers :—

THE AUTOMATIC COIL WINDER & ELECTRICAL EQUIPMENT CO., LT

'AVO' *Precision* **ELECTRICAL TESTING INSTRUMENTS**

Registered Trade Mark

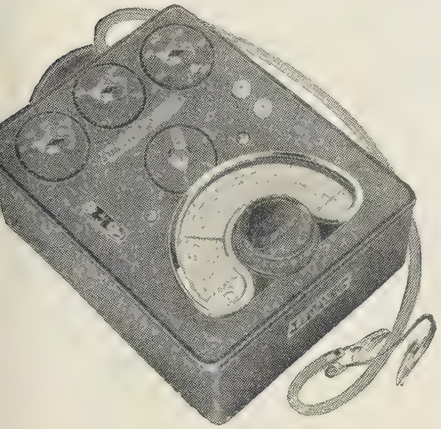

The "AVO" ALL-WAVE
OSCILLATOR

An inexpensive, accurate, modulated oscillator covering a continuous fundamental frequency band from 95 Kc. to 40 Mc. by means of 6 separate coils mounted on a rotary turret selector. A harmonic calibration extends the range to 80 Mc. A large, clearly marked dial is directly calibrated throughout, accuracy being within 1%. Externally modulated, internally modulated, or R.F. signals obtainable at will. Internal modulation at 30% at 400 cycles, the L.F. signal being available for external use. Calibrated double attenuator enables signal to be varied from a few microvolts to 50-millivolts, with a force output of 1 v. Self-contained, fully shielded. Shielded output lead and interchangeable dummy aerials. A.C. Mains and Battery Models.

Size: 10$\frac{1}{4}$" × 8$\frac{1}{4}$" × 4$\frac{1}{4}$" *Nett Weight: 13$\frac{1}{4}$ lbs*

•

THE "AVO" TEST BRIDGE

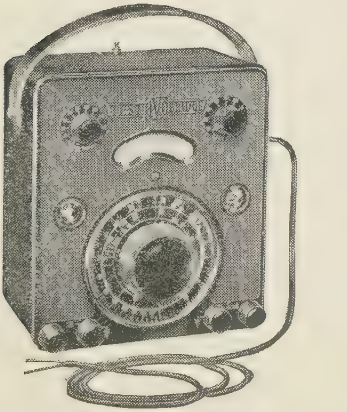

A portable self-contained 50-cycles bridge of exceptional accuracy and utility for direct measurement of all normal values of condensers and resistances. Except at the extreme ends of the scale, accuracy is within 5%.

CAPACITY
.000005—.005mFd
.0005 —.5 mFd.
.05 —50 mFd.

RESISTANCE
5—5,000 ohms
500—5,00000ohms
50,000 ohms to
50 Megohms.

Facilities also provided for condenser power factor measurements and leakage tests by the flashing neon method; resistance, capacity and large inductance measurements against external standards. May also be used as a highly efficient valve voltmeter indicator for measurement of both audio and radio frequency voltages.

The "AVO" VALVE TESTER

Complete with Universal valve panel fitted with Selector Switch enabling all English, American and Continental valves to be easily tested. Comprehensive valve data booklets, containing test details of nearly 2,000 English and American valves, also supplied.

Indicates mutual conductance direct in mA/V. Tests at makers' specified electrode voltages. One panel for all types of English and American valves. Any valve base arrangement set up; easily operated multi-roller Universal Selector Switch. Tests Cathode, Heater insulation of an indirectly heated valve when the valve is hot; emission of diodes and rectifiers; indicates filament continuity and electrode "shorts." Coloured scale indicates state of valve as "Good," "Indifferent" or "Replace." No calculations of any kind involved. Works entirely from A.C. mains.

DER HOUSE, DOUGLAS STREET, LONDON, S.W.1 *Telephone: VICtoria* **3404-8**

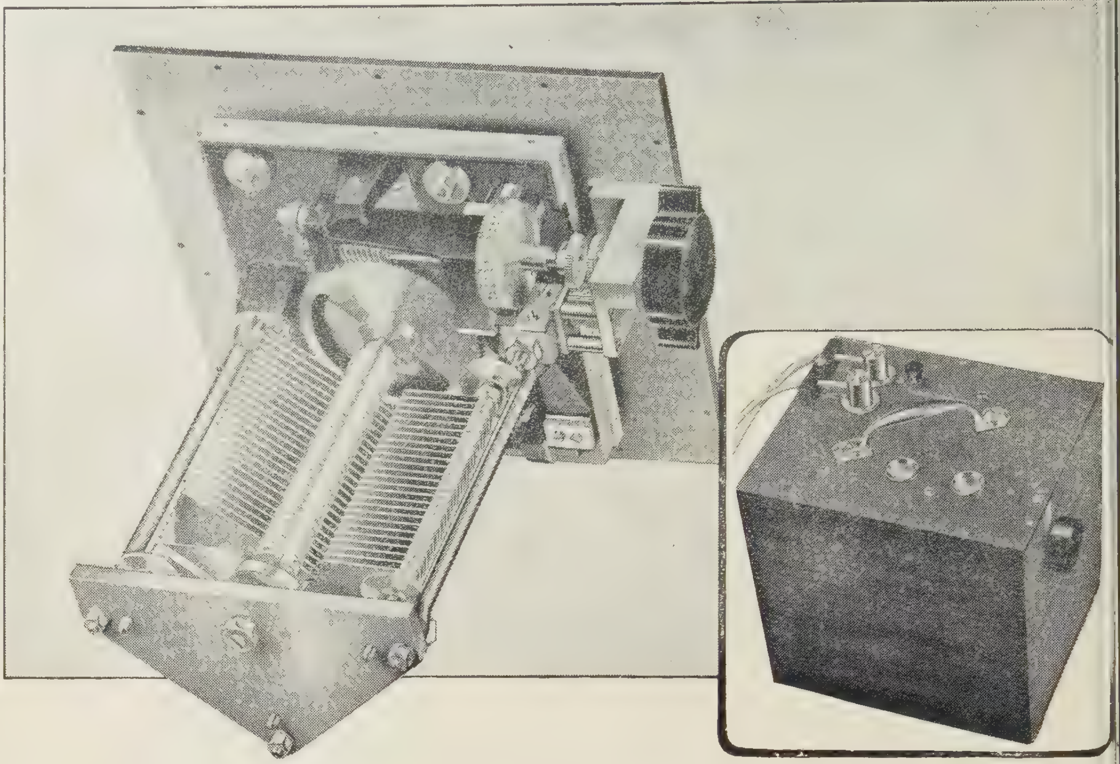

A Standard of Zero Loss Angle

VARIABLE AIR CONDENSER TYPE D-14-A

This three-terminal double-screened condenser is provided with a guard circuit which ensures that the dielectric of the plate-to-plate capacitance is composed entirely of air. This, together with the special surface treatment of the plates reduces the plate-to-plate power loss to a quantity which can be disregarded even when measuring the smallest power factors.

BRIEF SPECIFICATION

CAPACITANCE. 50 μμF min. 1,250 μμF max.

LOSS ANGLE. Approximately 1 micro-radian in a dry atmosphere: 7 micro-radians in 75% relative humidity, for the frequency range 50 c.p.s. to 10,000 c.p.s.

DRIVE. Worm reduction gear, 50: 1 ratio.

SCALE READING. To 1 part in 5,000 direct reading; To 1 part in 20,000 by interpolation.

BACKLASH. Not exceeding 1 part in 20,000.

DIMENSIONS. 12. 7/8″ x 10″ x 13 5/8″.

Write for Bulletin B-537-A giving further particulars.

MUIRHEAD

MUIRHEAD & COMPANY LTD., ELMERS END, BECKENHAM, KENT. TEL: BECKENHAM 0041-2.

FOR OVER 60 YEARS DESIGNERS AND MAKERS OF PRECISION INSTRUMEN

C.R.C. 45

B
T-H

RESEARCH &
ENGINEERING

BTH Products are available as instruments and apparatus for research, development, and engineering, including all branches of electronic control.

• • • •

THYRATRONS MAGNETRONS
CRYSTAL RECTIFIERS
SPECIAL VACUUM ELECTRONIC DEVICES
GLASS, AND GLASS METAL SEALS
RECTIFIERS
FRACTIONAL HORSEPOWER MOTORS
ETC.

BTH RUGBY
THE BRITISH THOMSON-HOUSTON COMPANY LIMITED, RUGBY, ENGLAND.

A3595N

AEI

CATHODE
RAY TUBES

Whenever the Oscillograph trace requires recording **ILFORD LIMITE** can supply the **MOST SUITABLE** photographic material. Ilford Limited marke a full range of papers, films and plates for photographic recording of all type used in scientific and industrial investigations. The following is a selection c materials specially made for **OSCILLOGRAPH RECORDING**:

CODE	NATURE	CHIEF USES
5R101	Film—Panchromatic. Very high speed. Medium contrast.	Specially suitable for recording traces on red fluorescen screens (Phosphate screens) and sometimes used fo green and blue screens.
H.P.3	Plate—Panchromatic. Medium contrast.	Sometimes used for recording single transients as it slightly faster than 5R101.
5G91	Film—Orthochromatic. Very high speed. Medium contrast.	The fastest material for recording traces on green an blue fluorescent screens. Specially suitable for recor ing single fast transients.
5B52	Film—Blue sensitive. High speed. Medium contrast. On orange base.	A new film specially for recording traces on blu fluorescent screens. On account of its special metho of manufacture there is a minimum of image sprea enabling traces, in which the spot velocity varies ove a wide range, to be successfully recorded. Also suitab for high-speed processing.
BP1	Paper—Glossy. Blue sensitive. High speed. High contrast.	Very widely used for recording traces on blue fluor escent screens and also for many other forms of recor ing where a paper base is required.
8B21	Film—Blue sensitive. Medium speed. High contrast.	Suitable for the direct recording of high-speed electror in an evacuated tube.

For an explanation of the code numbers used and for fuller details of these and other recommende materials, write for a copy of the Ilford booklet "Photography as an Aid to Scientific Work.

ILFORD LIMITED · ILFORD · LONDON

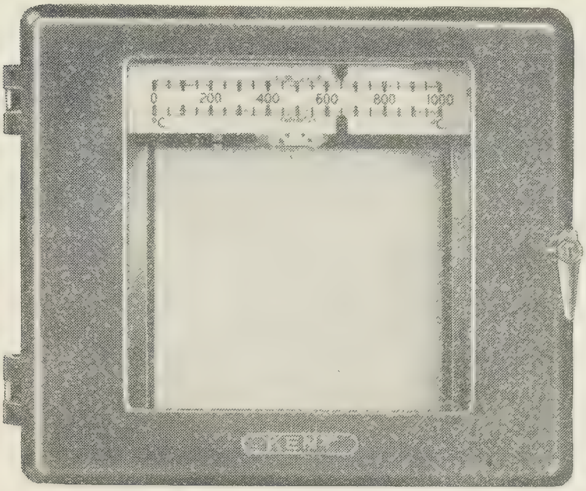

THE KENT

MULTELEC

is a strong and sturdy instrument which, upon activation at two-second intervals by any minute change of potential, sets up a powerful servo-motor force for controlling any desired form of correction, yet without imposing any restraint upon the sensitivity of the instrument. Furthermore, it indicates and records.

VARIOUS USES :

The Kent Multelec is extensively used in various industries for recording, indicating and controlling temperatures, its potentiometric basis ensures a fine degree of accuracy under industrial conditions.

It is also used in the control of *p*H value in various processes, and for the correction of boiler feed water by measurement of electrical conductivity.

It will be recognised that the Multelec can be adapted to many forms of controlling, recording or indicating besides the above.

George Kent, Ltd., also supply meters for accurate measurement of the flow of steam, water, gas, air, oil or any other fluid, whatever the quantity or pressure.

The Multelec booklet (No. 897) is available on request.

GEORGE KENT

GEORGE KENT, LTD. LUTON & LONDON

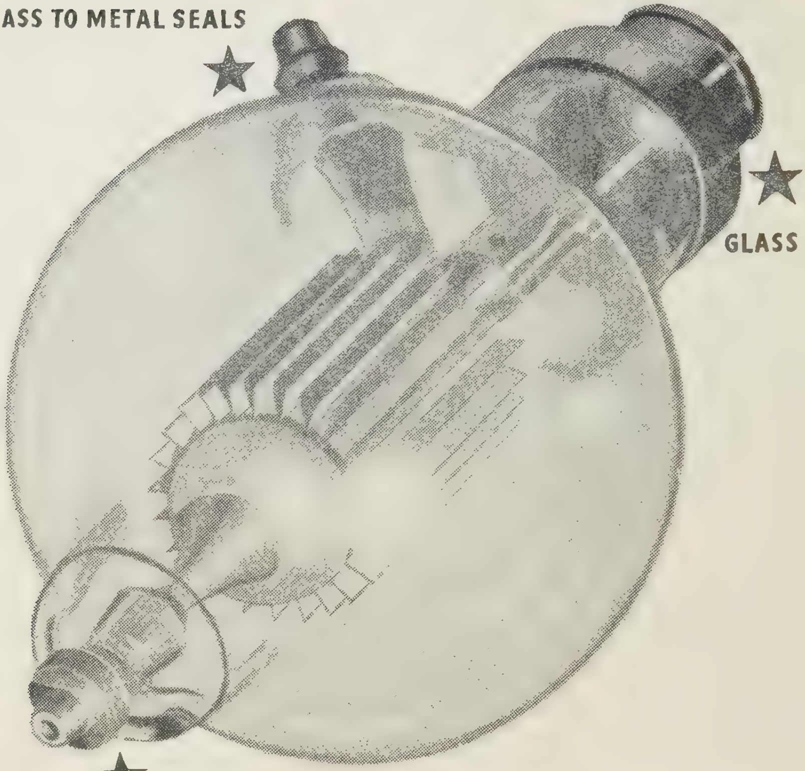

"NICOSEL"

(LOW EXPANSION STEEL)

SPECIAL ALLOY STEEL

" Nicosel " is a valuable British contribution to the Arts of electric lamp and vacuum tube manufacture. Its low co-efficient of expansion makes it eminently suitable for modern developments of the glass and electrical industries.

FIRTH-BROWN

THOS. FIRTH & JOHN BROWN LTD SHEFFIELD

BERCO RESISTANCES

Although present circumstances render it difficult for us to give our pre-war service to all customers, we are still working in their interests.

New materials and manufacturing processes, which we are now using to increase output, also contribute in large measure to improved performance and reliability of our products. Thus, when normal times return, all users of Berco Resistances will benefit by our work to-day.

THE BRITISH ELECTRIC RESISTANCE CO. LTD.
QUEENSWAY, PONDERS END, MIDDLESEX

Telephone: HOWARD 1492.
Telegrams: "VITROHM, ENFIELD."

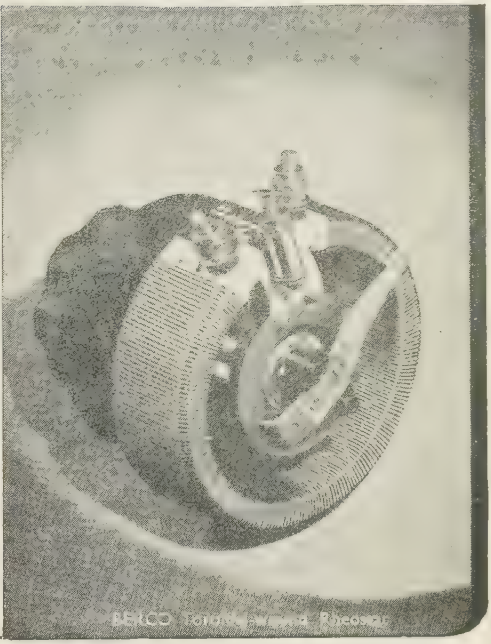

for HEAVY DUTY
LECTRICAL AND INSTRUMENT SPRINGS

GREATER tensile, elastic and fatigue strengths than any other non-ferrous alloy, a higher conductivity than any of the bronzes and excellent resistance to corrosion and wear—these characteristics of Mallory 73 Beryllium Copper have made it first choice for instrument springs, diaphragms and bellows, current-carrying springs, snap action switch blades, contact blades and clips.

Supplied annealed or lightly cold worked, it has good forming properties and is readily fabricated into springs and parts of complicated shape. A simple heat treatment then develops its remarkable properties.

Available as sheet, strip and wire, in a range of tempers to suit users' requirements, and as rod, tube, precision rolled hair-spring strip, and silver-faced contact bi-metal strip.

MALLORY

MALLORY METALLURGICAL PRODUCTS LTD.
An Associate Company of JOHNSON, MATTHEY & CO. LTD.
78 Hatton Garden, London, E.C.1
Telephone: HOLborn 5027

BERYLLIUM COPPER 73

Properties of
MALLORY 73 BERYLLIUM COPPER
after heat treatment

Ultimate tensile stress *tons per sq. inch*	**75-100**
Limit of proportionality *tons per sq. inch*	**47-50**
Fatigue limit *tons per sq. inch*	**±19-20**
Vickers pyramid hardness	**350-420**
Electrical Conductivity *per cent I.A.C.S.*	**23-25**

Full details are given in our booklet, which will be sent on request.

CAMBRIDGE
POLAROGRAPH

(HEYROVSKY DROPPING MERCURY ELECTRODE METHOD)

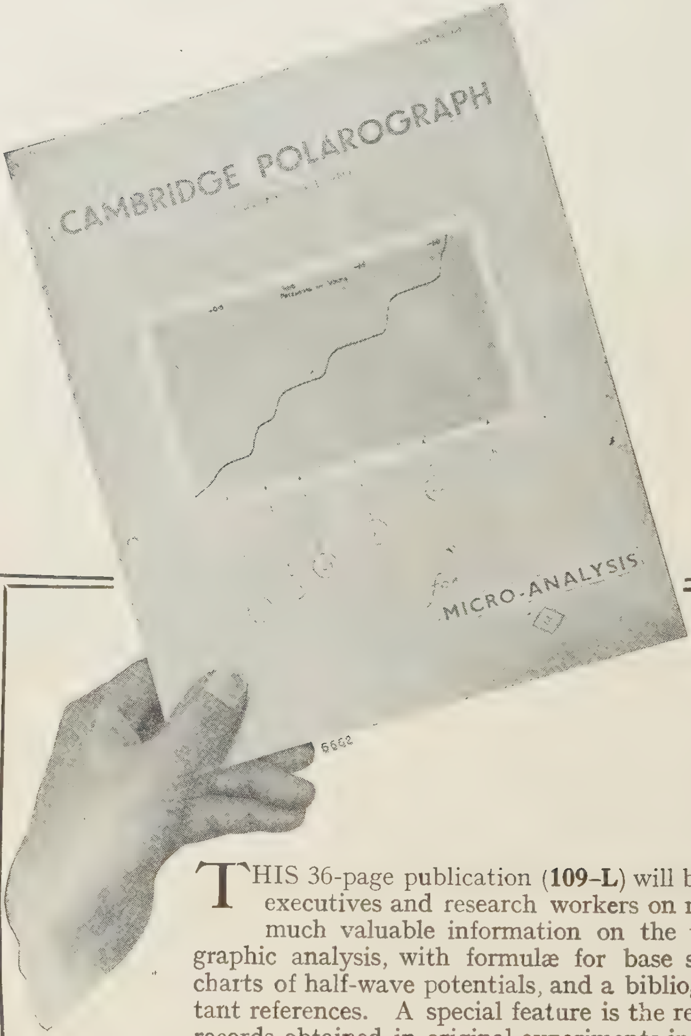

Some Fields of Application :

PHYSICAL CHEMISTRY
METALLURGY
MINERALOGY
SUGAR
EXPLOSIVES
GASES
AGRICULTURE
MEDICINE
OIL DISTILLING
DYEING & BLEACHING
CERAMICS
WATER PURIFICATION

THIS 36-page publication (**109-L**) will be sent to responsible executives and research workers on request. It contains much valuable information on the technique of polarographic analysis, with formulæ for base solutions, tables and charts of half-wave potentials, and a bibliography of 168 important references. A special feature is the reproduction of actual records obtained in original experiments in our own laboratory. A supplement describes the new Cambridge Voltamoscope, for routine determinations, which performs the same functions, but is non-recording.

91

CAMBRIDGE INSTRUMENT COMPANY LTD.
13, GROSVENOR PLACE, LONDON, S.W.I.
WORKS: LONDON & CAMBRIDGE.

THE PROCEEDINGS OF
THE PHYSICAL SOCIETY

VOL. 58, PART 1 1 January 1946 No. 325

COLOURS OF TOTAL RADIATORS EXPRESSED ON THE C.I.E. TRICHROMATIC SYSTEM FOR THE TEMPERATURE RANGE 0-1-660 MIREDS (C_2=14384·8)

By H. G. W. HARDING,
National Physical Laboratory, Teddington

MS. received 15 *July* 1945

ABSTRACT. Six-figure tables of the trichromatic coefficients of the colours of Planckian (total or black-body) radiators expressed on the C.I.E. trichromatic system (1931) are given for the temperature range 0–1–660 mireds. The colours refer to energy distributions calculated from Planck's formula with a value 14384·8 micron degrees for the constant C_2. Additional tables give the differences in the coefficients of the colours from the tabulated values for a change in the value of C_2 from 14384·8 to 14320 and from 14384·8 to 14350. These additional tables can be used to calculate the colours if other values of C_2 are used in Planck's formula.

TABLES which give the trichromatic coefficients of the colours of total radiators expressed on the C.I.E. system (1931) for the temperature range 1500–10–9000° K. have been published (Harding, 1944). These six-figure tables enable the coefficients of the colours of total radiators at any temperature within the given range to be calculated to five-figure accuracy by linear interpolation. To extend the range of these tables to cover the temperature range between 9000° K. and infinite temperature, the colours have been recalculated on a mired temperature scale and the range extended to infinite temperature. A mired, or micro-reciprocal-degree, is a million divided by the temperature of the radiator expressed in °K. (Priest, 1933).

The colours of the total radiators for the range 0–1–660 mireds were obtained by calculating the coefficients of the colours first for 0–10–660 mireds, then interpolating these coefficients to tenths.

The colours of the total radiators for 0–10–110 mireds had not been published and so they were calculated in the following way. The spectral distributions of the energies of the radiators were calculated from Planck's formula,

$$E_{\lambda, M}\, d\lambda = C_1 \lambda^{-5} \left[\exp \frac{C_2 M}{\lambda\, 10^6} - 1 \right]^{-1} d\lambda,$$

where $E_{\lambda, M}\, d\lambda$ represents the amount of energy radiated at M mireds between the wave-lengths $\lambda \pm \frac{d\lambda}{2}$ (microns) and C_1 and C_2 are constants. Since the energy values were made equal to 100·0000 at 0·56μ, the value of C_1 was not required. The value 14384·8 micron degrees was given to C_2 (Birge, 1941). The distributions of energy were checked by fifth differences and were estimated to be correct to about one part in a million. The trichromatic coefficients of the colours of the radiators were then calculated from the spectral distributions of energy, using the

Condensed Tables for Colour Computation for the equal-energy stimulus (Smith, 1934).

The colours of the radiators at 120–10–660 mireds were calculated from the previously published tables and the trichromatic coefficients were altered in some instances by a unit in the sixth decimal place to make the fifth differences smooth.

The trichromatic coefficients obtained by the methods just explained for the range 0–10–660 mireds were then interpolated to tenths, giving values at 0–1–660 mireds. Alterations of a unit in the sixth decimal place were made to the Z coefficients where necessary to make the sum of all three coefficients exactly unity. These coefficients are given in table 1.

The alterations to be made to the trichromatic coefficients if C_2 is changed from 14384·8 to 14320 were calculated for the mired range 0–10–660 mireds in the following way. Two illuminants have the same spectral distribution of energy, consequently the same colour, if the value of C_2M in Planck's formula remains unaltered. It follows that the trichromatic coefficients of the colour of a total radiator at M_{14320} mireds, calculated with $C_2=14320$, will be the same as those of a radiator at $14320\,(14384{\cdot}8)^{-1}M_{14384\cdot8}=0{\cdot}9954952\,M_{14384\cdot8}$ mireds if 14384·8 has been used for the colour calculation. The differences between the trichromatic coefficients for $M_{14384\cdot8}$ mireds and $0{\cdot}9954952\,M_{14384\cdot8}$ mireds were therefore calculated from the trichromatic coefficients in table 1 and are tabulated in table 2. If the value of C_2 is 14350, the alterations to the coefficients in table 1 are given by the differences between the coefficients for $M_{14384\cdot8}$ mireds and $14350\,(14384{\cdot}8)^{-1}M_{14384\cdot8}=0{\cdot}9975808\,M_{14384\cdot8}$ mireds. These differences are tabulated in table 3. All the differences in tables 2 and 3 were differenced to the third order and an alteration of a unit in the sixth decimal place was made to a few values to make the third differences smooth.

For other likely values of C_2 different from 14320 or 14350, linear interpolation of the values given either in table 2 or table 3 gives the differences with errors less than one or two units in the sixth decimal place; for instance, if $C_2=14360$ the X coefficient corresponding to 150 mireds is equal to

$$0{\cdot}310998-0{\cdot}000237\,\frac{14384{\cdot}8-14360}{14384{\cdot}8-14350}=0{\cdot}310998-0{\cdot}000169=0{\cdot}31083.$$

The six figures for the trichromatic coefficients are only quoted here in order that the smoothed tables might serve as a basis for the preparation of other tables that might be required with a value of C_2 other than 14384·8.

The values quoted in tables 1, 2 and 3 might in a few instances be one or two units in the sixth decimal place different from those in the previously published tables. These differences were considered to be necessary to smooth the values in the present tables.

ACKNOWLEDGMENTS

These calculations have been carried out as a part of the research programme of the National Physical Laboratory, and this paper is published by permission of the Director of the Laboratory.

REFERENCES

Birge, R. T., 1941. *Rev. Mod. Phys.* **13,** 237.
Harding, H. G. W., 1944. *Proc. Phys. Soc.* **56,** 305.
Priest, I. G., 1933. *J. Opt. Soc. Amer.* **23,** 41.
Smith, T., 1934. *Proc. Phys. Soc.* **46,** 372.

Table 1

Mireds $(T\ ^\circ\mathrm{K.})^{-1} \times 10^6$ $(C_2 = 14384{\cdot}8)$	Trichromatic coefficients		
	$x \times 10^6$	$y \times 10^6$	$z \times 10^6$
0	239906	234131	525963
1	240163	234513	525324
2	240423	234898	524679
3	240687	235287	524026
4	240953	235680	523367
5	241221	236077	522702
6	241493	236477	522030
7	241768	236882	521350
8	242046	237290	520664
9	242327	237702	519971
10	242610	238118	519272
11	242897	238538	518565
12	243187	238961	517852
13	243479	239388	517133
14	243775	239819	516406
15	244074	240254	515672
16	244376	240692	514932
17	244680	241134	514186
18	244988	241580	513432
19	245299	242030	512671
20	245613	242483	511904
21	245930	242940	511130
22	246250	243401	510349
23	246574	243865	509561
24	246900	244333	508767
25	247229	244805	507966
26	247562	245280	507158
27	247897	245759	506344
28	248236	246241	505523
29	248578	246727	504695
30	248923	247216	503861
31	249271	247709	503020
32	249622	248206	502172
33	249977	248705	501318
34	250334	249209	500457
35	250695	249715	499590
36	251058	250225	498717
37	251425	250739	497836
38	251795	251255	496950
39	252168	251775	496057
40	252545	252299	495156
41	252924	252825	494251
42	253307	253355	493338
43	253692	253888	492420
44	254081	254424	491495

Table 1 (*continued*)

Mireds $(T\ ^\circ\text{K.})^{-1} \times 10^6$ $(C_2 = 14384{\cdot}8)$	Trichromatic coefficients		
	$x \times 10^6$	$y \times 10^6$	$z \times 10^6$
45	254473	254963	490564
46	254868	255505	489627
47	255266	256050	488684
48	255668	256598	487734
49	256072	257150	486778
50	256480	257704	485816
51	256890	258261	484849
52	257304	258821	483875
53	257721	259384	482895
54	258141	259950	481909
55	258564	260518	480918
56	258990	261090	479920
57	259419	261664	478917
58	259851	262240	477909
59	260287	262820	476893
60	260725	263402	475873
61	261166	263986	474848
62	261611	264573	473816
63	262058	265162	472780
64	262509	265754	471737
65	262962	266349	470689
66	263419	266945	469636
67	263879	267544	468577
68	264341	268145	467514
69	264807	268749	466444
70	265275	269355	465370
71	265747	269962	464291
72	266221	270572	463207
73	266698	271184	462118
74	267178	271798	461024
75	267662	272414	459924
76	268148	273032	458820
77	268636	273652	457712
78	269128	274274	456598
79	269623	274898	455479
80	270120	275523	454357
81	270621	276150	453229
82	271124	276779	452097
83	271630	277409	450961
84	272138	278041	449821
85	272650	278675	448675
86	273164	279310	447526
87	273681	279946	446373
88	274201	280584	445215
89	274723	281224	444053

Table 1 (*continued*)

Mireds $(T\,^\circ\text{K.})^{1}\times 10^6$ $(C_2=14384{\cdot}8)$	Trichromatic coefficients		
	$x\times 10^6$	$y\times 10^6$	$z\times 10^6$
90	275249	281864	442887
91	275776	282506	441718
92	276307	283150	440543
93	276840	283794	439366
94	277376	284440	438184
95	277914	285086	437000
96	278455	285734	435811
97	278999	286383	434618
98	279545	287033	433422
99	280093	287684	432223
100	280644	288336	431020
101	281197	288989	429814
102	281754	289642	428604
103	282313	290296	427391
104	282874	290951	426175
105	283437	291607	424956
106	284003	292263	423734
107	284572	292920	422508
108	285143	293578	421279
109	285716	294236	420048
110	286291	294894	418815
111	286869	295553	417578
112	287449	296212	416339
113	288031	296872	415097
114	288615	297533	413852
115	289202	298193	412605
116	289791	298853	411356
117	290382	299514	410104
118	290976	300175	408849
119	291571	300836	407593
120	292169	301497	406334
121	292769	302158	405073
122	293371	302819	403810
123	293975	303480	402545
124	294581	304141	401278
125	295190	304802	400008
126	295800	305463	398737
127	296412	306123	397465
128	297027	306783	396190
129	297643	307443	394914
130	298261	308103	393636
131	298881	308762	392357
132	299503	309421	391076
133	300127	310080	389793
134	300752	310738	388510

Table 1 (*continued*)

Mireds $(T\,^\circ\mathrm{K.})^{-1}\times10^6$ $(C_2=14384\cdot8)$	Trichromatic coefficients		
	$x\times10^6$	$y\times10^6$	$z\times10^6$
135	301379	311396	387225
136	302009	312053	385938
137	302640	312709	384651
138	303273	313365	383362
139	303908	314020	382072
140	304544	314675	380781
141	305182	315329	379489
142	305822	315982	378196
143	306463	316634	376903
144	307106	317286	375608
145	307751	317937	374312
146	308397	318587	373016
147	309045	319236	371719
148	309695	319884	370421
149	310346	320531	369123
150	310998	321177	367825
151	311652	321822	366526
152	312307	322466	365227
153	312964	323109	363927
154	313623	323751	362626
155	314282	324392	361326
156	314943	325031	360026
157	315606	325669	358725
158	316270	326307	357423
159	316935	326942	356123
160	317601	327577	354822
161	318269	328210	353521
162	318937	328842	352221
163	319608	329473	350919
164	320279	330102	349619
165	320951	330730	348319
166	321625	331356	347019
167	322300	331980	345720
168	322976	332604	344420
169	323653	333226	343121
170	324331	333846	341823
171	325010	334465	340525
172	325691	335082	339227
173	326372	335697	337931
174	327054	336311	336635
175	327738	336923	335339
176	328422	337534	334044
177	329108	338142	332750
178	329794	338749	331457
179	330481	339355	330164

Table 1 (*continued*)

Mireds $(T\ \text{K.})^{-1}\times 10^6$ $(C_2=14384{\cdot}8)$	Trichromatic coefficients		
	$x\times 10^6$	$y\times 10^6$	$z\times 10^6$
180	331169	339958	328873
181	331858	340560	327582
182	332548	341159	326293
183	333238	341757	325005
184	333929	342353	323718
185	334621	342947	322432
186	335314	343539	321147
187	336008	344129	319863
188	336702	344717	318581
189	337397	345304	317299
190	338093	345888	316019
191	338789	346470	314741
192	339486	347050	313464
193	340184	347629	312187
194	340882	348205	310913
195	341581	348779	309640
196	342281	349351	308368
197	342981	349920	307099
198	343681	350488	305831
199	344382	351054	304564
200	345084	351617	303299
201	345786	352178	302036
202	346489	352737	300774
203	347192	353294	299514
204	347895	353849	298256
205	348599	354401	297000
206	349303	354951	295746
207	350007	355499	294494
208	350712	356045	293243
209	351418	356588	291994
210	352123	357129	290748
211	352829	357668	289503
212	353535	358204	288261
213	354241	358738	287021
214	354947	359270	285783
215	355654	359799	284547
216	356361	360326	283313
217	357068	360851	282081
218	357775	361373	280852
219	358482	361893	279625
220	359190	362410	278400
221	359898	362925	277177
222	360606	363437	275957
223	361314	363947	274739
224	362022	364454	273524

Table 1 (*continued*)

Mireds $(T^\circ\text{K.})^{-1}\times 10^6$ $(C_2=14384{\cdot}8)$	Trichromatic coefficients		
	$x\times 10^6$	$y\times 10^6$	$z\times 10^6$
225	362730	364959	272311
226	363438	365461	271101
227	364146	365961	269893
228	364854	366458	268688
229	365563	366953	267484
230	366271	367445	266284
231	366979	367935	265086
232	367688	368422	263890
233	368396	368906	262698
234	369104	369389	261507
235	369812	369868	260320
236	370520	370345	259135
237	371228	370819	257953
238	371935	371291	256774
239	372643	371760	255597
240	373350	372227	254423
241	374057	372691	253252
242	374764	373152	252084
243	375470	373611	250919
244	376177	374067	249756
245	376883	374521	248596
246	377589	374972	247439
247	378294	375420	246286
248	378999	375866	245135
249	379704	376309	243987
250	380409	376749	242842
251	381113	377187	241700
252	381817	377622	240561
253	382521	378054	239425
254	383224	378483	238293
255	383927	378910	237163
256	384630	379335	236035
257	385332	379756	234912
258	386034	380175	233791
259	386735	380591	232674
260	387436	381005	231559
261	388136	381416	230448
262	388836	381824	229340
263	389535	382230	228235
264	390234	382632	227134
265	390933	383033	226034
266	391630	383430	224930
267	392328	383825	223847
268	393024	384217	222759
269	393720	384606	221674

Table 1 (*continued*)

Mireds $(T°\text{K.})^{1}\times 10^{6}$ $(C_2=14384{\cdot}8)$	Trichromatic coefficients		
	$x\times10^6$	$y\times10^6$	$z\times10^6$
270	394416	384993	220591
271	395111	385377	219512
272	395805	385758	218437
273	396499	386137	217364
274	397193	386513	216294
275	397885	386886	215229
276	398577	387257	214166
277	399269	387625	213106
278	399959	387990	212051
279	400650	388352	210998
280	401339	388712	209949
281	402028	389069	208903
282	402716	389423	207861
283	403403	389775	206822
284	404090	390124	205786
285	404776	390470	204754
286	405461	390814	203725
287	406146	391154	202700
288	406830	391493	201677
289	407513	391828	200659
290	408195	392161	199644
291	408876	392491	198633
292	409557	392819	197624
293	410237	393144	196619
294	410915	393466	195619
295	411593	393786	194621
296	412271	394103	193626
297	412947	394417	192636
298	413623	394729	191648
299	414297	395038	190665
300	414971	395344	189685
301	415644	395648	188708
302	416316	395949	187735
303	416987	396248	186765
304	417657	396543	185800
305	418327	396837	184836
306	418995	397127	183878
307	419663	397415	182922
308	420330	397701	181969
309	420995	397984	181021
310	421660	398264	180076
311	422324	398542	179134
312	422987	398816	178197
313	423648	399089	177263
314	424309	399358	176333

Table 1 (*continued*)

Mireds $(T\ ^\circ\mathrm{K.})^{-1}\times10^6$ $(C_2=14384{\cdot}8)$	Trichromatic coefficients		
	$x\times10^6$	$y\times10^6$	$z\times10^6$
315	424969	399626	175405
316	425628	399890	174482
317	426286	400152	173562
318	426943	400412	172645
319	427599	400669	171732
320	428254	400923	170823
321	428908	401175	169917
322	429561	401424	169015
323	430213	401671	168116
324	430863	401915	167222
325	431513	402157	166330
326	432162	402397	165441
327	432809	402633	164558
328	433456	402868	163676
329	434102	403100	162798
330	434746	403329	161925
331	435389	403556	161055
332	436032	403780	160188
333	436673	404002	159325
334	437313	404222	158465
335	437952	404439	157609
336	438590	404654	156756
337	439226	404866	155908
338	439862	405076	155062
339	440497	405283	154220
340	441130	405488	153382
341	441762	405691	152547
342	442394	405891	151715
343	443024	406089	150887
344	443653	406284	150063
345	444280	406477	149243
346	444907	406668	148425
347	445533	406856	147611
348	446157	407042	146801
349	446780	407226	145994
350	447402	407407	145191
351	448023	407586	144391
352	448642	407763	143595
353	449261	407937	142802
354	449878	408109	142013
355	450494	408279	141227
356	451109	408446	140445
357	451722	408611	139667
358	452335	408774	138891
359	452946	408935	138119

Table 1 (*continued*)

Mireds $(T\ ^\circ\mathrm{K.})^{-1}\times10^6$ $(C_2=14384{\cdot}8)$	Trichromatic coefficients		
	$x\times10^6$	$y\times10^6$	$z\times10^6$
360	453556	409093	137351
361	454165	409249	136586
362	454772	409403	135825
363	455379	409555	135066
364	455984	409704	134312
365	456588	409851	133561
366	457191	409997	132812
367	457793	410139	132068
368	458393	410280	131327
369	458992	410419	130589
370	459590	410555	129855
371	460187	410689	129124
372	460782	410821	128397
373	461376	410951	127673
374	461969	411079	126952
375	462561	411205	126234
376	463152	411329	125519
377	463741	411450	124809
378	464329	411569	124102
379	464916	411687	123397
380	465501	411802	122697
381	466085	411915	122000
382	466668	412026	121306
383	467250	412135	120615
384	467830	412242	119928
385	468409	412347	119244
386	468987	412450	118563
387	469564	412550	117886
388	470139	412649	117212
389	470713	412746	116541
390	471286	412841	115873
391	471858	412934	115208
392	472428	413025	114547
393	472997	413114	113889
394	473565	413202	113233
395	474131	413287	112582
396	474697	413370	111933
397	475261	413452	111287
398	475823	413532	110645
399	476385	413609	110006
400	476945	413685	109370
401	477504	413759	108737
402	478062	413831	108107
403	478618	413901	107481
404	479173	413969	106858

Table 1 (*continued*)

Mireds $(T\ ^\circ\text{K.})^{-1}\times 10^6$ $(C_2=14384{\cdot}8)$	Trichromatic coefficients		
	$x\times 10^6$	$y\times 10^6$	$z\times 10^6$
405	479727	414035	106238
406	480280	414100	105620
407	480831	414163	105006
408	481381	414224	104395
409	481930	414283	103787
410	482477	414340	103183
411	483023	414396	102581
412	483568	414449	101983
413	484112	414501	101387
414	484654	414552	100794
415	485195	414600	100205
416	485735	414647	99618
417	486273	414692	99035
418	486810	414735	98455
419	487346	414777	97877
420	487881	414817	97302
421	488414	414855	96731
422	488946	414892	96162
423	489477	414927	95596
424	490007	414960	95033
425	490535	414992	94473
426	491062	415022	93916
427	491588	415050	93362
428	492112	415077	92811
429	492635	415102	92263
430	493157	415126	91717
431	493678	415148	91174
432	494197	415168	90635
433	494715	415187	90098
434	495232	415204	89564
435	495748	415220	89032
436	496262	415234	88504
437	496775	415247	87978
438	497287	415258	87455
439	497798	415267	86935
440	498307	415275	86418
441	498815	415281	85904
442	499322	415286	85392
443	499827	415290	84883
444	500332	415292	84376
445	500835	415292	83873
446	501336	415291	83373
447	501837	415289	82874
448	502336	415285	82379
449	502834	415280	81886

Table 1 (*continued*)

Mireds $(T°\text{K.})^{-1}\times 10^6$ $(C_2=14384\cdot 8)$	Trichromatic coefficients		
	$x \times 10^6$	$y \times 10^6$	$z \times 10^6$
450	503331	415273	81396
451	503827	415265	80908
452	504321	415255	80424
453	504814	415244	79942
454	505306	415232	79462
455	505796	415218	78986
456	506286	415203	78511
457	506774	415186	78040
458	507261	415169	77570
459	507747	415149	77104
460	508231	415129	76640
461	508714	415107	76179
462	509196	415084	75720
463	509677	415060	75263
464	510156	415034	74810
465	510635	415007	74358
466	511112	414979	73909
467	511588	414950	73462
468	512062	414919	73019
469	512536	414887	72577
470	513008	414854	72138
471	513479	414820	71701
472	513949	414784	71267
473	514418	414747	70835
474	514885	414709	70406
475	515351	414670	69979
476	515817	414630	69553
477	516280	414588	69132
478	516743	414545	68712
479	517205	414501	68294
480	517665	414456	67879
481	518124	414410	67466
482	518582	414362	67056
483	519039	414314	66647
484	519494	414264	66242
485	519949	414213	65838
486	520402	414161	65437
487	520854	414108	65038
488	521305	414054	64641
489	521754	413998	64248
490	522203	413942	63855
491	522650	413885	63465
492	523097	413826	63077
493	523542	413767	62691
494	523986	413706	62308

Table 1 (*continued*)

Mireds $(T\,°\text{K.})^{-1}\times 10^6$ $(C_2=14384{\cdot}8)$	Trichromatic coefficients		
	$x\times 10^6$	$y\times 10^6$	$z\times 10^6$
495	524428	413644	61928
496	524870	413582	61548
497	525310	413518	61172
498	525750	413453	60797
499	526188	413388	60424
500	526625	413321	60054
501	527061	413253	59686
502	527496	413185	59319
503	527929	413115	58956
504	528362	413044	58594
505	528793	412973	58234
506	529223	412900	57877
507	529652	412826	57522
508	530080	412752	57168
509	530507	412676	56817
510	530933	412600	56467
511	531358	412523	56119
512	531781	412444	55775
513	532204	412365	55431
514	532625	412285	55090
515	533045	412204	54751
516	533464	412122	54414
517	533882	412039	54079
518	534299	411956	53745
519	534715	411871	53414
520	535130	411786	53084
521	535544	411700	52756
522	535956	411613	52431
523	536368	411525	52107
524	536778	411437	51785
525	537187	411347	51466
526	537596	411257	51147
527	538003	411166	50831
528	538409	411074	50517
529	538814	410981	50205
530	539218	410888	49894
531	539621	410794	49585
532	540023	410699	49278
533	540424	410603	48973
534	540824	410507	48669
535	541223	410409	48368
536	541620	410311	48069
537	542017	410213	47770
538	542413	410113	47474
539	542807	410013	47180

Table 1 (*continued*)

Mireds $(T\ °\text{K.})^{-1}\times10^6$ $(C_2=14384\cdot8)$	Trichromatic coefficients		
	$x\times10^6$	$y\times10^6$	$z\times10^6$
540	543201	409912	46887
541	543594	409810	46596
542	543985	409708	46307
543	544376	409605	46019
544	544765	409501	45734
545	545154	409397	45449
546	545541	409292	45167
547	545928	409186	44886
548	546313	409080	44607
549	546698	408973	44329
550	547081	408865	44054
551	547463	408757	43780
552	547845	408647	43508
553	548225	408538	43237
554	548604	408427	42969
555	548983	408316	42701
556	549360	408205	42435
557	549737	408092	42171
558	550112	407980	41908
559	550487	407866	41647
560	550860	407752	41388
561	551233	407637	41130
562	551604	407522	40874
563	551975	407406	40619
564	552344	407290	40366
565	552713	407173	40114
566	553081	407056	39863
567	553447	406937	39616
568	553813	406819	39368
569	554178	406700	39122
570	554542	406580	38878
571	554905	406460	38635
572	555267	406339	38394
573	555628	406218	38154
574	555988	406096	37916
575	556348	405973	37679
576	556706	405850	37444
577	557063	405727	37210
578	557420	405603	36977
579	557775	405479	36746
580	558130	405354	36516
581	558484	405229	36287
582	558836	405103	36061
583	559188	404977	35835
584	559539	404850	35611

Table 1 (*continued*)

Mireds $(T°\text{K.})^{-1}\times 10^6$ $(C_2=14384\cdot 8)$	Trichromatic coefficients		
	$x\times 10^6$	$y\times 10^6$	$z\times 10^6$
585	559889	404723	35388
586	560239	404595	35166
587	560587	404467	34946
588	560934	404338	34728
589	561280	404209	34511
590	561626	404080	34294
591	561971	403950	34079
592	562314	403820	33866
593	562657	403689	33654
594	562999	403558	33443
595	563340	403426	33234
596	563680	403294	33026
597	564019	403162	32819
598	564358	403029	32613
599	564695	402896	32409
600	565032	402762	32206
601	565368	402628	32004
602	565703	402494	31803
603	566037	402359	31604
604	566370	402224	31406
605	566703	402088	31209
606	567035	401952	31013
607	567366	401816	30818
608	567696	401679	30625
609	568025	401542	30433
610	568353	401405	30242
611	568681	401267	30052
612	569007	401129	29864
613	569333	400991	29676
614	569658	400852	29490
615	569982	400713	29305
616	570306	400573	29121
617	570628	400433	28939
618	570950	400293	28757
619	571271	400153	28576
620	571591	400012	28397
621	571910	399871	28219
622	572229	399730	28041
623	572547	399588	27865
624	572863	399446	27691
625	573180	399304	27516
626	573495	399161	27344
627	573809	399018	27173
628	574123	398875	27002
629	574436	398732	26832

Table 1 (*contined*)

Mireds $(T\,^{\circ}\text{K.})^{-1}\times 10^6$ $(C_2=14384{\cdot}8)$	Trichromatic coefficients		
	$x\times 10^6$	$y\times 10^6$	$z\times 10^6$
630	574748	398588	26664
631	575059	398444	26497
632	575370	398300	26330
633	575680	398156	26164
634	575989	398011	26000
635	576297	397866	25837
636	576604	397721	25675
637	576911	397576	25513
638	577217	397430	25353
639	577522	397284	25194
640	577826	397138	25036
641	578130	396992	24878
642	578432	396845	24723
643	578734	396698	24568
644	579036	396551	24413
645	579336	396404	24260
646	579636	396256	24108
647	579935	396109	23956
648	580234	395961	23805
649	580531	395812	23657
650	580828	395664	23508
651	581124	395515	23361
652	581420	395367	23213
653	581714	395218	23068
654	582008	395068	22924
655	582301	394919	22780
656	582594	394769	22637
657	582886	394620	22494
658	583177	394470	22353
659	583467	394319	22214
660	583757	394169	22074

Table 2

Mireds $(T\,^{\circ}\text{K.})^{-1}\times 10^6$ $(C_2=14384{\cdot}8)$	Change in trichromatic coefficients if C_2 is altered from 14384·8 to 14320		
	$x\times 10^6$	$y\times 10^6$	$z\times 10^6$
0	− 0	− 0	+ 0
10	13	19	32
20	28	41	69
30	47	66	113
40	68	94	162

Table 2 (*continued*)

Mireds $(T\ ^{\circ}\mathrm{K.})^{-1}\times 10^6$ $(C_2=14384{\cdot}8)$	Change in trichromatic coefficients if C_2 is altered from 14384·8 to 14320.		
	$x\times 10^6$	$y\times 10^6$	$z\times 10^6$
50	− 92	−125	+217
60	119	157	276
70	148	191	339
80	179	225	404
90	213	260	473
100	248	294	542
110	285	326	611
120	323	357	680
130	362	386	748
140	401	413	814
150	441	436	877
160	480	458	938
170	519	475	994
180	558	489	1047
190	595	500	1095
200	632	508	1140
210	667	512	1179
220	701	513	1214
230	734	510	1244
240	765	505	1270
250	794	496	1290
260	821	485	1306
270	846	471	1317
280	870	454	1324
290	891	436	1327
300	911	415	1326
310	929	392	1321
320	944	368	1312
330	959	342	1301
340	971	315	1286
350	981	287	1268
360	990	258	1248
370	997	229	1226
380	1003	199	1202
390	1007	168	1175
400	1010	138	1148
410	1012	107	1119
420	1013	77	1090
430	1012	47	1059
440	1011	17	1028
450	−1009	+ 13	+996
460	1005	41	964
470	1002	69	933
480	997	96	901
490	992	123	869

Table 2 (*continued*)

Mireds $(T\ °\text{K.})^{-1}\times 10^6$ $(C_2=14384{\cdot}8)$	Change in trichromatic coefficients if C_2 is altered from 14384·8 to 14320		
	$x\times 10^6$	$y\times 10^6$	$z\times 10^6$
500	−986	−149	+ 837
510	980	174	806
520	973	198	775
530	966	221	745
540	959	244	715
550	952	266	686
560	944	286	658
570	936	306	630
580	928	325	603
590	920	343	577
600	912	360	552
610	904	377	527
620	896	392	504
630	888	407	481
640	880	421	459
650	871	434	437
660	863	447	416

Table 3

Mireds $(T\ °\text{K.})^{-1}\times 10^6$ $(C_2=14384{\cdot}8)$	Change in trichromatic coefficients if C_2 is altered from 14384·8 to 14350		
	$x\times 10^6$	$y\times 10^6$	$z\times 10^6$
0	− 0	− 0	+ 0
10	7	10	17
20	15	22	37
30	25	36	61
40	36	51	87
50	49	67	116
60	64	84	148
70	79	103	182
80	96	121	217
90	114	140	254
100	133	158	291
110	153	175	328
120	173	192	365
130	194	208	402
140	215	222	437

Table 3 (*continued*)

Mireds. $(T^{\circ}\text{K.})^{-1}\times 10^6$ $(C_2=14384{\cdot}8)$	Change in trichromatic coefficients if C_2 is altered from 14384·8 to 14350		
	$x\times 10^6$	$y\times 10^6$	$z\times 10^6$
150	−237	+234	+471
160	258	246	504
170	279	255	534
180	299	263	562
190	320	268	588
200	340	272	612
210	358	275	633
220	377	275	652
230	394	274	668
240	411	271	682
250	426	266	692
260	441	260	701
270	454	253	707
280	467	244	711
290	479	233	712
300	489	222	711
310	499	210	709
320	507	197	704
330	515	183	698
340	521	169	690
350	526	154	680
360	531	138	669
370	535	122	657
380	538	106	644
390	540	90	630
400	542	73	615
410	543	57	600
420	544	41	585
430	544	25	569
440	543	9	552
450	542	7	535
460	540	22	518
470	538	37	501
480	535	52	483
490	532	66	466
500	529	81	448
510	526	94	432
520	522	107	415
530	519	119	400
540	515	131	384
550	511	143	368
560	507	154	353
570	503	165	338
580	498	175	323
590	494	185	309

Table 3 (*continued*)

Mireds $(T\,°\mathrm{K.})^{-1}\times10^6$ $(C_2=14384{\cdot}8)$	Change in trichromatic coefficients if C_2 is altered from 14384·8 in 14350		
	$x\times10^6$	$y\times10^6$	$z\times10^6$
600	−489	+194	+295
610	485	202	283
620	481	211	270
630	476	219	257
640	472	226	246
650	467	233	234
660	463	240	223

HYSTERESIS AND EDDY LOSSES IN SINGLE CRYSTALS OF AN ALLOY OF IRON AND SILICON

By A. J. C. WILSON,
Cavendish Laboratory, Cambridge: now at University College, Cardiff

MS. received 23 *June* 1945

ABSTRACT. The total energy dissipated, in an alternating magnetic field, in single crystals of iron containing 2·1% silicon has been measured calorimetrically. Results are given for the field applied in the three crystallographic directions [100], [110], [111]. The total losses are separated into the conventional "hysteresis" and "eddy" components by means of measurements at different frequencies. The "eddy" losses do not appear to be dependent on direction; the "hysteresis" losses for [100] are about one-third of those for the other directions measured. A tentative explanation is suggested.

§1. INTRODUCTION

The calorimetric method is convenient for measuring the rate of continuous heat production, even when the rate is small. A striking application was the measurement of the energy of beta-disintegration of Radium E (Ellis and Wooster, 1928). Other examples of its use are the measurement of losses in dielectrics at radio frequencies (MacGregor Morris and Grisedale, 1939) and the study of the breakdown of dielectrics under high voltage (Whitehead and Nethercot, 1935). Bates and his co-workers have applied a calorimetric method to the somewhat different problem of the energy changes taking place in various parts of a single magnetic cycle (Bates and Weston, 1941; Bates and Healey, 1943).

In an investigation of electrical sheet steels undertaken at the Cavendish Laboratory for the Electrical Research Association, it was necessary to devise means for measuring energy losses in small samples of material (~5 grams). The normal methods require considerably more material, so the possibilities of using a calorimetric method were investigated. It has proved somewhat slow for routine use, but results have been obtained on single crystals magnetized in three important crystallographic directions.

The principle of the method is very simple. A thermocouple is enclosed in a pack of two or more sheets, and the increase in temperature caused by applying an alternating field for a known time is noted. The loss in ergs per gram per cycle is then given by

$$L=\frac{C\theta}{Mft}, \qquad \ldots\ldots (1)$$

where C is the heat capacity of the assembly in ergs per degree, θ is the temperature increase, t is the time of application of the field in seconds, M is the mass of the iron and f is the frequency. Two difficulties prevent the use of equation (1) in this simple form; first, the observed temperature increase is less than it should be because of heat losses during the time of application of the field, and secondly, the heat capacity of the assembly is doubtful, because of uncertainties in the heat capacity of Fe-Si alloys and lack of knowledge as to how much of the thermocouple leads and the surrounding air is effectively part of the assembly. It is therefore necessary to correct the observed temperature rise, and to calibrate the assembly by means of a small heating coil incorporated for the purpose. This calibration has the advantage that the thermocouple acts only as a transfer instrument, and it is unnecessary to know the factor for converting change in e.m.f. to change in temperature.

§ 2. APPARATUS, SPECIMEN AND MEASUREMENTS

The " calorimeter " was constructed so as to have as small a heat capacity as possible; it consisted merely of six junctions of a copper-constantan thermo-element, a 1-ohm constantan heating element, and a coil to measure the magnetic induction in the specimen. The junctions and the heating element were placed side by side, making a flat plate about 1 cm. square, and held in position with cotton thread and varnish. The coil was wound to a length of about 0·4 cm. on a rectangular former about 0·25 by 2·8 cm., varnished to prevent it from uncoiling, and then fixed to the thermocouple leads so that the junctions and heater were supported in the middle of it. There were thus two pockets, one on each side of the junctions and heater, into which the specimen to be investigated could be put.

The specimen consisted of four single-crystal discs of Fe-Si, cut from a single crystal about 7 cm. across. After the discs had been annealed at 1000°c. for half an hour, their orientation was found by means of back-reflection Laue photographs. It was found that [100] made an angle of $26° \pm 2°$ with the rolling direction, and that the plane of the sheet was within 6° of (011). The lattice parameter of a portion of the large crystal was 2·8581 kx. (2·8638 A.), corresponding to a silicon content of 2·1%. The average diameter of the discs was $2{\cdot}42_0$ cm., the measured total thickness $0{\cdot}15_9$ cm., and the total mass $5{\cdot}32_5$ g. The thickness calculated from the mass, density and diameter would be about $0{\cdot}15_1$ cm. A pair of the discs, separated by a sheet of thin paper to prevent electrical contact, was placed in each of the pockets mentioned above, and secured by tying with fine thread. The whole assembly was suspended in a Dewar flask and placed in a solenoid.

The flux-measuring coil was connected directly to a rectifier voltmeter whose resistance was high compared with that of the coil. It is easily shown that for an ideal rectifier the maximum flux linking the coil is given by

$$N=\frac{10^8E}{\sqrt{2}\pi f}, \qquad \ldots\ldots(2)$$

where E is the voltmeter reading, and that therefore

$$4\pi I'=\frac{10^8E}{\sqrt{2}\pi fnA}, \qquad \ldots\ldots(3)$$

where I' is the maximum magnetic intensity uncorrected for the field, n is the number of turns in the coil and A is the area of cross-section of the iron. The value of $4\pi I'$ needs correction for the actual magnetic field; the correction was zero within the limits of error for $4\pi I$ less than about 10000, and amounted to about 300 at $4\pi I=15000$. The apparent fields varied from 150 to 1000. The largest error in the corrected values of $4\pi I$ is uncertainty in what ought to be taken as the area of cross-section of the discs, since the measured thickness is about 5% greater than the calculated thickness. The measured thickness was used, so that the values of $4\pi I$ may all be low by 5%. In addition, there are individual errors due to the calibration of the voltmeter, uncertainty in the demagnetizing factor and the like. It is estimated that the values of $4\pi I$ are relatively correct within 3% and absolutely within 8%.

Before the assembly is heated, either by an alternating magnetic field or the heating coil incorporated, the temperature was nearly constant. During heating it rose almost linearly, and after heating fell fairly rapidly. The actual temperature rise was therefore somewhat less than that corresponding to the heat input, and a correction was made by extrapolating the initial and final portions of the temperature-time curve to the mid-point of the heating period. This was a simple straight-line extrapolation for the initial portion of the curve, but the fall was so steep in the final portion that analytical extrapolation had to be used. The fall was found to be exponential well within the limits of error, and a graphical method was devised for finding the constant of the curve rapidly. From observations of the temperature rise for a measured input to the heating element and the temperature rise produced by the magnetic field in a known time, the energy loss per magnetic cycle is easily calculated. The time of application of the field was usually 180 seconds. The largest errors in the losses so found would seem to be due to the extrapolation of the final portion of the time-temperature curve to the mid-point of the heating period. The percentage error produced depends somewhat on the temperature interval, increasing if it is made unduly small or unduly large. For most of the measurements it may be estimated at 3 to 4%. The error in the calibration measurements will of course affect all determinations of the energy loss in the same way, and so produce a systematic error, estimated at 2 to 3%. Other sources of error in the calorimetric measurements are small compared with these two; it is estimated, therefore, that the energy losses are relatively correct in general within 5% and absolutely within 8%.

§ 3. RESULTS

Measurements of the total loss per cycle were made with the applied field in the plane of the discs and having as nearly as possible the directions [100], [110], [111], at values of $4\pi I$ from about 5000 to 15000, and at three different frequencies. From these measurements values of the total loss at integral values of $4\pi I$ were interpolated. It was found convenient to use graphs of log (total loss) plotted against log ($4\pi I$), as such plots are nearly linear, whereas plots of total loss against $4\pi I$ are strongly curved. The interpolated values are given in table 1. A few values involving a slight extrapolation are also given in the table, but are distinguished by being enclosed in parentheses.

Table 1. Smoothed losses at integral values of $4\pi I$
(Extrapolated values are enclosed in parentheses)

		Loss, ergs per gram per cycle						
	$4\pi I$	3000	5000	7500	10000	12500	15000	17500
Direction	Frequency							
[100]	38	—	(41)	91	156	(240)	(340)	—
	50	17	46	103	181	280	406	586
	82	24	63	143	248	(380)	(540)	—
	121	—	81	180	316	496	787	(1150)
[110]	50	39	92	185	303	461	700	977
	81	—	(98)	210	359	578	916	(1480)
	145	57	145	302	510	809	1236	(1780)
[111]	50	31	87	197	358	537	741	(980)
	85	(34)	108	225	405	670	(1020)	—
	145	(48)	145	298	527	891	1390	(2040)

Table 2. "Hysteresis" loss and "eddy" loss at 50~
(Extrapolated values are enclosed in parentheses)

		Ergs per gram per cycle						
	$4\pi I$	3000	5000	7500	10000	12500	15000	17500
	Direction							
Hysteresis loss	[100]	6	20	48	79	120	140	(190)
	[110]	29	68	120	200	280	400	(480)
	[111]	(22)	55	140	270	350	390	(420 ?)
Eddy loss per cycle at 50~	[100]	11	26	55	100	160	270	(400)
	[110]	10	24	62	110	180	300	(500)
	[111]	(9)	32	57	90	180	350	(560 ?)
	Mean	10	27	58	100	170	310	—

The total loss per cycle for a given value of $4\pi I$ is, as is usually found, nearly a linear function of frequency. Several typical plots are shown in figure 1.

The loss extrapolated to zero frequency is conventionally attributed to hysteresis, and the linear increase with frequency to eddy currents. The losses separated in this way are given in table 2. The relative errors are estimated to be not more than 10%. It will be noticed that the "hysteresis" component varies markedly with crystallographic direction, being almost three times as great for [110] or [111] as for [100], while the "eddy" component is nearly independent of direction, at any rate for $4\pi I$ less than 13000.

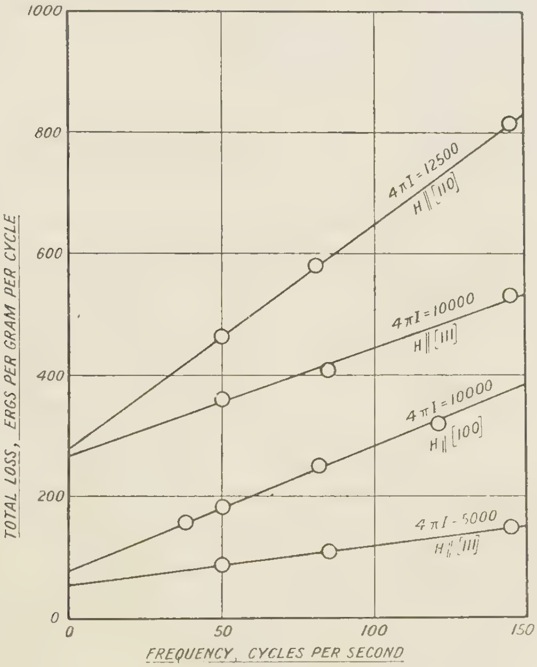

Figure 1. Extrapolation curves for hysteresis loss.

§4. DISCUSSION OF RESULTS

"*Eddy*" *losses*

It seems somewhat doubtful if the "eddy" component of the losses is due entirely to eddy currents. The heating due to this cause can be calculated with fair certainty; the theoretical formula for the loss per unit volume per second at low frequencies (flux density uniform throughout the sheet) is

$$W = \frac{\sigma b^2}{12 c^2} \overline{\left(\frac{\partial B}{\partial t}\right)^2}, \qquad \ldots\ldots(4)$$

where σ is the conductivity of the material, $\partial B/\partial t$ is time rate of change of the magnetic induction (the bar represents the time average over a complete cycle), b is the thickness of the sheet, and c is the speed of light. For a sinusoidal variation of B at 50~ this becomes

$$W = \frac{82 b^2 B^2_{\max}}{\rho\delta} \text{ ergs per gram per cycle}, \qquad \ldots\ldots(5)$$

where ρ is the resistivity of the sheet and δ its density, both in c.g.s. units. For the sheet used, $b=0{\cdot}040$ cm., $\rho \sim 35000$, $\delta \sim 7{\cdot}7$, so the loss at $B_{\max}=10000$ should be about 49 erg/gm. cycle. The observed value is 100 erg/gm. cycle, which is almost exactly twice as big. A discrepancy of this order is usually found in such comparisons (Brailsford, 1943), and has not yet been satisfactorily explained. In some cases it is due, at least in part, to non-sinusoidal variation of B, but it may also be necessary to postulate some magnetic viscosity effect. In the present experiments B was very nearly sinusoidal, since discs have a very large demagnetizing factor and the field in the absence of the specimen was sinusoidal.*

The "eddy" losses are very similar for the three directions, as is shown in figure 2. Up to $4\pi I \sim 12500$ they are identical within the estimated limits of error ; at 15000 they differ by scarcely more. The separation of "eddy" and "hysteresis" losses at 17500 is little better than guess-work, but it confirms the impression given by the losses at 15000 that at high inductions the "eddy" losses increase in the order $[100]<[110]<[111]$. It seems doubtful if eddy losses in the strict sense would behave in this way; magneto-resistance effects should not amount to more than a few tenths per cent. This is perhaps confirmatory of the hypothesis that "eddy" losses include magnetic viscosity effects dependent on the frequency as well as eddy losses proper, but Richer (1944) has advanced a theory which would suggest that eddy currents ought to depend on the direction of magnetization.

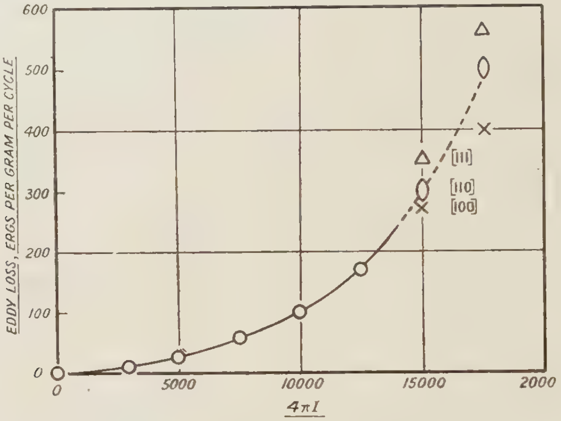

Figure 2. Eddy losses for the three directions at 50$\sim$. Up to $4\pi I=12500$ the losses are hardly separated on this scale.

"Hysteresis" losses

As has been seen, the losses in the [100] direction are much smaller than those in the [110] and [111] directions, in fact only about one-third as big. There is no great difference between the [110] and [111] directions ; [111] tends to be higher in the centre of the range, [110] at the ends. The following tentative discussion of the relation between the losses suggests itself. The argument is similar to that of Richer for eddy currents.

---

* The effect of a large demagnetizing factor is to reduce the actual field to a very small value, in such a way as to make the magnetic induction in the specimen very nearly proportional to the value of the field in the absence of the specimen.

The first step in magnetization along any non-[100] direction is to increase the number of domains whose [100] magnetization makes a small angle with the field direction, and decrease the number of domains whose [100] magnetization makes a large angle with the field direction. Now, all [100] directions are symmetrically placed with respect to [111], and one may therefore suppose that all [100] directions behave similarly, and, indeed, as they would behave if the field were in a [100] direction, except that it will be the component of the field in the [100] direction that is important. An externally measurable value of I in a [111] direction will then correspond to an actual internal value of I in the [100] directions that is $\sqrt{3}$ times as big. The curve of hysteresis loss against $4\pi I$ might therefore be expected to coincide with the similar curve for [100] if the values of $4\pi I$ are multiplied by $\sqrt{3}$. The postulated mechanism for magnetization in the [111] direction is almost certainly that predominant for values of the externally-measured $4\pi I$ less than about $1/\sqrt{3}$ of the saturation value, so that the relation between the [111] and the [100] losses should hold over the entire range for which the latter have been measured.

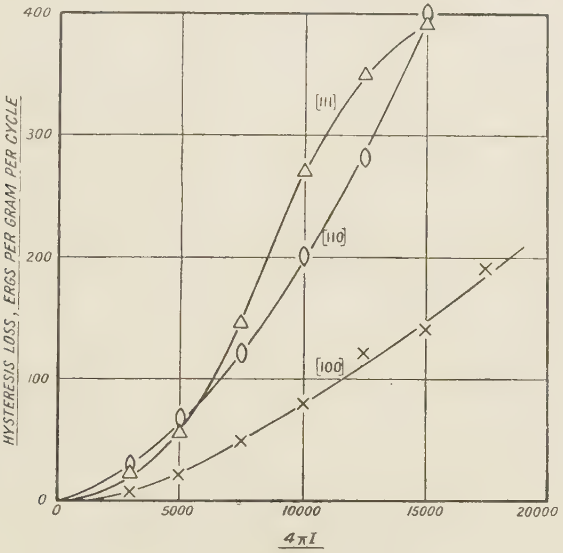

Figure 3. Hysteresis losses for the three directions.

The behaviour of the [110] direction is more difficult to predict. The [100] directions are not symmetrically placed with respect to [110] : two-thirds of them make angles of 45° (or 135°), one-third of them make angles of 90°. The assumption that immediately suggests itself is that the domains making angles of 90° with [110] make a 90° shift into one of the directions making angles of 45°. One might therefore expect that the curve of hysteresis loss againt $4\pi I$ would coincide with the similar curve for [100] if the values of $4\pi I$ are multiplied by $\sqrt{2}$. As in the case of [111], the relation should hold over the measured range of [100] losses.

In figure 3 the measured hysteresis losses are plotted against the externally measured value of $4\pi I$ for the three directions, and in figure 4 they are re-plotted with the co-ordinates treated as the foregoing argument suggests: [100] plotted without change (crosses), [110] plotted with the polarizations multiplied by $\sqrt{2}$ (ellipses with long axes vertical), [111] plotted with the polarizations multiplied by $\sqrt{3}$ (triangles). The vertical lines are of a length corresponding to errors of 10%. It will be seen that up to $4\pi I = 15000$ the curves for [111] and [100] agree within this amount.

The agreement is quite impressive, and may perhaps be taken as some confirmation of the not quite rigorous theoretical argument. On the other hand [110] shows no agreement at all, and this probably indicates that the assumption made about the behaviour of the domains making angles of 90° with the [110] direction is erroneous. Qualitatively one may say that these domains are less effective in increasing the polarization than if they behaved as assumed. By what is probably no more than a curious coincidence, the assumption of the opposite extreme (that these domains are entirely ineffective) gives good quantitative agreement. On this assumption one would have two-thirds of the iron magnetized to an intensity of $(3/2)\sqrt{2}$ times the externally measured intensity, and the curve of hysteresis loss against $4\pi I$ should coincide with that for [100] if the losses are multiplied by 3/2 and the values of $4\pi I$ by $3/\sqrt{2}$. The [110] losses treated in this way are also plotted in the figure (ellipses with long axes horizontal), and it will be seen that they agree well with those for [100] and [111].

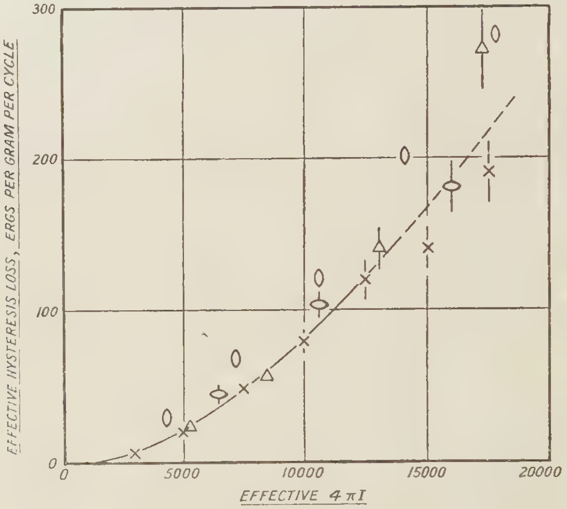

Figure 4. Comparable hysteresis losses for the three directions. For explanation of the points see text.

This explanation of the apparently anomalous behaviour of the [110] losses is confirmed by the tendency, postulated by Becker and Döring (1939), for the domains whose directions of magnetization lie nearly in the plane of the sheet to be favoured at the expense of those whose directions of magnetization make large angles with the plane of the sheet. In the present case domains effective for the [100] measurements have their directions in the plane of the sheet, whereas those effective for the [110] measurements have their directions of magnetization at 45° to the plane of the sheet. This explanation might be regarded as qualitatively satisfactory, but the fraction one-third would be the result of coincidence. A little consideration shows that the [111] losses would not be affected if the greater part of, or even all, the domains had their direction of magnetization in the plane of the sheet. Richer (private communication), however, has suggested that the apparently anomalous behaviour of the [110] losses might be explained by a non-isotropic distribution of interstitial impurities set up in the process of rolling the sheet.

ACKNOWLEDGMENTS

This work forms part of a programme sponsored by the British Electrical and Allied Industries Research Association, to whom the author is indebted for permission to publish. It has been carried out under the direction first of Dr. J. T. Randall and then of Dr. D. Shoenberg. The sheet from which the single-crystal discs were cut was provided through the kindness of Mr. G. C. Richer of Messrs. J. Lysaght, Ltd., and the determination of their orientation and lattice parameter was done by Mrs. L. E. R. Rogers.

REFERENCES

Bates, L. F. and Healey, D. R., 1943. *Proc. Phys. Soc.* **55**, 188–202.
Bates, L. F. and Weston, J. C., 1941. *Proc. Phys. Soc.* **53**, 5–34.
Becker, R. and Döring, W., 1939. *Ferromagnetismus*, p. 153.
Brailsford, F., 1943. *J. Instn. Elect. Engrs.* **90**, 307.
Ellis, C. D. and Wooster, W. A., 1928. *Proc. Roy. Soc.* A, **117**, 109.
MacGregor Morris, J. T. and Grisedale, G. L., 1939. *Phil. Mag.* **28**, 34–63.
Richer, G. C., 1944. *Report* T.C. 31 of Lysaght-Sankey Technical and Research Committee.
Whitehead, S. and Nethercot, W., 1934. *Proc. Phys. Soc.* **47**, 974.

COMPLETE COMPUTATION OF ELECTRON OPTICAL SYSTEMS

By H. MOTZ and LAURA KLANFER,
Engineering Laboratory, Oxford

MS. received 5 *April* 1945

ABSTRACT. This paper shows how electron-optical systems can be completely calculated, without appeal to model experiments, by methods capable of great accuracy.

The computation method is a numerical one. It is explained with reference to the example of an electrostatic lens consisting of two cylinders with diameter ratio 1·5. The electric potential and the field are found by relaxation methods.

Electron paths for paraxial and non-paraxial electrons are computed by means of a step-by-step integration method which allows a close check on accuracy. The position of focal and cardinal points and the spherical aberration of the lens are found to be in fair agreement with experimental and semi-empirical determinations by other authors.

§1. INTRODUCTION

The theoretical treatment of any electron-optical system proceeds in two steps : calculation of the electric or magnetic field of the focusing system and determination of the path of charged particles in these fields. In some cases analytic expressions for the fields are known, but in the majority of arrangements in practical use this is not the case. It is then usual to determine the field by experiment, either with the help of an electrolytic tank or by other means.

When analytic expressions for the field are known, the second step, path determination, can sometimes be carried out analytically. Again, in most cases this is not possible, and approximation methods have to be used. In a recent paper L. S. Goddard (1944) has given a summary of path-tracing methods. In that paper a step-by-step method of path computation is proposed which is used by Klemperer and Goddard (1944) for treatment of a magnetic lens. L. J. Comrie pointed out in the discussion that other step-by-step methods may be preferable. Goddard also indicates that the relaxation method may be used for the first step, the field computation.

We have been using both the relaxation method and a step-by-step method proposed by L. J. Comrie during the last few years for electron-optical calculations, and it will be shown in this paper that a complete numerical computation of electron-optical systems, without appeal to experiment, is practicable.

An electrostatic lens will be taken as an example, and the agreement of the result of the determination of focal length with the results of other authors will be discussed.

The methods used are, *mutatis mutandis*, equally applicable to axially symmetrical magnetic focusing systems. Even saturation effects in ironclad coils can be taken into account. A discussion of magnetic field computation will shortly appear in the *Journal of the Institution of Electrical Engineers*, where the application of the relaxation method to potential problems will be fully explained.

§ 2. THE FINITE-DIFFERENCE METHOD OF FIELD CALCULATION

For the purpose of the field determination, Laplace's equation,

$$\frac{\partial^2\phi}{\partial r^2}+\frac{1}{r}\frac{\partial\phi}{\partial r}+\frac{\partial^2\phi}{\partial z^2}=0, \qquad \ldots\ldots(1)$$

for the potential ϕ has to be solved with certain boundary conditions. For this equation a system of difference equations for the values of ϕ at points of a net of small but finite mesh length is substituted. The choice of the net depends on the shape of the boundary. In the present paper a study is made of an electrostatic lens, consisting of two semi-infinite cylinders placed end to end and separated by a finite gap. The cylinders as shown in figure 1 have diameters D_1 and D_2, with $D_2/D_1=1{\cdot}5$, and their potentials are 200 v. and 1200 v. respectively. This choice fixes the boundary conditions. The voltage ratio is thus $V_2/V_1=6$, but when a solution is found for this ratio, a solution for any other voltage ratio can be obtained quite simply (see Maloff and Epstein, 1938, p. 102). Three quadratic nets of successively finer mesh length are shown in figure 3. Consider at first the coarsest net, of mesh-length a. At any point P of this net the potential ϕ can be expressed in terms of the potentials ϕ_{Q}, ϕ_{R}, ϕ_{S}, ϕ_{T} of the four neighbouring mesh points, Q, R, S, T, figure 2. It can be seen, with the help of an expansion in Taylor series of the potential at these points, that

$$\phi_{\mathrm{Q}}\left(1-\frac{1}{2\rho_{\mathrm{P}}}\right)+\phi_{\mathrm{S}}\left(1+\frac{1}{2\rho_{\mathrm{P}}}\right)+\phi_{\mathrm{R}}+\phi_{\mathrm{T}}-4\phi_{\mathrm{P}}=0, \qquad \ldots\ldots(2)$$

where $\rho=r/a$ and $\rho_{\mathrm{P}}=r_{\mathrm{P}}/a$, so that r_{P} is the radial distance of point P from the axis. If there are n mesh points, excluding points on the boundary where $\phi=$ const., n simultaneous equations have to be satisfied. Owing to the symmetry of the figure, the equations on both sides of the axis are the same, so that only one-half of figure 1 is used for the computation.

A solution of these equations can be found by various methods, e.g. the Gauss-Doolittle elimination method or R. V. Southwell's relaxation method (Christopherson and Southwell, 1938). We have used the latter method, which we prefer because it is self-checking in so far as mistakes made at some stage of the calculation are corrected later with little loss of time and effort. At any stage of the process, the residuals

$$\phi_{\mathrm{Q}}\left(1-\frac{1}{2\rho_{\mathrm{P}}}\right)+\phi_{\mathrm{S}}\left(1+\frac{1}{2\rho_{\mathrm{P}}}\right)+\phi_{\mathrm{R}}+\phi_{\mathrm{T}}-4\rho_{\mathrm{P}}=\delta_{\mathrm{P}} \qquad \ldots\ldots(3)$$

are found and reduced in successive steps until they are negligible. A further description of the process is given in a forthcoming paper by Motz and Worthy in the *Journal of the Institution of Electrical Engineers*.

At the end a further test should be applied. The system of finite-difference equations (2) is accurate only to the second order in a, and we are only justified in using it when ϕ does not change rapidly in the neighbourhood of any mesh-point. It is possible to locate points or regions where second-order approximation is not good enough by forming the higher differences of ϕ in rows and

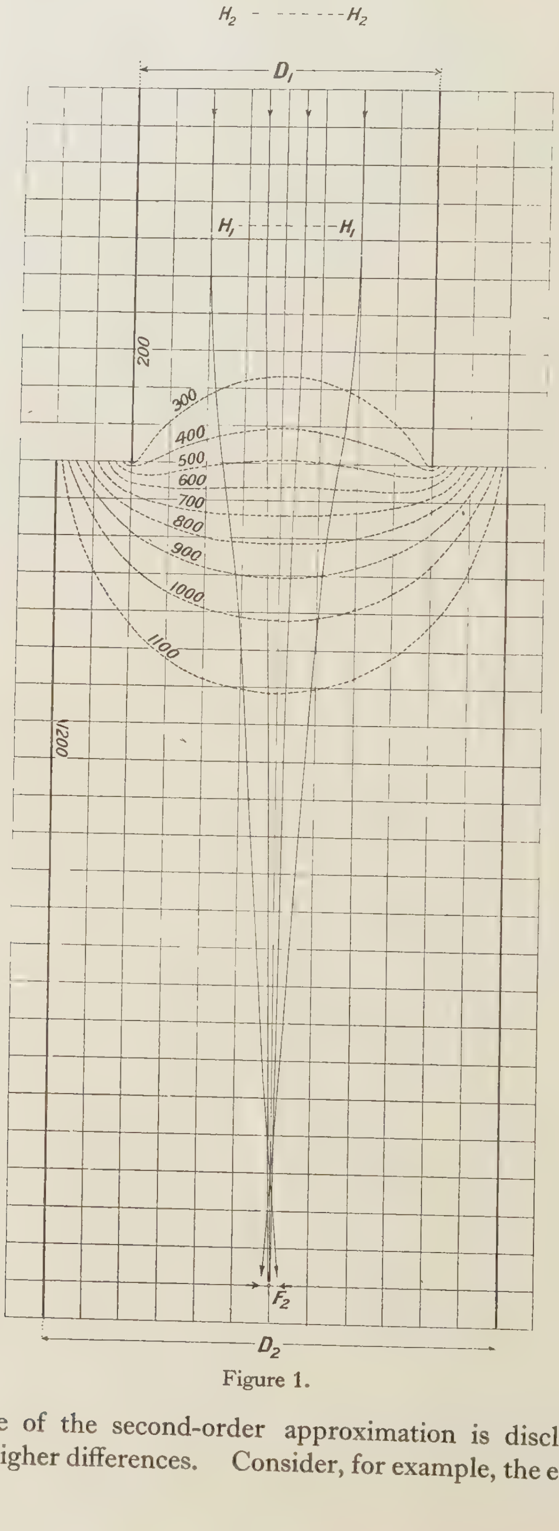

Figure 1.

columns. Failure of the second-order approximation is disclosed by erratic behaviour of the higher differences. Consider, for example, the effect of a change of ϕ at one mesh point by ± 1 on the higher differences. If the fourth differences fluctuate by an amount larger than the one which would be produced by errors of ± 1 in the last significant figure of the result, it must be concluded that this

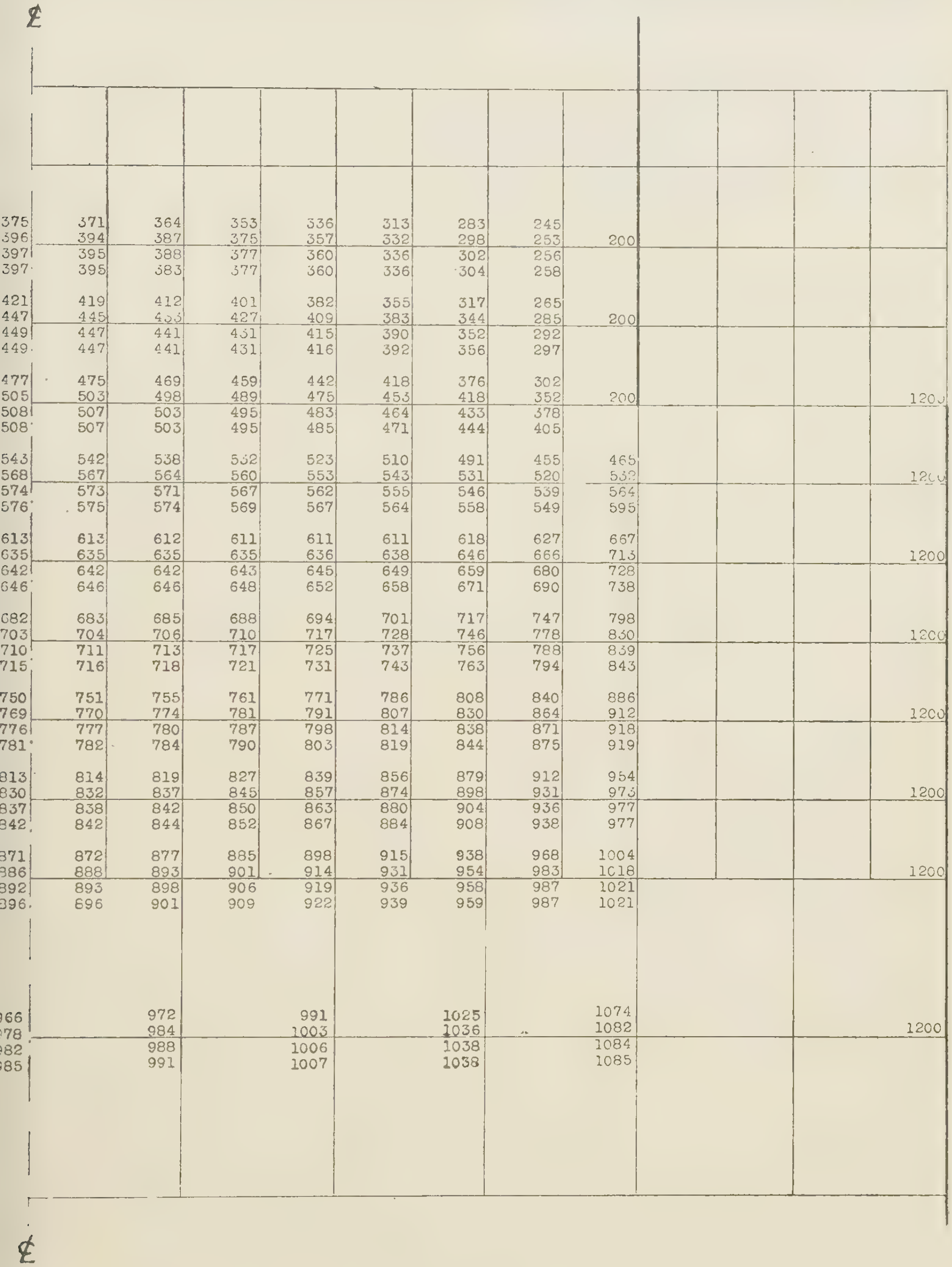

375	371	364	353	336	313	283	245		
396	394	387	375	357	332	298	253	200	
397	395	388	377	360	336	302	256		
397	395	383	377	360	336	304	258		
421	419	412	401	382	355	317	265		
447	445	433	427	409	383	344	285	200	
449	447	441	431	415	390	352	292		
449	447	441	431	416	392	356	297		
477	475	469	459	442	418	376	302		
505	503	498	489	475	453	418	352	200	1200
508	507	503	495	483	464	433	378		
508	507	503	495	485	471	444	405		
543	542	538	532	523	510	491	455	465	
568	567	564	560	553	543	531	520	532	1200
574	573	571	567	562	555	546	539	564	
576	575	574	569	567	564	558	549	595	
613	613	612	611	611	611	618	627	667	
635	635	635	635	636	638	646	666	713	1200
642	642	642	643	645	649	659	680	728	
646	646	646	648	652	658	671	690	738	
682	683	685	688	694	701	717	747	798	
703	704	706	710	717	728	746	778	830	1200
710	711	713	717	725	737	756	788	839	
715	716	718	721	731	743	763	794	843	
750	751	755	761	771	786	808	840	886	
769	770	774	781	791	807	830	864	912	1200
776	777	780	787	798	814	838	871	918	
781	782	784	790	803	819	844	875	919	
813	814	819	827	839	856	879	912	954	
830	832	837	845	857	874	898	931	973	1200
837	838	842	850	863	880	904	936	977	
842	842	844	852	867	884	908	938	977	
871	872	877	885	898	915	938	968	1004	
886	888	893	901	914	931	954	983	1018	1200
892	893	898	906	919	936	958	987	1021	
896	696	901	909	922	939	959	987	1021	
66		972		991		1025		1074	
78		984		1003		1036		1082	1200
82		988		1006		1038		1084	
85		991		1007		1038		1085	

Figure 2.

figure is uncertain by more than ± 1. Difference formulae, of higher than second-order accuracy, may then be used, or the net may be subdivided.

It is clear that the cylinder edges, figure 1, are singularities for ϕ, and it can be shown that near them ϕ varies as the square root of the distance from the edge. Hence in the neighbourhood of sharp edges, the higher-order residuals cannot be neglected. Methods for dealing with this singularity have been evolved which are based on the behaviour of the potential near the singularity, but in this paper the simplest expedient has been used. It consists in the use of two successive finer nets as shown in figure 1. When the net is subdivided in a particular region, the computation is carried on in alternative steps (i) and (ii).

(i) Values of the potential at fine mesh points on the boundary between the fine and coarse net region are found by interpolation. ϕ-values on this boundary are then kept constant and, with these values, ϕ is found at points of the fine-mesh region by the relaxation process. Some of those points belong also to the coarse net.

(ii) ϕ-values at these latter points are next kept constant and new ϕ-values in the coarse net are found. The fine-net values are redetermined according to (i), etc., until the process converges. The result of the computation with the coarse, medium and finest net are retained. Figure 2 shows the middle region of figure 1 with the medium net. The three successive ϕ-values are recorded and the fourth figure is found by parabolic extrapolation to mesh-length zero. At points not too near the edges the convergence is good. The extrapolation has only been carried out in a region where electron paths have been computed. In any practical focusing system the wall thickness of cylinders is finite. The mesh length of the finest net should be of the order of the radius of curvature of the edge. It will be seen later that the focal lengths of a lens with a wall thickness given by our finest net differ insignificantly from those of an ideal lens having cylinder walls of zero thickness.

§ 3. TREATMENT OF THE REGION OUTSIDE THE CYLINDERS

In any practical system, electrostatic shields will be found outside the focusing electrodes. We shall later compare the results of our path computation with those given by Maloff and Epstein (1938) and by Spangenberg and Field (1943). Neither of these papers gives information about shielding, and we have, therefore, not included a shield. To treat the infinite space outside, we have carried out an inversion with respect to a cylinder of radius $r_0 = 9a$. A new variable, $s = r_0/r$, is introduced.

Equation (1) becomes

$$\frac{\partial^2 \phi}{\partial z^2} + \frac{s^4}{r_0^{\,2}} \frac{\partial^2 \phi}{\partial s^2} + \frac{s^3}{r_0^{\,2}} \frac{\partial \phi}{\partial s} = 0. \qquad \ldots\ldots.(4)$$

The mesh length b of the s-net outside the inversion cylinder was taken as $b = \frac{1}{4}$ (s is non-dimensional).

Corresponding values are then :

$s =$	0	$\frac{1}{4}$	$\frac{1}{2}$	$\frac{3}{4}$	1
$r =$	∞	$36a$	$18a$	$12a$	$9a$

The cylinders are long, but finite, compared with D_1 and D_2. At large distances, the field due to the cylinders will behave as a dipole field. Thus at $r = \infty$, $\phi = 0$. The effect of the end charges of the cylinders is neglected, but it is clear that these

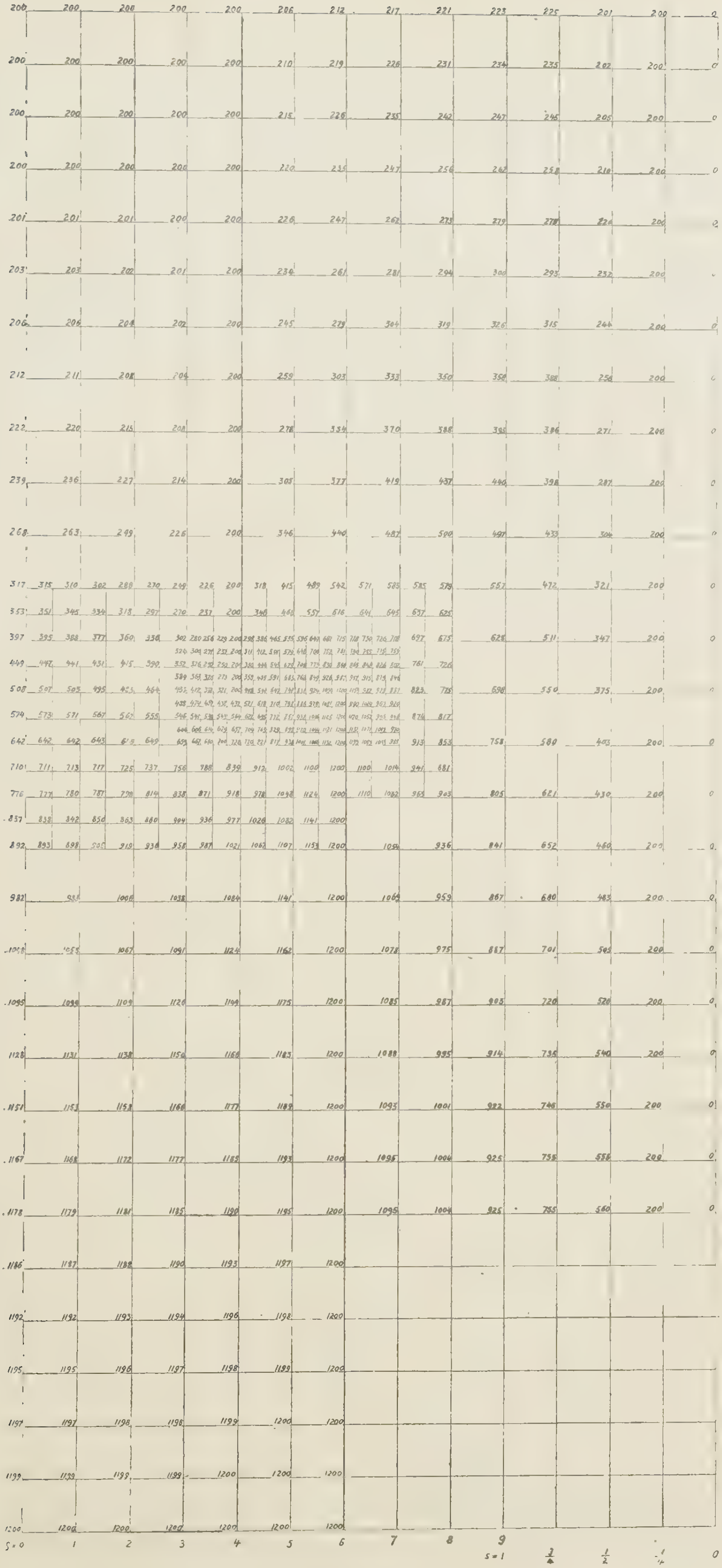
200 200 200 200 200 206 212 217 221 223 225 201 200 0
200 200 200 200 200 210 219 226 231 234 235 202 200 0
200 200 200 200 200 215 228 235 242 247 245 205 200 0
200 200 200 200 200 220 235 247 256 263 258 210 200 0
201 201 201 200 200 226 247 262 273 279 278 224 200 0
203 203 202 201 200 234 261 281 294 300 293 232 200
206 205 204 202 200 245 278 304 319 326 315 244 200 0
212 211 208 204 200 259 303 333 350 358 388 258 200
222 220 215 208 200 278 334 370 388 395 386 271 200 0
239 236 227 214 200 305 377 419 437 440 398 287 200 0
268 263 249 226 200 346 440 487 500 497 435 304 200
317 315 310 302 288 270 249 226 200 318 415 489 542 571 585 585 579 557 472 321 200 0
353 351 345 334 318 297 270 237 200 348 468 557 616 641 645 637 625
397 395 388 377 360 338 697 675 628 511 347 200 0
449 447 441 431 415 390 761 726
508 507 503 495 483 464 823 775 698 550 375 200
574 573 571 567 562 555 874 817
642 642 642 643 645 649 913 853 758 580 403 200 0
710 711 713 717 725 737 756 788 839 912 1002 1100 1200 1100 1014 941 881
776 777 780 787 798 814 838 871 918 978 1048 1124 1200 1110 1032 965 903 805 621 430 200 0
837 838 842 850 863 880 904 936 977 1028 1082 1141 1200
892 893 898 905 919 938 958 987 1021 1062 1107 1153 1200 1054 936 841 652 460 200 0
982 985 1006 1038 1084 1141 1200 1069 959 867 680 483 200 0
1048 1055 1067 1091 1124 1162 1200 1078 975 887 701 505 200 0
1095 1099 1109 1126 1149 1175 1200 1085 987 903 720 526 200 0
1128 1131 1138 1150 1166 1183 1200 1088 995 914 735 540 200 0
1151 1153 1158 1166 1177 1189 1200 1093 1001 922 746 550 200 0
1167 1168 1172 1177 1185 1193 1200 1095 1004 925 755 556 200 0
1178 1179 1181 1185 1190 1195 1200 1095 1004 925 755 560 200 0
1186 1187 1188 1190 1193 1197 1200
1192 1192 1193 1194 1196 1198 1200
1195 1195 1196 1197 1198 1199 1200
1197 1197 1198 1198 1199 1200 1200
1199 1199 1199 1199 1200 1200 1200
1200 1200 1200 1200 1200 1200 1200
S=0 1 2 3 4 5 6 7 8 9
S=1 3/4 1/2 1/4 0

Figure 3.

effects must cancel at radial distances small compared with the length of the cylinders where we wish the potential to be accurately determined.*

The finite-difference equations corresponding to (4) become

$$\left(\frac{16}{81}\rho_P{}^4-\frac{2}{81}\rho_P{}^3\right)\phi_Q+\left(\frac{16}{81}\rho_P{}^4+\frac{2}{81}\rho_P{}^3\right)\phi_S+\phi_R+\phi_T-\left(\frac{32}{81}\rho_P{}^4+2\right)\phi_P=0. \qquad \ldots\ldots(5)$$

There is a slight ambiguity on the line $r=9a$, where (2) or (5) may be used. Both (2) and (5) are difference equivalents of (1), and we have used the mean of the coefficients of these equations. The result of the potential calculations is shown in figure 3.

§ 4. DETERMINATION OF THE PATH

Two paraxial electron paths have been computed and one non-paraxial one. In figure 1 one paraxial path is seen entering the smaller cylinder at $r=D_1/16$. Another path entering the larger cylinder in a direction parallel to the axis at the same radial distance has also been computed. These two paths determine focal length and principal planes. The non-paraxial path gives a measure of the spherical aberration in the forward direction accelerating lens.

The equation for the path of a negatively charged particle is

$$\frac{d^2r}{dz^2}+\frac{\partial V}{dz}\,\frac{\left[1+\left(\frac{dr}{dz}\right)^2\right]\frac{dr}{dz}}{2V}-\frac{1}{2V}\frac{\partial V}{\partial r}\left[1+\left(\frac{dr}{dz}\right)^2\right]=0. \qquad \ldots\ldots(6)$$

The method of path computation is based on a process suggested by L. J. Comrie in *Interpolation and Allied Tables* (1936).

Define

$$F=4\frac{d^2\rho}{d\zeta^2} \qquad f=2\frac{d\rho}{d\zeta},$$

where $\rho=r/a$, $\zeta=z/a$, and use steps

$$\rho_{n+1}-\rho_n=z_{n+1}-z_n=a.$$

Equation (6) can be written

$$F=-\frac{\partial V}{\partial z}\,\frac{\left(1+\frac{f^2}{4}\right)}{V}f+2\frac{\partial V}{\partial r}\,\frac{\left(1+\frac{f^2}{4}\right)}{V}. \qquad \ldots\ldots(7)$$

The procedure consists in computing entries of the following table :—

Table 1

z/a	ρ	d'	d''	d'''	f	F	Δ'	Δ''
0	ρ_0		d_0''		f_0	F_0		Δ_0''
		$d_{1/2}'$		$d_{1/2}'''$			$\Delta_{1/2}'$	
1	ρ_1		d_1''		f_1	F_1		Δ_1''
		$d_{3/2}'$		$d_{3/2}'''$			$\Delta_{3/2}'$	
2	ρ_2		d_2''		f_2	F_2		Δ_2''
		$d_{5/2}'$		$d_{5/2}'''$			$\Delta_{5/2}'$	
3	ρ_3		d_3''		f_3	F_3		
.		.		.				
.			.		.			

---

* Alternatively one might interpret the field as due to infinite cylinders and a zero potential field at infinity.

where d', d'', d''' are successive central differences of ρ, and Δ', Δ'', Δ''', . . . are successive central differences of F.

Assume ρ_0, ρ_1, ρ_2 known; in our example

$$\rho_0 = \rho_1 = \rho_2 = D_1/16.$$

Calculate f_0, f_1, f_2 from, for example,

$$f_1 = \left(2d_1'\right) - \frac{1}{6}\left(2d_1'''\right) + \frac{1}{30}\left(2d_1^{(V)}\right) - \dots \qquad \dots\dots (8)$$

and F_0, F_1, F_2 from equation (7) and difference. Δ_1'' is already found in this way, but not Δ_2''.

$$\frac{1}{V}\frac{\partial\phi}{\partial z}, \quad \frac{1}{V}\frac{\partial\phi}{\partial r} \qquad \dots\dots (9)$$

are taken from the field plot, figure 3. (Tables of these values are prepared beforehand so that appropriate values of (9) can be interpolated for each value of ρ. For interpolation we use a four-point formula (Comrie, 1936, p. 685)).

From now on the following steps are carried out:

(i) Estimate Δ_2'', e.g. take $\Delta_2'' = \Delta_1''$ and calculate d_2'' from

$$d_2'' = \frac{1}{4}\left(F_2 + \frac{1}{12}\Delta_2'' - \frac{1}{240}\Delta_2^{(iv)} + \dots\right). \qquad \dots\dots (10)$$

(ii) Form ρ_3 by building up from d_2''.

(iii) Verify by calculating f_1 from (8) and, if necessary, make a correction.

(iv) Now extrapolate $f_3 = f_1 + F_2 + \frac{1}{6}\Delta_2'' - \frac{1}{180}\Delta_2^{(iv)} + \dots$ $\qquad \dots\dots (11)$

(v) Compute F_3 and difference;

(vi) Verify that correct value of d_2'' has been used in (ii); correct if necessary.

The steps of z used in the path computation are conveniently chosen so that $\frac{1}{48}$ of Δ_2'' is not larger than a few units of the last decimal figure of F which is retained during computation. It should be assumed that one significant figure is lost in about ten steps of the integration. It is therefore necessary, if absolute certainty of the result is desired, to retain during the computation more decimal figures than the final accuracy claimed for the path warrants.

If, in our table 2, the last figure of F is uncertain by ± 1, then the r might, in any step, acquire an error of one-third of the last figure retained. There are 30 steps; the errors accumulate in arithmetic progression so that, if all the errors are in the same direction, the final result may be in error by 0·150 and the position of the focal points in error by two mesh lengths (cf. the end of the path given in table 2). Now it is very unlikely that all the errors are in fact in the same direction, and we estimate that the error is less than one mesh length.

The process outlined above leads to table 2 for the paraxial path shown in figure 1. We have found it convenient to use the steps of the relaxation net for the path computation. Thus the first eight steps are carried out in the coarsest net. To start the path in the middle region medium net, two values of ρ are interpolated at mid-points of the last two steps. The last part, again in the coarse net, is started by selecting the last three values of ρ belonging to the coarse net in the middle region. At the end the path is a straight line and the first differences are 0·147. The point of intersection is found by interpolation. The paraxial path was first determined in the coarse net throughout, and F_2, the distance of the focal

Table 2

ζ	ρ	d'	d''	d'''	f	F	Δ'	Δ''
−10	0·500		0·000		0·000	0·000		
		0·000		0·000			0·000	
− 9	0·500		−0·001		−0·001	0·000		−0·002
		−0·001		0·000			−0·002	
− 8	0·499		0·000		−0·002	−0·002		−0·001
		−0·001		−0·001			−0·003	
− 7	0·498		−0·001		−0·003	−0·005		−0·002
		−0·002		0·000			−0·005	
− 6	0·496		−0·002		−0·006	−0·010		0·000
		−0·004		−0·001			−0·005	
− 5	0·492		−0·004		−0·012	−0·015		−0·003
		−0·008		−0·002			−0·008	
− 4	0·484		−0·006		−0·021	−0·023		−0·001
		−0·014		−0·001			−0·006	
− 3	0·470		−0·007		−0·035	−0·029		+0·004
		−0·021		−0·001			−0·002	
− 2	0·449		−0·006		−0·048	−0·031		+0·009
		−0·027		0·000			+0·007	
− 1	0·422		−0·006		−0·061	−0·024		+0·015
		−0·033		+0·006			+0·022	
0	0·389		0·000		−0·067	+0·002		−0·010
		−0·033		+0·004			+0·012	
+ 1	0·356		+0·004		−0·063	+0·014		−0·012
		−0·029		−0·001			0·000	
+ 2	0·327		+0·003		−0·055	+0·014		0·000
		−0·026		+0·001			0·000	
+ 3	0·301		+0·004		−0·048	+0·014		+0·004
		−0·022		−0·002			+0·004	
+ 4	0·279		+0·002		−0·042	+0·009		−0·002
		−0·020		0·000			−0·002	
+ 5	0·259		+0·002		−0·038	+0·007		+0·001
		−0·018		−0·001			−0·003	
+ 6	0·241		+0·001		−0·035	+0·004		+0·002
		−0·017		0·000			−0·001	
+ 7	0·224		+0·001		−0·034	+0·003		0·000
		−0·016		0·000			−0·001	
+ 8	0·208		+0·0005		−0·032	+0·002		0·000
		−0·0155		0·000			−0·001	
+ 9	0·1925		+0·0003		−0·031	+0·0012		+0·001
		−0·0152		0·000			0·000	
+10	0·1773		+0·0002		−0·030	+0·0007		0·000
		−0·0150		0·000			0·000	
+11	0·1623		+0·0001		−0·030	+0·0005		0·000
		−0·0149		0·000			0·000	
+12	0·1474		+0·0001		−0·030	+0·0002		0·000
		−0·0148		0·000			0·000	
+13	0·1326		0·0000		−0·030	+0·0002		0·000
		−0·0148		0·000			0·000	
+14	0·1178		−0·0001		−0·030	+0·0002		0·000
		−0·0147 etc.						

Table 2—*continued*

Medium region computed in half-intervals

2ζ	2ρ	d'	d''	d'''	f	F	Δ'	Δ''
−7	0·956		−0·000		−0·028	−0·013	interpolated	
		−0·016		−0·000			−0·002	
−6	0·940		−0·004		−0·036	−0·015		+0·001
		−0·020		+0·002			−0·001	
−5	0·920		−0·002		−0·042	−0·016	interpolated	+0·001
		−0·022		−0·002			0·000	
−4	0·898		−0·004		−0·048	−0·016		+0·003
		−0·026		+0·001			+0·003	
−3	0·872		−0·003		−0·055	−0·013		−0·002
		−0·029		0·000			+0·001	
−2	0·843		−0·003		−0·061	−0·012		+0·005
		−0·032		+0·001			+0·006	
−1	0·811		−0·002		−0·067	−0·006		+0·001
		−0·034		+0·002			+0·007	
0	0·777		0·000		−0·069	+0·001		−0·002
		−0·034		+0·002			+0·005	
+1	0·743		+0·002		−0·066	+0·006		−0·004
		−0·032		0·000			+0·001	
+2	0·711		+0·002		−0·062	+0·007	end path start	0·000
		−0·030		0·000			+0·001	
+3	0·681		+0·002		−0·058	+0·008		−0·002
		−0·028		0·000			−0·001	
+4	0·653		+0·002		−0·054	+0·007	end path	0·000
		−0·026		−0·001			−0·002	
+5	0·627		+0·001		−0·051	+0·005		
		−0·025						
+6	0·602				−0·049		end path	

point from the cylinder junction, was $F_2 = +15$. Then it was redetermined with the more exact figures of the medium net, and finally again with the best extrapolated figures; the last two results for F_2 were the same, although the paths were slightly different, and we therefore considered our result as the final answer. The distances of the focal planes F_1, F_2 and the cardinal planes H_1, H_2, from the plane through the cylinder junction, are given in table 3.

§ 5. COMPARISON WITH THE RESULTS OF OTHER AUTHORS

Maloff and Epstein (1938) on p. 105 give data for a lens similar to the one computed in this paper with $D_2/D_1 = 1{\cdot}5$, $V_2/V_1 = 6$.

There is no precise information in the book concerning the method by which these results were obtained. In particular, no details are given about position and potential of shielding electrodes outside the lens either in the electrolytic trough experiments determining the field or in the experimental verification of focal length, etc., given on p. 114. It is, however, likely that one grounded shield was used. The wall thickness of the cylinders is not stated. All these data are also omitted by Spangenberg and Field (1942), p. 195, who give a chart for a similar lens with the same parameters. It must be concluded from the nature of the experimental arrangement that two shields at different potentials were used. The results taken from these papers are summarized in table 3.

It is difficult to say how much of the disagreement is due to the difference in shielding and wall thickness in the three cases. It will be seen that the distances between focal points agree wthin one mesh length, and this is within the accuracy of our calculation. In our result the whole system of principal planes and focal planes seems to be shifted bodily by about three mesh lengths towards the high-potential electrode.

Table 3

	F_1	F_2	H_1	H_2
Maloff and Epstein	−21·6	20	−8·8	−13·2
Spangenberg and Field	−21·68	18·11		
Our result : Paraxial	−18·56	22	−6·37	−12·01
Non-paraxial		19·25		

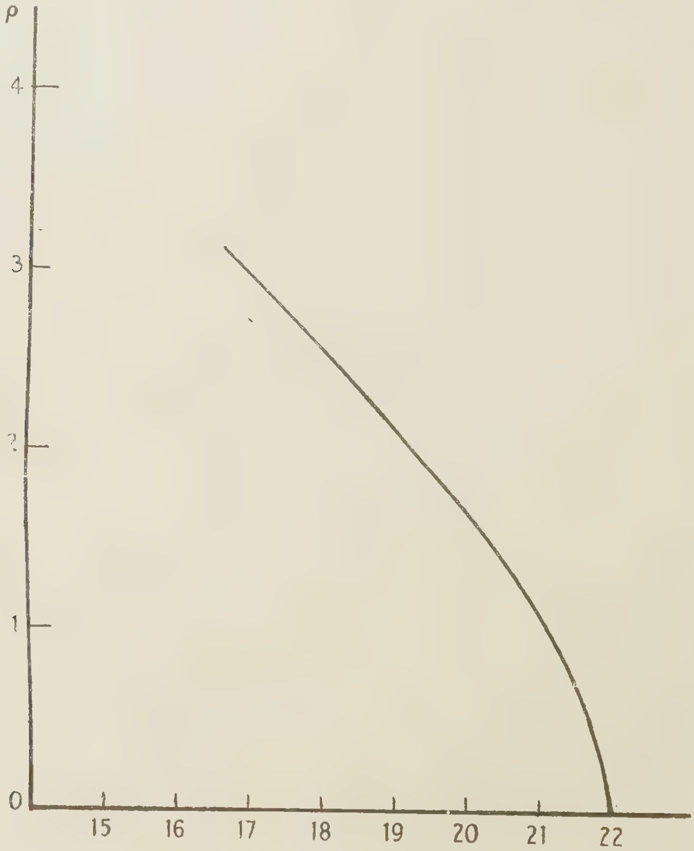

Figure 4.

Spangenberg and Field (1942) give on p. 312 a graph for the reduction of length for a non-paraxial path in an accelerating lens. They state that this reduction curve is almost universal if percentage reductions are considered. We have computed a non-paraxial path (figure 1 and table 3). The reduction in focal length is 87·5%, whereas the reduction read off the universal curve mentioned above is 87%.

In order to obtain the full spherical-aberration curve, several other non-paraxial paths were computed, and the curve obtained is given in figure 4.

We conclude that our path determinations are internally consistent and that the differences between our results and those of the authors quoted are mostly due to errors in the field computation and the uncertainty of the geometrical data. We could, of course, increase the accuracy of our field determination. Such a further effort is not likely to effect our results materially and does not seem justified in view of the experimental errors.

REFERENCES

Comrie, L. J., 1936. *Interpolation and Allied Tables* (London : H.M. Stationery Office).
Goddard, L. S., 1944. *Proc. Phys. Soc.* 56, 342.
Goddard, L. S. and Klemperer, O., 1944. *Proc. Phys. Soc.* 56, 348.
Maloff, I. G. and Epstein, D. W., 1938. *Electron Optics in Television* (New York and London : McGraw-Hill Publishing Co. Inc.).
Motz, H. and Worthy, W. D. " Calculation of the Magnetic Field in Dynamo-electric Machines." (To appear shortly in *J. Instn. Elect. Engrs.*)
Spangenberg, K. and Field, Lester M., 1942. *Electrical Communications*, **20**, 305 ; *ibid.* **21**, 194.

ADDITIONAL BIBLIOGRAPHY

Christopherson, D. G. and Southwell, R. V., 1938. *Proc. Roy. Soc.* A, **168**, 317.
Fox, L., 1944. *Q. J. Appl. Math.* 2, 251.
Southwell, R. V. and Vaisey, G., 1943. *Proc. Roy. Soc.* A, **132**, 129.

A MODIFIED HELMHOLTZ LINE-ELEMENT IN BRIGHTNESS-COLOUR SPACE

By W. S. STILES,
Teddington

MS. received 6 *July* 1945

ABSTRACT. Helmholtz, Schrödinger and others have considered the relation between the trichromatic coordinates, x, y, z and $x+\delta x$ $y+\delta y$, $z+\delta z$, of two juxtaposed light patches which can just be discriminated by the eye. The Helmholtz expression,

$$\left(\frac{\delta x}{a+x}\right)^2+\left(\frac{\delta y}{b+y}\right)^2+\left(\frac{\delta z}{c+z}\right)^2=\text{const.}=\delta s^2,$$

is the most readily interpretable in terms of the trichromatic theory, but to explain the observed variation of the hue limen through the spectrum it demands double-peak fundamental response curves which are at variance with other evidence. It also leads to a step-by-step visibility curve of wrong shape. The difficulties mentioned are removed by introducing different constant factors in the three terms. Such a modification is indicated independently by recent measurements of the liminal brightness increment, from which appropriate values of the factors have been derived. The factor in each term is simply related to the limiting Fechner fraction of the corresponding trichromatic mechanism, i.e., the Fechner fraction $\Delta B/B$ which would be observed at sufficiently high brightnesses B if visual discrimination depended on that mechanism only. The modified expression for δs^2 is applied to the calculation of hue limens, the step-by-step visibility curve, the Fechner fraction curves, and the general colour limen at different points of the colour triangle. Certain main features of the experimental results are correctly reproduced, but discrepancies with Wright and MacAdam's measurements of general colour limens may indicate that the modified element ignores some factor which is operative in their experiments.

§1. INTRODUCTION

THE examination of the properties of the proposed line-element will be preceded by a brief comment on earlier work. It was Helmholtz (1891) who first attempted to express in mathematical form the condition for two juxtaposed light patches to be on the limit of discrimination by the eye. He suggested that any two just-distinguishable patches would have trichromatic co-ordinates x, y, z and $x+\delta x$, $y+\delta y$, $z+\delta z$ respectively, satisfying a relation of the form,

$$3\delta s^2 \equiv \left(\frac{\delta x}{a+x}\right)^2 + \left(\frac{\delta y}{b+y}\right)^2 + \left(\frac{\delta z}{c+z}\right)^2 = 3F^2, \qquad \ldots\ldots (1)^*$$

where a, b, c and F are constants. The trichromatic co-ordinates here are the actual quantities of a particular set of primaries required to match the light patch—not the actual quantities divided by their sum (the unit co-ordinates). It is customary to regard the quantity δs defined in (1) as the length of the line-element in a non-Euclidean space of co-ordinates x, y, z. In this so-called brightness-colour space, the points corresponding to any pair of just-distinguishable light patches are the same elementary distance F apart. If a change is made to a different set of primaries and the relation (1) is expressed in terms of the new co-ordinates of the light patches, the simple form of the relation is lost and it is no longer the case that each term depends on one co-ordinate only. Thus, if the original form is valid at all, it is valid for only one set of the infinitely many sets of primaries which would serve equally well for the statement of the results of colour-matching measurements. The Helmholtz line-element implies, in fact, a particular set of primaries which, on the usual physiological interpretation of the trichromatic theory, we should expect to be the fundamental set such that each primary stimulates one, and only one, of the cone mechanisms. The quantities of the fundamental primaries required to match a monochromatic patch of unit energy intensity define three functions of wave-length—the spectral *sensitivity curves* or *fundamental response curves* of the three mechanisms.

Helmholtz took König's measurements of the trichromatic co-ordinates of the spectrum colours and sought to express them in terms of a set of primaries for which the relation (1) would be valid. The test was that the values of the hue limen through the spectrum as derived from (1) should agree with the measurements of this quantity made by König and Dieterici (1884). Helmholtz actually used the simpler form,

$$3\delta s^2 \equiv \left(\frac{\delta x}{x}\right)^2 + \left(\frac{\delta y}{y}\right)^2 + \left(\frac{\delta z}{z}\right)^2 = 3F^2, \qquad \ldots\ldots (2)$$

to which (1) reduces at sufficiently high intensities when a, b, c can be neglected compared with x, y, z respectively. He was able to find a set of primaries which

---

[*] The factor 3 is introduced so that F has a simple physical meaning, as explained below. Relation (1) is sometimes referred to as *the threshold condition.*

satisfied this test fairly well. But the corresponding fundamental response curves (reproduced as figure 8 in Peddie's **Colour Vision**) each have two pronounced maxima and are quite unlike the *Grundempfindungen* proposed by König from a consideration of the properties of colour-blinds. Moreover, as Schrödinger (1920) pointed out, they lead to an impossible double-peak form for the step-by-step visibility curve (the curve showing the relative energies of neighbouring spectrum colours which appear equally bright).

Schrödinger raised a further objection to the Helmholtz line-element. Although the step-by-step visibility curve can be derived from the line-element and its associated fundamental response curves, some additional assumption is necessary to determine when the eye will judge as equally bright two juxtaposed patches which differ widely in colour. Schrödinger assumed that two patches would appear equally bright if any change in the intensity of one of them would increase the minimum number of just-perceptible steps needed to pass from one to the other. The minumum number for any two light patches A and B is proportional to the integral

$$\int_{A}^{B} ds$$

taken along the geodesic in b.c. space. Thus the assumption is that A will match B when the intensity of B is adjusted to make this integral a minimum. While mathematically attractive, this definition of equality of brightness is not very plausible from a physiological standpoint. Applied to the Helmholtz element, it makes brightness a non-additive property of lights, in conflict with Abney's law. Schrödinger proposed an alternative line-element,

$$\delta s^2 \equiv \frac{1}{\alpha x+\beta y+\gamma z}\left[\frac{\alpha\delta x^2}{x}+\frac{\beta\delta y^2}{y}+\frac{\gamma\delta z^2}{z}\right]=F^2, \qquad \ldots\ldots(3)$$

which, on his assumption, makes brightness proportional to $\alpha x+\beta y+\gamma z$ and, therefore, strictly additive. An adequate criticism of this line-element will not be attempted, but it appears to the writer inconsistent with the threshold measurements considered below.

Since Schrödinger's theoretical work, several investigators have determined by experiment sets of pairs of just-distinguishable patches on various lines and surfaces in b.c. space. Most of these measurements were made at fairly high intensities and were confined to a particular class of just-distinguishable pairs, namely, those in which the members of each pair appeared equally bright (colour-limen type *). The observations on which the modified line-element of this paper is based were of a rather different nature, and are best introduced by considering the application of the Helmholtz element to another special class of just-distinguishable pairs of patches (liminal-increment type).

§ 2. APPLICATION OF THE HELMHOLTZ LINE-ELEMENT TO PAIRS OF JUST-DISTINGUISHABLE PATCHES OF LIMINAL INCREMENT TYPE

A pair is of this type if the physical stimulus in one patch is obtained from that of the other by the *addition* of a further stimulus. Consider the special case when one patch is monochromatic, of wave-length μ and energy intensity W_μ, while the other is a mixture of wave-lengths μ and λ (λ in general different from μ), of energy intensities W_μ and U_λ respectively. The threshold condition (1) takes the form,

---

* Measurements of the hue limen amd the minimum perceptible colorimetric purity (Priest and Brickwedde, 1926) are of this type, as well as the more general colour limens recently determined by Wright (1941).

$$\left[\frac{U_\lambda r_\lambda'}{a+W_\mu r_\mu'}\right]^2+\left[\frac{U_\lambda g'}{b+W_\mu g_\mu'}\right]^2+\left[\frac{U_\lambda b_\lambda'}{c+W\ b_\mu'}\right]^2=3F^2, \qquad \ldots\ldots(4)$$

where r_λ', g_λ', b_λ' are the fundamental response functions of the x, y, z or "red", "green", "blue" mechanisms respectively. Equation (4) may be written

$$\left(\frac{1}{U_\lambda}\right)^2=[r_\lambda\eta(R_\mu W_\mu)]^2+[g_\lambda\eta(G_\mu W_\mu)]^2+[b_\lambda\eta(B_\mu W_\mu)]^2 \qquad \ldots\ldots(5)$$

or

$$\left(\frac{1}{U_\lambda}\right)^2=\left(\frac{1}{U_{\lambda r}}\right)^2+\left(\frac{1}{U_{\lambda g}}\right)^2+\left(\frac{1}{U_{\lambda b}}\right)^2, \qquad \ldots\ldots(6)$$

where

$$\eta(p)=\left(\frac{1}{1+9p}\right)$$

and

$$\left.\begin{array}{lll} r_\lambda=r_\lambda'/aF\sqrt{3}, & R_\lambda=r_\lambda'/9a, & \dfrac{1}{U_{\lambda r}}=r_\lambda\eta(R_\mu W_\mu), \\ g_\lambda=g_\lambda'/bF\sqrt{3}, & G_\lambda=g_\lambda'/9b, & \dfrac{1}{U_{\lambda g}}=g_\lambda\eta(G_\mu W_\mu), \\ b_\lambda=b_\lambda'/cF\sqrt{3}, & B_\lambda=b_\lambda'/9c, & \dfrac{1}{U_{\lambda b}}=b_\lambda\eta(B_\mu W_\mu). \end{array}\right\} \qquad \ldots\ldots(7)$$

$U_{\lambda r}$, $U_{\lambda g}$ amd $U_{\lambda b}$ may be regarded as the values which U_λ would assume if, in turn, each of the three mechanisms were acting alone. Since $\eta(0)=1$, then, since $\dfrac{1}{U_{\lambda r}}=r_\lambda$ when $W_\mu=0$, and r_λ is the reciprocal of the absolute threshold (in energy units) of the red mechanism for light of wave-length λ. Also, since $\eta(1)=0{\cdot}1$, R_μ is the reciprocal of the energy intensity W_μ of light of wave-length μ required to raise $U_{\mu r}$, the difference threshold of the red mechanism, to ten times the absolute threshold ($1/r_\lambda$). Similar interpretations apply to g_λ, G_μ, b_λ, B_μ. For $\lambda=\mu$, we have

$$\frac{R_\lambda}{r_\lambda}=\frac{G_\lambda}{g_\lambda}=\frac{B_\lambda}{b^\lambda}=\frac{F\sqrt{3}}{9}. \qquad \ldots\ldots(8)$$

For fixed λ and μ it is convenient to illustrate relation (5) by a plot of $\log(1/U_\lambda)$ against $\log W_\mu$, and to show plots of $\log(1/U_{\lambda r})$, $\log(1/U_{\lambda g})$ and $\log(1/U_{\lambda b})$ in the same diagram (figure 1). The latter curves (component curves) all have the same shape, but their respective positions in the diagram are determined by the values of r_λ, g_λ, b_λ (position on the ordinate axis) and R_μ, G_μ, B_μ (position on the abscissa axis). If $\mu=\lambda$, the component curves all tend asymptotically at high values of W_μ to the line : *ordinate* $=\log(1/F\sqrt{3})-$ *abscissa*, while the resultant curve ($\log 1/U_\lambda$) tends to the line: *ordinate* $=\log(1/F)-$ *abscissa*. If $\mu\neq\lambda$, the component curves may intersect so that the resultant curve exhibits a more or less pronounced "change of law" as illustrated.

§ 3. BASIC MEASUREMENTS

Given the seven functions $\eta(p)$, r_λ . . . . B_μ the resultant curve for any combination (λ, μ) can be drawn at once. An attempt at the converse problem of determining the seven functions from a number of experimental curves of $\log(1/U_\lambda)$ against $\log W_\mu$ has recently been made. The main points of this work (Stiles, 1939) will be briefly indicated. The present application was not in mind and the conditions of observation differed considerably from those implied in the foregoing discussion.

(*a*) The subject viewed, not two small juxtaposed patches but a large (10° diam.) patch of wave-length μ and energy intensity W_μ, at whose centre a small (1° square) patch of wave-length λ and energy intensity U_λ' was applied in flashes (0·063 sec.) as an additional stimulus. Thus within the 1° square during the flash the energy intensity equalled $W_\mu + U_\lambda'$, while that of the surrounding field remained at W_μ throughout. The subject fixated the centre of the 10° patch, and great care was taken to ensure that the observations corresponded to foveal and cone (rod-free) vision of the additional stimulus. By repeated exposures of the latter at different energies U_λ', W_μ being kept constant, the critical intensity U_λ was determined at which the subject had a 50% chance of seeing the 1° patch.

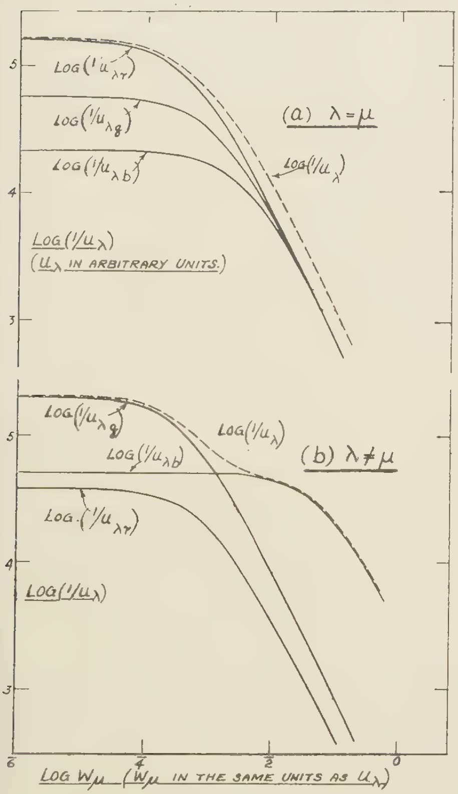

Figure 1.

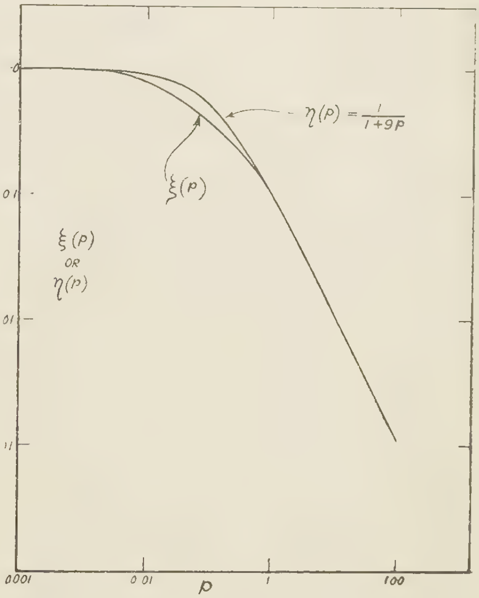

Figure 2.

(*b*) By measuring U_λ in this way for a series of values of W_μ from zero upwards, a curve of $\log(1/U_\lambda)$ against $\log W_\mu$ was obtained for various pairs of wave-lengths λ and μ. These experimental curves corresponded to the broken-line curves in figure 1. For example, with $\lambda = 480$ mμ, $\mu = 540$ mμ, the experimental curve closely resembled the broken-line curve of figure 1 (*b*). It was the characteristic form of such experimental curves which first suggested that they were really resultant curves derivable from component curves of fixed shape. This view was supported by the fact that when λ was kept constant at 480 mμ and μ was varied, the experimental curve was modified as though (referring to figure 1 (*b*)) the component curves $\log(1/U_{\lambda g})$ and $\log(1/U_{\lambda b})$ were displaced parallel to the axis of $\log W_\mu$, while remaining in the same position along the axis of $\log(1/U_\lambda)$. On the other hand, when μ was kept constant and λ varied, the experimental curve was modified as though the component curves were displaced parallel to the axis of $\log(1/U_\lambda)$. These regularities in the results may be called the "displacement rules".

From nearly 100 curves of $\log(1/U_\lambda)$ against $\log W_\mu$ for the writer's left eye, it was concluded that all such curves for this eye could be regarded as resultants of three component curves of a common fixed shape whose positions in the diagram depended on λ and μ. The most satisfactory fixed shape to suit all the results was chosen by trial, and the positions in the diagram at which component curves of this shape had to be placed to yield a resultant curve agreeing with the experimental curve were determined for the various combinations of λ and μ studied. Actually no more than two component curves contributed to the experimental curve for any particular combination, but to cover all combinations in accordance with the displacement rules three components were necessary.

(*c*) The common shape of the component curves was represented as a function $\xi(p)$ (figure 2) defined so that $\xi(p) = 1$ for $p = 0$, $\xi(p) = 0{\cdot}1$ for $p = 1$. Thus $\xi(p)$ played the rôle of the function $\eta(p)$ above. It is apparent from figure 2 that the difference between the two functions is small and confined to values of p below 1. The expression for a particular component, say the "red" component, then took the form,

$$\log(1/U_{\lambda r}) = \log[r_\lambda \xi(R_\mu W_\mu)],$$

where for given λ and μ the constants r_λ and R_μ fix the position of the curve in the diagram. Conversely, when the position had been determined as explained above, the values of r_λ and R_μ were obtained. Although this method yielded values for each of the functions r_λ, R_μ, g_λ, etc., in a part only of the visible spectrum, the ranges were extended by assuming the ratios $\frac{R_\lambda}{r_\lambda}$, $\frac{G_\lambda}{g_\lambda}$, $\frac{B_\lambda}{b_\lambda}$ to be approximately independent of λ. This appeared to be nearly true in regions where both numerator and denominator functions could be followed. The tentative determinations of the six functions r_λ to B_μ are plotted as the continuous-line curves of figures 3 to 5. The absolute values depend on the unit in which energy intensity is expressed. Here and elsewhere in this paper, by *energy intensity* is to be understood the flux of radiation entering the eye, expressed in ergs per sec. per square degree of the light patch. The values given refer to the case when the pupil of entry at the eye is small and concentric with the natural pupil. Rather different values apply when the pupil is large or eccentric, on account of the directional properties of retinal sensitivity.

(*d*) On the assumption that $\frac{R_\lambda}{r_\lambda}$, $\frac{G_\lambda}{g_\lambda}$ and $\frac{B_\lambda}{b_\lambda}$ are constants independent of λ, the values of these ratios were found to be (very approximately) in the proportion

$$\frac{R_\lambda}{r_\lambda} : \frac{G_\lambda}{g_\lambda} : \frac{B_\lambda}{b_\lambda} = 0{\cdot}78 : 1 : 4{\cdot}46.$$

(*e*) The resultant curve was related to the component curves by the following rough rule: for a given $\log W_\mu$, $\log 1/U_\lambda \ldots$ equals the greatest of $\log(1/U_{\lambda r})$ $\log(1/U_{\lambda g})$ and $\log(1/U_{\lambda b})$, except when the greatest and next greatest have nearly the same value. In the latter case $\log(1/U_\lambda)$ exceeds the greatest by a small amount, of the order of 0·1.

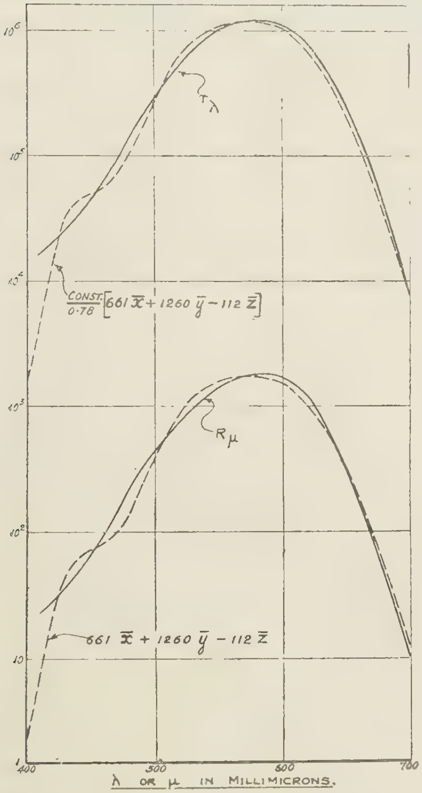

Figure 3.

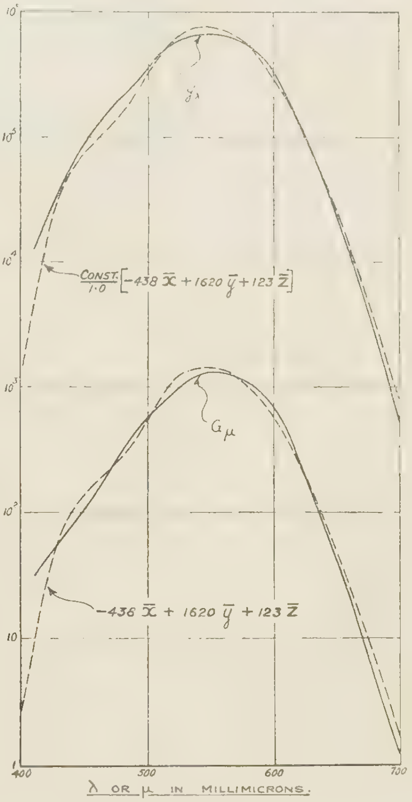

Figure 4.

(*f*) A breakdown in the analysis of the results on the above lines occurred when the 10° patch was orange or red and of very high intensity (about 30,000 photons) and when the additional stimulus was blue (*limited conditioning effect* of red light on the blue mechanism). Colour-match equations also break down after adaptation to intensities of this order (Wright, 1936).

Setting aside the effect noted in (*f*), the experimental results differ from the predictions of the line-element and associated primaries of Helmholtz in the following respects:—

(i) The function $\eta(p)$ is replaced by a slightly different function $\xi(q)$.

(ii) The spectral sensitivity functions have the same general form as König's *Grundempfindungen.*

(iii) The ratios $\frac{R_\lambda}{r_\lambda}$, $\frac{G_\lambda}{g_\lambda}$, $\frac{B_\lambda}{b_\lambda}$ are not equal: $\frac{B_\lambda}{b_\lambda}$ is materially greater than the other two. It follows that for $\lambda = \mu$, the three component curves in diagrams such as figure 1 no longer tend to a common line at high intensities.

(iv) The effects of the three mechanisms add up, if anything, to a smaller extent than required by the sum of squares relation (6).

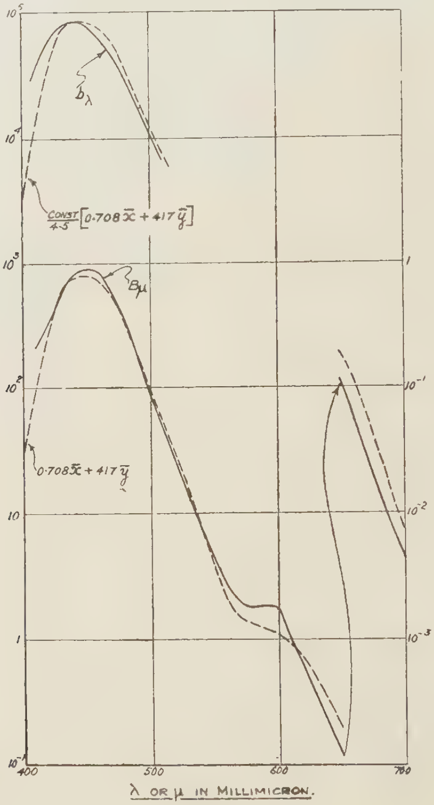

Figure 5.

For $\lambda = \mu$, the ratios $\frac{U_{\lambda r}}{W_\lambda}$, $\frac{U_{\lambda g}}{W_\lambda}$, $\frac{U_{\lambda b}}{W_\lambda}$ are the Fechner fractions * of the respective mechanisms. Since $\xi(p)$ tends to $\frac{1}{9p}$ as p becomes large, it is clear that $\frac{U_{\lambda r}}{W} = \frac{1}{W_\lambda r_r \xi(R_\lambda W_\lambda)}$ approaches $9\frac{R_\lambda}{r_\lambda}$ at high intensities W_λ. Thus the ratios $\frac{R_\lambda}{r_\lambda}$, $\frac{G_\lambda}{g_\lambda}$, $\frac{B_\lambda}{b_\lambda}$ are proportional respectively to the *limiting Fechner* fractions of the three mechanisms, and (iii) implies that, contrary to the assumption of Helmholtz, the different mechanisms have different limiting Fechner fractions.

---

* Historically it would be more accurate to call these ratios "Weber fractions", but it has seemed preferable to follow the more usual practice.

The precision of threshold measurements is low, and during a long investigation the properties of the eye may undergo systematic changes. There can be no question of a precise determination of the unknown functions by the methods used. All that can be claimed is that the derived functions reproduce the main features of the experimental curves.

§ 4. MODIFIED LINE-ELEMENT

Following the hints given by the basic measurements, we may construct a tentative line-element for application to any pair of just-distinguishable light patches, not necessarily of liminal increment type. Suppose the patches P′ and P have absolute energy distributions $W_\lambda' d\lambda$ and $W_\lambda d\lambda$ respectively. Put

$$\zeta(p)=9\xi(p), \qquad R=\int W_\lambda R_\lambda d\lambda, \qquad \delta R=\int (W_\lambda' - W_\lambda) R_\lambda d\lambda \quad \ldots\ldots(10)$$

and define G, δG, B, δB similarly, where $\xi(p)$, R_λ, G_λ, B_λ are the *experimental* functions* plotted in figures 2 to 5. Introduce the quantities ρ, γ, β proportional to the limiting Fechner fractions of the three mechanisms,

$$\rho:\gamma:\beta=\frac{R_\lambda}{r_\lambda}:\frac{G_\lambda}{g_\lambda}:\frac{B_\lambda}{b_\lambda}=0{\cdot}78:1:4{\cdot}46, \quad \ldots\ldots(11)$$

and satisfying

$$\frac{1}{\rho^2}+\frac{1}{\gamma^2}+\frac{1}{\beta^2}=1, \quad \ldots\ldots(12)$$

so that $\frac{1}{\rho^2}=0{\cdot}612$, $\frac{1}{\gamma^2}=0{\cdot}369$, $\frac{1}{\beta^2}=0{\cdot}0185$. The proposed line-element is then

$$\delta s^2\equiv\left[\frac{\delta R}{\rho}\zeta(R)\right]^2+\left[\frac{\delta G}{\gamma}\zeta(G)\right]^2+\left[\frac{\delta B}{\beta}\zeta(B)\right]^2=F^2, \quad \ldots\ldots(13)$$

which reduces at high intensities to

$$\delta s^2\equiv\left[\frac{1}{\rho}\frac{\delta R}{R}\right]^2+\left[\frac{1}{\gamma}\frac{\delta G}{G}\right]^2+\left[\frac{1}{\beta}\frac{\delta B}{B}\right]^2=F^2, \quad \ldots\ldots(14)$$

where F is a constant.

If the two patches have the same *relative* energy distributions, their intensities may be specified by their total energies T' and T (or by their total energies weighted according to any function of wave-length, such as the visibility curve). Their Fechner fraction is then given by

$$\frac{\delta T}{T}\equiv\frac{T'-T}{T}=\frac{\delta R}{R}=\frac{\delta G}{G}=\frac{\delta B}{B}.$$

Thus, by (14) and (12), $\frac{\delta T}{T}=F$ at high intensities, or F is the limiting Fechner fraction for any pair of patches of the same relative energy distribution whatever form that may take. The factor 3 introduced into (1) gives F a similar meaning for the Helmholtz line-element. Experimentally, the value of F depends on the precise conditions of observation. It is round about 0·01 for the conditions normally used in determining colour limens, and this value will be used in the calculations which follow.

---

* The definitions of R_λ, G_λ, B_λ are modified later.

For just distinguishable patches of liminal increment type, δR, δG and δB are all positive or all negative. In applying the line-element generally, it is assumed that the signs of δR, δG, δB are immaterial, so that, for example, slight excess stimulations of the red and green mechanisms make the same contribution to the limen whether the excesses occur both in the same or one in each patch.

§ 5. COLOUR MATCHING

Light patches whose representative points P′ in b.c. space lie within the small ellipsoid centred on P and defined by (13) are indistinguishable from, and therefore in colour match with, P. In colour-matching measurements the objective is to bring the variable colour to the centre of this ellipsoid, and the condition for an ideal match may be taken to be $\delta R = \delta G = \delta B = 0$, or $\int W_\lambda' R_\lambda \, d\lambda = \int W_\lambda R_\lambda \, d\lambda$, and two similar equations.* R_λ, G_λ, B_λ were, in fact, obtained by a method completely independent of colour-matching, but their introduction into the line-element relates them at once to the distribution coefficients $\bar{x}$, $\bar{y}$, $\bar{z}$ derivable from colour-matching measurements. In terms of these coefficients, the conditions for a colour match are

$$\int W_\lambda' \bar{x} \, d\lambda = \int W_\lambda \bar{x} \, d\lambda$$

and two similar equations. Thus R_λ, G_λ, B_λ should be linear forms in $\bar{x}$, $\bar{y}$, $\bar{z}$. The distribution coefficients for the writer's eye (a normal trichromat) have not been determined, but using the coefficients of the C.I.E. Standard Observer in the Standard Reference System (C.I.E. 1931) an approximate linear representation of R_λ, G_λ, B_λ is obtained as follows :—

$$\left.\begin{array}{ll} (R_\lambda) & 6{\cdot}61 \, . \, 10^2 \, \bar{x} + 1{\cdot}26 \, . \, 10^3 \bar{y} - 1{\cdot}12 \, . \, 10^2 \bar{z}, \\ (G_\lambda) & -4{\cdot}38 \, . \, 10^2 \, \bar{x} + 1{\cdot}62 \, . \, 10^3 \bar{y} + 1{\cdot}23 \, . \, 10^2 \bar{z}, \\ (B_\lambda) & 7{\cdot}08 \, . \, 10^{-1} \bar{x} + 0 \, . \, \bar{y} \qquad\qquad + 4{\cdot}17 \, . \, 10^2 \bar{z}, \end{array}\right\} \quad \ldots\ldots(15)$$

These linear forms are plotted as the broken lines in figures 3 to 5. The agreement between the broken and continuous curves is fairly satisfactory when it is recalled (*a*) that the experimental uncertainties in determining R_λ, G_λ, B_λ are considerable—much greater than for $\bar{x}$, $\bar{y}$, $\bar{z}$; (*b*) that results for a single eye and for an average eye are being compared. The basic measurements (§ 3) could be represented almost as well by using the expressions (15) in place of R_λ, G_λ, B_λ, and by making the same substitutions in the definitions of R, δR, etc., the line element would lead automatically to the correct colour-matching equations for the C.I.E. standard observer. From now on, therefore, R_λ, G_λ, B_λ are supposed defined by the expressions (15). We are, of course, still dependent on the basic measurements for the coefficients in (15) and for the relative values of ρ, γ, β.

---

* Even if an ideal colour match is not achieved, (13) ensures that these equations shall be approximately true, i.e. δR will be small compared with R, and so on.

§ 6. STEP-BY-STEP VISIBILITY CURVE

In the experimental determination of the visibility curve by the step-by-step method, the two juxtaposed patches have slightly different colours and the intensity of one is varied until the "difference" between the two patches is a minimum. If the colour difference is appropriately chosen, the two patches are just indistinguishable at this minimum setting of the intensity. The visibility curve is derived from the line-element (14) by a corresponding procedure. The unit co-ordinates (in the fundamental system) of the two patches, i', j', k' and i, j, k, are required, where

$$i' = \frac{R'}{R'+G'+B'} = \frac{R'}{\Sigma'}, \qquad i = \frac{R}{R+G+B} = \frac{R}{\Sigma}, \qquad \ldots\ldots(16)$$

and j', k' ; j, k are similarly defined.

In terms of these, the line-element (13) takes the form

$$\delta s^2 \equiv \left[\frac{\Sigma' i' - \Sigma i}{\rho}\zeta(i)\right]^2 + \text{two similar terms.} \qquad \ldots\ldots(17)$$

By varying Σ', keeping i', j', k' constant, the intensity of patch P′ is varied without altering its colour. The minimum value of δs^2 under such a variation is reached when

$$0 = \frac{1}{\rho^2}\,[2i'(\Sigma' i' - \Sigma i)\zeta(\Sigma i)]^2 + \text{two similar terms,}$$

or, reverting to the earlier notation and retaining only first-order quantities, when

$$0 = \frac{\delta R}{R}\left[\frac{R}{\rho}\zeta(R)\right]^2 + \frac{\delta G}{G}\left[\frac{G}{\gamma}\zeta(G)\right]^2 + \frac{\delta B}{B}\left[\frac{B}{\beta}\zeta(B)\right]^2. \qquad \ldots\ldots(18)$$

Strictly, the colour difference of the two patches should be chosen so that at the minimum setting $\delta s = F$, but it suffices both in the theory and in the experimental method for this condition merely to be approached.

The equality-of-brightness condition (18) applies to any pair of patches of nearly the same colour. In the special case of monochromatic patches of wave-lengths λ, $\lambda + \delta\lambda$ and energy intensities W_λ, $W_\lambda + \delta W_\lambda$, (18) becomes

$$-\frac{\delta W_\lambda}{W_\lambda} = \delta\lambda\left[\frac{C_r^2}{R_\lambda}\frac{dR_\lambda}{d\lambda} + \frac{C_g^2}{G_\lambda}\frac{dG_\lambda}{d\lambda} + \frac{C_b^2}{B_\lambda}\frac{dB_\lambda}{d\lambda}\right], \qquad \ldots\ldots(19)$$

where

$$C_r^2 = \frac{\left[\frac{R}{\rho}\zeta(R)\right]^2}{\left[\frac{R}{\rho}\zeta(R)\right]^2 + \left[\frac{G}{\gamma}\zeta(G)\right]^2 + \left[\frac{B}{\beta}\zeta(B)\right]^2} \qquad \ldots\ldots(20)$$

and C_g^2, C_b^2 are similarly defined. By successive applications of (19) we can determine the energy intensities of a series of monochromatic patches whose wave-lengths increase in small steps from the blue to the red, and each of which matches in brightness its next neighbours in the series. The reciprocal of the patch energy plotted against wave-length represents a step-by-step visibility curve whose shape will depend in general on the intensity level, specified, say, by the value of W_λ at $\lambda = 555$ mμ. At sufficiently high intensity levels C_r^2, C_g^2, C_b^2 tend to $1/\rho^2$, $1/\gamma^2$, $1/\beta^2$ respectively, and the visibility curve approaches the limiting form

$$V_\lambda = \frac{\text{const.}}{W_\lambda} = \text{const. } R_\lambda^{1/\rho^2}\, G_\lambda^{1/\gamma^2}\, B_\lambda^{1/\beta^2}. \qquad \ldots\ldots\ldots (21)$$

As usual, the constant is adjusted so that V_λ has the maximum value unity.

The circle points in figure 6 represent relative visibilities calculated from the expression (21). Except in the blue, these points lie very close to the full-line curve, which is a plot of the C.I.E. visibility function. The discrepancy in the blue is greatly reduced if the comparison is made with the mean visibility curve obtained by Gibson and Tyndall (1923) for 52 observers (38 on ends) using the step-by-step method.* In the several investigations of the visibility curve in which large groups of observers have been used, the variations between observers are markedly greater in the blue (say 455 mμ) than in the red (say 655 mμ). On this general ground any theoretical derivation of the visibility curve may be expected to meet greater difficulties in the blue than in the red.

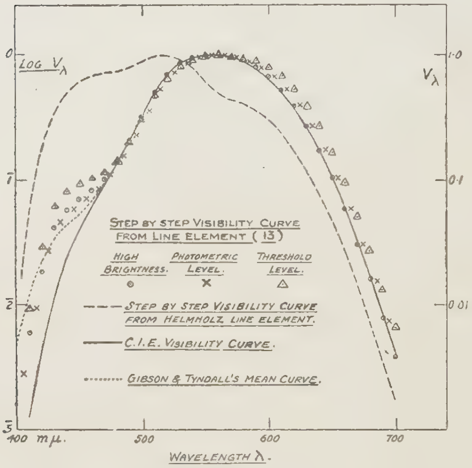

Figure 6. Step-by-step visibility curves.

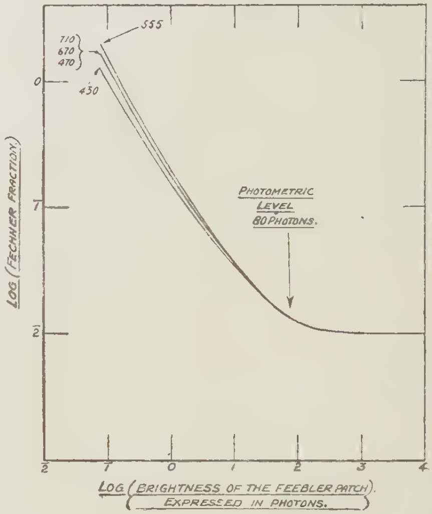

Figure 7. Fechner fraction curves.

The broken curve in figure 6 is the visibility function for the Helmholtz line-element, but assuming the response functions (15). It is derived from (21) by putting

$$\frac{1}{\rho^2} = \frac{1}{\gamma^2} = \frac{1}{\beta^2} = \frac{1}{3}.$$

Equally unacceptable curves are obtained by applying to the Helmholtz element König's *Grundemfindungen* or the double-peak response curves of Helmholtz. The Hecht response curves (Hecht, 1932), each of which is a fair approximation to the visibility curve, would make the Helmholtz or the modified line-element consistent with the visibility curve, but would render it incapable of explaining the basic measurements (§ 4).

---

* I am indebted to Prof. Hecht for drawing my attention to this point. He also points out that the mean curve of Coblenz and Emerson (1917) shows a hump in the blue, and that a protanope studied by Hecht and Shlaer gave a curve similar in this respect to a normal observer.

The standard photometric brightness level at which the C.I.E. visibility curve applies may be taken as 25 equivalent metre candles seen through an eye pupil of 10 sq. mm. area, or 79·5 photons. A monochromatic patch of wavelength 555 mμ has this brightness when its energy intensity W_λ equals $3{\cdot}66 \times 10^{-4}$ erg per sec. per square degree. The limiting form (21) of the derived visibility curve is barely reached at this value of W_{555}, and the curve must be derived from (19) by a method of successive approximation. The results of the calculation are shown as the cross-points in figure 6. The agreement with the C.I.E. curve is substantial, although in the red it is rather less close than for the high-intensity curve. As the intensity is reduced below the photometric level, the derived curve undergoes some further modification, to assume finally the form shown by the triangle-points of figure 6, when the absolute threshold is reached. The second limiting form (22) can be obtained from (19) or directly from the line-element (13) by using the principle that at the absolute threshold all light patches are equally bright :

$$V_\lambda = \text{const.} \sqrt{\left(\frac{R_\lambda}{\rho}\right)^2 + \left(\frac{G_\lambda}{\gamma}\right)^2 + \left(\frac{B_\lambda}{\beta}\right)^2}. \qquad \ldots\ldots (22)$$

The main effects of lowering the intensity level are to increase slightly the visibilities in the orange and red and in the blue. It must be emphasized that the line-element (13) is intended to represent foveal and strictly cone vision. The small changes in the visibility curve just considered are quite distinct from the very much larger changes (Purkinje effect) which occur when, by the use of a large or eccentrically fixated matching field, the rods participate in the matching process.

No determinations of the foveal cone visibility curve by the step-by-step method have been made at low intensities. Walters and Wright (1943) used a fixed red comparison patch and worked with the full-colour difference. They found that at low intensities the visibility curve showed a slight shift of the maximum towards the blue, which they think may have resulted from some admixture of rod vision, and a " lump " in the curve at about 600 mμ, which they attribute to a tendency of the red mechanism to retain its sensitivity over a greater intensity range than the green or blue mechanisms.

Relation (18) is the differential of the function

$$P(R,\ G,\ B) = P_r(R) + P_g(G) + P_b(B),$$

where

$$P_r(R) = \int^R \frac{dR}{R}\left[\frac{R\zeta(R)}{\rho}\right]^2,$$

and P_g, P_b are similarly defined. All lights (not necessarily monochromatic) for which $P(R, G, B)$ has the same value can be linked in small steps by series of intermediate lights, adjacent lights in any series having the same brightness. We may say that all such lights have the same " small-step " brightness. But P_r, P_g and P_b are not linear functions of their arguments, so that " small-step " brightness is not additive. To estimate the magnitude of the breakdown in the additive law, we will use for $P(R, G, B)$ the form to which it reduces at high intensities, namely,

$$\log_e [R^{1/\rho^2} G^{1/\gamma^2} B^{1/\beta^2}].$$

If lights 1 and 2 have the same small-step brightness,

$$R_1^{1/\varrho^2} G_1^{1/\gamma^2} B_1^{1/\beta^2} = R_2^{1/\varrho^2} G_2^{1/\gamma^2} B_2^{1/\beta^2},$$

and the equality of brightness still holds if their intensities are changed by the same factor, α say, since

$$(R_1\alpha)^{1/\varrho^2} (G_1\alpha)^{1/\gamma^2} (B_1\alpha)^{1/\beta^2} = (R_2\alpha)^{1/\varrho^2} (G_2\alpha)^{1/\gamma^2} (B_2\alpha)^{1/\beta^2}.$$

But if lights 1 and 2 each match light 3 in brightness, the mixture of 1 and 2 will not in general match light 3 increased to double its original intensity, since

$$(R_1+R_2)^{1/\varrho^2} (G_1+G_2)^{1/\gamma^2} (B_1+B_2)^{1/\beta^2} = (2R_3)^{1/\varrho^2} (2G_3)^{1/\gamma^2} (2B_3)^{1/\beta^2}$$

is not in general true. The discrepancy may be expected to be greatest when the colours of 1 and 2 are most widely different, and it is estimated that about the worst case arises with monochromatic lights in the blue (470 mμ) and red (680 mμ). The colour of light 3 is immaterial. Calculation for this case shows that

$$(R_1+R_2)^{1/\varrho^2} (G_1+G_2)^{1/\gamma^2} (B_1+B_2)^{1/\beta^2} = (2{\cdot}63R_3)^{1/\varrho^2} (2{\cdot}63G_3)^{1/\gamma^2} (2{\cdot}63G_3)^{1/\beta^2}.$$

The breakdown in additivity corresponds to the difference between 2 and 2·63, or about 27%. As a second example, take a white of energy distribution $W_\lambda d\lambda$ appropriate to a black body of temperature 2060° K. and compare its small-step brightness with the sum of the small-step brightnesses of its component wavelengths. Additivity would require

$$\int R_\lambda^{1/\varrho^2} G_\lambda^{1/\gamma^2} B_\lambda^{1/\beta^2} W_\lambda d\lambda = \left\{\int W_\lambda R_\lambda d\lambda\right\}^{1/\varrho^2} \left\{\int W_\lambda G_\lambda d\lambda\right\}^{1/\gamma^2} \left\{\int W_\lambda B_\lambda d\lambda\right\}^{1/\beta^2},$$

but calculation shows that the equation is in error by about 8%. This second case is the one used by Ives to test the additivity of brightness as assessed in the flicker photometer. He found additivity held good within the experimental error (1 or 2%). No similar check of additivity for small-step brightness has been made, and it cannot be said with certainty that discrepancies of the kind indicated by the line-element would not be observed, although there is no positive evidence for them. The results of brightness matching by flicker photometry, like those obtained by direct-comparison photometry with full colour difference, cannot be derived from the line-element without additional assumptions and will not be discussed.

§7. FECHNER FRACTION CURVES

Although the modified line-element assumes that the red, green and blue mechanisms have different limiting Fechner fractions at high intensities, it still leads to a common value F for the limiting Fechner fraction of a pair of just-distinguishable and similarly-coloured light patches, whatever that colour may be. This is in accordance with König and Brodhun's classic measurements of the Fechner fractions of white and monochromatic light. These measurements were made with large patches, each 3° × 4½°, and it is only at the higher intensities studied that the results can be accepted as referring to cone vision. The wide divergence in the observed values of the Fechner fraction at lower intensities is caused by the intrusion of the rods. The change with intensity in the Fechner fraction of monochromatic patches as predicted by the modified line-element (13) is shown in figure 7. The Fechner fraction, plotted as ordinate, is the just-distinguishable difference in patch intensity divided by the intensity of the *feebler* patch, and the intensity level, plotted as abscissa, is the intensity of the feebler patch. For $\lambda = 555 m\mu$, this intensity is expressed in photons and for other wave-lengths in units such that all colours have the same brightness when compared on the basis of the calculated step-by-step visibility curve for the photometric level (figure 6). The Fechner fraction curves for different wave-lengths are not very different, but for the extreme blue the Fechner fraction has a rather smaller value at low intensities than for other colours.

§ 8. HUE LIMEN

The hue limen, or the difference of wave-length of two just-distinguishable monochromatic patches of equal brightness, is obtained from relations (13) and (18) by the substitutions,

$$R = W_\lambda R_\lambda, \quad \delta R = R_\lambda \delta W_\lambda + W_\lambda \frac{dR_\lambda}{d\lambda} \delta\lambda, \text{ etc.}$$

On eliminating W_λ, the equation for the hue limen $\delta\lambda$ takes the form :

$$F^2 = \delta\lambda^2 \left[\left\{ \frac{C_r^2 - 1}{R_\lambda} \frac{dR_\lambda}{d\lambda} + \frac{C_g^2}{G_\lambda} \frac{dG_\lambda}{d\lambda} + \frac{C_b^2}{B_\lambda} \frac{dB_\lambda}{d\lambda} \right\}^2 \left\{ \frac{R}{\rho} \zeta(R) \right\}^2 + \text{two similar terms} \right] \qquad \text{.....(23)}$$

At high intensities this reduces to

$$F^2 = \delta\lambda^2 \left[\left\{ \frac{1/\rho^2 - 1}{R_\lambda} \frac{dR_\lambda}{a\lambda} + \frac{1/\gamma^2}{G_\lambda} \frac{dG_\lambda}{d\lambda} + \frac{1/\beta^2}{B_\lambda} \frac{dB}{d\lambda} \right\}^2 1/\rho^2 + \text{two similar terms} \right]. \qquad \text{......(24)}$$

The equation used by Helmholtz is the special case of (24), when ρ, γ, β are made equal.

The values of the hue limen through the spectrum have been calculated from (23), assuming a common brightness for all colours on the basis of the calculated step-by-step visibility curve for the photometric level (figure 6) and an actual brightness of 80 photons for $\lambda = 550$ $m\mu$.

Table 1. Values of hue limen at the photometric level derived from the modified line element

λ (mμ)	$\delta\lambda$ (mμ)	λ (mμ)	$\delta\lambda$ (mμ)	λ (mμ)	$\delta\lambda$ (mμ)
410	5·7	510	2·06	610	1·43
420	3·9	520	2·74	620	1·88
430	2·22	530	2·88	630	2·42
440	1·75	540	2·87	640	3·2
450	1·41	550	2·62	650	4·7
460	1·63	560	2·03	660	6·8
470	1·14	570	1·72	670	11
480	0·82	580	1·44	680	18
490	0·97	590	1·27	690	29
500	1·45	600	1·26		

The calculated values are plotted in figure 8 together with five experimental curves obtained by Wright and Pitt (1934) at an average intensity level (480 to

650 mμ) of 70 photons. An outstanding difference between the theoretical and experimental curves is that in the former the limens in the blue are relatively low.

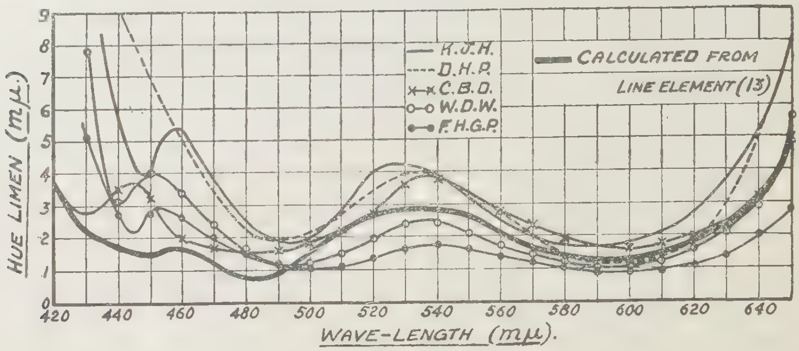

Figure 8. Observed (Wright and Pitt, 1934) and calculated values of the hue limen.

In the determination of the experimental curves it was necessary to use lower intensities in the extreme blue, the total range being about 20 to 1. This may account for some of the difference.

§ 9. GENERAL COLOUR LIMEN

If two patches P and P′, not necessarily monochromatic, have the same brightness and are just distinguishable, they define a general colour limen. The general colour limens for a given common brightness level are conveniently displayed in a C.I.E. (x, y) chart (*a*) by marking pairs of just-distinguishable colours on various lines joining spectrum colours to other spectrum colours or to purples (Wright, 1941), or (*b*) by drawing small closed curves (ellipses) about various points in the chart, the colours corresponding to all points on each such curve being just distinguishable from the central colour. The modified line-element will now be applied to calculate the g.c.l. (general colour limen) ellipses for the 25 colours used in the recent investigation by MacAdam (1942). Using an ingenious optical system, MacAdam arranged that, by turning a single control knob, the colour of a light patch was varied along a line in the C.I.E. chart while its brightness (C.I.E.) was automatically held constant. Repeated colour matches were made with a second juxtaposed patch of the same brightness and of a fixed colour on the given line. The standard deviations of the settings were determined, a setting being specified by the distance in the chart between the variable and fixed points. The standard deviation is closely related to, and may be taken as proportional to, the diameter of the g.c.l. ellipse at the fixed colour in the direction of the given line. MacAdam determined for one subject the complete ellipses for 25 fixed colours distributed fairly evenly over the domain between the spectrum locus and the line of purples.

Denoting by $t_{mn}(m, n=1, 2, 3)$ the coefficients in the forms (15), the R co-ordinate of a patch of absolute energy distribution $W_\lambda d\lambda$ is given by

$$R = t_{11}x' + t_{12}y' + t_{13}z', \qquad \ldots\ldots (25)$$

where $$x' = \int W_\lambda \bar{x}\, d\lambda, \qquad y' = \int W_\lambda \bar{y}\, d\lambda, \qquad z' = \int W_\lambda \bar{z} d\lambda,$$

and similar equations hold for G and B. The C.I.E. unit co-ordinates x, y, z are then $x = x'/w'$, $y = y'/w'$, $z = z'/w'$, where $w' = x' + y' + z'$. The quantity y' is proportional to the C.I.E. brightness of the patch and, in fact, recalling the units in which $W_\lambda d\lambda$ is expressed, we have :

$$\text{patch brightness in photons} = 2{\cdot}19 \,.\, 10^5 \int W_\lambda \bar{y}\, d\lambda,$$

where the mechanical equivalent of light has been taken as 0·0015 watts per lumen. MacAdam worked with a C.I.E. brightness of 15 millilamberts seen through a pupil of 2·6 mm. diameter, that is, with a brightness of 271 photons. The calculation will be applied, therefore, to the case,

$$\int W_\lambda \bar{y}\, d\lambda = y' = w'y = \frac{271}{2{\cdot}19 \,.\, 10^5} = 1{\cdot}24 \,.\, 10^{-3}.$$

The R co-ordinate of the just-distinguishable patch is $R + \delta R$, where

$$\delta R = t_{11}\delta x' + t_{12}\delta y' + t_{13}\delta z',$$

and similar equations hold for δG and δB. In MacAdam's observations $\delta y' = 0$. The differentials $\delta x'$, $\delta z'$, expressed in terms of dx, δy, are then :

$$\delta x' = \frac{y'}{y}\left\{\delta x - \frac{x}{y}\delta y\right\},$$

$$\delta z' = \frac{y'}{y}\left\{\frac{\overline{x-1}}{y}\delta y - \delta x\right\}.$$

Thus,

$$\delta R = \delta x \,.\, \frac{y'}{y}\,(t_{11} - t_{13}) + \delta y \,.\, \frac{y'}{y^2}(x\,\overline{t_{13} - t_{11}} - t_{13}),$$

$$R = x \,.\, \frac{y' t_{11}}{y} + y' t_{12} + z \,.\, \frac{y'}{y}\, t_{13}, \qquad \ldots\ldots (26)$$

and, inserting these expressions, the line-element (13) takes the form

$$\begin{aligned} F^2 = {} & \delta x^2 \left[\left\{\frac{p_{11}}{\rho}\zeta(R)\right\}^2 + \left\{\frac{p_{21}}{\gamma}\zeta(G)\right\}^2 + \left\{\frac{p_{31}}{\beta}\zeta(B)\right\}^2\right. \\ & + 2\delta x\, \delta y\left[p_{11}p_{12}\left\{\frac{\zeta(R)}{\rho}\right\}^2 + p_{21}p_{22}\left\{\frac{\zeta(G)}{\gamma}\right\}^2 + p_{31}p_{32}\left\{\frac{\zeta(B)}{\beta}\right\}^2\right] \\ & + \delta y^2\left[\left\{\frac{p_{12}}{\rho}\zeta(R)\right\}^2 + \left\{\frac{p_{22}}{\gamma}\zeta(G)\right\}^2 + \left\{\frac{p_{32}}{\beta}\zeta(B)\right\}^2\right], \qquad \ldots\ldots (27) \end{aligned}$$

where

$$p_{11} = \frac{y'}{y}(t_{11} - t_{13}), \qquad p_{12} = \frac{y'}{y^2}(x\,\overline{t_{13} - t_{11}} - t_{13}),$$

$$p_{21} = \frac{y'}{y}(t_{21} - t_{23}), \qquad p_{22} = \frac{y'}{y^2}(x\,\overline{t_{23} - t_{21}} - t_{23}),$$

$$p_{31} = \frac{y'}{y}(t_{31} - t_{32}), \qquad p_{32} = \frac{y'}{y^2}(x\,\overline{t_{33} - t_{31}} - t_{33}),$$

For a given colour x, y, the g.c.l. ellipse is completely determined by the equation

(27). The semi-axes and orientation of the ellipse have been calculated for MacAdam's 25 colours and are as follows:—

Table 2

Colour MacAdam's figure number	C.I.E. co-ordinates			Semi-axes		Angle between major axis and axis of x (degrees)
	x	y	z	Major	Minor	
23	0·160	0·057	0·783	0·235 . 10^{-2}	0·139 . 10^{-2}	85
24	0·187	0·118	0·695	0·62	0·285	75
25	0·253	0·125	0·622	0·71	0·272	53
26	0·150	0·680	0·170	2·84	1·26	106
27	0·131	0·521	0·348	2·60	1·04	101
28	0·212	0·550	0·238	2·37	1·13	97
29	0·258	0·450	0·292	1·90	0·97	86
30	0·152	0·365	0·483	1·86	0·76	96
31	0·280	0·385	0·335	1·67	0·85	78
32	0·380	0·498	0·122	1·53	1·04	83
33	0·160	0·200	0·640	1·10	0·44	92
34	0·228	0·250	0·522	1·24	0·57	76
35	0·305	0·323	0·372	1·43	0·72	68
36	0·385	0·393	0·222	1·47	0·83	63
37	0·472	0·399	0·129	1·23	0·78	54
38	0·517	0·350	0·123	1·14	0·61	44
39	0·475	0·300	0·225	1·27	0·52	43
40	0·510	0·236	0·254	1·17	0·31	35
41	0·596	0·283	0·121	1·02	0·35	33
42	0·344	0·284	0·372	1·30	0·60	57
43	0·390	0·237	0·373	1·18	0·44	45
44	0·441	0·198	0·361	1·13	0·284	36
45	0·278	0·223	0·499	1·14	0·49	62
46	0·300	0·163	0·537	0·91	0·33	50
47	0·365	0·153	0·482	0·99	0·24	39

In figures 9 and 10 the calculated and MacAdam's ellipses are plotted in the C.I.E. chart. There is some similarity. The orientations of the ellipses correspond rather well (figure 11), and their areas show a correlation (figure 12). The computed areas exceed MacAdam's on the average by a factor of 20·7 (4·5^2), but MacAdam's refer to standard deviations, which he estimates to be about one-third the corresponding limens. The axis ratios of the ellipses cover a range of about 2·5 to 1 and have average values 2·3 (calculated) and 2·9 (MacAdam's), but they show no correlation (figure 13).

MacAdam reports a limited number of observations for a second subject. The ratio of the g.c.l.s of the two subjects varies, for different points and directions in the chart, over a range of about 0·8 to 2·5. For colour No. 35 sufficient results are given to construct the ellipse for the second subject (figure 14*), and in table 3 the characteristics of the ellipses of the two subjects are compared.

* The plotted points in this figure were read off the smooth curves of MacAdam's figures 8 to 19, and there will be some reading error.

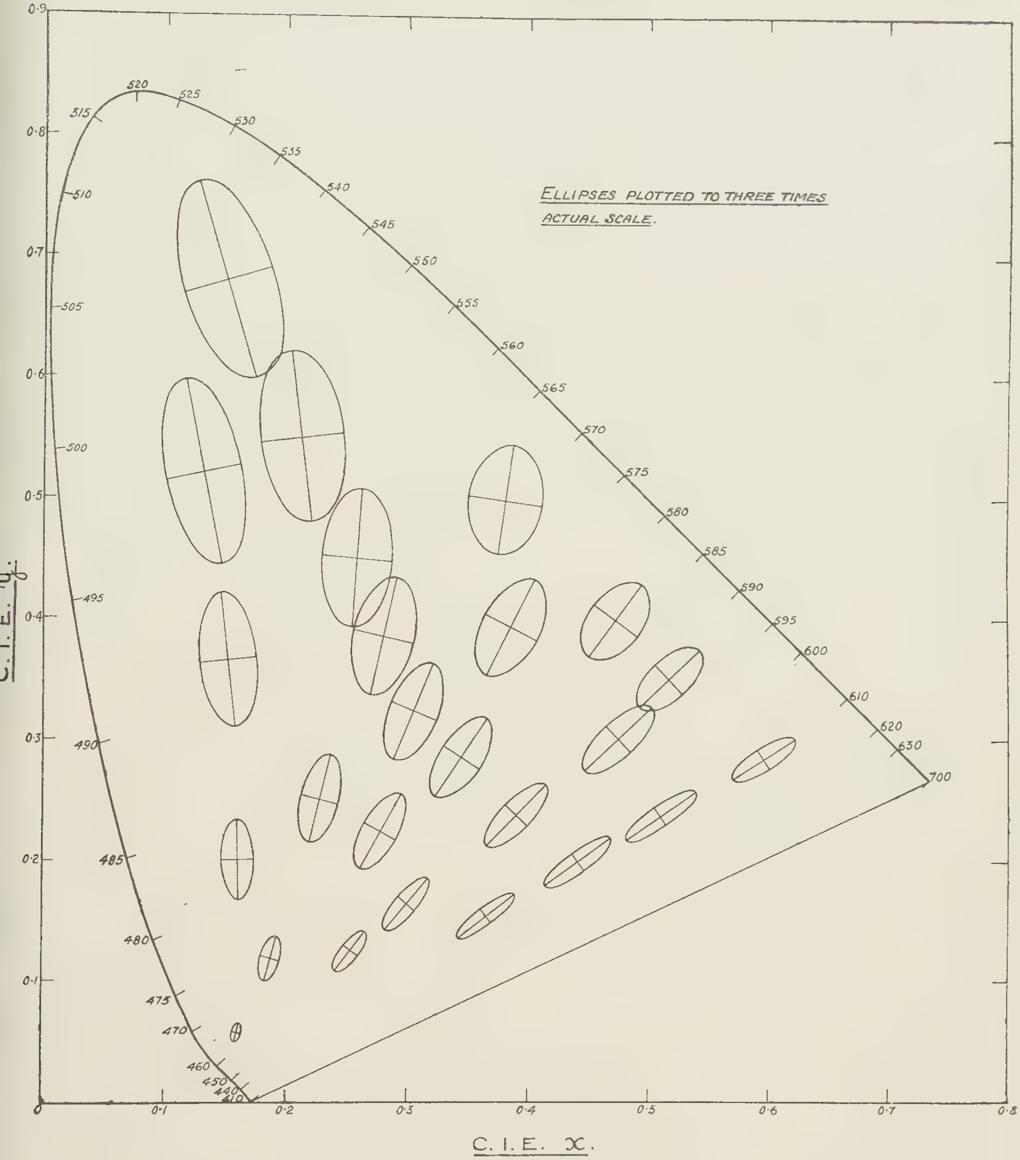

Figure 9. G.C.L. ellipses calculated from the line-element (13).

Table 3

	Major semi-axis	Minor semi-axis	Ratio of axes	Area of ellipse	Inclination of major axis to axis of x (degrees)
Principal subject (P.G.N.)	0·25 . 10^{-2}	0·086 . 10^{-2}	2·9	6·7 . 10^{-6}	70
Second subject (D.L.M.)	0·31	0·165	1·88	16·1	44

In Wright's investigation (1941), the subjects determined equal colour steps on various lines in the C.I.E. chart, and in figure 15 the logarithm of the observed colour step is plotted against distance from one end of the line for four of the principal lines studied. Wright's colour steps were not actual limens but

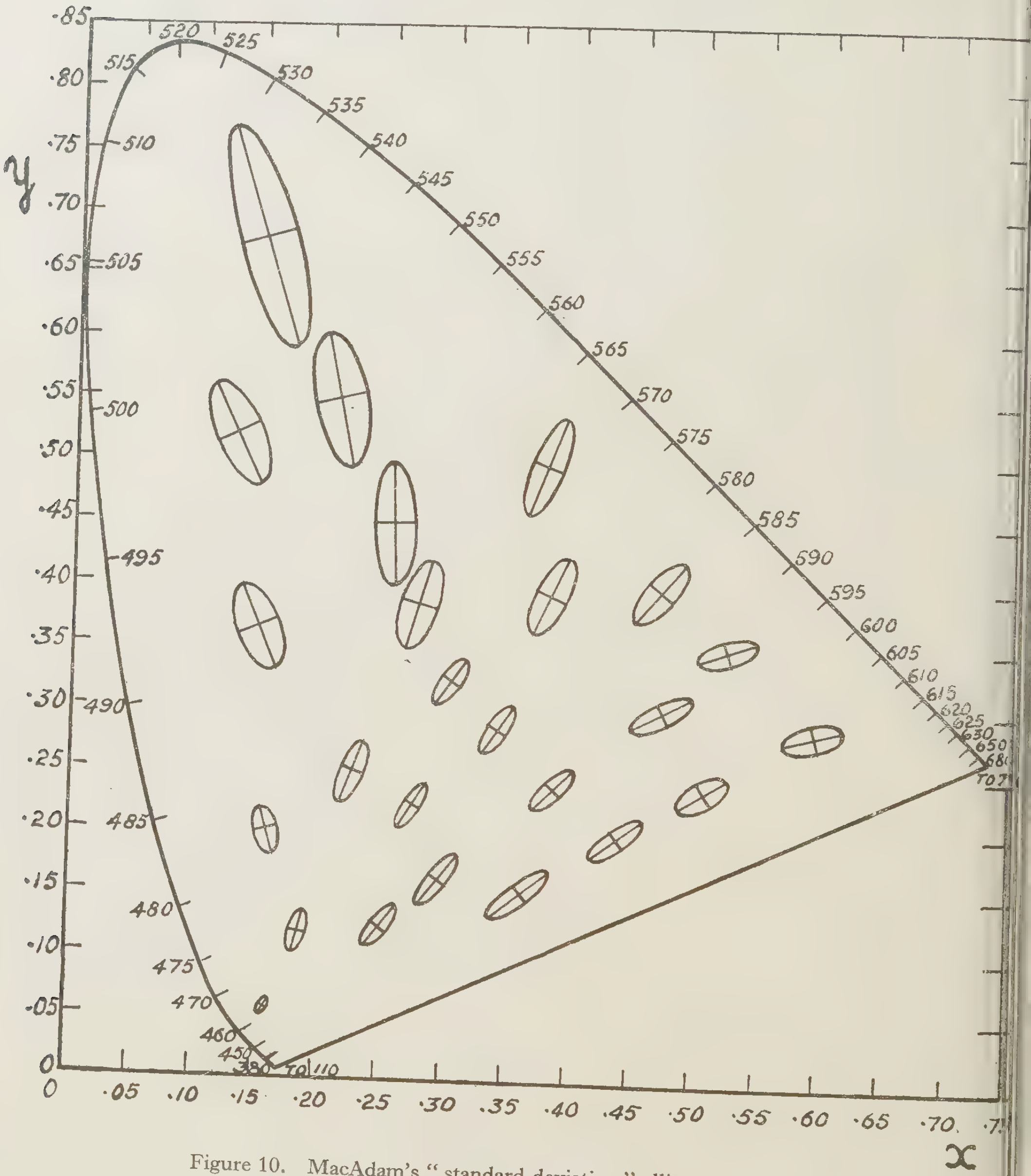

Figure 10. MacAdam's "standard deviation" ellipses for P.G.N.

"equal small colour differences"; he found that after practice a subject could maintain a reasonably steady criterion. On the average, the colour step was about three times the limen. In reporting his results, Wright reduced the steps for the four subjects to about the same average values by applying suitable constant factors: figure 15 shows the results before the application of these factors.

No direct calculations from the line-element were made for comparison with Wright's results, but a fair idea of the variations along the several lines was obtained by interpolation from the 25 computed ellipses of figure 9. A similar derivation was made from MacAdam's ellipses for P.G.N (figure 10). In figure 15 the computed colour limens times 3 are shown as the thick-line graphs and MacAdam's standard deviations times 9 as the broken-line graphs. These factors allow for the average systematic differences between small colour step and limen, limen and standard deviation, as estimated by Wright and MacAdam respectively. Admitting that these factors may differ for different subjects, and that F may also differ, it is fair to suppose the four line-element curves in figure 15 all shifted up or down by the same amount when comparing with the experimental curves of each subject. Even then there is no close agreement with

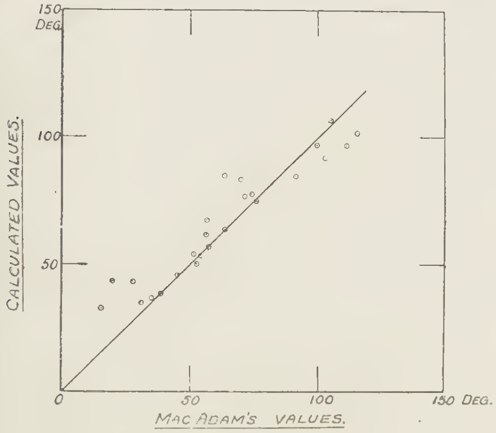

Figure 11. Inclination of the major axis of ellipse to the axis of x.

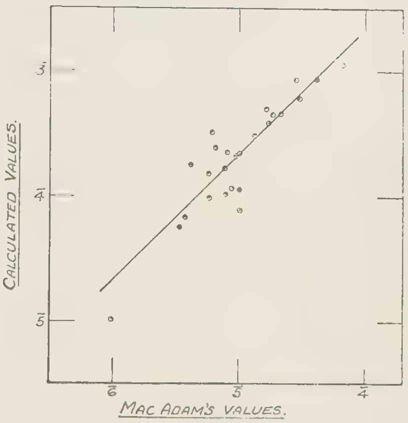

Figure 12. Log (area of ellipse).

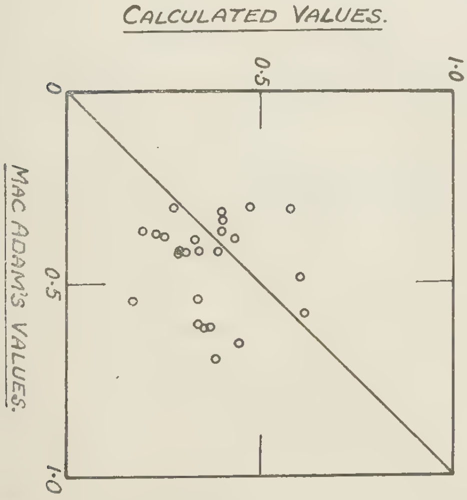

Figure 13. Log $\left(\frac{\text{major axis of ellipse}}{\text{minor axis of ellipse}}\right)$.

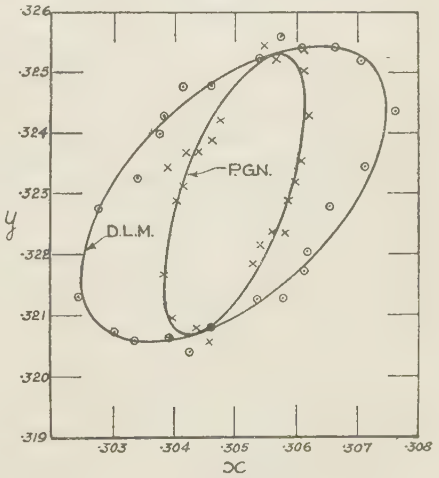

Figure 14. G.C.L. ellipses for two subjects (MacAdam).

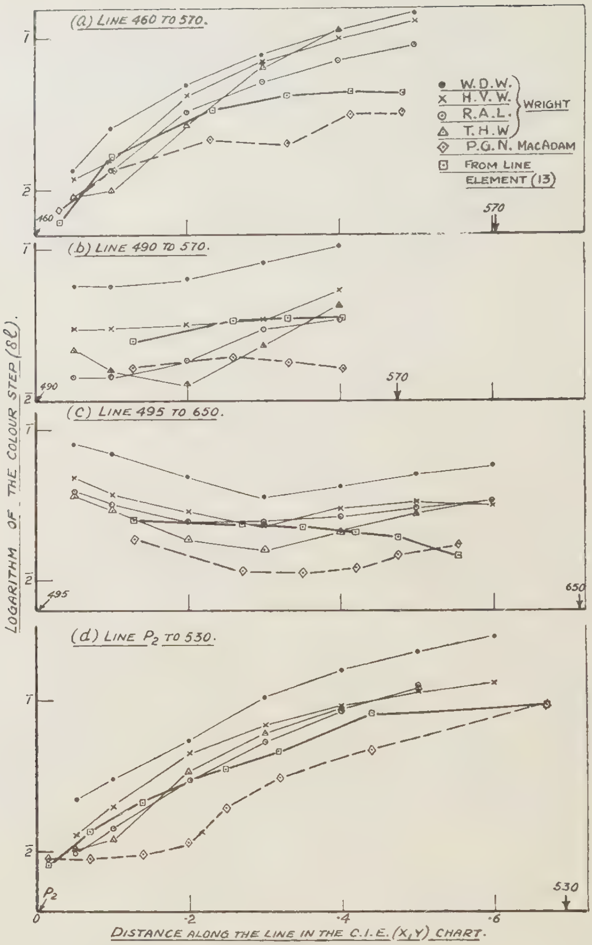

Figure 15.

the curves of any of the five subjects. It may be noted that the experimental curves of different subjects, compared in the same way, show differences which are hardly less marked.

§ 10. DISCUSSION

The line-element may be regarded as a mathematical model of the mechanism underlying a particular group of visual properties (increment threshold, colour-matching relations, visibility curve, etc.). In the Helmholtz and modified elements, the respective terms correspond to three component mechanisms, with each of which is associated a unique spectral sensitivity curve. A difference between adjacent light patches will be perceived by the action of one of these component mechanisms, say the red, if the product,

$$|\delta x|\left(\frac{\sqrt{3}}{a+x}\right)\text{(Helmholtz element)}\quad\text{or}\quad|\delta R|\left(\frac{\zeta(R)}{\rho}\right)\text{ (modified element),}$$

exceeds F. The first factor in these products is the difference of stimulation of the red mechanism in the two patches, evaluated on the basis of the red spectral-sensitivity curve. The second factor defines the sensitivity of the red mechanism in the state to which it is brought by the total stimulation, x or R, which may be taken here as approximately the same in the two patches. The product, on this view, is a measure of the response of the red mechanism to the difference of stimulation. The only interaction between the red, green and blue component mechanisms contemplated by these line-elements is a certain degree of summation of their responses, $\frac{\delta x\sqrt{3}}{a+x}$, etc., according to the sums of squares relation.

The Schrödinger element (3) is an example of the wider class represented by

$$\delta s^2 \equiv [\delta x \cdot g_x(x, y, z)]^2 + [\delta y \cdot g_y(x, y, z)]^2 + [\delta z \cdot g_z(x, y, z)]^2 = F^2. \qquad \ldots\ldots(28)$$

For line-elements in this class, the component mechanisms preserve their individuality—with each is associated a unique spectral sensitivity curve *—but they are so linked that the state of each as indicated by the sensitivity factors g_x, g_y, g_z depends on the stimulations of all three mechanisms. This linkage is additional to the summation of responses according to the sum of squares relation.

For the above elements, the axes of the small ellipsoid defined by the line-element at each point of f.c. space are parallel to the co-ordinated axes. In the more general element,

$$\delta s^2 \equiv \sum_{m,n} g_{mn}\delta x_m \delta x_n = F (m, n = 1, 2, 3), \qquad \ldots\ldots(29)$$

the axes of the elementary ellipsoids at different points are not necessarily parallel to the axes of the ellipsoid at any one point in the space, but different rotations are in general required for different points. A rotation of the axes corresponds to a change of the primaries so that on this model the spectral-sensitivity curves of the three mechanisms are progressively modified as the stimulation (defined by the position in b.c. space) is varied.

To what extent does the simple model defined by the modified line-element (13) fit the facts? The matter is complicated by the very considerable differences in the experimental results of different subjects. To be satisfactory, the line-element (13) with a particular numerical determination of R_λ, G_λ, B_λ, ρ, γ, β, F and $\zeta(p)$ should reproduce the colour-matching values, the step-by-step visibility curve, the increment and colour limens and possibly some other visual properties of a particular eye, or, more precisely, of a particular rod-free area of a given retina. Changes in the visual properties in passing from one rod-free area to another in the same or a different eye should all be accounted for at a stroke by a change in the numerical determination of the line-element. For the comparisons made in this paper, a single numerical determination has been used: for the distribution coefficients $\bar{x}$, $\bar{y}$, $\bar{z}$ the C.I.E. values, for the fundamental response curves the function defined in (15) for the limiting Fechner fractions numbers in the proportion 0·78 : 1 : 4·46, and for F the value 0·01. While certain main features of the experimental results are reproduced, satisfactory quantitative agreement with the measurements of all the visual properties for some particular subject has not been demonstrated. In fact no such complete set of measurements is available. For the restricted group of

---

* Except in the degenerate case when any two of g_x, g_y, g_z stand in a constant ratio.

colour-limen measurements, the comparisons made (figures 8 to 15) show differences which could no doubt be reduced by a different numerical determination of the line-element for each subject. But in the case of MacAdam's subject P.G.N. it can be shown that complete agreement could not be reached by any change in which the fundamental response functions R_λ, G_λ, B_λ remained always positive, linear forms in the C.I.E. distribution coefficients. (See Appendix.) Our conclusion must be that the modified line-element, constructed to suit measurements of increment limens, leads to the right kind of step-by-step visibility curve, but is in difficulties when applied to measurements of colour limens.

§ 11. ACKNOWLEDGMENT

This paper is published by permission of the Director of the National Physical Laboratory.

APPENDIX

The Gaussian curvature of the surface of constant C.I.E. brightness according to the modified line-element

Following Silberstein (1943), the unit C.I.E. co-ordinates x, y for colours of a given constant C.I.E. brightness can be regarded as curvilinear co-ordinates on a surface embedded in a three-dimensional Euclidean space, the distance apart of neighbouring points on this surface being defined by the expression for the line-element δs. This expression, for the modified line-element, is the square root of the right-hand side of equation (27). Silberstein uses an empirical expression for δs derived from MacAdam's measurements for the subject P.G.N. (figure 10), and shows that the Gaussian curvature K of the surface is not only not constant, but that it is positive in some areas, negative in others.

The Gaussian curvature is invariant to transformations, linear or non-linear, of the co-ordinates x, y, and it is permissible to employ R, G in place of x, y. For the modified line-element, an expression for K is obtained quite easily if we accept for $\zeta(p)$ the approximation $\dfrac{9}{1+9p}$, to which it reduces when p exceeds 1. This corresponds to using curve $\eta(p)$ instead of curve $\xi(p)$ (figure 2). K is then given by

$$K=\frac{\rho^2\gamma^2\beta^2(1+9R)(1+9G)(1+9B)v_r v_g v_b(9y'+v_r+v_g+v_b)}{[\rho^2 v_r{}^2(1+9R)^2+\gamma^2 v_g{}^2(1+9G)^2+\beta^2 v_b{}^2(1+9B)^2]^2}, \quad \ldots\ldots(30)$$

where $y'=v_r R+v_g G+v_b B=\text{const.}$ This condition is obtained by solving the equation (25) for x', y', z' ; it expresses the fact that the colours considered all have a constant C.I.E. brightness (equal to $2{\cdot}19\ .\ 10^5\,y'$ photons).

Since for real colours R, G and B are all positive, it is clear that the Gaussian curvature will have the same sign at all points of the surface of constant C.I.E. brightness.

Computation gives

$$\begin{aligned} v_r &= 2{\cdot}70\times10^{-4}\\ v_g &= 4{\cdot}07\times10^{-4}\\ v_b &= -4{\cdot}76\times10^{-5}\\ v_r+v_g+v_b &= 6{\cdot}29\times10^{-4}. \end{aligned}$$

Thus $v_r v_g v_b(9y' + v_r + v_g + v_b)$, and hence K, is negative for any value of y', i.e. for any C.I.E. brightness.

It follows that the modified line-element is inconsistent with MacAdam's results for P.G.N., which for different colours yield K values of opposite sign. This inconsistency persists however ρ, γ, β be chosen and whatever change be made in the fundamental response curves R_λ, G_λ, B_λ provided these remain linear forms in the C.I.E. distribution coefficients, and lead to all positive co-ordinates R, G, B for real colours.

REFERENCES

Coblenz, W. W. and Emerson, W. B., 1917. *Sci. Pap. U.S. Bur. Stand.* No. 303.
Gibson, K. S. and Tyndall, E. P. T., 1923. *Sci. Pap. U.S. Bur. Stand.* No. 475.
Hecht, S., 1932. *Discussion on Vision*, Phys. and Opt. Societies, 126.
Helmholtz, H. von, 1891. *Z. Sinnesphysiol.* 3, 517.
König, A. and Dieterici, C., 1884. *Ann. Phys., Lpz.*, **22**, 579.
MacAdam, D. L., 1942. *J. Opt. Soc. Amer.* **32**, 247.
Priest, I. G. and Brickwedde, F. G., 1926. *J. Opt. Soc. Amer.* **13**, 306.
Schrödinger, E., 1920. *Ann. Phys., Lpz.*, 63.
Silberstein, L., 1943. *J. Opt. Soc. Amer.* **33**, 1.
Stiles, W. S., 1939. *Proc. Roy. Soc.* B, **127**, 64.
Walters, H. V. and Wright, W. D., 1943. *Proc. Roy. Soc.* B, **131**, 340.
Wright, W. D., 1936. *J. Physiol.* **87**, 23.
Wright, W. D., 1941. *Proc. Phys. Soc.* **53**, 93.
Wright, W. D. and Pitt, F. H. G., 1934. *Proc. Phys. Soc.* **46**, 459.

ON DECENTRED ASPHERIC PLATES

By E. H. LINFOOT,
University of Bristol

MS. received 31 *May* 1945

ABSTRACT. The main purpose of the paper is to discuss the effects of errors of centring on the optical performance of plate-mirror systems. Such errors may occur during the aspheric grinding of the plates and also in the lining up of the system. It is first shown that if a grinding technique is used which builds up the asphericity at a proportionately equal rate all over the surface, the result of a large number of small centring errors at different stages of the grinding is very nearly equivalent to a simple decentring of the asphericity on the surface, combined with a small amount of primary astigmatism. Next, general formulae are obtained for the effects on the Seidel errors of a centred system of decentring and tilting its components, and it is shown that in the case of a plate-mirror system the formulae can be used to estimate the practical tolerances for disturbances of this kind. Lastly, the general formulae are applied to discuss the lining up of a two-sphere one-plate Schmidt-Cassegrain camera.

§1. EFFECT OF ERRORS IN GRINDING

In the construction and use of plate-mirror systems, problems of centring are met with at two stages. The first is during the actual aspherizing of the surfaces; the second during the lining up of the system. An error in centring at the first stage will in general lead to an asymmetrical error in the figure of the surface. This will result in a slight change in the centring chosen for the surface when the complete system comes to be lined up, for the centring chosen will be that at which the optical effect of the asymmetry appears as small as possible. Thus the practical effect of the asymmetry depends not so much on its actual amount as on the extent to which it cannot be compensated by lateral shift of the surface which bears it.

Broadly speaking, the most successful methods of figuring aspheric plates are those in which the asphericity is built up at a proportionately equal rate all over the surface. One such method, well suited to the resources of the amateur astronomer, has been described in an ably written paper by H. W. Cox (1939). It depends on the use of a flexible grinding lap consisting of lead facets arranged in petal-shaped areas on a Sorbo rubber backing, operated by a mechanical traverse. The lap is traversed in short, fairly rapid strokes as the plate slowly rotates. With such an arrangement, asymmetry arising from random variations in the stroke is eliminated for all practical purposes, and inaccuracy of centring of the plate in its holder, or of the plate-holder on its spindle, becomes a potentially important source of error.

To estimate the practical effect of errors arising in this way, we observe that if the grinder is adjusted to generate a true curve, with only small relative errors, whose depth increases at proportionately equal rates all over the surface, then the effect of having the plate wrongly centred for part of the time is to contribute a weak "Schmidt plate" with displaced centre to the figure instead of adding its strength to the main (i.e. truly centred) figuring.

Suppose that m errors of this type are made and that the plate is centred by trial in the final assembly. The plate figure is then the sum of m figurings, each with a slight decentring, whose strengths together make up the full plate-strength B. We can investigate the properties of such a plate by applying the methods of Conrady (1919).

The deviation (Δx, Δy) of the point of intersection with the Petzval surface of the ray through the point P with polar co-ordinates (S, E) in the entry pupil is given in the case of pure primary spherical aberration by

$$\Delta x = BS^3 \cos E, \qquad \Delta y = BS^3 \sin E,$$

where the coefficient B measures the amount of the aberration. From a decentred spherical aberration of centre (ξ_r, η_r) and amount B_r we therefore have deviation-contributions

$$\Delta x = B_r S_r^3 \cos E_r, \qquad \Delta y = B_r S_r^3 \sin E_r,$$

where (see figure 1)

$$S_r \cos E_r = S \cos E - \xi_r, \qquad S_r \sin E_r = S \sin E - \eta_r\,;$$
$$S_r^2 = S^2 - 2S(\xi_r \cos E + \eta_r \sin E) + (\xi_r^2 + \eta_r^2).$$

If ξ_r, η_r are so small that their squares can be neglected, the deviation-contributions can be written

$$\begin{aligned}\Delta x &= B_r[S^2 + (\xi_r^2 + \eta_r^2) - 2S(\xi_r \cos E + \eta_r \sin E)](S \cos E - \xi_r)\\ &= B_r S^3 \cos E - B_r \xi_r S^2 (2 + \cos 2E) - B_r \eta_r S^2 \sin 2E,\\ \Delta y &= B_r S^3 \sin E - B_r \xi_r S^2 \sin 2E - B_r \eta_r S^2 (2 - \cos 2E),\end{aligned}$$

and the total deviations effected by the plate are accordingly

$$\Delta x = \left(\sum_{r=1}^{m} B_r\right) S^3 \cos E - \left(\sum_{r=1}^{m} B_r\xi_r\right) S^2(2+\cos 2E) - \left(\sum_{r=1}^{m} B_r\eta_r\right) S^2 \sin 2E,$$

$$\Delta y = \left(\sum_{r=1}^{m} B_r\right) S^3 \sin E - \left(\sum_{r=1}^{m} B_r\xi_r\right) S^2 \sin 2E - \left(\sum_{r=1}^{m} B_r\eta_r\right) S^2(2-\cos 2E), \qquad \ldots\ldots(1)$$

i.e. are those corresponding to primary spherical aberration of amount $B = \sum_{r=1}^{m} B_r$, together with a coma contribution which is measured by the sum of the vectors $B_r(\xi_r, \eta_r)$. This coma will be annulled if the plate is given a lateral displacement (Ξ, H), where

$$B\Xi = -\sum_{r=1}^{m} B_r\xi_r, \qquad B\mathrm{H} = -\sum_{r=1}^{m} B_r\eta_r, \qquad \ldots\ldots(2)$$

when the system is assembled. Since the plate will in practice be centred by trial, such a displacement will be given automatically. The largest errors then remaining are the second-order terms (neglected above), and, as will appear later, these give rise to astigmatism, in second-order small quantity, uniform over the image-field.

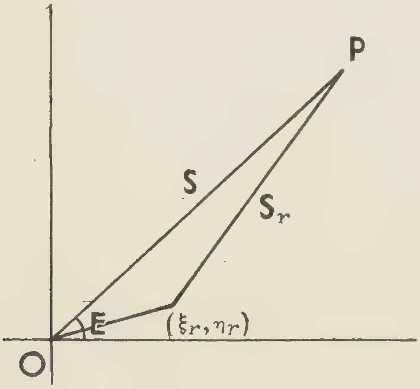

Figure 1.

In certain important cases* this astigmatism also can be compensated by adjustments of the components perpendicular to the axis ; it follows that in these cases a first-order centring error in aspherical grinding, *provided it is of the type specified above*, leads only to errors of the third order of small quantities in the finally adjusted system, i.e. to extra terms in the expressions for the displacements Δx, Δy in the final system whose coefficients are third-order small quantities. Such terms have no perceptible effect on the physical image in many practical cases. In general, a second-order amount of astigmatism remains after the coma has been removed by empirical plate-adjustment.

The general conclusion is that, provided the grinding is arranged so as to generate the asphericity at proportionately equal rates all over the surface, the effect of the centring errors, which must always be present in some degree, is far less serious than might appear at first sight. It seems likely that this circumstance plays a large part in determining the success or failure of a grinding technique.

---

* For example, in the monocentric Schmidt-Cassegrain systems and in the two-plate Schmidt-Cassegrains.

§ 2. EMPIRICAL LINING-UP OF A CENTRED OPTICAL SYSTEM

Consider the "equivalent plate system".* Let B_1, $B_2 \ldots, B_n$ be the plate-strengths; $\sigma_1, \sigma_2 \ldots . \sigma_n$ the respective distances of the (real or virtual) plates in front of the entry pupil; (ξ_1, η_1), (ξ_2, η_2), $\ldots . (\xi_n, \eta_n)$ their respective lateral displacements. For the present, we suppose the components of the system to be free from errors of figure.

Then, as before, the displacement-contribution from the first plate to the intersection with the Petzval surface of a ray, originally parallel to the axis, through the point of the entry pupil whose polar co-ordinates are (S, E), is

$$\Delta x = B_1 S_1{}^3 \cos E_1, \qquad \Delta y = B_1 S_1{}^3 \sin E_1,$$

where

$$S_1 \cos E_1 = S \cos E - \xi_1, \qquad S_1 \sin E_1 = S \sin E - \eta_1,$$
$$S_1{}^2 = S^2 + (\xi_1{}^2 + \eta_1{}^2) - 2S(\xi_1 \cos E + \eta_1 \sin E).$$

Thus

$$\begin{aligned}\Delta x &= B_1[S^2 + (\xi_1{}^2 + \eta_1{}^2) - 2S(\xi_1 \cos E + \eta_1 \sin E)][S \cos E - \xi_1] \\ &= B_1[S^3 \cos E - S^2(\xi_1(2 + \cos 2E) + \eta_1 \sin 2E) \\ &\qquad + S((3\xi_1{}^2 + \eta_1{}^2) \cos E + 2\xi_1\eta_1 \sin E) - \xi_1(\xi_1{}^2 + \eta_1{}^2)], \\ \Delta y &= B_1[S^3 \sin E - S^2(\xi_1 \sin 2E + \eta_1(2 - \cos 2E)) \\ &\qquad + S((\xi_1{}^2 + 3\eta_1{}^2) \sin E + 2\xi_1\eta_1 \cos E) - \eta_1(\xi_1{}^2 + \eta_1{}^2)].\end{aligned}$$

If we write

$$\xi_1 + i\eta_1 = \rho_1 e^{i\phi_1},$$

these equations can be given the more compact form

$$\begin{aligned}\Delta x + i\Delta y = B_1 e^{i\phi'}[S^3 e^{i(E-\phi_1)} &- S^2\rho_1(2 + e^{2i(E-\phi_1)}) \\ &+ S\rho_1{}^2 e^{i(E-\phi_1)}(2 + e^{2i(E-\phi_1)}) - \rho_1{}^3].\end{aligned}$$

For the complete plate-system we therefore have, in Seidel approximation,

$$\begin{aligned}\Delta x + i\Delta y = S^3 e^{iE} \sum_{r=1}^{n} B_r &- S^2\left(2\sum_{r=1}^{n} B_r\rho_r e^{i\phi_r} + e^{2iE}\sum_{r=1}^{n} B_r\rho_r e^{-i\phi_r}\right) \\ &+ S\left(2e^{iE}\sum_{r=1}^{n} B_r\rho_r{}^2 + e^{-iE}\sum_{r=1}^{n} B_r\rho_r{}^2 e^{2i\phi_r}\right) - \sum_{r=1}^{n} B_r\rho_r{}^3 e^{i\phi_r}, \qquad \ldots\ldots (3)\end{aligned}$$

where B_r denotes the strength of the rth plate and $\rho_r e^{i\phi_r} = \xi_r + i\eta_r$ its lateral displacement. Here Δx, Δy measure the lateral displacements in the Petzval surface and $B_1, B_2, \ldots\ldots$ measure the plate-strengths, both in suitable units. The connection between the two sets of units can be expressed by saying that if for the unit of plate-strength we choose the strength of the Schmidt plate of a concave spherical mirror of paraxial focal length f_1, then the actual linear displacements δx, δy in the Petzval surface are obtained on multiplying Δx, Δy by $f/8f_1{}^3$, where f is the focal length of the system.

---

* In the sense of the method of plate-diagram analysis. *See* C. R. Burch, *Mon. Not. R. Astr. Soc.* **102,** 159–165 (1942); E. H. Linfoot, *ibid.* **104,** 48–64 (1944), for an account of this method.

The first three terms on the right-hand side of equation (3) are easily recognized, on separating them into real and imaginary parts once more, as arising respectively from spherical aberration, coma, and astigmatism combined with change of focus. The fourth term, being independent of E and S, represents a lateral shift of the image as a whole.

We shall suppose the system designed so that $\sum_{r=1}^{n} B_r = 0$, i.e. spherically corrected. Then the conditions for the axial image to be error-free are, if we do not permit a change of focus,

$$\sum_{r=1}^{n} B_r\rho_r e^{i\phi_r} = 0, \qquad \sum_{r=1}^{n} B_r\rho_r^2 e^{2i\phi_r} = 0, \qquad \sum_{r=1}^{n} B_r\rho_r^2 = 0. \quad \ldots\ldots (4)$$

In practice, however, the focus is usually determined empirically and the term $2Se^{iE}\sum_r B_r\rho_r^2$ will not show itself as a defect in the image. It follows that the conditions to be satisfied are

$$\sum_{r=1}^{n} B_r = 0, \qquad \sum_{r=1}^{n} B_r\rho_r e^{i\phi_r} = 0, \qquad \sum_{r=1}^{n} B_r\rho_r^2 e^{2i\phi_r} = 0. \quad \ldots\ldots (5)$$

We can express this result as follows : *If the (real or virtual) elements of the plate-system associated with an optical system are given lateral displacements* $\boldsymbol{v}_1, \boldsymbol{v}_2 \ldots$ *($\boldsymbol{v}$ a vector) satisfying the conditions*

$$\sum_r B_r\boldsymbol{v}_r = 0, \qquad \sum_r B_r\boldsymbol{v}_r^2 = 0, \qquad \ldots\ldots (6)$$

the axial image will not develop spherical aberration, coma or astigmatism. It will be laterally displaced by an amount proportional to $\sum_r B_r|\boldsymbol{v}_r|^2\boldsymbol{v}_r$ *and will be moved along the axis, away from the system, through a distance proportional to* $2\sum_r B_r|\boldsymbol{v}_r^2|$.

Equation (3) gives a simple proof of the property, mentioned in § 1, that when a plate suffering from errors of figure of the type there described is centred empirically, the residual error is effectively primary astigmatism, in second-order small quantity. It is only necessary to set $\sigma_1 = \sigma_2 \ldots . \sigma_m$ in the present discussion ($\sigma_{m+1}, \ldots . \sigma_n$ remaining arbitrary) and to observe that the operation of centring the plate empirically is expressed by adding to each of $\rho_1 e^{i\phi_1}, \ldots . \rho_m e^{i\phi_m}$ the complex constant

$$\alpha = -\sum_{r=1}^{n} B_r\rho_r e^{i\phi_r} \Big/ \sum_{r=1}^{m} B_r.$$

After this operation, the coefficient of S^2 in (3) vanishes and the third term becomes the leading term.

Off-axis images

To determine the effect on the off-axis errors of a system of decentring its plates, we consider a parallel beam coming in at an angle V with the axis, the azimuth of this angle being χ. The principal ray meets a plane distant σ in fron of the entry pupil in the point

$$X = \sigma V \cos\chi, \qquad Y = \sigma V \sin\chi,$$

and the effect of the plate is, therefore, the same (in Seidel approximation) as if it were situated in the entry-pupil but with a lateral displacement $(-\sigma V\cos\chi, -\sigma V\sin\chi)$, and the pencil were parallel to the axis.* It follows that the off-axis errors for laterally displaced plates are obtained on replacing (ξ_r, η_r) by $(\xi_r-\sigma_r V\cos\chi, \eta_r-\sigma_r V\sin\chi)$ in (3). Set

$$\xi_r-\sigma_r V\cos\chi=P_r\cos\Phi_r, \qquad \eta_r-\sigma_r V\sin\chi=P_r\sin\Phi_r,$$

which gives

$$P_r e^{\pm i\Phi_r}=\rho_r e^{\pm i\phi_r}-\sigma_r V e^{\pm i\chi},$$

and we obtain in place of (3) the equation

$$\Delta x+i\Delta y=S^3e^{iE}\sum_{r=1}^{n}B_r-S^2\left(2\sum_{r=1}^{n}B_rP_re^{i\Phi_r}+e^{2iE}\sum_{r=1}^{n}B_rP_re^{-i\Phi_r}\right)$$
$$+S\left(2e^{iE}\sum_{r=1}^{n}B_rP_r^2+e^{-iE}\sum_{r=1}^{n}B_rP_r^2e^{2i\Phi_r}\right)-\sum_{r=1}^{n}B_rP_r^3e^{i\Phi_r}. \qquad \ldots\ldots(7)$$

The four terms of this new equation have the same significance as before, and they now specify the spherical aberration, coma, astigmatism with change of focus, and lateral displacement† at any point of the image-field of the system with decentred plates.

We assumed above that the optical components were free from errors of figure. The same analysis suffices, however, to cover the more general case where the plates suffer from errors of figure of the type discussed in § 1. It is only necessary to represent each plate as a cluster of mutually decentred, error-free component-plates held rigidly in contact, and to apply (7) to the system of component-plates so obtained.

An inspection of the terms on the right of (7) enables us to draw one or two general conclusions about the effect of these errors of figure on the performance of an empirically lined up system.

Since the first term $S^3e^{iE}\sum_r B_r$, which represents the spherical aberration, does not involve V or the quantities ρ_r, ϕ_r, it follows that the spherical aberration of the system is unaffected by the errors and remains constant all over the field.

The second term, which represents the coma, falls into two parts :

$$-S^2(2\sum_r B_re^{i\Phi_r}+e^{2iE}\sum_r B_rP_re^{-i\Phi_r})$$
$$=-S^2(2\sum_r B_r\rho_re^{i\phi_r}+e^{2iE}\sum_r B_r\rho_re^{i\phi_r})$$
$$+S^2V(2e^{i\chi}+e^{2iE-i\chi})\sum_r B_r\sigma_r. \qquad \ldots\ldots(8)$$

The second part represents off-axis coma of the usual kind, and vanishes identically if, as we suppose, the system is designed to satisfy the aplanatism condition $\sum_r B_r\sigma_r=0$. The first part does not depend on V or χ, and so represents a coma uniform over the whole field, which can be eliminated by a lateral shift of any one of the plates in the plate-system, or of several plates together, so as to secure the fulfilment of the condition $\sum_r B_r P_r e^{i\Phi_r} = 0$.

---

* The effect of the small relative tilt between plate and off-axis pencil is zero in Seidel approximation.

† The last term is associated with the distortion of the system, but does not by itself measure the distortion. See *Mon. Not. R. Astr. Soc.* **104,** 49 (1944).

The third term,

$$\begin{aligned}
&S(2e^{iE}\sum_r B_r P_r^2 + e^{-iE}\sum_r B_r P_r^2 e^{2i\Phi_r}) \\
&\quad = S(2e^{iE}\sum_r B_r \rho_r^2 + e^{-iE}\sum_r B_r \rho_r^2 e^{2i\phi_r}) \\
&\qquad - 2SV(2e^{iE}\sum_r B_r \rho_r \sigma_r \cos(\phi_r - \chi) + e^{-iE}\sum_r B_r \rho_r \sigma_r e^{i(\phi_r + \chi)}) \\
&\qquad\quad + SV^2(2e^{iE} + e^{2i\chi - iE})\sum_r B_r \sigma_r^2, \qquad \ldots\ldots (9)
\end{aligned}$$

represents astigmatism and focus shift.* It falls into three parts, in accordance with (9) ; the third part contains the ordinary off-axis astigmatism of the system, which vanishes in systems (the so-called Seidel anastigmats) in which $\sum_r B_r \sigma_r^2 = 0$. The remaining parts represent the effect of the decentring ; we shall consider them in more detail, in the next section, in the particular case of a three-plate system.

Finally, the fourth term,

$$\begin{aligned}
&\sum_r B_r P_r^3 e^{i\Phi_r} = \sum_r B_r P_r e^{i\Phi_r} | P_r e^{i\Phi_r} |^2 \\
&\quad = \sum_r B_r \rho_r^3 e^{i\phi_r} - V\sum_r B_r \rho_r^2 \sigma_r (2e^{i\chi} + e^{2i\phi_r - i\chi_r}) \\
&\qquad + V^2 \sum_r B_r \rho_r \sigma_r^2 (2e^{i\phi_r} + e^{2i\chi - i\phi_r}) \\
&\qquad\quad - V^3 e^{i\chi}\sum_r B_r \sigma_r^3, \qquad \ldots\ldots (10)
\end{aligned}$$

which represents the plate-contribution to the distortion of the system, remains independent of S and E when the plates are decentred, and so does not affect the sharpness of the images. But it does depend on V and on the quantities ρ_r, ϕ_r, so that, as was pointed out by Conrady in the paper already referred to, a system lined up to give satisfactory images may still contain centring errors which appreciably modify its distortion.

The above analysis applies in principle to ordinary lens systems with spherical surfaces ; their associated plate systems, to which we can apply (7), consist entirely of virtual plates. But the application is not very satisfactory in the case of wide-aperture lens systems, since in these the Seidel theory is far from giving a true picture of the image-errors, especially in the outer parts of the field. In its application to plate-mirror systems of the Schmidt-Cassegrain type, however, the theory supplies information of practical value even at nominal apertures as high as F/2. This different state of affairs can be attributed to the much smaller size of the fifth-order error-coefficients which results when mirrors are used in place of lenses as optical power-surfaces, together with the circumstance that vignetting restricts the field diameter of an F/2 Schmidt-Cassegrain to something less than 15°.

---

* An incidental advantage of the complex notation used in this section is that the terms representing focus-shift appear separated from those representing astigmatism. The former are the terms in Se^{iE}, the latter those in Se^{-iE}.

§ 3. APPLICATION TO SCHMIDT-CASSEGRAIN CAMERAS

As a practical example, we consider the lining-up of a Schmidt-Cassegrain camera consisting of two spherical mirrors and one aspheric plate. The general appearance of such a system is shown in figure 2.

The optical lining-up of a correctly figured system of this type can be carried out as follows :

(*a*) place the primary mirror M_1 symmetrically in its mounting by measurement ;

(*b*) place the plate P at the measured distance from M_1 and centre it by measurement ;

(*c*) move the secondary mirror M_2 along the axis, keeping it roughly centred, until spherical aberration is zero, when P is moved laterally so as to annul coma, and thus allow the spherical aberration to be observed ;

(*d*) *tilt* M_2, readjusting P laterally each time, until the astigmatism is zero on axis ;

(*e*) move P along the axis until the coma remains zero for small image-displacements off axis.

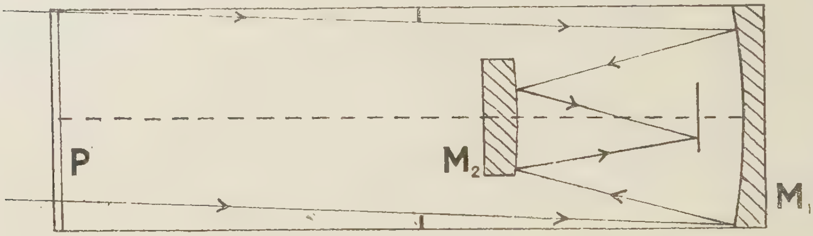

Figure 2.

The system is then in " Seidel adjustment ". This adjustment must now be altered, by an amount which depends on the field to be covered, in order to balance the higher errors by suitable amounts of opposing Seidel error over the required field.

In the monocentric Schmidt-Cassegrains, the change consists in moving M_2 and P along the axis to balance the lateral spherical aberration against primary spherical aberration, while keeping the coma zero. This gives a system which is extremely close to a monocentric system. The last operation is always to adjust P laterally to bring the coma to zero on axis. In the flat-fielded aplanats, the compromises to be made are of a more complicated nature.

In a practical case, however, the plate-figure usually contains a little primary astigmatism arising (in the manner already described) from centring errors during grinding. The amount of this astigmatism can be kept within tolerable limits by the use of proper precautions during the aspherizing process. For example, the plate of an F/2 Schmidt-Cassegrain system might be regarded as satisfactory if the astigmatic confusion-circle corresponding to its astigmatism of figure did not exceed $^1/_{5000}$ inch in diameter. But the presence of this astigmatism complicates the task of lining up the system ; if the above procedure be adopted it results in a decentred line-up which Seidel theory and experiment agree in condemning as unsatisfactory in most cases because of its effect on the images in the outer parts of the field.* It is therefore better to begin by placing the two mirrors M_1, M_2 in correct alignment by mechanical means (with provision for varying the position of M_2 along the axis) and to confine the empirical adjustments to operations (*c*), (*e*) and the annulling of coma by lateral plate-shift.

The question then arises, how accurate the mechanical alignment of M_1 and M_2 needs to be. We shall investigate this by applying the general formulae of the last section. To be of practical value, the investigation must take account of the higher aberrations as well as the Seidel properties of the system. In the case of wide-aperture lens systems, where the higher aberrations have to be carefully compensated over a relatively large field, a general theoretical discussion of centring tolerances would seem to be hardly practicable at the present time, since it would at once involve us in the formidable analytical complications of fifth-order optics. We should need to rely instead upon conclusions drawn from experiment, and these conclusions would only remain valid for systems very close in design to those on which the experimental observations had been made. In the case of the Schmidt-Cassegrain systems, comprising only three or four effective optical surfaces and working over a smaller field, high definition is a consequence of the intrinsic smallness of the higher aberrations of each element rather than of their mutual compensation.† A small error in the lining up of the system therefore results in only a small percentage change in the amounts of its higher aberrations. Since the Seidel coma and the primary spherical aberration are under continuous control,‡ it is the size of these higher aberrations which determines the actual confusion-spreads in a Seidel anastigmat (or near-anastigmat) in correct adjustment. It follows that small centring errors will not markedly affect the confusion-spreads of a Schmidt-Cassegrain system provided that their contribution to the Seidel errors is small compared with the image-spreads of the correctly adjusted system. A more convenient formulation, practically equivalent to the first, is that the centring errors can be tolerated if their Seidel contribution to the displacement $\Delta x + i\Delta y$ is everywhere small compared with the allowed upper limit to the size of this quantity for the system.

We can obtain a reasonable estimate of the amount of decentring which can be tolerated in the line-up of the secondary mirror of a Schmidt-Cassegrain camera by laying down that the resulting final disturbance $\delta x + i\delta y$ of the Seidel displacement-vector in the Petzval surface must nowhere exceed one fifth of the allowed image-spread for the system. In a practical case, the allowed image-spread might be 0·001 inch, and the tolerance would then be given by the condition

$$|\delta x + i\delta y| < \frac{1}{5000}\,\text{inch}$$

over the whole field.

---

* The monocentric Schmidt-Cassegrains are to a certain extent an exception to this rule.

† Higher spherical aberration (zonal aberration) appears as an exception to this statement, inasmuch as it is usually fully compensated in the plate-figuring. But this aberration also is intrinsically very small, as can be shown in a striking manner in a particular case by removing the secondary mirror of an F/2 two-sphere aplanat, placing the plate in contact with the primary and Foucault-testing the pair with a pinhole at an adjustable distance along the axis. When the pinhole-distance is suitably chosen, the residual spherical aberration is found to be scarcely detectable with the knife-edge.

‡ They can be varied at will by altering the spacings of the components.

The disturbance of the Seidel properties due to centring errors in the line-up can be calculated from the general formulae of the last section as soon as the errors have been expressed in terms of displacements of the elements in the associated plate system. To do this, we image the surface-figurings, aspheric plates and missing Schmidt plates of the system through into object-space in the usual way, taking account of the errors in tilt and in lateral adjustment of the mirrors when calculating the images according to Gaussian optics. The associated plate system thus obtained has its elements laterally displaced and tilted. The tilts of the elements have no effect on the Seidel aberrations and are therefore disregarded ; their lateral displacements are a set of parameters which describe, sufficiently fully for the present purpose, the errors in the line-up of the original system.

A Schmidt-Cassegrain with both mirrors spherical is a "three plate system" ; that is to say, its plate-diagram consists of three plates and an aperture stop. Two of these plates are virtual ; they are the missing anastigmatizing plate P_1 of the primary M_1, and the image P_2 in M_1 of the missing anastigmatizing plate of M_2 (both with strengths reversed, since the plates are missing). The third plate P_3 is the glass aspheric plate P of the system.

In the aplanats, the plate-strengths B_1, B_2, B_3 and the distances σ_1, σ_2, σ_3 of the plates in front of the aperture-stop satisfy the relations *

$$B_1+B_2+B_3=0, \qquad B_1\sigma_1+B_2\sigma_2+B_3\sigma_3=0, \qquad \ldots\ldots(11)$$

while the off-axis astigmatism is proportional to

$$B_1\sigma_1{}^2+B_2\sigma_2{}^2+B_3\sigma_3{}^2. \qquad \ldots\ldots(12)$$

Taking M_1 as defining the axis of the system by means of the normal through its pole, we set $\rho_1=0$ in the general formulae (8), (9), which then become, for an off-axis beam of azimuth χ,

Coma :

$$-S^2[2B_2\rho_2e^{i\phi_2}+2B_3\rho_3e^{i\phi_3}+e^{2iE}(B_2\rho_2e^{-i\phi_2}+B_3\rho_3e^{-i\phi_3})]. \qquad \ldots\ldots(13)$$

Astigmatism and focus-shift :

$$\begin{aligned} &S[2e^{iE}(B_2\rho_2{}^2+B_3\rho_3{}^2)+e^{-iE}(B_2\rho_2{}^2e^{2i\phi_2}+B_3\rho_3{}^2e^{2i\phi_3})] \\ &\quad -2SV[2e^{iE}\{B_2\rho_2\sigma_2\cos(\phi_2-\chi)+B_3\rho_3\sigma_3\cos(\phi_3-\chi)\} \\ &\qquad\qquad +e^{-iE+i\chi}\{B_2\rho_2\sigma_2e^{i\phi_2}+B_3\rho_3\sigma_3e^{i\phi_3}\}] \\ &\qquad +SV^2(2e^{iE}+e^{2i\chi-iE})(B_1\sigma_1{}^2+B_2\sigma_2{}^2+B_3\sigma_3{}^2)\,; \qquad \ldots\ldots(14) \end{aligned}$$

as already remarked, the terms Se^{iE} represent the focus-shift and those in Se^{-iE} the astigmatism.

In the lining-up procedure described above, the decentring (ρ_3, ϕ_3) given to the plate P_3 is determined by the condition that the coma shall vanish, i.e. by the equation

$$B_2\rho_2e^{i\phi_2}+B_3\rho_3e^{i\phi_3}=0,$$

---

* The notation here and below is that of a previous paper (*Mon. Not. R. Astr. Soc.* **104**, 48 (1944)). Since the unit of plate-strength is there defined as the strength of the Schmidt plate of M_1, it follows that expressions (13) and (14) below must be multiplied by $f/8f_1{}^3$ to obtain their contributions to the actual displacements in the Petzval surface, and that the value of B_1 is -1.

which is equivalent, since B_2 and B_3 are both positive, to the relations

$$\phi_3 = \pi + \phi_2, \qquad B_3\rho_3 = B_2\rho_2. \qquad \ldots\ldots(15)$$

Expression (14) then reduces to

$$S(2e^{iE} + e^{2i\phi_2 - iE})\,\frac{B_2}{B_3}\,\rho_2{}^2$$
$$-2SV(\sigma_2 - \sigma_3)[2e^{iE}\cos(\phi_2 - \chi) + e^{-iE + i\phi_2 + i\chi}]B_2\rho_2$$
$$+SV^2(2e^{iE} + e^{2i\chi - iE})(B_1\rho_1{}^2 + B_2\sigma_2{}^2 + B_3\rho_3{}^2), \qquad \ldots\ldots(16)$$

in which $B_1 = -1$, $B_2 + B_3 = 1$.

If the plate and mirrors are free from errors of figure, the reduction of the observed astigmatism in the axial image to zero by tilting M_2 (operation (*d*)) is equivalent to setting $\rho_2 = 0$ in (16), i.e. to the correct alignment of M_2 relative to M_1. It then follows from (15) that $\rho_3 = 0$ and the system is correctly centred.

The practically important case, however, is that in which the secondary mirror M_2 is slightly out of alignment in relation to the primary ; that is to say, the virtual plate P_2 is decentred and the consequent decentring of P_3 is given by (15). The decentring of P_2 may represent the result of applying operation (*d*) to a system whose plate is not quite free from astigmatism of figure, or it may represent an inaccuracy in the mechanical positioning of M_2 relative to M_1. In either case, we only need to consider lateral shifts of P_2, since the longitudinal adjustment of M_2 is made empirically.*

To fix ideas, we consider the special case of the two-sphere one-plate astrographic camera

$$q = 0{\cdot}30, \qquad A = 0, \qquad B = 0, \qquad \Gamma = 0{\cdot}7399, \qquad \sigma = 2{\cdot}1447, \qquad \ldots\ldots(17)$$

constructed with $f_1 = f_2 = 20$ inches. We suppose that the aperture stop, 10 inches in diameter, is situated 20 inches in front of the pole of the primary mirror† and that the system, of focal length approximately 28 inches, covers a field of 6° diameter at a nominal aperture of *F*/3. Then in the plate-diagram of the system

$$B_1 = -1, \qquad B_2 = q^2(2-q)^2 = 0{\cdot}2601, \qquad B_3 = \Gamma = 0{\cdot}7399,$$
$$\sigma_1 = 1, \qquad \sigma_2 = \frac{3-q}{2-q} - 1 = 0{\cdot}5882, \qquad \sigma_3 = \sigma - 1 = 1{\cdot}1447, \qquad \ldots\ldots(18)$$

and the unit of length $f_1 = 20$ inches.

To express the effect of decentring P_2 in the azimuth $\phi_2 = 0$ and readjusting P_3 to annul coma all over the field, we set

$$\phi_2 = 0, \qquad \rho_3 = \frac{B_2}{B_3}\,\rho_2 = 0{\cdot}3515\rho_2, \qquad \phi_3 = \pi.$$

Expression (16) then becomes

$$S(2e^{iE} + e^{-iE}) \times 0{\cdot}3515\,\rho_2{}^2 + SV(2e^{iE}\cos\chi + e^{-iE + i\chi}) \times 0{\cdot}2895\,\rho_2$$
$$+SV^2(2e^{iE} + e^{2i\chi - iE}) \times 0{\cdot}0596,$$

---

* An error in the longitudinal adjustment of M_2 would cause a change in the strength of P_2 as well as in its position.

† The stop is placed about half-way between the plate and the primary mirror in order to obtain uniform lighting of the field with the least possible increase in the diameters of plate and primary over that of the stop.

since

$$B_1\sigma_1^{\,2}+B_2\sigma_2^{\,2}+B_3\sigma_3^{\,2}=\frac{q^2(1-q)^2}{B_3}=0{\cdot}0596.$$

The actual displacement-contribution in the Petvzal surface for the ray through the point (S, E) of the aperture stop is therefore,

$$\begin{aligned}\delta x+i\delta y&=\frac{f}{8f_1^{\,3}}(\Delta x+i\Delta y)\\&=\frac{S}{8(1-q)}[(2e^{iE}+e^{-iE})\times 0{\cdot}3515\,\rho_2^{\,2}/f_1^{\,2}\\&\qquad+(2e^{iE}\cos\chi+e^{-iE+\chi})\times 0{\cdot}2895\,V\rho_2/f_1\\&\qquad+(2e^{iE}+e^{2i\chi-iE})\times 0{\cdot}0596\,V^2], \qquad \ldots\ldots(20)\end{aligned}$$

where V denotes the off-axis angle of the incident pencil and χ its azimuth.

In the case $\rho_2=0$ of a correctly lined-up system, the contribution of the off-axis astigmatism to the displacement is

$$(2e^{iE}+e^{2i\chi-iE})\times 0{\cdot}0596\,SV^2/8(1-q).$$

Since the absolute value of this expression never exceeds

$$3\times 0{\cdot}06\times 5\times\left(\frac{1}{20}\right)^2\times\frac{10}{56}=0{\cdot}0004 \text{ inch},$$

we see that the system is for all practical purposes anastigmatic.

In the case $\rho_2>0$ we have at the edge of the field:

$$\begin{aligned}&(\text{Change in } \delta x+i\delta y \text{ due to decentring})\\&\quad=\frac{S}{8(1-q)}[(2e^{iE}+e^{-iE})\times 0{\cdot}00072\,\rho_2\\&\qquad\qquad+(2e^{iE}\cos\chi+e^{-iE+i\chi})\times 0{\cdot}00072\,\rho_2],\end{aligned}$$

where ρ_2, S are measured in inches. Since $S\leqslant 5$, the absolute value of this expression never exceeds

$$0{\cdot}001(2{\cdot}35\,\rho_2^{\,2}+1{\cdot}94\,\rho_2) \text{ inch}.$$

A decentring in which ρ_2 does not exceed 0·1 therefore disturbs the contribution from astigmatism and focus-shift to the Seidel displacement $\delta x+i\delta y$ in the Petzval surface by an amount which nowhere exceeds 0·00022 inch in absolute value. Its effect on the image-quality will therefore be harmlessly small.

There is, however, another consequence of the decentring which needs to be considered, namely a disturbance in the distortion of the system, called "dislocation of the image" by Conrady. Only if this also is harmlessly small can the decentring be tolerated in a system whose images are to be used for measurements of position. To settle this point, we use expression (10), which in the case $\phi_2=0$, $\phi_3=\pi$, $B_2\rho_2=B_3\rho_3$ becomes

$$\begin{aligned}&(B_2\rho_2^{\,3}-B_3\rho_3^{\,3})-V(B_2\rho_2^{\,2}\sigma_2+B_3\rho_3^{\,2}\sigma_3)(e^{i\chi}+2\cos\chi)\\&\qquad+V^2(B_2\rho_2\sigma_2^{\,2}-B_3\rho_3\sigma_3^{\,2})(2e^{i\chi}\cos\chi+1)-V^3e^{i\chi}\sum_r B_r\sigma_r^{\,3}.\end{aligned}$$

The first term merely represents a lateral displacement of the whole field, while the last term is the ordinary plate-contribution to the Seidel distortion of the system. The effect of the decentring is represented by the terms in V and V^2, whose contribution to the actual displacement $\delta x + i\delta y$ in the Petzval surface is

$$\frac{f}{8f_1^3}\Big[-VB_2\rho_2^2\left(\sigma_2+\frac{B_2}{B_3}\sigma_3\right)\left(e^{i\chi}+2\cos\chi\right) + V^2B_2\rho_2(\sigma_2^2-\sigma_3^2)(2e^{i\chi}\cos\chi+1)\Big]$$

$$=\frac{1}{2240}[-0\cdot2576\,V\rho_2^2(2e^{i\chi}+e^{-i\chi})-0\cdot2508\,V^2\rho_2(2e^{2i\chi}+1)].$$

Since $V \leqslant \frac{1}{20}$, the absolute value in inches of this contribution never exceeds

$$(17\cdot5\rho_2^2+\rho_2)10^{-5},$$

which for $\rho_2 \leqslant 0\cdot1$ is utterly negligible.

It follows that a decentring for which $\rho_2 \leqslant 0\cdot1$ causes no appreciable dislocation of the image, nor any serious deterioration in the image-quality. Centring of this accuracy is readily obtainable by mechanical methods.*

Finally, we remark that the compensation of an axial astigmatism

$$\delta x + i\delta y = \tfrac{1}{5}Se^{-iE} \times 0\cdot00022$$

due to error in the plate-figure can be shown by the same methods to involve a decentring, of approximately five times the above tolerance limit, which introduces astigmatism near the edge of the field several times greater than that removed at the centre. The use of an intentionally decentred line-up is therefore not to be recommended.

REFERENCES

Burch, C. R., 1942. *Mon. Not. R. Astr. Soc.* **102,** 159.

Conrady, A. E., 1919. *Mon. Not. R. Astr. Soc.* **79,** 384.

Cox, H. W., 1939. *J. Sci. Instrum.* **16,** 257.

Linfoot, E. H., 1944. *Mon. Not. R. Astr. Soc.* **104,** 48 ; 1945. *Proc. Phys. Soc.* **57,** 199.

---

* If it is more convenient to line-up the two mirrors optically, an adaptation of the method described by A. Couder (*Bull. Astronomique*, 1932, **7,** 278–280) can be used with advantage.

THE FUNDAMENTAL FREQUENCY OF VIBRATION OF RECTANGULAR WOOD AND PLYWOOD PLATES

By R. F. S. HEARMON,
Princes Risborough

Communicated by W. W. Barkas 24 *September* 1945

ABSTRACT. Equations are derived expressing the frequency of vibration of rectangular wood and plywood plates in terms of elastic constants, dimensions and density. For supported edges, the solution is exact and gives the complete series of overtones. For clamped edges, the fundamental frequency is estimated by the approximate Rayleigh method, but evidence is presented which indicates that the errors introduced by the use of the Rayleigh method are, in fact, negligible. A method of measuring the frequencies is described; comparison of calculated with observed frequencies shows that the former are on the average about 23% high for clamped edges and about the same amount low for supported edges. This discrepancy is attributed to lack of correspondence between the experimental edge conditions and those assumed in the theoretical treatment. Finally, an empirical method, based on the rough proportionality between elastic constants and density of wood, is suggested and justified for obtaining approximate estimates of the fundamental frequencies in terms of plate dimensions only.

INTRODUCTION

CONSIDERABLE advances have recently been made in the elastic theory of wood and plywood. This theory has been used to calculate stresses and deflections under lateral loading and critical buckling stresses of plywood plates ; the agreement with experiment is reasonable though not exact. The frequency of vibration can be obtained theoretically by closely allied methods, and one of the objectives of the present investigation is to extend the comparison between theory and experiment to this frequency. A second objective is to gain some information regarding the frequency, which does not appear to have been studied hitherto.

§ 1. DEFINITIONS AND BASIC EQUATIONS

As is usual in problems of this type, it is assumed that the material is homogeneous and perfectly elastic and that, in the two-dimensional case, its elastic behaviour is determined by the existence of two perpendicular symmetry axes. For the particular purpose of the present investigation, it is further assumed that the symmetry axes (i.e. the directions parallel and perpendicular to the grain) are parallel with the sides of the plate. The dimensions of the plate are a, b and h, where

a = length of side parallel with Ox.
b = ,, ,, ,, ,, ,, Oy.
h = thickness of plate, parallel with Oz.
(h is small in comparison with a and b.)

Under these conditions the differential equation governing the small deflections w in the Oz direction is (March, 1936, 1942)

$$D_1\frac{\partial^4 w}{\partial x^4}+D_2\frac{\partial^4 w}{\partial y^4}+2D_3\frac{\partial^4 w}{\partial x^2\partial y^2}-P=0, \qquad \ldots\ldots (1.1)$$

where

$$\left.\begin{aligned} D_1&=\frac{E_1h^3}{12\lambda}\,; \\ D_2&=\frac{E_2h^3}{12\lambda}\,; \\ D_3&=\frac{E_1\sigma_{21}h^3}{12\lambda}+\frac{G_{12}h^3}{6} \\ &=D_4+2D_5\,; \end{aligned}\right\} \qquad \ldots\ldots (1.2)$$

E_1 = Young's modulus in bending in Ox direction ;

E_2 = " " " " " Oy " ;

G_{12} = Rigidity modulus for shear stresses in Ox and Oy directions ;

$\sigma_{21}=\dfrac{\text{contraction in O}x\text{ direction}}{\text{extension in O}y\text{ direction}}$ for tension in Oy direction ;

$\lambda=1-\sigma_{21}\sigma_{12}\approx 0{\cdot}99$ for wood and plywood ;

P = pressure acting in Oz direction.

The differential equation governing the vibration of the plate can be found by substituting $\rho h(\partial^2 w/\partial t^2)$ for $-P$ in (1.1) :

$$D_1\frac{\partial^4 w}{\partial x^4}+D_2\frac{\partial^4 w}{\partial y^4}+2D_3\frac{\partial^4 w}{\partial x^2\partial y^2}+\rho h\frac{\partial^2 w}{\partial t^2}=0, \qquad \ldots\ldots (1.3)$$

where ρ = density of material (weight at test/volume at test) and t = time.

The boundary conditions for a plate clamped at the edges are (Timoshenko, 1940, § 22) :

$$\left.\begin{aligned} w&=0 \text{ at :— } && x=0, \quad x=a, \quad y=0, \quad y=b\,; \\ \frac{\partial w}{\partial x}&=0 \text{ at :— } && x=0, \quad x=a\,; \\ \frac{\partial w}{\partial y}&=0 \text{ at :— } && y=0, \quad y=b; \end{aligned}\right\} \qquad \ldots\ldots (1.4)$$

while for a plate simply supported at the edges they are (Timoshenko, 1940, §§ 22, 26) :

$$\left.\begin{aligned} w&=0 \text{ at :— } && x=0, \quad x=a, \quad y=0, \quad y=b\,; \\ \frac{\partial^2 w}{\partial x^2}&=0 \text{ at :— } && x=0, \quad x=a\,; \\ \frac{\partial^2 w}{\partial y^2}&=0 \text{ at :— } && y=0, \quad y=b. \end{aligned}\right\} \qquad \ldots\ldots (1.5)$$

The potential energy of bending (V) is (March, 1942 ; Goland, 1942) :

$$V=\frac{1}{2}\int_0^a\int_0^b\left\{D_1\left(\frac{\partial^2 w}{\partial x^2}\right)^2+D_2\left(\frac{\partial^2 w}{\partial y^2}\right)^2+2D_4\frac{\partial^2 w}{\partial x^2}\frac{\partial^2 w}{\partial y^2}+4D_5\left(\frac{\partial^2 w}{\partial x\,\partial y}\right)^2\right\}dx\,dy, \qquad \ldots\ldots(1\cdot 6)$$

and the kinetic energy T is

$$T=\frac{\rho h}{2}\int_0^a\int_0^b\left(\frac{\partial w}{\partial t}\right)^2 dx\,dy. \qquad \ldots\ldots(1\cdot 7)$$

§ 2. DERIVATION OF THE FREQUENCY EQUATIONS

In the case of supported edges, an exact solution can be obtained by expressing w as

$$w=w_0\sin\frac{m\pi x}{a}\sin\frac{n\pi y}{b}\sin pt, \qquad \ldots\ldots(2.1)$$

where $p=2\pi\times$ frequency (ν), m and n are integers, and w_0 is a constant. Substitution of (2.1) in (1.5) shows that the boundary conditions are satisfied, and substitution of (2.1) in the differential equation (1.3) leads directly to

$$\nu_s=\frac{\pi}{2a^2b^2}\left\{\frac{1}{\rho h}\left[D_1m^4b^4+D_2n^4a^4+2D_3m^2n^2a^2b^2\right]\right\}^{\frac{1}{2}}, \qquad \ldots\ldots(2.2)$$

where the suffix s indicates supported edges.

The fundamental is given by $m=n=1$, and the overtones by higher values of m and n.

In view of the complexity of the problem involved in a complete solution, the fundamental frequency for clamped edges has been derived by the Rayleigh method (see e.g. Timoshenko, 1937, § 16), supplemented to some extent by the use of the more accurate Ritz modification. For comparison both with the exact solution (2.2) and with the results for clamped edges, the Rayleigh and Ritz methods have also been applied to the case of simply supported edges.

The Rayleigh method consists in working out the potential energy V and the kinetic energy T from the equation

$$w=f(x,y)g(t), \qquad \ldots\ldots(2.3)$$

which expresses the deflection w as a function of time t and of position on the plate. If the system is conservative, then

$$V_{\max}=T_{\max}, \qquad \ldots\ldots(2.4)$$

and the frequency of vibration is found from this condition.

The virtue of the Rayleigh method is that in general it is possible to use an approximate expression of $f(x, y)$ in (2.3) and still obtain estimates of the frequency sufficiently accurate for all practical purposes. In the present instance, the simplest algebraic expressions consistent with the boundary conditions have been chosen to represent $f(x, y)$. Assuming a sinusoidal vibration, this leads to

$$w=K_cx^2y^2(a-x)^2(b-y)^2\sin pt, \qquad \ldots\ldots(2.5)$$

for clamped edges, and to

$$w=K_sxy(a-x)(b-y)(a^2+ax-x^2)(b^2+by-y^2)\sin pt, \qquad \ldots\ldots(2.6)$$

for supported edges, where K_c and K_s are constants, the suffix indicating the boundary conditions. It should be noted that, although (2.5) and (2.6) satisfy the boundary conditions, they are not solutions of (1.3).

The potential energy can now be found for clamped edges by inserting w, as given by (2·5), in (1·6) :

$$V_c = \frac{a^5b^5K_c^2}{1575}\left[D_1b^4 + D_2a^4 + \frac{4}{7}D_3a^2b^2\right]\sin^2 pt, \qquad \ldots\ldots(2.7)$$

and for supporting edges by inserting (2.6) in (1.6) :

$$V_s = \frac{62a^5b^5K_s^2}{525}\left[D_1b^4 + D_2a^4 + \frac{867}{434}D_3a^2b^2\right]\sin^2 pt. \qquad \ldots\ldots(2.8)$$

The kinetic energy is given similarly for clamped edges by (2.5) and (1.7) as

$$T_c = \frac{\rho h a^9b^9K_c^2p^2\cos^2 pt}{793800}, \qquad \ldots\ldots(2.9)$$

and for supported edges by (2.6) and (1.7) as

$$T_s = \frac{961\rho h a^9b^9K_s^2p^2\cos^2 pt}{793800}. \qquad \ldots\ldots(2.10)$$

In each case the potential energy can be written $V = MK^2\sin^2 pt$ and the kinetic energy $T = NK^2p^2\cos^2 pt$. The maximum V occurs when $\sin^2 pt = 1$ and the maximum T when $\cos^2 pt = 1$. Hence from condition (2.4), $p^2(=4\pi^2\nu^2) = M/N$. Thus from equations (2.7) and (2.9)

$$\nu_c = \frac{1}{\pi a^2b^2}\left\{\frac{126}{\rho h}\left[D_1b^4 + D_2a^4 + \frac{4}{7}D_3a^2b^2\right]\right\}^{\frac{1}{2}}, \qquad \ldots\ldots(2.11)$$

and from (2.8) and (2.10)

$$\nu_s = \frac{1}{\pi a^2b^2}\left\{\frac{756}{31\rho h}\left[D_1b^4 + D_2a^4 + \frac{867}{434}D_3a^2b^2\right]\right\}^{\frac{1}{2}}. \qquad \ldots\ldots(2.12)$$

Comparison of equation (2.12) with the accurate solution (2.2), putting $m=n=1$, shows that the form of the equations is identical, and further, the numerical coefficients are very close in the two cases. The coefficient outside the brackets in the accurate equation (2.2) is $\pi/2 = 1{\cdot}5708$, while the corresponding coefficient in (2.12) is $\pi^{-1}\sqrt{(756/31)} = 1{\cdot}5719$; the coefficient of the term in $D_3a^2b^2$ is 2 in equation (2.2) and 867/434 ($=1{\cdot}998$) in equation (2.12).

In order to obtain an estimate of the degree of approximation involved in the clamped-edge solution (2.11), the Ritz modification of the Rayleigh method has been applied to the present problem. The procedure, with an example on the one-dimensional case of the vibrating string, is given in Timoshenko's book (1937, § 62). The application of the method to the two-dimensional case of the vibrating anisotropic plate does not present any special difficulties, although it leads to somewhat laborious algebra and arithmetic. For the above reasons, only the final results, and such description of the process as is required for their presentation, will be given here.

The forms assumed for w are generalizations of (2.5) and (2.6) :

(1) Clamped edges, $w=X^2Y^2(K_1+K_2XY)\sin pt$;

(2) Supported edges, $w=XY(a^2+ax-x^2)(b^2+by-y^2)(K_1+K_2XY)\sin pt$, where $X=x(a-x)$, $Y=y(b-y)$.

If $K_2=0$, the above equations reduce respectively to (2.5) and (2.6). An essential feature of the Ritz method is that the values of K_1 and K_2 are adjusted at one stage in the process so as to make the frequency a minimum. With two constants, this leads to a quadratic in the frequency, one root of which gives a more accurate estimate of the fundamental frequency than that given by the Rayleigh method.

For the purpose of comparing the various estimates, it is convenient to confine attention to square plates, and, in the case of wood and plywood, to particular values of the elastic constants. For square plates, equations (2.2), (2.11) and (2.12) are of the form

$$\nu=c_1/a^2\sqrt{\rho h}. \qquad \ldots\ldots(2.13)$$

Values of the constant c_1 have been calculated by the Ritz method for plates of birch 5-ply and birch veneer having the following "flexural rigidities" D (C.G.S. units ; values based on elastic constants given in table 2 below).

	D_1	D_2	D_3
Birch 5-ply	$0\cdot191\times10^{10}$	$0\cdot071\times10^{10}$	$0\cdot044\times10^{10}$
Birch veneer	$2\cdot97\times10^{8}$	$0\cdot21\times10^{8}$	$0\cdot69\times10^{8}$

For an isotropic solid $D_1=D_2=D_3$, and it is therefore possible, by introducing this condition, to reduce any of the equations so far given to the isotropic case. The exact value of c_1 for a square isotropic plate with supported edges is known (Timoshenko, 1937, equation 214) to be $\pi\sqrt{D_1}$, where $D_1=Eh^3/12(1-\sigma^2)$, and Tomotika (1936) has given an estimate of c_1 for a square plate with clamped edges which, though not strictly exact, gives a highly accurate lower limit. The various estimates for c_1 are collected in table 1.

Table 1. Calculated values of c_1 in equation (2.13)
(Square plates)

Method	Clamped edges			Supported edges		
	Isotropic	Birch		Isotropic	Birch	
		5-ply	Veneer		5-ply	Veneer
Rayleigh	$5\cdot730\sqrt{D_1}$	$1\cdot914\times10^5$	$0\cdot6755\times10^5$	$3\cdot1429\sqrt{D_1}$	$0\cdot9300\times10^5$	$0\cdot3357\times10^5$
Ritz	$5\cdot729\sqrt{D_1}$	$1\cdot912\times10^5$	$0\cdot6750\times10^5$	$3\cdot1420\sqrt{D_1}$	$0\cdot9294\times10^5$	$0\cdot3355\times10^5$
Exact	$5\cdot727\sqrt{D_1}$	—	—	$3\cdot1416\sqrt{D_1}$	$0\cdot9293\times10^5$	$0\cdot3354\times10^5$

Even the largest difference in the above table is only just greater than 0·1%, and it can be concluded that the fundamental frequencies estimated by the

Rayleigh method are mathematically sufficiently accurate for the purpose of comparing theoretical with observed frequencies. The Rayleigh equations (2.11) and (2.12) have, therefore, been used in all subsequent calculations.

§ 3. EXPERIMENTAL

The general features of the method used to determine the frequencies can be seen from figures 1, 2 and 3. The wood or plywood plate was held in a suitable frame and two small iron plates A and C (figure 1) were attached by means of soft wax, one (A) at the centre of the test plate, and the other (C) a convenient distance away. A small iron-cored solenoid (B), fed by alternating current from a beat-frequency oscillator, was placed near to plate A, while a telephone receiver, stripped of its diaphragm and case, was placed so that the magnets were close to plate C. Any currents induced in the coils of the telephone were fed to a cathode-ray oscillograph, and the experiment consisted in varying the frequency of the driving current supplied to B until the response, as indicated by the oscillograph, was a maximum. The telephone receiver D was connected to the vertical plates of the oscillograph, and the driving current from the oscillator connected to the horizontal plates, in parallel with the coil B. In this way, a Lissajous figure was obtained on the oscillograph screen, and it was found that, with the present experimental arrangement, the plates tended to respond to integral submultiples of the resonant frequency, in agreement with results, so far unpublished, on wooden strips. The most powerful response in all cases occurred when the frequency of the driving current was one-half the true resonant frequency, as is shown by the fact that the Lissajous figure indicated two vibrations of the plate for each cycle of the forcing current. The results given in table 2 are all based on this response mode.

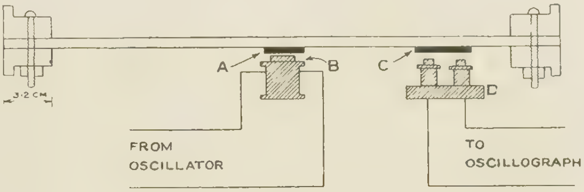

Figure 1. Experimental arrangement.

The apparatus can, of course, be used to measure overtones, and a number of observations were actually made of the frequencies at which these occurred. Owing to certain difficulties, mainly theoretical, a satisfactory interpretation of these measurements is not available at present, and they will not be discussed further.

The frames for holding the plates were made of wood and are shown in figures 1, 2 and 3. The frame for clamped edges (general view, figure 2; cross-section, figure 1) consisted of two halves bolted together, with the plate sandwiched between them. The frame for supported edges (figure 3) consisted of four separate grooved members held together by brass bolts and wing nuts, with the edges of the plate at the base of the grooves, as shown in the section diagram, figure 3 (*b*).

For convenience of lining up and adjustment, the apparatus was assembled on an optical-bench base. The frames were held at opposite corners by ordinary laboratory clamps attached to vertical rods ; the solenoid B and telephone receiver D were also mounted on rods, all of which were held in optical-bench stands.

The plates were originally cut to 45·8 cm. squares, and were progressively reduced in size in order to provide measurements over a range of lateral dimensions. It can be seen from equations (2.11) and (2.12) that if D_1 and D_2 differ, the frequency of an oblong plate of given dimensions depends on whether the direction of greater flexural rigidity coincides with the longer or shorter side of the plate, and provision was made for the testing of plates fulfilling both of these conditions. For example, two 45·8 × 45·8 cm. plates of obeche veneer were originally available (table 2). The first reduction in size was accomplished on plate 1 by shortening to 30·6 cm. the side *a*, lying parallel to the greater Young's modulus, and on plate 2 by shortening to the same length the side *b*, lying parallel to the smaller Young's modulus. On the second reduction in size, side *b* on plate 1 and side *a* on plate 2 were shortened to 30·6 cm., thus giving square plates again. This procedure was repeated once more, finally leading to the smallest size of plate, 20·4 × 20·4 cm. The dimensions given refer to the supported-edge condition ; the clamped dimensions are smaller owing to the overlap of the frames (see figures 1 and 2).

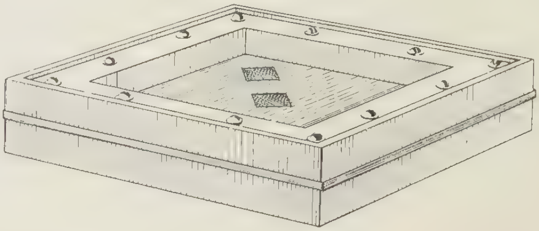

Figure 2. Clamped edge frame.

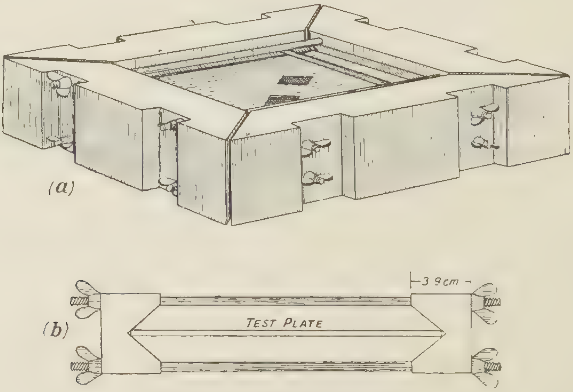

Figure 3. Supported edge frame.
(*a*) General view ; (*b*) cross-section.

Young's moduli in bending (E), and rigidity modulus (G), on which, by equations (1.2), the " flexural rigidities " depend, were determined respectively

	Veneers								Plywoods				
	Obeche		Gaboon			Beech		Birch	Birch 5-ply	Birch 3-ply		Opepe 3-ply	Douglas fir 3-ply
	(1)	(2)	(1)	(2)	(3)	(1)	(2)			(1)	(2)		
(1) Elastic constants													
E_1	6·9	7·4	7·8	7·9	8·7	13·3	13·3	11·7	9·3	12·0	12·4	9·3	8·4
E_2 $\times 10^{-10}\ \frac{\text{dynes}}{\text{sq. cm.}}$	0·17	0·05	0·30	0·19	0·14	0·55	0·54	0·82	3·45	1·19	1·21	0·80	1·08
$E_1\sigma_{21}$	0·17	0·17	0·19	0·19	0·22	0·33	0·33	0·37	0·37	0·37	0·37	0·25	0·25
G_{12}	0·30	0·34	0·58	0·45	0·41	0·85	0·86	1·19	0·90	0·88	0·93	0·54	0·90
h (cm.)	0·291	0·323	0·318	0·310	0·315	0·309	0·309	0·311	0·626	0·532	0·525	0·479	0·415
ρ (gm./cc.	0·330	0·390	0·400	0·399	0·393	0·670	0·659	0·719	0·690	0·716	0·711	0·774	0·533
(2) Observed fundamental frequencies (cycles/sec.). Clamped edges													
$a=b=39{\cdot}3$ cm.	67	82	76	76	78	89	82	—	160	140	148	—	—
$a=24{\cdot}2,\ b=39{\cdot}3$	172	—	192	—	—	—	182	—	—	—	254	—	—
$a=39{\cdot}3,\ b=24{\cdot}2$	—	88	—	96	92	95	—	96	254	197	—	155	162
$a=b=24{\cdot}2$ cm.	189	191	202	156	202	200	225	212	392	320	326	270	278
$a=14{\cdot}0,\ b=24{\cdot}2$	506	—	496	—	—	—	440	—	—	—	706	—	—
$a=24{\cdot}2,\ b=14{\cdot}0$	—	201	—	229	224	241	—	248	650	486	—	375	382
$a=b=14{\cdot}0$ cm.	444	502	556	510	524	530	514	544	980	830	850	654	618
(3) Observed fundamental frequencies (cycles/sec.). Supported edges													
$a=b=45{\cdot}8$ cm.	35	39	40	34	38	41	43	—	73	67	61	—	—
$a=30{\cdot}6,\ b=45{\cdot}8$	92	—	94	—	—	—	95	—	—	—	152	—	—
$a=45{\cdot}8,\ b=30{\cdot}6$	—	60	—	68	50	53	—	52	150	82	—	77	90
$a=b=30{\cdot}6$ cm.	81	114	105	88	92	84	94	108	187	190	180	120	137
$a=20{\cdot}4,\ b=30{\cdot}6$	186	—	181	—	—	—	166	—	—	—	320	—	—
$a=30{\cdot}6,\ b=20{\cdot}4$	—	94	—	109	92	106	—	123	281	200	—	167	168
$a=b=20{\cdot}4$ cm.	184	190	218	182	182	186	191	228	420	390	374	296	278

by flexural and torsional vibration experiments (Hearmon and Barkas, 1941) on approximately 2·5-cm. wide strips of the material cut parallel to and near the sides of the largest plates. The Poisson's ratios (σ) were not measured, but were obtained from published values of σ for the appropriate solid wood. In some cases, no relevant measurements could be found, and it was then assumed that the Poisson's ratio for solid wood, $\frac{\text{contraction along the grain}}{\text{extension across the grain}}$ for tension across the grain, had the value 0·025. As in much work on wood and plywood, the contribution of the terms involving the Poisson's ratios is small, and the exact values adopted are not very important.

§4. RESULTS AND DISCUSSION

The complete experimental results are given in table 2 ; the side *a* is taken as parallel with the direction of E_1 and *b* with E_2, where $E_1 > E_2$.

In order to compare the observed and theoretical frequencies, it is convenient to express the equations for the latter in terms of elastic constants, rather than flexural rigidities, by substituting equations (1.2) in (2.11) and (2.12). Thus,

$$\nu_c = \frac{1{\cdot}04h}{a^2\sqrt{\rho}}\left[E_1 + \left(\frac{a}{b}\right)^4 E_2 + \left(\frac{a}{b}\right)^2 (0{\cdot}57E_1\sigma_{21} + 1{\cdot}13G_{12})\right]^{\frac{1}{2}} \qquad \ldots\ldots(4.1)$$

and

$$\nu_s = \frac{0{\cdot}456h}{a^2\sqrt{\rho}}\left[E_1 + \left(\frac{a}{b}\right)^4 E_2 + \left(\frac{a}{b}\right)^2 (2{\cdot}00E_1\sigma_{21} + 3{\cdot}96G_{12})\right]^{\frac{1}{2}}, \qquad \ldots\ldots(4.2)$$

where λ has been put equal to 0·99, and the numerical coefficients are given to three significant figures.

The observed frequencies are plotted against those calculated from (4.1) and (4.2) in figures 4 and 5. The lines in these figures are not necessarily the "best" fit, but are drawn through the origin with slope determined by the average value of the ratio (observed frequency/calculated frequency) for all the observations. Numerically, this average is 0·772 for clamped edges and 1·238 for supported edges. Thus, the calculated frequencies with edges clamped are consistently higher than the observed frequencies, while the reverse is true for the supported edges. This suggests that the actual conditions at the edges of the plates are always intermediate between the conditions appropriate to strictly clamped and supported edges (equations (1.4) and (1.5)). The difficulty of realizing experimentally the exact boundary conditions assumed in the theoretical treatment of this type of problem is well known, and has been encountered, for example, in buckling tests of plywood panels in shear (Norris, Voss and Palma, 1945).

Ideally, of course, the points in figures 4 and 5 should lie on a line passing through the origin, and having a slope of 45° ; the general tendency of the points to depart from this line is a measure of the effect just discussed. In addition, there is also a certain amount of random scatter, which is partly accounted for by casual experimental errors in the frequency measurements, or by variation in the material between the test plates and the strips used in the determination of elastic constants.

Superimposed on all these effects, however, there is definite indication that with clamped edges (figure 4) the best line through the points is curved, and not straight ; the curvature is such that the ratio (ν observed/ν calculated) becomes smaller at higher frequencies. The physical interpretation of this result is that the frame used for clamped edges becomes less effective with thicker plates and smaller lateral dimensions, and under these conditions departures from the ideal clamped-edge conditions tend to be higher.

In order to obtain further information on this effect, a mild steel frame was made to hold the smallest square plates in the clamped-edge condition. This frame was of the same dimensions as the corresponding wooden frame ; the two halves, however, were held together by twelve $\frac{1}{4}$-in. bolts instead of the $\frac{1}{8}$-in. size used with the wooden frame. The observed frequencies in the steel and wooden frames and the theoretical frequencies (equation (4.1)) are given in table 3.

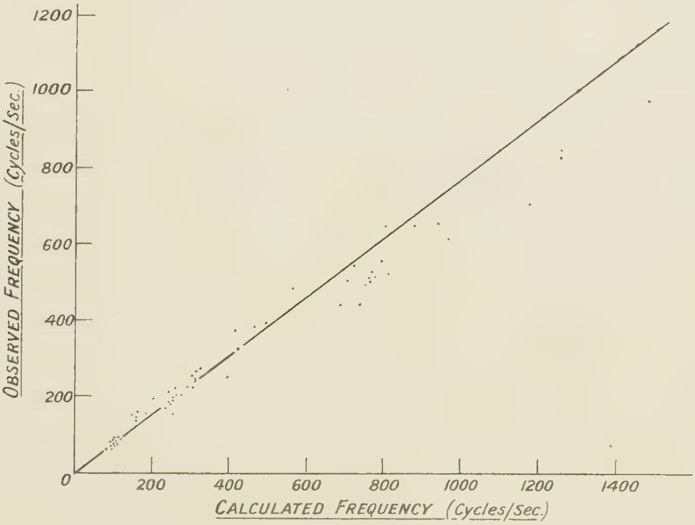

Figure 4. All results, clamped edges.

In each case the frequency is higher in the steel frame than in the wooden frame, and is, therefore, closer to the calculated frequency. The average ratio (observed frequency/calculated frequency) is 0·67 for the wooden frame and 0·83 for the mild-steel frame. These results confirm that a considerable part at least of the discrepancy between observed and calculated frequencies can be attributed to the conditions at the edges of the plates.

With the exception of the opepe 3-ply, the observed frequencies in the steel frame are lower than those calculated. This suggests that, even in the steel frame, the restraint at the edges is not sufficient to realize fully the ideal clamped-edge conditions.

Inspection of figure 5 (simply supported edges) does not reveal any marked tendency to curvature, though statistical analysis (see table 4) shows that there is in fact a slight tendency to curvature such that the ratio (observed frequency/calculated frequency) *increases* somewhat as the frequency rises. It is rather surprising that the supported-edge frame should prove more

Table 3. Frequencies in cycles/sec. Edges clamped ; $a=b=14{\cdot}0$ cm.

Material	Obeche		Gaboon			Beech		Birch	Birch 5-ply	Birch 3-ply		Opepe 3-ply	Douglas fir 3-ply
	(1)	(2)	(1)	(2)	(3)	(1)	(2)			(1)	(2)		
Frequency (wooden frame)	444	502	556	510	524	530	514	544	980	830	850	654	618
Frequency (steel frame)	514	585	642	593	613	637	628	647	1220	1110	1110	960	770
Frequency (calculated)	740	770	800	770	810	780	790	730	1490	1260	1270	950	980

satisfactory in this respect than the clamped-edge frame, because the former has quite apparent defects. There is a small area near each corner which is unrestrained, but, perhaps more important, the degree to which the wing nuts holding the frame together (figure 3) are tightened is a matter for personal judgment in obtaining a sufficiently firm fixing of the test plate without applying appreciable compressions in its plane. Nevertheless, the experimental results indicate that, although the conditions at the edges do not constitute true simple support, they are to a first approximation independent of the dimensions of the plate.

In view of the rough proportionality between elastic constants and density of timber, it is possible to derive certain empirical relations which enable the frequencies to be estimated even if the elastic constants and densities are not known. If it is assumed that elastic constants are exactly proportional to density, then equations (4.1) and (4.2) take the form

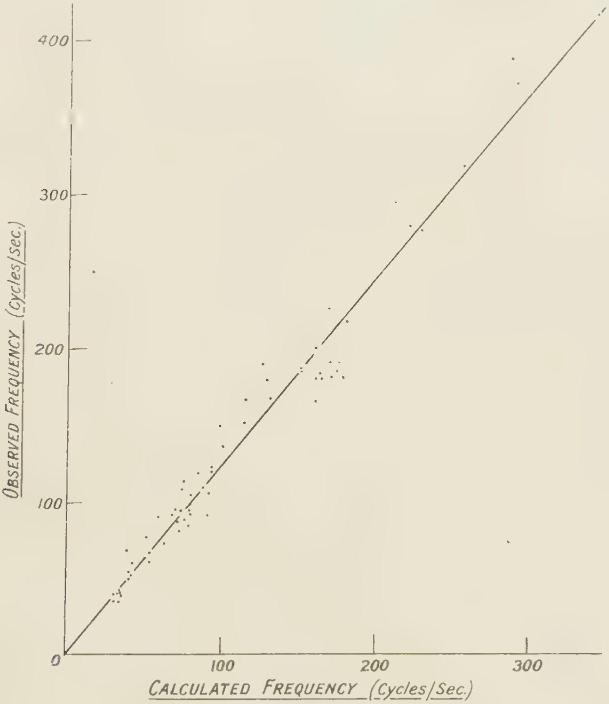

Figure 5. All results, supported edges.

$$\nu = c_2 h/a^2, \qquad \ldots\ldots (4.3)$$

where c_2 is a numerical factor which depends only on the edge conditions and on the ratio a/b.

Two related consequences follow from (4.3) :

(1) For given edge conditions, and given ratios a/b and h/a^2, the frequency should be constant irrespective of the values of elastic constants and density. Examination of the experimental results for the veneers in table 2, all of which have a thickness of about 0·3 cm., shows that this prediction is approximately verified.

(2) For given edge conditions, and a given value of a/b, a plot of ν against h/a^2 should give a straight line passing through the origin. The theoretical frequencies for square plates are plotted on this basis in figures 6 and 7, and it will be seen that, apart from three exceptionally low frequencies in each figure, the points lie very close to the lines

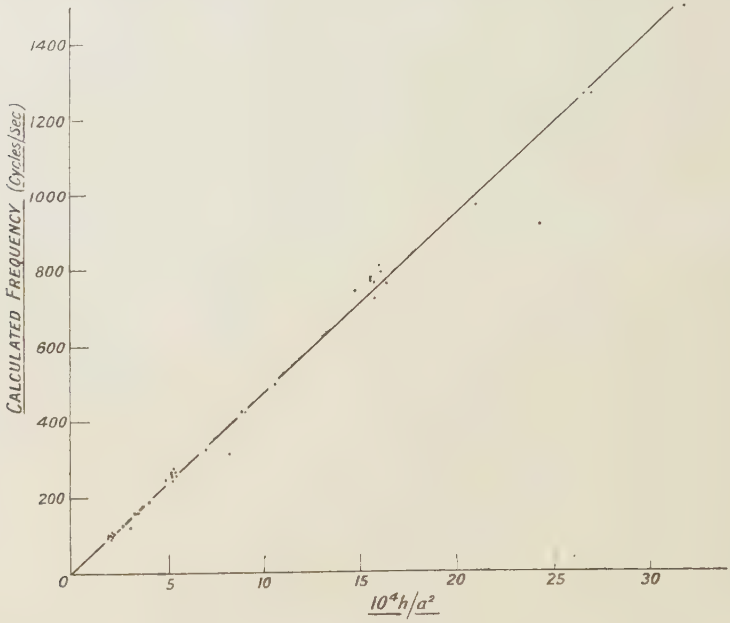

Figure 6. Square plates, clamped edges.

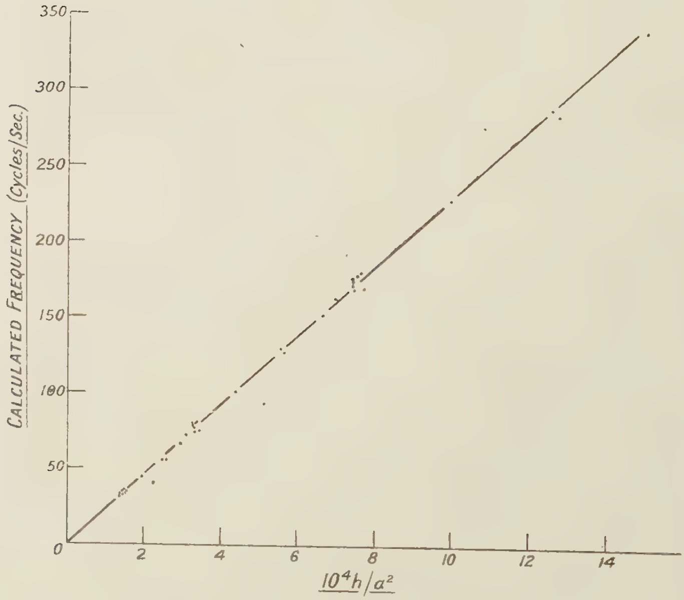

Figure 7. Square plates, supported edges.

$$\nu_c = 47 \times 10^4 h/a^2 \text{ (clamped edges),} \qquad \ldots\ldots(4.4)$$

$$\nu_s = 23 \times 10^4 h/a^2 \text{ (supported edges).} \qquad \ldots\ldots(4.5)$$

The exceptionally low frequencies all refer to the opepe 3-ply, and serve as a reminder that this method of estimating frequencies must necessarily give results somewhat in error in those cases where the assumed proportionality between elastic constants and density does not hold.

The theoretical frequencies for oblong plates have been analysed in the same way and have given the following equations :

Clamped edges :

$$a/b=2/3, \qquad \nu_c \approx 45\times 10^4 h/a^2\,;$$
$$a/b=3/2, \qquad \nu_c \approx 55\times 10^4 h/a^2.$$

Supported edges :

$$a/b=2/3, \qquad \nu_s \approx 21\times 10^4 h/a^2\,;$$
$$a/b=3/2, \qquad \nu_s \approx 29\times 10^4 h/a^2.$$

It will be remembered that a is the length of side parallel to the direction of greatest Young's modulus. The scatter of the points for $a/b=2/3$ is greater than that shown for square plates in figures 6 and 7, and the uncertainty in the predicted frequency is therefore greater in this case.

The experimental results for square plates (table 2) have been analysed statistically on the above basis, both as a whole and in groups corresponding with the different sizes of plate. The regression equations for predicting the experimentally observed frequencies in terms of $y(=10^4 h/a^2)$ are summarized in table 4.

Table 4. Summary of regression equations
(ν = observed frequency, $y=10^4 h/a^2$)

Clamped edges		Supported edges	
$a=b=39\cdot 3$ cm.	$\nu=42\cdot 9y-7\cdot 3$	$a=b=45\cdot 8$ cm.	$\nu=23\cdot 6y+3\cdot 8$
$a=b=24\cdot 2$ cm.	$\nu=34\cdot 4y+14\cdot 9$	$a=b=30\cdot 6$ cm.	$\nu=30\cdot 7y-6\cdot 1$
$a=b=14\cdot 0$ cm.	$\nu=27\cdot 7y+70\cdot 2$	$a=b=20\cdot 4$ cm.	$\nu=31\cdot 8y-44\cdot 0$
All results	$\nu=29\cdot 3y+38\cdot 7$	All results	$\nu=28\cdot 3y-2\cdot 9$

For the largest sizes, the equations are not very different from (4.4) and (4.5), which are derived from the theoretical frequencies. With clamped edges there is a noticeable decrease in the slope of the lines and an increase in the intercept on the y axis with decreasing size of plate. These effects are reflections of the tendency to curvature already discussed in connection with figure 4. The supported-edge results show a slight tendency to curvature in the opposite direction when analysed in this way, although, as already mentioned, this tendency is not obvious on inspection of figure 5. In other words, the edge conditions in the frames tend to approach each other at the higher frequencies, and there are indications that at the highest frequencies the "clamped"-edge frame may even impose less restraint at the edges than the "supported"-edge frame.

ACKNOWLEDGMENTS

The work described above was carried out in the Physics Section, Forest Products Research Laboratory, as part of the programme of the Forest Products

Research Board, and publication is by permission of the Department of Scientific and Industrial Research. The statistical analyses summarized in table 4 were carried out under the direction of Miss C. B. Pettifor, B.Sc.

REFERENCES

GOLAND, M., 1942. Curtiss-Wright Corporation, Airplane Division, *Research Report*, 5 S, 13.
HEARMON, R. F. S. and BARKAS, W. W., 1941. *Proc. Phys. Soc.* **53**, 674.
MARCH, H. W., 1936. *Physics*, **7**, 32.
MARCH, H. W., 1942. *U.S. Dept. Agric. Forest Prod. Lab., Madison*, Mimeo. 1312.
NORRIS, C. B., VOSS, A. W. and PALMA, J., 1945. *U.S. Dept. Agric. Forest Prod. Lab., Madison*, Mimeo. 1316 H.
TIMOSHENKO, S., 1937. *Vibration Problems in Engineering* (New York : Van Nostrand).
TIMOSHENKO, S., 1940. *The Theory of Plates and Shells* (New York : McGraw-Hill).
TOMOTIKA, S., 1936. *Phil. Mag.* **21**, 745.

THE OPTICAL SINE-CONDITION

BY H. H. HOPKINS,
W. Watson and Sons, Barnet, Herts

MS. received 20 *September* 1945

ABSTRACT. The Sine-Condition is formulated on the basis of optical path differences, leading to an expression which is valid in the presence of spherical aberration. It is shown to contain results obtained previously by means of a " ray-intersection " analysis. The " next terms " are estimated and serve as an approximate measure of the error involved ; or, alternatively, as an indication of the size of field over which the sine-condition is a valid measure of off-axis aberration.

It is well known that fulfilment of the so-called *Sine-Condition* by an optical system ensures freedom from the aberration of coma for objects that are but a small angular distance from the axis. Because of this fact, the sine-condition has been used extensively by lens designers as a check on the off-axis performance of both telescope and microscope objectives. There are, however, respects in which this usage has been unsatisfactory.

In the first place the condition is a valid measure of off-axis aberration only when the angular distance off-axis of the object point is so small that its square can be neglected. There is an uncertainty in the size of field over which this approximation is permissible, given a required order of accuracy in the result. Secondly, the physical meaning which can be attached to the violation of the condition is—in my experience—generally not appreciated. The permitted departures from exact fulfilment of the sine-condition are consequently either wholly arbitrary or based on experience of " what works ". It is true that Conrady (*Applied Optics and Optical Design*, vol. i, p. 393) gave a "Rayleigh tolerance " for coma, but this was simply quoted without proof.

In what follows, an account of the imagery of off-axis object points is given which leads to a simple interpretation of departures from the sine-condition and also provides an approximate rule giving the size of field over which the condition is a valid measure of off-axis aberration.

In figure 1, O_1 and Q_1 are object points (real or virtual), the one situated on, and the other a small angular distance off, the axis, O_1O_λ', of an optical system having λ refracting surfaces. The diagram shows a meridian section containing the off-axis object point Q_1. ST is a section of a spherical wave-front with centre O_1 : S_QT_Q is a section of a spherical wave-front with centre Q_1. Thus O_1P_0, $Q_1R_0P_0$ and O_1E_1, Q_1E_1 are rays along which elements of the waves proceed from the object points O_1, Q_1. R_0 is on the sphere S_QT_Q.

O_λ', Q_λ' are the Gaussian images of O_1, Q_1 respectively; $S'T'$, S_Q' T_Q' are spheres centred on O_λ', Q_λ'. The forms of the wave-fronts emerging from the system and proceeding towards O_λ', Q_λ' can be specified by their departures at a given moment from the appropriate one of the spheres centred on O_λ', Q_λ'. Such a procedure has been used before.*

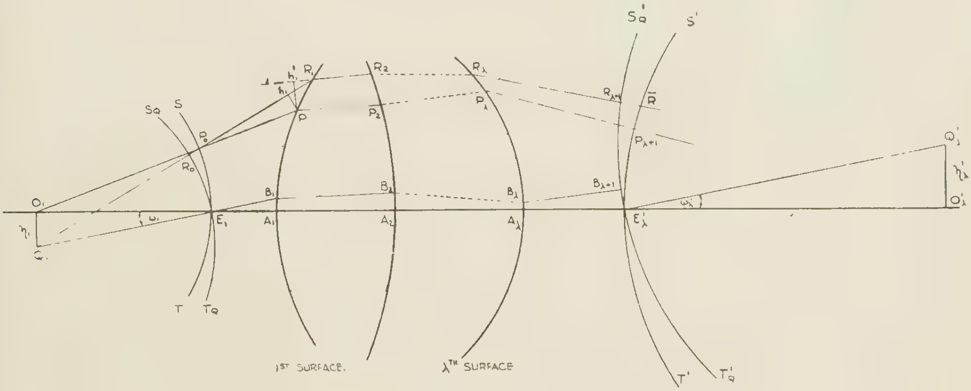

Figure 1.

When the departure from the appropriate reference sphere is zero (or constant) for the whole aperture, the corresponding image point is free from aberration. The departure at a given point on the wave-front will be referred to as the wave-front aberration. It is a function of the position of the wave element on the emergent wave-front, and will be measured, not as a geometrical, but as an optical, path-length.

The incident wave-fronts and the reference-spheres of the emergent wave-fronts are conveniently chosen so that they intersect in E_1, E_λ' the axial points of the entrance and exit pupils. In the diagram (simply for the purposes of clarity) these latter have been taken to be external to the system. Thus Q_1E_1 is the initially incident principal ray from Q_1.

An element of the wave from O_1 proceeds along the ray $O_1P_0P_1P_2 \ldots \ldots P_\lambda P_{\lambda+1}$, intersecting the O_λ'-reference sphere in $P_{\lambda+1}$. Suppose the final wave-front aberration of this element is W_λ', measured positively when the element is in advance of the O_λ'-reference sphere, and such that this latter and the emergent wave coincide at E_λ'—that is, W_λ' is zero for the element of wave which proceeds from O_1 along the axis O_1O_λ'. Then the wave-front aberration of the wave-element considered is

---

* For a derivation of the theory of the aberrations of lens-systems on this basis, see the writer's "Monochromatic Lens Aberration Theory", *Phil. Mag.* (publication impending.)

$$W_\lambda' = (E_1A_1A_2\ldots\ldots A_\lambda E_\lambda') - (P_0P_1P_2\ldots\ldots P_\lambda P_{\lambda+1}), \qquad \ldots\ldots(1)$$

where the brackets denote optical path lengths.

A second element of wave proceeds from Q_1 along the ray $Q_1R_0P_0R_1R_2\ldots\ldots R_\lambda R_{\lambda+1}$, intersecting the Q_λ'-reference sphere in $R_{\lambda+1}$. If this element has a wave-front aberration V_λ', measured positively when the element is in advance of the Q_λ'-reference sphere, and such that this latter and the emergent wave coincide at $B_{\lambda+1}$—that is, V_λ' is zero for the element of wave which proceeds from Q_1 along the principal ray $E_1B_1B_1\ldots\ldots B_\lambda B_{\lambda+1}$—then the wave-front aberration of the element considered is

$$V_\lambda' = (E_1B_1B_2\ldots\ldots B_\lambda B_{\lambda+1}) - (R_0P_0R_1R_2\ldots\ldots R_\lambda R_{\lambda+1}), \qquad \ldots\ldots(2)$$

where $B_{\lambda+1}$, $R_{\lambda+1}$ are the points of intersection of the emergent rays with the Q_λ'-reference sphere. Rewriting (2),

$$V_\lambda' = (E_1B_1B_2\ldots\ldots B_\lambda B_{\lambda+1}) - (P_0R_1R_2\ldots\ldots R_\lambda R_{\lambda+1}\bar{R}) + (R_{\lambda+1}\bar{R} - R_0P_0),$$

where $\bar{R}$ is the point of intersection of $R_\lambda R_{\lambda+1}$ with the O_λ'-reference sphere, it follows, using (1), that :

$$V_\lambda' = W_\lambda' + (R_{\lambda+1}\bar{R} - R_0P_0) + C_1, \qquad \ldots\ldots(3)$$

where

$$\begin{aligned} C_1 = &\{(E_1B_1B_2\ldots\ldots B_\lambda B_{\lambda+1}) - (E_1A_1A_2\ldots\ldots A_\lambda E_\lambda')\} \\ &- \{(P_0R_1R_2\ldots\ldots R_\lambda R_{\lambda+1}\bar{R}) - (P_0P_1P_2\ldots\ldots P_\lambda P_{\lambda+1})\}. \end{aligned}$$

It can be shown that C_1 is zero (or negligible) for small angles of field.

From P_1 draw P_1h_1, P_1h_1' perpendicular to P_0P_1, P_1P_2, and meeting P_0R_1, R_1R_2 (produced if necessary) in h_1, h_1'. Then the following are differences in optical path length :

$$\begin{aligned} (P_0R_1 - P_0P_1) &= N_1 . l_1 \sin I_1 + N_1 . D_0 (\sec x_1 - 1) \\ (R_1R_2 - P_1P_2) &= N_2' . l_2' \sin I_2' - N_1' . l_1 \sin I_1' + N_2 . D_1 (\sec x_2 - 1) \\ &\cdot\quad\cdot\quad\cdot\quad\cdot\quad\cdot\quad\cdot\quad\cdot\quad\cdot\quad\cdot\quad\cdot \\ (R_\lambda\bar{R} - P_\lambda P_{\lambda+1}) &= -N_\lambda' . l_\lambda \sin I_\lambda' + N_{\lambda+1} . D_\lambda (\sec x_{\lambda+1} - 1), \end{aligned}$$

where $l_1 = P_1R_1$, $l_2 = P_2R_2$, ... etc. ; $x_1 = R_1\hat{P}_0P_1$, ... etc. ; $D_0 = P_0P_1$, $D_1 = P_1P_2$, ... $D_\lambda = P_\lambda P_{\lambda+1}$; N_1, $N_2 = N_1'$, ... etc., are refractive indices ; and I, I' are the angles of incidence and emergence of the ray $P_0P_1P_2\ldots\ldots P_\lambda$ at the successive surfaces of the system. Addition of these equations gives, the angles x being assumed small,

$$\begin{aligned} &\{(P_0R_1R_2\ldots\ldots R_\lambda R_{\lambda+1}\bar{R}) - (P_0P_1P_2\ldots\ldots P_\lambda P_{\lambda+1})\} \\ &\quad = \tfrac{1}{2}x_1^2 . N_1D_0 + \tfrac{1}{2}x_2^2 . N_2D_1 + \ldots\ldots + \tfrac{1}{2}x_{\lambda+1}^2 . N_{\lambda+1} . D_\lambda, \qquad \ldots\ldots(4) \end{aligned}$$

the other items cancelling because of the law of refraction between I and I'.

By a similar argument applied to the principal ray it can be shown that

$$\begin{aligned} &\{(E_1B_1B_2\ldots\ldots B_\lambda B_{\lambda+1}) - (E_1A_1A_2\ldots\ldots A_\lambda E_\lambda')\} \\ &\quad = \tfrac{1}{2}y_1^2 . N_1d_0 + \tfrac{1}{2}y_2^2 . N_2d_1 + \ldots\ldots + \tfrac{1}{2}y_{\lambda+1}^2 . N_{\lambda+1}d_\lambda, \qquad \ldots\ldots(5) \end{aligned}$$

where $d_0 = E_1A_1$, $d_1 = A_1A_2$, ... etc. ; and $y_1 = B_1\hat{E}_1A_1$, and so on.

From (4) and (5)

$$C_1 = \tfrac{1}{2}y_1^2 . N_1(d_0 - D_0) + \tfrac{1}{2}y_2^2 . N_2(d_1 - D_1) + \ldots\ldots + \tfrac{1}{2}y_{\lambda+1}^2 . N_{\lambda+1}(d_\lambda - D_\lambda), \qquad \ldots\ldots(6)$$

where a "paraxial" approximation has been made in putting $x_2 = y_2$, $x_3 = y_3$, ... etc., and where $x_1 = y_1 = \omega_1$; ω_1 being the angle of field $Q_1\hat{E}_1O_1$, which is small. If, now, retaining the paraxial approximation, there is written

$$y_1 = \frac{\omega_1}{V_1} . V_1, \quad y_2 = \frac{\omega_1}{V_1} . V_2, \ldots\ldots y_{\lambda+1} = \frac{\omega_1}{V_1} . V_{\lambda+1},$$

where V_1, V_2 ..... $V_{\lambda+1}$ are angles from a traced paraxial principal ray, then

$$C_1 = \tfrac{1}{2}\left(\frac{\omega_1}{V_1}\right)^2 \{N_1(d_0 - D_0) . V_1^2 + N_2(d_1 - D_1) . V_2^2 + \ldots\ldots$$
$$+ N_{\lambda+1}(d_\lambda - D_\lambda) . V_{\lambda+1}^2\} \qquad \ldots\ldots(7)$$

which gives an approximate value for C_1. For small angles of field, powers of ω_1 higher than the first are neglected, and C_1 is regarded as zero. Equation (7) then provides an estimate of the most significant error arising from this approximation. On the other hand, given a "safe" limit for C_1, (7) provides an expression for ω_1, the size of field over which the approximation is sufficiently valid. C_1 is on an optical path length, and is one of the principal errors involved in V_λ', when C_1 is assumed zero in equation (3).

Attention has been confined so far to rays from Q_1, lying in the meridian section. It is, however, easy to show that the result (4), and therefore (7), hold equally for skew rays from Q_1. For, in this case, the elements of refracting surfaces at P_1, P_2 ..... P_λ are regarded as plane. Planes are constructed through each of these points perpendicular to the rays incident and emergent at the points. The differences in optical path length then become

$$(P_0R_1 - P_0P_1) = N_1 . l_1 \sin I_1 . \cos\phi_1 + N_1 . D_0 (\sec x_1 - 1)$$
$$(R_1R_2 - P_1P_2) = N_2 . l_2 \sin I_2 . \cos\phi_2 - N_1 . l_1 \sin I_1' . \cos\phi_1 + N_2 . D_1(\sec x_2 - 1)$$

and so on, where ϕ_1, ϕ_2, ... etc., are the azimuths of the points of incidence R_1, R_2, ... R_λ. On addition, terms on the right-hand side again cancel, giving the result (4). Thus C_1 is zero for both meridian and skew rays, providing powers of ω_1 higher than the first are neglected. Furthermore, equation (7) still provides an estimate of the error involved in the approximation.

Construct, then, rectangular co-ordinates having O_1 as origin, O_1O_λ' as x-axis, and Q_1 in the XOZ-plane. Let $O_1E_1 = r$, $Q_1E_1 = p$; and let P_0 (on the incident wave from O_1) have co-ordinates (x, y, z). Then if Q_1 is the point (o, o, η), the length Q_1P_0 is given by

$$Q_1P_0^2 = x^2 + y^2 + (z - \eta)^2 = p^2 - 2z\eta.$$

In the diagram η_1 and ω_1 are shown negative, following the usual optical convention of signs.

Thus, since $O_1\hat{E}_1Q_1 = \omega_1$ is assumed small,

$$R_0P_0 = Q_1P_0 - p = -\frac{z . \eta}{p} - \tfrac{1}{2}\frac{z^2 . \eta^2}{p^3},$$

or, substituting $\frac{1}{p}=\frac{1}{r}\left(1-\frac{1}{2}\frac{\eta^2}{r^2}\right)$,

$$\mathrm{R}_0\mathrm{P}_0=-\frac{z\,.\,\eta}{r}-\frac{1}{2}\frac{z\,.\,\eta^2}{r^2}\left[\frac{\eta}{r}-\frac{z}{r}\right].$$

Replacing z by polar co-ordinates $(\rho_1,\ \phi)$, where $\phi=0$ is the positive direction of z, and ρ_1 is the perpendicular distance of P_0 from the axis, this becomes

$$\mathrm{R}_0\mathrm{P}_0=-\frac{\eta_1\rho_1}{r_1}\,.\cos\phi-\frac{\eta_1\rho_1}{r_1}\,.\cos\phi\,.\,\tfrac{1}{2}\tan^2\omega_1\left(\tan\omega_1-\frac{\rho_1\cos\phi}{r_1}\right),\quad\ldots\ldots(8)$$

where the suffix 1 has also been given to η, ω and r.

Similarly if Q_λ' be joined to $\mathrm{P}_{\lambda+1}$ (and continued), the intercept between the two reference spheres is very closely equal to $\mathrm{R}_{\lambda+1}$; and, therefore,

$$\mathrm{R}_{\lambda+1}\,\overline{\mathrm{R}}=-\frac{\eta_\lambda'\rho_\lambda'}{r_\lambda'}\,.\cos\phi-\frac{\eta_\lambda'\rho_\lambda'}{r_\lambda'}\cos\phi\,.\,\tfrac{1}{2}\tan^2\omega_\lambda'\left(\tan\omega_\lambda'-\frac{\rho_\lambda'\cos\phi}{r_\lambda'}\right),\quad\ldots\ldots(9)$$

where ρ_λ' is measured at the exit pupil.

Subtraction of (8) and (9) gives for the optical path difference

$$(\mathrm{R}_{\lambda+1}\overline{\mathrm{R}}-\mathrm{R}_0\mathrm{P}_0)=\left(\frac{N_1\eta_1\rho_1}{r'}-\frac{N_\lambda'\rho_\lambda'\rho_\lambda'}{r_\lambda'}\right)\cos\phi+C_2,\quad\ldots\ldots(10)$$

where C_2, a second-order term, is

$$C_2=\frac{N_1\eta_1\rho_1}{r_1}\,.\cos\phi\,.\,\tfrac{1}{2}\tan^2\omega_1{}^2\left(\tan\omega_1-\frac{\rho_1\cos\phi}{r_1}\right)$$
$$-\frac{N_\lambda'\eta_\lambda'\rho_\lambda'}{r_\lambda'}\,.\cos\phi\,.\,\tfrac{1}{2}\tan^2\omega_\lambda'\left(\tan\omega_\lambda'-\frac{\rho_\lambda'\cos\phi}{r_\lambda'}\right).$$

It will be seen that C_2 is zero in the sagittal section, $\phi=\pi/2$. In the meridian section it has the value

$$C_2=\frac{N_1\eta_1\rho_1}{r_1}\,.\,\tfrac{1}{2}\tan^2\omega_1\left(\tan\omega_1-\frac{\rho'}{r_1}\right)$$
$$-\frac{N_\lambda'\eta_\lambda'\rho_\lambda'}{r_\lambda'}\,.\,\tfrac{1}{2}\tan^2\omega_\lambda'\left(\tan\omega_\lambda'-\frac{\rho_\lambda'}{r_\lambda'}\right).\quad\ldots\ldots(11)$$

This is zero if powers of ω_1 higher than the first are ignored. (11) then estimates the error involved in the approximation.

Substitution of (10) in (4) gives, ignoring C_1 and C_2,

$$V_\lambda'=W_\lambda'+\left[\frac{N_1\eta_1\rho_1}{r_1}-\frac{N_\lambda'\eta_\lambda'\rho_\lambda'}{r_\lambda'}\right].\cos\phi,\quad\ldots\ldots(12)$$

where r_1, r_λ' have signs such that, in figure 1, r_1 is positive and r_λ' negative. This will be so if

$$\left.\begin{aligned}r_1&=l_{\mathrm{pr}_1}-l_{\mathrm{parax}_1},\\ r_\lambda'&=l_{\mathrm{pr}_\lambda}-l'_{\mathrm{parax}_\lambda},\end{aligned}\right\}\quad\ldots\ldots(13)$$

with an obvious notation. Thus the wave-front aberration associated with the wave proceeding to Q_λ' consists of the spherical aberration W_λ' of the wave proceeding to O_λ', together with a coma-type term, which is zero in the sagittal section ($\phi = \pi/2$) and has a maximum value in the meridian section ($\phi = 0$). The latter is merely reversed in sign in the section $\phi = \pi$. In the section $\phi = 0$, (12) becomes

$$V_\lambda' = W_\lambda' + \left[\frac{N_1 \eta_1 \rho_1}{l'_{\text{pr}_1} - l_{\text{parax}_1}} - \frac{N_\lambda' \eta_\lambda' \rho_\lambda'}{l'_{\text{pr}_\lambda} - l'_{\text{parax}_\lambda}}\right], \qquad \ldots\ldots(14)$$

and this can readily be given forms suited to special cases.

Thus, for telescopic systems in air ($N_1 = N_\lambda' = 1$),

$$V_\lambda' = W_\lambda' + [\rho_1 \,.\, \tan\omega_1 - \rho_\lambda' \,.\, \tan\omega_\lambda'], \qquad \ldots\ldots(15)$$

where ρ_1, ρ_λ' are measured in the (paraxially defined) entrance and exit pupils along the marginal ray. If h_1, h_λ' are the initial and final incidence heights of a paraxial ray trace, the magnification is

$$\frac{h_1}{h_\lambda'} = \frac{\tan\omega_\lambda'}{\tan\omega_1},$$

so that

$$V_\lambda' = W_\lambda' + \left[\rho_1 - \frac{h_1}{h_\lambda} \,.\, \rho_\lambda'\right] \tan\omega_1. \qquad \ldots\ldots(16)$$

Using the notation of figure 2, in which $\delta u_\lambda'$, the final angular aberration is

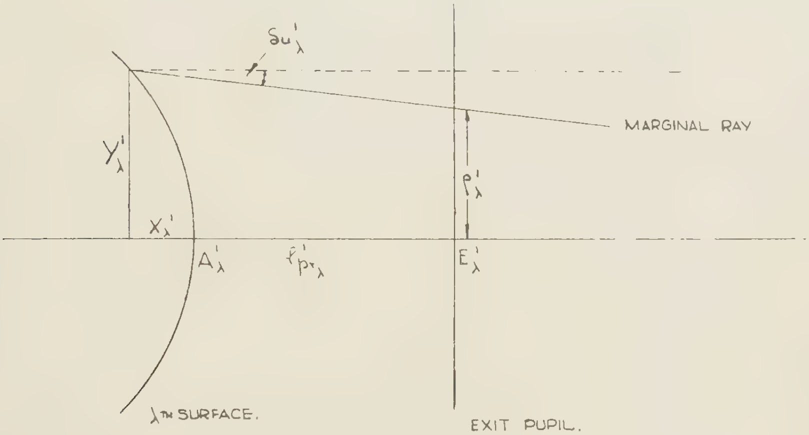

Figure 2.

shown as positive,

$$\rho_\lambda' = Y_\lambda' - (l'_{\text{pr}_\lambda} - X_\lambda') \,.\, \tan\delta u_\lambda'. \qquad \ldots\ldots(17)$$

From this it will be seen that, in the presence of spherical aberration ($\delta u_\lambda \neq 0$), ρ_λ', and hence the coma part of V_λ', will vary with l'_{pr_λ}, the position of the exit pupil.

The case of telescopic and photographic objectives in air gives

$$V_\lambda' = W_\lambda' + \left[\rho_1 - \frac{F}{l'_{\text{pr}_\lambda} - l'_{\text{parax}_\lambda}} \,.\, \rho_\lambda'\right] \tan\omega_1, \qquad \ldots\ldots(18)$$

where use has been made of the relationship $\eta_\lambda' = F \,.\, \tan\omega_1$, F being the equivalent focal length of the system. In figure 3, u_λ' is the angle between the finally emergent marginal ray and the axis, $\delta u_\lambda'$, $\delta s_\lambda'$ are the angular and longitudinal spherical aberration respectively of the marginal ray $P_{\lambda+1}O'_{m\lambda}$. Evidently, the angle $\delta u_\lambda'$ being small, and negative as shown,

$$\begin{aligned}\rho_\lambda' &= r_\lambda' \,.\, \sin(u_\lambda' - \delta u_\lambda') \\ &= r_\lambda'\{\sin u_\lambda' + \delta s_\lambda' \,.\, \sin u_\lambda' \,.\, \cos u_\lambda' / r_\lambda'\},\end{aligned} \qquad \ldots\ldots(19)$$

since, with the given sign convention,

$$\delta u_\lambda' = -\frac{\delta s_\lambda' \,.\, \sin u_\lambda'}{r_\lambda'}$$

Using this in (18) gives

$$V_\lambda' = W_\lambda' + \left[\rho_1 - F\sin U_\lambda'\left(1 + \frac{\delta s_\lambda' \,.\, \cos U_\lambda'}{l'_{\mathrm{pr}_\lambda} - l'_{\mathrm{parax}_\lambda}}\right)\right] .\, \tan\omega_1. \qquad \ldots\ldots(20)$$

It will again be seen that the coma part of V_λ' is independent of shifts of the diaphragm in the absence of spherical aberration ($\delta s_\lambda' = 0$) : on the other hand, V_λ' is independent of the spherical aberration when $l'_{\mathrm{pr}_\lambda} = \infty$—that is, with a diaphragm in the anterior focal plane (telecentric stop). With the exit pupil at the posterior nodal point, $F = -(l'_{\mathrm{pr}_\lambda} - l'_{\mathrm{parax}_\lambda}) = -r_\lambda'$, and

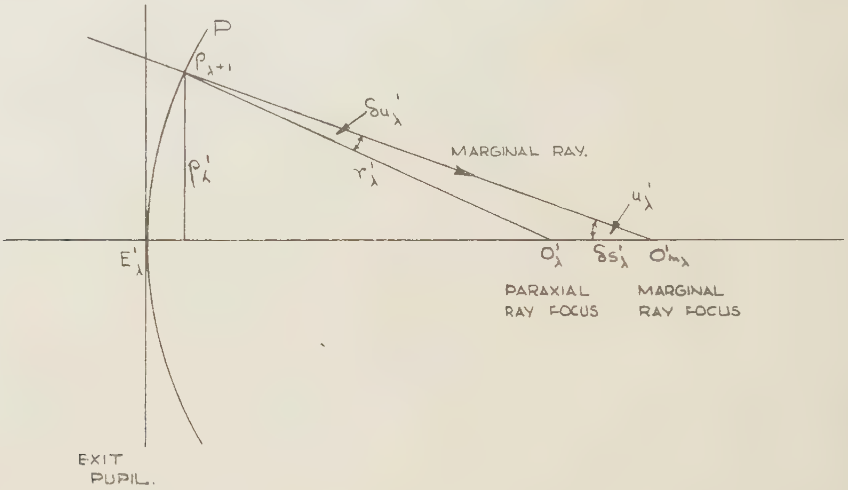

Figure 3.

$$V_\lambda' = W_\lambda' + [\rho_1 - (F - \delta s_\lambda' \,.\, \cos U_\lambda') \,.\, \sin U_\lambda'] \tan\omega_1, \qquad \ldots\ldots(21)$$

or, since in this case $\omega_1 = \omega_\lambda'$,

$$V_\lambda' = W_\lambda' + \left[u'_{\mathrm{parax}_\lambda} - \frac{F - \delta s_\lambda' \,.\, \cos U_\lambda'}{F} \,.\, \sin U_\lambda'\right] \eta_\lambda', \qquad \ldots\ldots(22)$$

where $u'_{\mathrm{parax}_\lambda}$ refers to a paraxial trace having the same initial incidence height as the marginal ray.

For systems in which both object and image distances are finite, (14) becomes

$$V_\lambda' = W_\lambda' + \left[N_1\eta_1 \sin U_1 - N_\lambda'\eta_\lambda' \sin U_\lambda' \,.\, \left(1 + \frac{\delta s_\lambda' \,.\, \cos U_\lambda'}{l'_{\mathrm{pr}_\lambda} - l'_{\mathrm{parax}_\lambda}}\right)\right], \qquad \ldots\ldots(23)$$

use having again been made of the result (19). Again it will be seen that V_λ' is independent of $\delta s_\lambda'$ when $l_{\mathrm{pr}_\lambda}' = \infty$; and independent of l'_{pr_λ} when $\delta s_\lambda' = 0$. These results were obtained by Conrady (*loc. cit.* p. 375) using a "ray-intersection" investigation. (23) can be put into a different form, thus

$$V_\lambda' = W_\lambda' + \left[\frac{\sin U_1}{u_1} - \frac{\sin U_\lambda'}{u_\lambda'}\left(1 + \frac{\delta s_\lambda' \,.\, \cos U_\lambda'}{l'_{\mathrm{pr}_\lambda} - l_{\mathrm{parax}_\lambda}}\right)\right] H, \qquad \ldots\ldots(24)$$

where $H = N_1 u_1 \eta_1 = N_1' u'_1 \eta_1' = \ldots\ldots = N_\lambda' u_\lambda' \eta_\lambda'$ (the Lagrange Invariant) ; and small u's refer to paraxial angles. When $\delta s_\lambda' = 0$, or $l'_{\mathrm{pr}_\lambda} = \infty$, this gives for the absence of coma the classical (but very restricted) result

$$\frac{\sin U_1}{u_1} = \frac{\sin U_\lambda'}{u_\lambda'}, \qquad \ldots\ldots(25)$$

The above formulae will give the coma part of the wave-front aberration even in the presence of large amounts of spherical aberration. The Rayleigh tolerance states simply that the total V_λ' must not exceed $\lambda/4$; Conrady's tolerance applies only to the coma part of V_λ'. Given the same tolerance on W_λ', N_λ' might thus reach $\lambda/2$ at some parts of the aperture.

The coma-part of the expression for V_λ' includes all the coma terms depending on the first power of the field, i.e. those in which the wave-front aberration is proportional to the cube, fifth, seventh ..... powers of the aperture. The accuracy of the results can be easily checked by noting the values of C_1 and C_2. If, as in a good many telescope objectives, the incidence heights of the principal rays are all small, there can be written in (7)

$$V_2/V_1 = N_1 \; N_2$$

and so on, giving the useful result

$$C_1 = \tfrac{1}{2} N_1 \omega_1^2 [(d_0 - D_0) + (d_1 - D_1) + (d_2 - D_2) + \ldots\ldots + (d_\lambda - D_\lambda)]. \qquad \ldots\ldots(26)$$

The correction term C_2, depending on powers of ω_1 higher than the square, will generally be smaller than C_1.

Although the above demonstrations have assumed the (more usual) system consisting of centred spherical refracting interfaces, it will be appreciated that essentially the results apply to other systems. Moreover, it will be seen that a similar analysis yields a " Sine-Condition " (based on an accurate principal ray-trace and another ray from the same object point) which will give the wave-front aberration associated with image points in the neighbourhood of an off-axis image point.

HERSCHEL'S CONDITION

By H. H. HOPKINS,

W. Watson and Sons, Barnet, Herts

MS. received 12 *October* 1945

ABSTRACT. The change in spherical aberration introduced by a change in object distance is discussed. Herschel's condition is shown to be valid for originally corrected conjugates. It follows as a special case of the general formulae derived.

The satisfying of Herschel's condition by an optical system which is free from spherical aberration for given conjugates ensures freedom from spherical aberration for neighbouring pairs of conjugates. Attention does not seem to have been called to the invalidity of the usual form of the condition in the case when the system is not corrected for the original conjugates. It is, however, possible to formulate the condition in such a manner that it not only applies to such uncorrected systems, but such that the resulting generalized condition also measures directly the change in spherical aberration consequent upon a small change in the conjugates. The treatment resembles closely that which has been used elsewhere in connection with the Sine Condition (Hopkins, *Proc. Phys. Soc.* **58**, 92 (1946)).

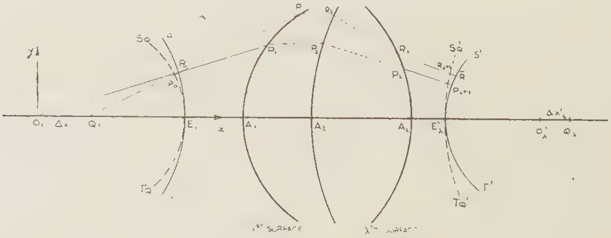

In the figure, O_1 is an object point (real or virtual) situated on the axis O_1O_λ' of an optical system consisting of λ refracting surfaces. O_λ' is the Gaussian image of O_1 after λ refractions. Spheres ST, S′T′ centred on O_1, O_λ' serve as reference surfaces, with respect to which the initially incident and finally emergent wave-fronts can be specified (*vide* Hopkins, 1945). These are conveniently chosen to intersect the axial points of the (paraxially defined) entrance and exit pupils. The latter are, respectively, E*s* and E_λ'.*

Assume the incident and emergent wave-fronts to coincide with the O_1- and O_λ'-reference spheres, respectively, at the points E_1, E_λ'. Let the element of wave from O_1 which is associated with the ray through P_0 be in advance of the O_1-reference sphere by an amount W_1, which is an optical path length. This is, then, the initial wave-front aberration of the wave-element. Let W_λ' be the amount this element is in advance of the O_λ'-reference sphere upon emergence. This is, then, the final wave-front aberration of the wave-element. Since optical path lengths along rays between corresponding wave-fronts are equal,

---

* In the presence of spherical aberration the outer parts of the wave-front close up (or open out) more rapidly than the central parts. Because of this, the angular distribution of wave-front aberration depends upon the radii of the reference spheres. These are conventionally chosen, in each case, to refer the aberration to the entrance and exit pupils.

$$W_\lambda' - W_1 + (P_0P_1P_2 \ldots\ldots P_1P_{\lambda+1}) = (E_1A_1A_2 \ldots A_\lambda E_\lambda'), \qquad \ldots\ldots(1)$$

where the brackets denote optical path lengths.

Suppose, now, the object point be moved to Q_1, whose Gaussian image is Q_λ'. Let a wave-element, having initial wave-front aberration W_1, proceed from Q_1 along the ray $R_0P_0R_1R_2 \ldots\ldots R_\lambda R_{\lambda+1}$ (where R_0, $R_{\lambda+1}$ are on the spheres S_QT_Q, $S_Q'T_Q'$, which are centred on Q_1, Q_λ'. There can then be written

$$V_\lambda' - W_1 + (R_0P_0R_1R_2 \ldots\ldots R_\lambda R_{\lambda+1}) = (E_1A_1A_2 \ldots\ldots A_\lambda E_\lambda'), \qquad \ldots\ldots(2)$$

where V_λ' is the final wave-front aberration of the wave-element on emergence from the system, measured with reference to S'_QT_Q', the Q_λ-reference sphere.

On subtraction (1) and (2) give

$$\begin{aligned} V_\lambda' - W_\lambda' &= (P_0P_1P_2 \ldots\ldots P_\lambda P_{\lambda+1}) - (R_0P_0R_1R_2 \ldots\ldots R_\lambda R_{\lambda+1}) \\ &= (P_0P_1P_2 \ldots\ldots P_\lambda P_{\lambda+1}) - (P_0R_1R_2 \ldots\ldots R_\lambda R_{\lambda+1}\bar{R}) \\ &\qquad + (R_{\lambda+1}\bar{R} - R_0P_0). \end{aligned}$$

The first two brackets have been shown elsewhere to be equal, and they cancel, providing the angle $O_1R_0Q_1 = \Delta U_1$ is sufficiently small for powers of ΔU_1 higher than the first to be ignored. The error implied in this approximation has also been discussed elsewhere (Hopkins, *loc. cit.*). To this accuracy, the change in the wave-front aberration of the element considered is, therefore,

$$dW = (R_{\lambda+1}\bar{R} - R_0P_0). \qquad \ldots\ldots(3)$$

Construct, then, plane rectangular co-ordinates having O_1 as origin, x-axis along the line O_1O_λ', and y-axis in the plane of the diagram and positive above the optical axis. Let P_0 have co-ordinates (x, y), and let E_1 be the point $(r_1, 0)$. Then

$$\begin{aligned} P_0Q_1^2 &= (x - \Delta x_1)^2 + y^2 \\ &= r_1^2 - 2x \,.\, \Delta x_1, \end{aligned}$$

since P_0 is on the circle $x^2 + y^2 = r_1^2$. $\Delta x_1 = O_1Q_1$ is assumed small compared with r_1, and powers of $\Delta x_1/r_1$ higher than the first are therefore ignored. Taking square roots,

$$P_0Q_1 = r_1 - \frac{x \,.\, \Delta x_1}{r_1}$$

to the required accuracy ; and further,

$$Q_1R_0 = Q_1E_1 = r_1 - \Delta x_1.$$

Thus

$$P_0Q_1 - Q_1R_0 = \Delta x_1\left(1 - \frac{x_1}{r_1}\right)$$

or

$$P_0R_0 = \Delta x_1 \,.\, (1 - \cos\theta_1), \qquad \ldots\ldots(4)$$

where θ_1 is the angle $P_0\hat{O}_1E_1$, O_1 being the paraxial object point.

If, now, O_λ' be joined to $P_{\lambda+1}$ (and continued), the intercept between the spheres S′T′, $S_Q'T_Q'$ is very closely equal to $R_{\lambda+1}\overline{R}$. Using, therefore, an expression for $R_{\lambda+1}\overline{R}$ similar to (4), the expression (3) becomes

$$dW = N_\lambda' \,.\, \Delta x_\lambda'(1-\cos\theta_\lambda') - N_1 \,.\, \Delta x_1(1-\cos\theta_1).$$

Thus, using the (paraxial) longitudinal magnification formula

$$N_\lambda' u_\lambda'^2 \,\Delta x_\lambda' = N_1 u_1^2 \Delta x_1 = H_L, \qquad \ldots\ldots(5)$$

the change in spherical aberration produced by the change of conjugates denoted by H_L is given by

$$dW = \left[\frac{1-\cos\theta_\lambda'}{u\lambda'^2} - \frac{1-\cos\theta_1}{u_1^2}\right] . H_L, \qquad \ldots\ldots(6)$$

where u_λ', u_1 refer to paraxial angles associated with the original conjugates. This formula can be given forms suited to special cases.

Thus, in the absence of spherical aberration, $\theta_1 = U_1$, $\theta_\lambda' = U_\lambda'$, where U_1, U_λ' are angles from a marginal ray trace. (6) becomes

$$dW = \left[\left(\frac{\sin\frac{1}{2}U_\lambda'}{u_\lambda'/2}\right)^2 - \left(\frac{\sin\frac{1}{2}U_1}{u_1/2}\right)\right] . \tfrac{1}{2}H_L\,, \qquad \ldots\ldots(7)$$

which leads to the usual form of the Herschel condition. For dW will be zero, providing

$$\frac{\sin\frac{1}{2}U_\lambda'}{u_\lambda'/2} = \frac{\sin\frac{1}{2}U_1}{u_1/2}. \qquad \ldots\ldots(8)$$

If the system is uncorrected for the original conjugates, $\theta_\lambda' \neq U_\lambda'$, $\theta_1 \neq U_1$: (7), (8) are then no longer valid.

If, now,

$$\delta u_1 = -\frac{\delta s_1 \,.\, \sin U_1}{l_{\mathrm{pr}_1} - l_{\mathrm{parax}_1}}\,, \qquad \delta u_\lambda' = -\frac{\delta s_\lambda' \,.\, \sin U_\lambda'}{l'_{\mathrm{pr}_\lambda} - l'_{\mathrm{parax}_\lambda}}$$

are the initial and final angular spherical aberrations associated with a given ray, defined when the axial parts of the incident and emergent wave-fronts are at E_1, E_λ' respectively, and with the notation of an earlier paper (*loc. cit.*), then

$$\theta_1 = U_1 - \delta u_1, \qquad \theta_\lambda' = U_\lambda' - \delta u_\lambda'$$

and

$$\cos\theta_1 = \cos U_1 + \sin U_1 \cdot \frac{\delta s_1 \sin U_1}{l_{\mathrm{pr}_1} - l_{\mathrm{parax}_1}}\,, \qquad \ldots\ldots(9)$$

$$\cos\theta_\lambda' = \cos U_\lambda' + \sin U_\lambda' \cdot \frac{\delta s_\lambda' \,.\, \sin U_\lambda'}{l'_{\mathrm{pr}_\lambda} - l'_{\mathrm{parax}_\lambda}}$$

Substitution of these in (6) gives, after some reduction,

$$dW = \left[\left(\frac{\sin\frac{1}{2}U_\lambda'}{u_\lambda'/2}\right)^2 \cdot \left(1 + \frac{1-\cos U_\lambda'}{l'_{\mathrm{pr}_\lambda} - l'_{\mathrm{parax}_\lambda}} . \delta s_\lambda'\right)\right.$$

$$\left. - \left(\frac{\sin\frac{1}{2}U_1}{u_1/2}\right) \cdot \left(1 + \frac{1-\cos U_1}{l_{\mathrm{pr}_1} - l_{\mathrm{parax}_1}} \cdot \delta s_1\right)\right] \tfrac{1}{2}H_L\,. \qquad \ldots\ldots(10)$$

In telescopic systems, the value of Δx is given in angular measure. Thus if h_1, h_λ are the paraxial incident heights at the first and last surfaces of any system and a change of conjugate Δu_1 results in a change $\Delta u_\lambda'$ in the object space, then generally

$$\Delta u = \frac{\Delta x \,.\, u}{r} = \frac{\Delta x \,.\, u^2}{h},$$

and, therefore, the longitudinal magnification formula becomes

$$N_\lambda' h_\lambda \Delta u_\lambda' = N_1 h_1 \Delta u_1 = H_L \,. \qquad \ldots\ldots(11)$$

It is this form which is used in telescopic systems. Let ρ_1, ρ_λ' be the intersection heights of a given ray in the paraxially defined entrance and exit pupils; then for small angles U_λ', U_1 (a "nearly" telescopic system), θ_λ', θ_1 are necessarily small, and

$$\theta_\lambda' = -\frac{\rho_\lambda'}{l'_{\mathrm{pr}\lambda} - l'_{\mathrm{parax}\lambda}}, \qquad u_\lambda' = \frac{h_\lambda}{l'_{\mathrm{parax}\lambda}}.$$

In the limit $l'_{\mathrm{parax}\lambda} \rightarrow \infty$, the ratio

$$\frac{\theta_\lambda'}{u_\lambda'} = \frac{\rho_\lambda'}{h_\lambda}.$$

Thus, for telescopic systems,

$$\frac{1-\cos\theta_\lambda'}{u_\lambda'^2} = \frac{1}{2}\left(\frac{\rho_\lambda'}{h_\lambda}\right)^2, \qquad \ldots\ldots(12)$$

with a similar expression in the object space. Using (11), (12) in (6), the change of spherical aberration, consequent upon the change of conjugates H_L, is

$$dW = \left[\left(\frac{\rho_\lambda'}{h_\lambda}\right)^2 - \left(\frac{\rho_1}{h_1}\right)^2\right] \,.\, \tfrac{1}{2} H_L. \qquad \ldots\ldots(13)$$

It has been shown before (*loc. cit.*) that

$$\rho_\lambda' = Y_\lambda - (l'_{\mathrm{pr}_\lambda} - X_\lambda) \,.\, \tan \delta u_\lambda',$$

with the notation of the earlier paper. In the absence of spherical aberration, Herschel's Condition for a telescope is thus

$$\frac{Y_\lambda}{h_\lambda} = \frac{Y_1}{h_1}. \qquad \ldots\ldots(14)$$

It will be apparent that use of one or other of the forms of $\left(\frac{1-\cos\theta}{u^2}\right)$ used in (10) and (13) will give results suited to photographic objectives (infinite object, finite image distance) and eyepieces (finite object, infinite image distance).

If it is assumed that for given conjugates a system is both free from spherical aberration and satisfies the sine-condition, there follow immediately results which have a bearing on a number of questions.

Thus, consider a corrected microscope objective of N.A. $= N_1 \sin U_1$, having a primary magnification m. A change of tube length $\Delta x_\lambda'$ gives, N_λ' being that of air $= 1$,

$$H_L = u_\lambda'^2 \,.\, \Delta x_\lambda' = \left(\frac{N_1 u_1}{m}\right)^2 \,.\, \Delta x_\lambda'.$$

The sine-condition is satisfied, so that

$$\frac{\sin \frac{1}{2} U_\lambda'}{u_\lambda'/2} \cdot \cos \frac{U_\lambda'}{2} = \frac{\sin \frac{1}{2} U_1}{u_1/2} \cdot \cos U_1/2 \,,$$

or, the light coming from the short conjugate, u_λ' is small, and

$$\left(\frac{\sin \frac{1}{2} U_\lambda'}{u_\lambda'/2}\right)^2 - \left(\frac{\sin \frac{1}{2} U_1}{u_1/2}\right) = -\left(\frac{1-\cos U_1}{u_1}\right)^2 .$$

Substituting in (7) gives

$$dW = -\left[\frac{N_1(1-\cos U_1)}{m}\right]^2 \cdot \tfrac{1}{2} \Delta x_\lambda' \quad . \qquad \ldots\ldots(15)$$

Thus for a $^1/_{12}$-in. objective having N.A. $=1{\cdot}20$, $m = \times 100$, and using an oil for which $1{\cdot}53$,

$$dW = -0{\cdot}0000167 \;.\; \Delta x_\lambda' ,$$

i.e. a change of wave-front aberration of $\frac{1}{2}$ wave-length of sodium D light follows a change in tube-length of 17·5 mm.* With an objective of this type "good observers" claim to estimate tube-length to this order of accuracy, although the effects are generally unnoticeable at the "best" focus.

In a corrected telescopic system the sine-condition takes the form

$$\frac{Y_\lambda}{h_\lambda} = \frac{Y_1}{h_1} ,$$

which is identical with equation (14). Thus, in this case, Herschel's condition and the sine-condition are simultaneously satisfied.†

Consider a corrected photographic objective, satisfying the sine-condition. Let the long-conjugate change from ∞ to L_1, and let h_1 be the radius of the entrance pupil. Then by (11),

$$H_L = \frac{h_1^2}{L_1} ,$$

assuming $N_1 = 1$. The sine-condition gives

$$\frac{\rho_1}{h_1} = \frac{\sin \frac{1}{2} U_\lambda'}{u_\lambda'/2} \cdot \cos \frac{U_\lambda'}{2} ,$$

or, F being the equivalent focal length,

$$\left(\frac{\rho_1}{h_1}\right)^2 - \left(\frac{\sin \frac{1}{2} U_\lambda'}{u_\lambda'/2}\right)^2 = \left(\frac{1-\cos U_\lambda'}{h_1}\right)^2 . \; F^2 .$$

---

* Since writing this, Mr. A. G. Sabin has given me a similar value for a $\frac{1}{8}$-in. versalic objective obtained by accurate ray-tracing methods. For N.A. $=1{\cdot}16$, $m = \times 98$, a change in aberration of 1·6 wave-lengths was found to be produced by a change in tube-length of 50 mm. The above approximate formula gives 1·3 wave-lengths.

† This is also true at unit magnification for a copying system corrected for spherical aberration at that magnification.

The change in spherical aberration is, therefore,

$$dW = \tfrac{1}{2}\left(1 - \cos U_\lambda'\right)^2 \cdot \frac{F^2}{L_1}. \qquad \ldots\ldots(16)$$

Thus for an $F/1{\cdot}0$ objective,

$$dW = 0{\cdot}0056 \,.\, \frac{F^2}{L_1},$$

and, for a 1-in. focus lens, a change in aberration of one wave-length occurs for $L_1 = 242$ inches. Further, for a given relative aperture, the value of L_1 for a given change in spherical aberration is proportional to the square of the equivalent focal length. For a given focal length it is approximately proportional to the fourth power of the relative aperture.

It will be seen that an identical analysis yields a "Herschel condition" applying to extra-axial object points. For first-order changes in the conjugates, the aberrational change is symmetrical about the principal ray (i.e. a "spherical aberration") and greater changes in the conjugates are required to introduce changes in the comatic and astigmatic aberrations.

THE THERMAL CONDUCTIVITY OF TEXTILES

By S. BAXTER,
Wool Industries Research Association, Leeds

MS. received 18 *September* 1945

ABSTRACT. A review is given of measurements of the thermal conductivity of natural clothing fibres and of formulae that have been proposed for the overall thermal conductivity of fibre-air mixtures in terms of their density and fibre conductivity.

Measurements of the conductivity of wool felts ranging in density from 0·01 to 1·0 gm./cc. have been made, using Hercus and Laby's method for determining the conductivity of air. The conductivity of solid keratin (horn) has also been measured by the Lees disc method, and it is suggested that wool fibres and horn have identical conductivities of $4{\cdot}62 \times 10^{-4}$ c.g.s. units at 0·7% regain and $5{\cdot}32 \times 10^{-4}$ c.g.s. units at 10·7% regain. The data given for wool felts and horn are used to obtain an empirical relation between conductivity and bulk density.

Results obtained with cotton fabrics indicate that published values of the thermal conductivity of cotton fibres are too high.

§ 1. INTRODUCTION

The thermal conductivity of fabrics or masses of fibres is made up of two components: the heat transmitted through the air spaces and the heat transmitted through the textile fibres. Typical wool fabrics, as used for clothing purposes, have densities ranging from 0·1 to 0·3 gm. per cc., i.e. the air space in the fabrics varies from 92% to 77% of the volume of the fabric. Clearly this means that in a fabric the thermal conductivity of the air will be the controlling factor and the conductivity of the fibres will exert only a secondary influence; in particular the conductivity of a fabric of low bulk density will be practically independent of the fibres used. This result has been shown by many workers investigating the thermal insulation of fabrics.

If any differences in the thermal conductivity of various fibres are to be shown, the thermal conductivity measurements must be made on fabrics of high density, where the conductivity of the fibre becomes increasingly effective.

Few attempts have been made to determine the thermal conductivity of textile fibres from measurements of the conductivity of fibre-air mixtures. It was well known that low-density fibre-air mixtures had thermal conductivities approaching the value for air, and Speakman and Chamberlain (1930) have shown that the conductivity increases with the bulk density, depending on the type of fibre used.

The present work is an attempt to find an empirical formula for the wool conductivity-density curve from measurements of the conductivity of felts of increasing density and also of the conductivity of solid keratin. A satisfactory formula has been obtained, and the conductivity of any natural fibre can be predicted from its conductivity-density curve. Also, if the thermal conductivity of the fibre can be determined directly, as is the case with most synthetic fibres, then the conductivity of a fibre-air mixture of any density can be predicted.

§ 2. HISTORICAL

According to Schuhmeister (1877) the first investigations of the conducting power of cotton and wool fabrics were made by Peclet and reported by him in his *Handbook of the Science of Heat*. He concluded that the conducting power of various fabrics was little different from that of air. Later, Forbes (1872) found that the conducting power of cotton decreased with compression, a result which Schuhmeister interpreted as meaning that the conductivity of cotton was less than that of air. The present results show that it is quite possible, under certain conditions, for the conductivity of a fibre-air mixture to decrease as the density increases, although the fibre conductivity is greater than that of air. The problem of the conductivity of textile fabrics was first attacked seriously by Schuhmeister, using the method developed by Stefan for investigating the thermal conductivity of gases. In this method, the fibres are packed into the space between two concentric cylinders, the centre cylinder acting as an air thermometer. Schuhmeister showed that his results could be expressed by the formula

$$k_m = k_1 + aP, \qquad \ldots\ldots(1)$$

where k_m is the conducting power of the mixture, k_1 the conducting power of the gas, P the weight of textile fibre present, and a is a constant.

Taking the volume occupied by the fibres into account, the formula reduces to

$$k_m = k_1 + b\rho, \qquad \ldots\ldots(2)$$

where ρ is the bulk density of the fibres and b is a constant. For wool the value of the constant is 2·71, for silk 2·50 and for cotton 7·35. The range of values of bulk density used was small, the highest value being 0·15 gm./cc. In calculating the thermal conductivity of the fibres, Schuhmeister assumed that the fibres were uniformly distributed in all directions, or, for the purposes of calculation, that one-third were plane slabs parallel to the direction of heat flow and touching both plates, and two-thirds were slabs at right angles to the direction of heat flow. On these assumptions,

$$k_m = \tfrac{1}{3}(k_1 v_1 + k_2 v_2) + \tfrac{2}{3}\left(\frac{k_1 k_2}{k_1 v_2 + k_2 v_1}\right), \qquad \ldots\ldots (3)$$

where k_1, k_2 and v_1, v_2 are the conductivity and fractional volume of air and of the fibres, so that

$$v_1 + v_2 = 1.$$

Using equation (3), and assuming the conductivity of air to be unity, Schuhmeister gave the value for cotton as 37, for wool 12 and for silk 11.

Rubner (1895), using the Stefan calorimeter and Schuhmeister's method of calculation, gave the conductivity of wool as 6·1, of silk 19·2 and of cotton and linen 29·9, taking the value for air as unity. Rubner measured the thermal conductivities of a wide range of keratin fibres and found no significant difference between them. The same result was also found for a wide range of cellulosic fibres, and for natural silks. His absolute values of conductivity are given in table 1, but it should be noted that they are not consistent with his ratios of the conductivities.

Table 1. Rubner's values

Substance	Thermal conductivity k (c.g.s. units)
Air	$0{\cdot}532 \times 10^{-4}$
Mammal hairs	4·791
Silk	8·870
Plant fibres	14·199

Rubner also investigated the increase in the value of k_m with increasing density, but again he investigated only the region of very low densities, his maximum value being 0·12 gm./cc. His values for the constant in equation (2) were 3·65 for wool, 3·62 for silk and 5·9 for cotton.

One of the main reasons for the discrepancy between the results of Schuhmeister and Rubner was their choice of working in the region of low bulk density, where, as will be shown later, the conductivity of fibre-air mixtures behaves in a peculiar manner. One might have expected, however, that the agreement would have been better since Rubner's work appears to be an exact replica of Schuhmeister's. The error in estimating k_2 from equation (3) must be very large when low bulk densities are used. The higher the bulk density used to determine k_m, the smaller will be the error in estimating k_2. The validity of equation (3) is discussed later.

The theory of the conductivity of heterogeneous media is complex and has only been attempted for certain simple cases. Maxwell in his *Electricity and Magnetism* has worked out the conductivity of a medium formed by embedding spheres of conductivity k_2 in a medium of conductivity k_1, the spheres being a large distance apart. He also worked out the cases where the media were separated by planes both parallel and at right angles to the direction of heat flow, and the case of right prisms of rectangular cross-section, one dimension being large compared with the other, and the length of the prisms being large compared with the larger cross-sectional dimension, placed either with their edges parallel or perpendicular to the direction of heat flow. These cases have limited application on account of the geometry implied. Lees (1900) has also worked out an expression for the conductivity of heterogeneous media from considerations of the heat flow through a medium formed by an equal number of equally long prisms of square cross-section having conductivities k_1 and k_2 and arranged in draught-board pattern, the planes of constant temperature being drawn through the diagonals of the cross-sections of the prisms. For this case Lees shows that the effective conductivity k_m is given by

$$k_m = k_1^{\frac{1}{2}} k_2^{\frac{1}{2}}. \qquad \ldots\ldots(4)$$

From this result he reasons that the thermal conductivity of a compound medium in the general case where the constituents are in the form of long prisms with their axes perpendicular to the direction of heat flow is given by

$$k_m = k_1^{v_1} k_2^{v_2}, \qquad \ldots\ldots(5)$$

where v_1 and v_2 are the fractional volumes of the media of thermal conductivity k_1 and k_2 respectively. It must be noted, however, that, even in the general case, equation (5) only holds when the prisms are square in cross-section and are arranged in some form of draught-board pattern with their edges touching along their length.

§ 3. EXPERIMENTS WITH THE LEES DISC

The experimental method first used by the author to determine the absolute conductivity of felts and fabrics was that of the Lees disc (1898). The apparatus is sufficiently well known only to require brief description here. Its essentials, shown in figure 1, are the brass plates C and U, which are screwed together with a heating coil between them. The fabric to be tested is placed between this hot plate and a lower plate M, and the whole block is then suspended in an enclosure of constant temperature until the readings of heater current and voltage and the plate temperatures, which are measured by thermocouples, become steady. The calculation of the results is somewhat tedious, and for details the original paper should be consulted.

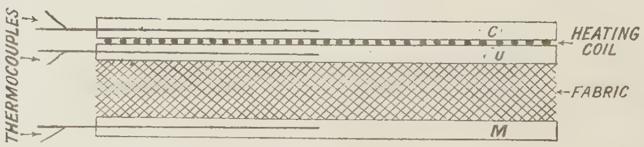

Figure 1. Lees' disc apparatus.

The conductivity of layers of thin cotton, wool and rayon fabrics were measured by this method, and in each case it was found that the thermal conductivity increased with the number of layers used. Figure 2 shows the values obtained using 1, 2, 4 and 8 layers of cotton fabric, both with the heater above and below the fabric. The results can be explained by assuming a constant air layer of thickness $d_a/2$ at each plate, the rest of the space being assumed to have a constant thermal conductivity k, figure 3. The measured conductivity K will be a function of the thickness d, and will be given by

$$K=\frac{kk_a d}{kd_a+k_a(d-d_a)}. \qquad \ldots\ldots(6)$$

From equation (6) it is seen that $K \to k$ as $d \to \infty$. Curve (1) of figure 2 is for equation (6) with $k_a=0{\cdot}6\times10^{-4}$ c.g.s. ; $k=2{\cdot}72\times10^{-4}$ and $d_a=1{\cdot}1\times10^{-2}$ cm. Curve (2) of figure 2 is for $k=2{\cdot}2\times10^{-4}$ and $d_a=1{\cdot}1\times10^{-2}$ cm. Although the curves fit the experimental points, the large value of d_a in comparison with the single fabric thickness 0·04 cm. gave rise to doubts as to their validity. In Lees' calculation the edges of the material tested were assumed to have the same emissivity as the metal plates. This equality can be achieved with a solid sample merely by varnishing the whole block after assembly with, say, shellac, but when using textiles such a course is impossible. Also, when working with textiles, heat can be lost from the edges of the fabric by convection of the air ; i.e. by hot air leaving the centre of the fabric and diffusing out at the edges. Such effects cannot easily be allowed for in the calculations, and almost certainly contribute to the results of figure 2. In view of these difficulties, the use of the Lees disc to measure the conductivity of textile-air mixtures was abandoned.

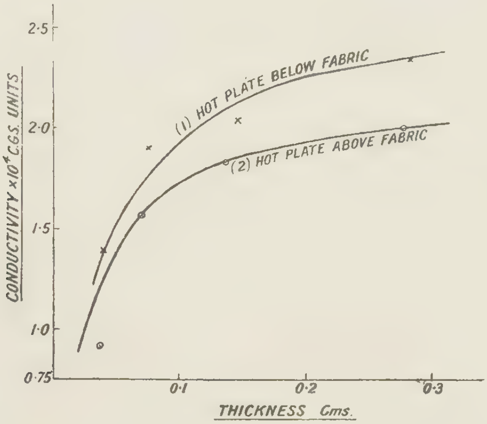

Figure 2. Conductivity of layers of cotton fabric as measured by Lees' disc apparatus.

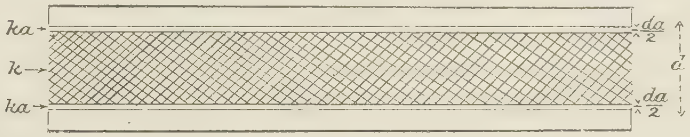

Figure 3. Boundary resistances.

An attempt was made to estimate the thermal conductivity of textile fibres by placing them in liquids and measuring the thermal conductivity of the mixture using Lees' disc. If this were done using liquids which had both higher and lower conductivities than the fibres, it was hoped that the conductivity of the fibres could be estimated. The results obtained using cotton and wool were somewhat erratic, depending on whether or not the liquid was absorbed by the fibres, but the value for the conductivity of wool appeared to be $3{\cdot}5 \times 10^{-4}$ c.g.s. units and for cotton $6{\cdot}0 \times 10^{-4}$ units. No great accuracy is claimed for these results.

§4. EXPERIMENTS WITH THE APPARATUS OF HERCUS AND LABY

As mentioned earlier, textile fabrics contain a very high proportion of air by volume, and in measuring the thermal conductivity of a fabric, it would appear better to use an apparatus designed to measure the thermal conductivity of gases rather than one designed to measure the thermal conductivity of solids. The types of apparatus used to measure the conductivity of gases fall generally into two classes : the hot-wire type, in which the heat losses from a heated wire in a cylindrical tube are measured, and the parallel-plate method, where the heat transmitted through the material from one plate to a colder plate is measured. An apparatus of the second type was most suitable for our purpose, and Hercus and Laby's (1919) design has been used. The apparatus, which is shown in figure 4, was made in two halves, one unit comprising the top plate, centre plate and guard ring, the other unit being the cold plate. Each plate was made of two sections which were screwed together. The top sections in the case of the top plate, centre plate and guard ring had spiral grooves cut into their lower faces, the heating coils being wound into these grooves. The bottom section of each of the three plates had a radial groove cut in its upper face to take the thermocouples. The top section of the bottom plate also had a radial groove cut into its underside for thermocouples. The cold plate was kept at a constant temperature by circulating cold water (26° C.) through it from a thermostated tank. The apparatus could be used with the hot plate above the fabric and the cold plate below or vice versa. Full details of the experimental technique and method of calculating the results will be found in Hercus and Laby's paper (1919). Briefly the method is to heat the guard ring and top plate to a temperature slightly higher than the centre plate, so that all the heat input into the centre plate is transmitted throught the material to the cold plate. Corrections are applied for the small amount of heat gained from the top plate and the guard ring. All the outer surfaces of the plates were silver-plated, and when radiation corrections

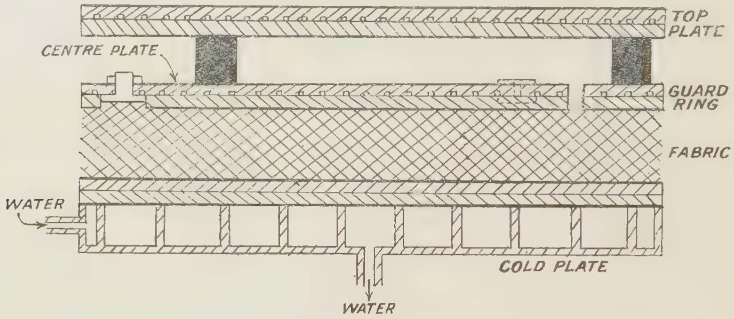

Figure 4. Apparatus based on that of Hercus and Laby.

were applied, the emissivity of the plates was taken as $4 \cdot 1 \times 10^{-12}$ cal./sec./cm.^{2}/deg.^{4} The e.m.f. generated by the thermocouples, which had previously been calibrated, was measured on a Cambridge potentiometer.

(a) *Results using air*

As a check on the apparatus, the thermal conductivity of air was determined. The air was room air. The results obtained were reduced to k_0, the value of the conductivity at 0° c. by use of the formula, $k_t = k_0(1 + 0{\cdot}003\,t)$, as used by Hercus and Sutherland (1934). The values obtained are given in table 2.

The values obtained with the heater below the air gap confirm the well-known result that convection plays no appreciable part until the thickness of the air gap becomes greater than about 1 cm., when the effect becomes quite large, as is seen by the last value of the table. The mean value obtained for the conductivity of air may be compared with some of the most accurate measurements made to date. Kannuluick and Martin (1934), using the hot-wire method, give k_0 as $5{\cdot}76 \times 10^{-5}$ c.g.s. units, and Hercus and Sutherland (1934), using the parallel-plate method of Hercus and Laby, give k_0 as $5{\cdot}72 \times 10^{-5}$ c.g.s. units. The agreement of the present results with these values serves as a check on the calibrations of the thermocouples and electrical measuring instruments and shows that no systematic error was present.

Table 2

Hot plate above		Hot plate below	
Thickness of layer (cm.)	k_0 (c.g.s. units)	Thickness of layer (cm.)	k_0 (c.g.s. units)
0·150	$5{\cdot}44 \times 10^{-5}$	0·171	$5{\cdot}58 \times 10^{-5}$
0·153	5·64	0·184	5·64
0·450	5·61	0·476	5·84
0·458	5·92	0·966	5·83
0·953	5·82		
1·946	6·09	1·968	12·48 *
Mean 5·75		Mean 5·72	

* Not taken into account in determining the mean value.

(b) *Results using fabrics*

The thermal conductivity of layers of thin fabrics made from wool, cotton and viscose rayon were determined. The wool and cotton cloths were made as nearly identical as possible, but the rayon cloth was thinner than the others. The wool and cotton cloths had weights of 4·3 oz. per sq. yd. and the rayon cloth weighed 3·1 oz. per sq. yd., the thicknesses under a pressure of 5 gm./cm.^{2} being 0·037 cm. for the wool fabric, 0·035 cm. for the cotton fabric and 0·023 cm. for the rayon fabric. The measurements of conductivity were done with the fabrics at room regain,* and with the hot plate both above and below the fabric,

---

* Regain is the moisture content expressed as a percentage of the dry weight.

Table 3

Number of layers	Bulk density (gm./cc.)	Thickness (cm.)	$10^4 \times$ conductivity (cal./cm./sec./°c.)	Mean temp. (c.)
Heater above fabric : Cotton				
8	0·450	0·252	1·70	27·9
8	0·450	0·252	1·69	28·0
17	0·467	0·515	1·74	32·1
	Mean 0·455		Mean 1·71	Mean 29·3
Wool				
9	0·475	0·310	1·25	29·3
18	0·480	0·612	1·26	32·3
	Mean 0·477		Mean 1·26	Mean 30·8
Rayon				
12	0·520	0·229	1·45	28·7
16	0·515	0·310	1·45	28·9
16	0·515	0·310	1·48	27·8
	Mean 0·517		Mean 1·46	Mean 27·5
All-wool greatcoat material				
1	0·295	0·241	1·05	28·1
1	0·295	0·241	1·02	29·1
2	0·285	0·501	1·07	29·4
2	0·285	0·501	1·07	29·5
3	0·287	0·740	1·09	31·6
4	0·287	0·986	1·13	32·8
5	0·296	1·201	1·12	33·6
	Mean 0·290		Mean 1·08	Mean 30·6
Heater below fabric : Cotton				
9	0·460	0·276	1·62	29·4
17	0·460	0·521	1·71	32·6
17	0·460	0·521	1·65	27·5
	Mean 0·460		Mean 1·66	Mean 29·8
Wool				
9	0·482	0·307	1·17	29·2
9	0·482	0·307	1·18	27·1
18	0·468	0·630	1·26	32·0
18	0·468	0·630	1·28	31·7
	Mean 0·475		Mean 1·22	Mean 30·0
Rayon				
10	0·531	0·189	1·35	29·0
15	0·524	0·287	1·40	30·1
	Mean 0·527		Mean 1·38	Mean 29·6
All-wool greatcoat material				
3.	0·290	0·735	1·08	33·8
5	0·287	1·239	1·09	33·3
	Mean 0·289		Mean 1·09	Mean 33·6

in order to determine whether or not convection losses through the fabric were possible. The values obtained are given in table 3.

The results show that there is little change in conductivity with increasing thickness, and that in most cases where an increase is shown, the higher value has been obtained at a higher temperature. The values obtained with the heated plate below the fabrics show that no convection took place through the fabrics. The bulk densities of the thin fabrics when in the apparatus and at room regain were very similar ; the mean values expressed as gm. of fibres per cc. were 0·476 for the wool fabric, 0·458 for the cotton fabric and 0·522 for the rayon fabric. Since the weaves of the fabrics were similar, it must be concluded that the wool fibre has the lowest conductivity of the three materials investigated.

(c) *Variation of conductivity with density*

In order to be able to make an estimate of the conductivity of the wool fibre, it is necessary to determine the curve of conductivity against density for wool at a constant regain and then to extrapolate the curve to find the conductivity corresponding to a density of 1·3 gm./cc. In order to do this, a length of felt was specially prepared with a density of approximately 0·1 gm./cc. and thickness approximately $\frac{1}{2}$ inch. Values at higher densities were obtained by compressing layers of the felt together at a temperature of 100° c. and allowing them to cool before releasing the compression. If the wool had a regain not less than about 20%, it was found that the heat and compression treatment caused a permanent set. Excess water was not necessary, as the saturation regain of wool at 100° c.

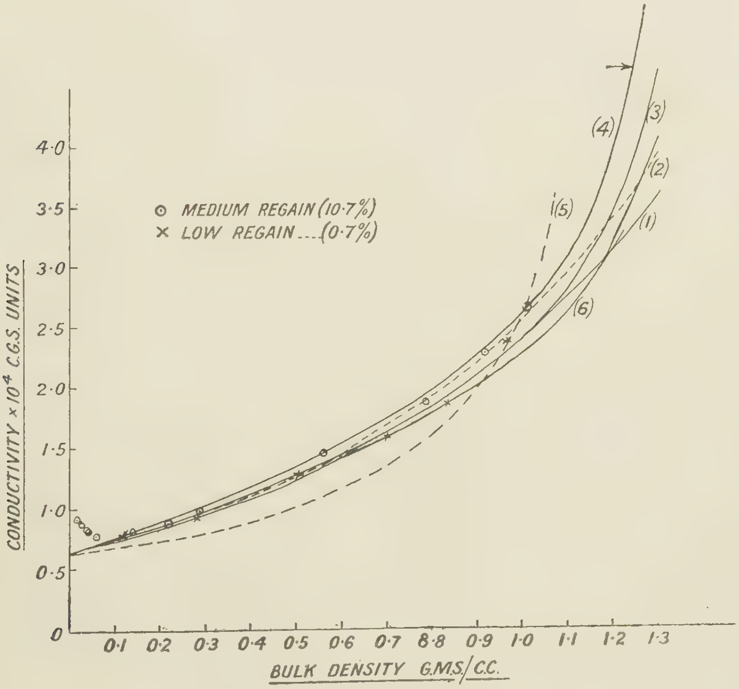

Figure 5. Conductivity against bulk density for wool.

is in the region of 20%. Using this technique, densities up to 1·0 gm./cc. were obtained. For densities less than 0·1 gm./cc. the felt was carded dry and placed in laps between the plates, which were separated by spacing blocks of ebonite between the guard ring and the cold plate. The conductivity of each felt of density greater than 0·1 gm./cc. was measured at a low (0·7%) and a medium (10·7%) regain, the regains being based on the dry weight obtained by placing the felt in an oven maintained at 100° c. The values obtained are shown graphically in figure 5.

(d) *Variation of conductivity with regain*

The effect of increasing the regain is to increase the bulk density and also the conductivity, the magnitude of the effect depending on the bulk density. At low densities the regain effect can hardly be detected owing to the small part played by the fibres and also as at low temperatures the conductivity of air is negligibly altered by increasing the relative humidity. This has been verified in the present investigations, which are in line with the results of Gruss and Schmick (1928), who showed that introducing 5% of water vapour into the air caused the thermal conductivity of air to increase by 1%.

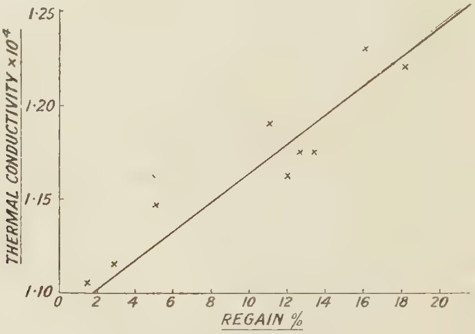

Figure 6. Effect of regain on conductivity of wool felt of density 0·335 gm./cc.

The effect of regain on a felt of density 0·30 gm. per cc. when dry was investigated. The density of the felt varied slightly with regain, and the values of the conductivity were corrected, using the curve of figure 5 to correspond in each case to a density of 0·335 gm./cc. The values are shown in figure 6, and the conductivity is seen to increase linearly with increasing regain. The slope of the line is $7 \cdot 7 \times 10^{-3}$ units of conductivity per unit change in regain. This value will of course depend on the bulk density of the material. The experimental points are all within 2% of the straight line.

§ 5. THE CONDUCTIVITY OF HORN

Since both wool and horn are keratin, the estimated values for the conductivity of wool would be expected to be similar to the conductivity of horn. The thermal conductivity of horn, in a direction at right angles to the axis of the long chain molecules, was determined at various regains by means of the Lees disc apparatus. A piece of horn was flattened by boiling whilst clamped in a flat position, and then turned on a lathe into a disc of the same diameter as the Lees discs, and of thickness 0·226 cm. when dry. The horn warps badly as the regain is altered, and the specimen was held clamped flat between the plates of the apparatus, paraffin wax being used to ensure good thermal contact between the specimen and the plates. The conductivity of the horn was investigated over a wide range of regains, and the values are given in figure 7.

The thermal conductivity of mixtures can in many cases be expressed by a formula of the type

$$k_m = k_0(1 + aC_m),$$

where k_m is the conductivity of the mixture, k_0 the conductivity of the pure substance, C_m the concentration of the added substance, and a a constant. Water molecules are absorbed by wool in two states, some being absorbed on to localized sites and others existing in the liquid state. The proportion of water in the two states at any regain has been worked out by Cassie (1945). Assuming these two types of water, the conductivity of horn may be expressed by the equation

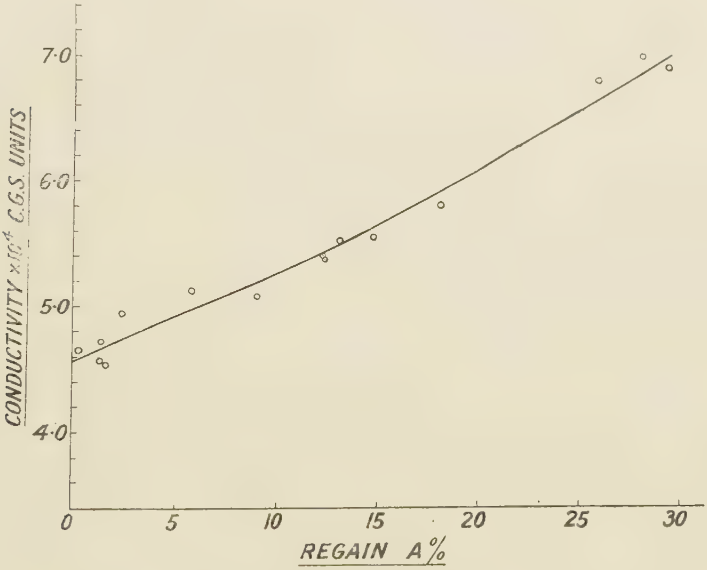

Figure 7. Effect of regain on the conductivity of horn.

$$k_m = k_0(1 + \alpha C_X + \beta C_{(A-X)}), \qquad \ldots\ldots(8)$$

where k_0 is the conductivity of the dry horn, k_m that of the horn when at regain m; C_X is the concentration of water absorbed on the localized sites, and $C_{(A-X)}$ is the concentration of water in the liquid state, whilst α and β are constants.

The values of C_A, C_X and $C_{(A-X)}$ for various regain values have been evaluated from table 3 of Cassie's paper, and are given in table 4.

The curve in figure 7 is for equation (8), the constants being obtained by making the curve to pass through the points $k_m = 5{\cdot}3 \times 10^{-4}$, $A = 10{\cdot}8\%$ and $k_m = 6{\cdot}6 \times 10^{-4}$, $A = 25{\cdot}2\%$. The values of the constants are $\alpha = 49{\cdot}4$ and $\beta = 133$, indicating that the free water contributes more to the thermal conductivity than the water found on localized sites.

Table 4

Regain (A)	C_A (gm./cc.)	C_X (gm./cc.)	$C_{(A-X)}$ (gm./cc.)
%			
3·6	0·045	0·041	0·004
7·2	0·086	0·082	0·004
10·8	0·125	0·113	0·012
14·4	0·165	0·141	0·024
18·0	0·200	0·159	0·041
21·6	0·232	0·169	0·063
25·2	0·260	0·174	0·086
28·8	0·286	0·174	0·112
32·5	0·314	0·174	0·140

§ 6. INTERPRETATION OF RESULTS

There are two possible equations which may be applied to the experimental points of figure 5 ; they are the Lees formula, equation (5), and Schuhmeister's formula, equation (3). The orientation of the wool fibres in the compressed felts used do not agree with the conditions assumed in deducing either of the two formulae, and any equation which fits the data must be taken as a purely empirical equation without any real theoretical foundation. Curve (1) of figure 5 is for Lees' equation (5), with $k_1 = 0{\cdot}63 \times 10^{-4}$, the conductivity of air at the temperature of the experiments, $k_2 = 3{\cdot}63 \times 10^{-4}$, and curve (2) is for equation (5), with $k_1 = 0{\cdot}63 \times 10^{-4}$ and $k_2 = 3{\cdot}92 \times 10^{-4}$. The two curves fit the experimental points quite well, except for densities less than 0·2 gm./cc., and predict the conductivity of wool at the lower regain (0·7%) as $3{\cdot}63 \times 10^{-4}$, and at the higher regain (10·7%) as $3{\cdot}95 \times 10^{-4}$. The values of the conductivity of horn at the same two regains are $4{\cdot}62 \times 10^{-4}$ and $5{\cdot}32 \times 10^{-4}$.

Schuhmeister's formula, equation (3), may be written

$$k_m = x(k_1 v_1 + k_2 v_2) + y \frac{k_1 k_2}{k_1 v_2 + k_2 v_1}, \qquad \ldots\ldots(9)$$

where $x + y = 1$.

If x is unity, we have k_m increasing linearly with density from k_1 to k_2, and if y is unity we have a hyperbolic relation with k_m, increasing slowly with density at first and then more rapidly as the density increases. Equation (9) has been used with $y = 1$ for water-vapour diffusion by Peirce, Rees and Ogden (1945), but this by no means fits the experimental points, as is seen by curve (5) of figure 5, which is equation (9) for $y = 1$, $k_2 = \infty$ and the density of the fibres 1·3 gm./cc. As there are no means of determining directly the values of x and y, the only method is to take the value of k_2 as determined for horn and then to fit the equation to the experimental points and so determine x and y. This method gives the values of x and y as 0·29 and 0·71 respectively. Curve 3 of figure 5 is for equation (6) with $x = 0{\cdot}29$, $y = 0{\cdot}71$, $k_1 = 0{\cdot}63 \times 10^{-4}$, $k_2 = 4{\cdot}62 \times 10^{-4}$, and curve 4 is with $k_2 = 5{\cdot}32 \times 10^{-4}$. The curves again fit the experimental points within experimental error. If we take $x = \frac{1}{3}$ and $y = \frac{2}{3}$, which are Schuhmeister's values, and fit the equation to the low regain experimental points, $k_m = 1{\cdot}425 \times 10^{-4}$ c.g.s. and $\rho = 0{\cdot}6$ gm./cc., we find that k_2 is $4{\cdot}04 \times 10^{-4}$ c.g.s. units, and with this value we get curve (6). This curve is almost identical with curves (1) and (2) over the region explored experimentally.

We have, therefore, to decide which equation, type (3) or type (5), should be used. Both equations give curves which fit the experimental points equally well over the range measured, but the Schuhmeister formula, with $x=0{\cdot}29$ and $y=0{\cdot}71$, takes in the values found for the conductivity of horn and, therefore, may be considered to give a better empirical formula than the Lees equation or Schuhmeister's equation with $x=\frac{1}{3}$, $y=\frac{2}{3}$.

At densities less than 0·1 gm./cc. neither formula fits the experimental points. The apparent increase in conductivity as the density falls below 0·1 gm./cc. is probably due to convection. The temperature gradient along a fibre will be different from the temperature gradient in the air adjacent to it. This will give convection currents whose magnitude will depend on the fibre surface area and the average distance between the fibres. As the density increases, the surface area increases, but the mean distance between the fibres decreases and a maximum would be expected in the (conductivity *v.* density) curve. This is seen to be the case: the convection effect rises to a maximum at a density of 0·01 gm./cc. and then decreases as the density increases, and becomes negligible at densities greater than 0·2 gm./cc.

Table 5

Substance	Density (gm./cm.^{3})	$10^4 \times$ thermal conductivity (c.g.s. units)
Polyvinyl chloride-acetate	1·34–1·37	3·95
Polyvinyl chloride	1·2 –1·6	3·9–4·0
Cellulose acetate (transparent)	1·27–1·32	5·4
Cellulose acetate (pigmented)	1·37–1·56	5·3–8·7
Ethyl cellulose	1·10–1·25	5·6

Equation (9) with $x=0{\cdot}21$ and $y=0{\cdot}79$, may be used to give estimates of the conductivities of the fibres for the three thin fabrics of table 3. Using the mean values of the density and fabric conductivity, the conductivity of the wool fibre is found to be $4{\cdot}6\times10^{-4}$, of the cotton fibres $11{\cdot}0\times10^{-4}$, and the viscose rayon fibres $6{\cdot}9\times10^{-4}$, the regains being approximately 10, 5 and 10% respectively. Taking the conductivity of air, $0{\cdot}63\times10^{-4}$, as unity, the relative conductivity of wool becomes 7·3, of cotton 17·5 and of viscose rayon 11·0. The value for wool lies between the estimates of Rubner and Schuhmeister, and the value for cotton is roughly half their values. The value obtained for the viscose rayon compares favourably with those given for cellulose derivatives in table 5 below, although the conductivity of viscose—regenerated cellulose—is not known. The result for cotton, taken together with the value indicated by the experiments with liquids, suggests that Schuhmeister and Rubner's values are too high.

The thermal conductivity of synthetic fibres can be measured directly, as the materials are readily available in sheet form, and, knowing the fibre conductivity, the conductivity of a fabric can be estimated from its density and equation (9). The thermal conductivities of many of the synthetic materials used as textiles are not available, but a few are given in table 5 (cf. Simonds and Ellis, 1943).

No mention is made of the regain of the material at which the measurements were made. Wool is seen to have a conductivity comparable with that of the artificial materials, whilst cotton appears to have a considerably higher conductivity.

ACKNOWLEDGMENTS

The author's thanks are due to Mr. B. H. Wilsden, Sir Charles Martin and Dr. A. B. D. Cassie for discussion; to Mr. R. Bownass and Miss B. Oughten for assistance in the experimental work; and to the Council of the Wool Industries Research Association for permission to publish this account.

REFERENCES

Cassie, 1945. *Trans. Faraday Soc.* **41**, 458.
Forbes, 1872. *Proc. Roy. Soc. Edin.* **18**, 66.
Gruss and Schmick, 1928. *Wiss. Veröff. Siemens-Konz.* **7**, 202.
Hercus and Laby, 1919. *Proc. Roy. Soc.* A, **95**, 190.
Hercus and Sutherland, 1934. *Proc. Roy. Soc.* A, **145**, 599.
Kannuluick and Martin, 1934. *Proc. Roy. Soc.* A, **144**, 496.
Lees, 1898. *Philos. Trans.* **191**, 399.
Lees, 1900. *Phil. Mag.* **49**, 221.
Peirce, Rees and Ogden, 1945. *J. Textile Inst.* T. 169.
Rubner, 1895. *Arch. Hyg.* **24**, 265.
Schuhmeister, 1877. *Ber. K. Akad. Wien (Math.-Naturw. Klasse)*, **76**, 283.
Simonds and Ellis, 1943. *Handbook of Plastics* (Chapman and Hall), pp. 40 and 48.
Speakman and Chamberlain, 1930. *J. Textile Inst.* T. 29.

THE DEPENDENCE OF PRESSURE-VARIATION, WITH DEPTH IN A LIQUID, ON THE VERTICAL ACCELERATION OF THE LIQUID

By KERR GRANT,
University of Adelaide

MS. received 22 *September* 1945

The experimental demonstration here illustrated was suggested to me by the obvious scepticism of a class of first-year students to a remark that water in a falling vessel would not issue from an orifice in the bottom of the vessel.

To demonstrate the truth of the statement, a flask filled with coloured water was attached to a spiral spring about 3 feet in length, which permitted of an oscillation of the flask in a vertical direction (*v.* figure 1). To the bottom of the flask was sealed a short tube, the opening of which was drawn down to a capillary of some 2 mm. diameter. The period of oscillation of the flask was about 2 sec. and an amplitude of 6 inches could be given to it. Thus it was subjected to a vertical acceleration ranging sinusoidally from about 5 ft./sec./sec. upwards to the same value downwards, and the value of gravity thus effectively varied from $(32+5)=37$ to $(32-5)=27$ ft./sec./sec.

This variation, producing, of course, a proportional variation in the pressure (above atmospheric) at the orifice, was sufficient to cause alternately cessation and occurrence of flow of the liquid from the orifice, as shown in figure 2.

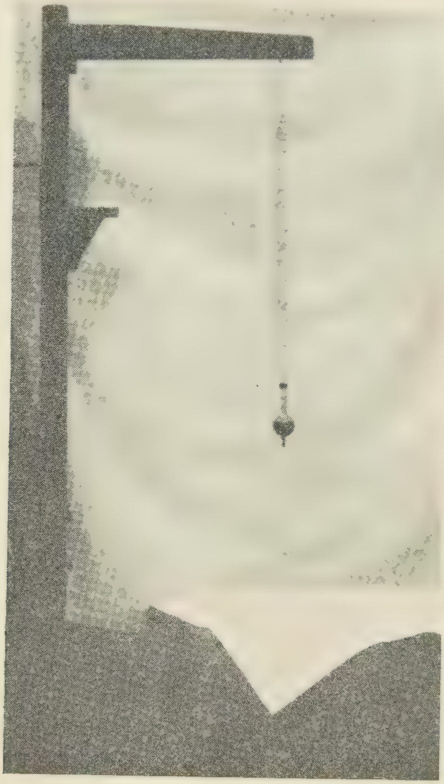

Figure 1. Flask containing inky water suspended on spiral spring and executing vertical oscillations of period about 3 seconds. Beneath flask is a rotating table covered with white paper.

Figure 2. Shows intermittent character of flow of fluid from opening of fine tube. Due to capillary effect at the orifice, the interval during which flow is inhibited is longer than that during which it occurs.

THE HYSTERESIS OF THE ANGLE OF CONTACT OF MERCURY

By The Rev. G. D. YARNOLD,
University College, Nottingham

MS. received 19 *July* 1945

ABSTRACT. A dynamical method is described for the observation of the advancing and receding angles of contact of mercury at very low velocities. It is suggested that the irreversible part of the work expended when the line of contact of the liquid traverses the solid surface is different for the two directions of motion.

§ 1. INTRODUCTION

The angle of contact of mercury differs widely according as the liquid is advancing or receding over the surface of a solid. It has already been shown (Yarnold, 1938, 1940) that the difference between the cosines of the advancing and receding angles of contact against walls of glass, Pyrex and quartz is independent of the velocity of the line of contact throughout the range from 3 to 30 cm./sec. The hysteresis of the angle of contact at very low velocities has now been studied by measurement of the force exerted by a rising or falling mercury surface on a suspended sphere which is partly immersed in the liquid. An expression for the force experienced by the sphere may be derived as follows.

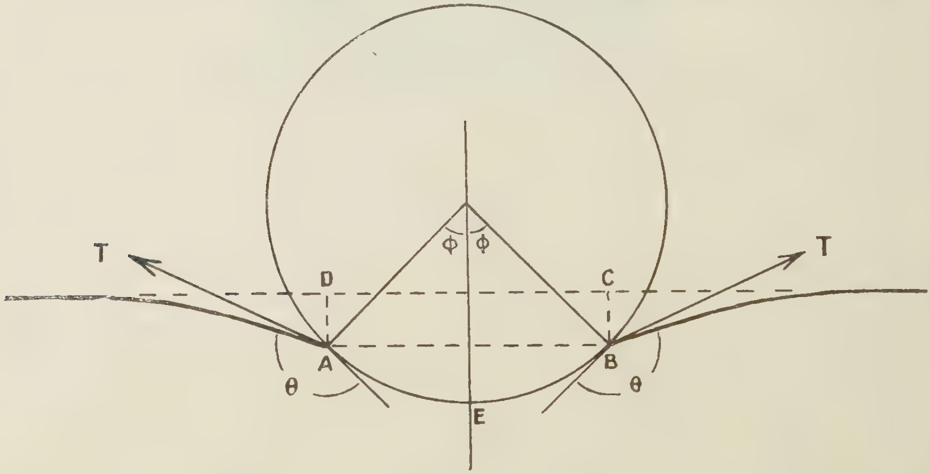

Figure 1.

Consider a sphere of radius a whose centre is at height y above the plane surface of the mercury. Whether the mercury surface is elevated or depressed in the neighbourhood of the sphere depends upon the value of y and upon the motion of the sphere. In figure 1 the mercury surface is represented as depressed in the region of the sphere, with which it makes an angle of contact θ. The lines joining the circle of contact with the centre of the sphere make an angle ϕ with the vertical. The upthrust of the liquid may be divided for convenience into two parts : that due to the displacement of the segment ABE and that due to the displacement of the cylinder ABCD. The forces due to surface tension act in directions inclined at an angle $(\theta+\phi-\pi)$ to the horizontal. The total upward force on the sphere is therefore given by the equation

$$U=\pi a^3\rho g\left(\frac{2}{3}-\cos\phi+\frac{1}{3}\cos^3\phi\right)+\pi a^2\rho g\sin^2\phi(a\cos\phi-y)$$

$$-2\pi aT\sin\phi\,.\,\sin(\theta+\phi),$$

where ρ is the density and T is the surface tension of the liquid.

If the sphere is immersed completely, the upthrust becomes

$$U_1=\tfrac{4}{3}\pi a^3\rho g.$$

Hence, in general,

$$\frac{U}{U_1}=\left(\frac{1}{2}-\frac{3}{4}\cos\phi+\frac{1}{4}\cos^3\phi\right)+\frac{3}{4}\sin^2\phi\left(\cos\phi-\frac{y}{a}\right)$$

$$-\frac{3}{2}\cdot\frac{T}{a^2\rho g}\,.\,\sin\phi\,.\,\sin(\theta+\phi). \qquad \ldots\ldots(1)$$

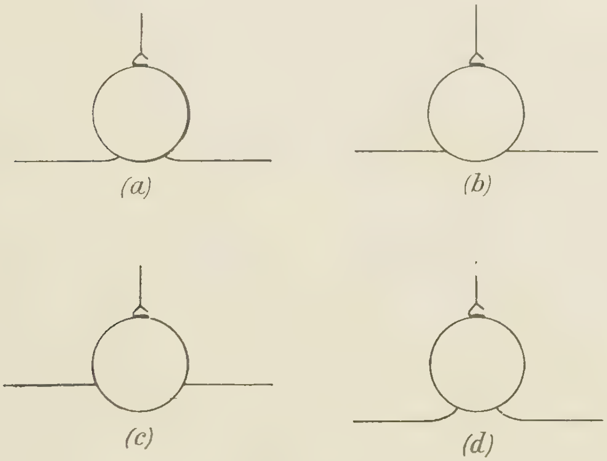

Figure 2.
(*a*), (*b*). Mercury rising. (*c*), (*d*). Mercury falling.

In this expression for U/U_1, the first term is always positive whatever the value of ϕ. The second term is positive or negative according as $\cos\phi$ is greater or less than y/a, i.e. according as $(\theta-\phi)$ is greater or less than π. Clearly, also, the same condition determines whether the effect of the third term is positive or negative.

Let it be supposed that the sphere is immersed so that the mercury is exactly horizontal right up to the lines of contact (figure 2 (*b*) or 2 (*c*)). It follows then that $(\theta+\phi)=\pi$ and that $\cos\phi=y/a$. If the upward force acting on the sphere under these conditions is denoted by U_0, then

$$\frac{U_0}{U_1}=\frac{1}{2}-\frac{3}{4}\left(\frac{y}{a}\right)+\frac{1}{4}\left(\frac{y}{a}\right)^3 \qquad \ldots\ldots(2)$$

This criterion makes it possible to recognize the point at which the liquid surface is horizontal right up to the surface of the sphere much more accurately than by direct visual observation. We have, therefore, a dynamical method of observing angles of contact which is entirely independent of the surface tension of the liquid.

§2. EXPERIMENTAL METHOD

Calculation suggests that the most suitable diameter of sphere is about 1 cm. In some of the experiments, steel ball-bearings were used ; in others, small glass spheres suitably weighted with mercury before being sealed. Each sphere in turn was suspended from a Sucksmith ring balance (Sucksmith, 1929) of simplified design, by the displacement of which the force, upwards or downwards, exerted by the mercury could be measured. The ring was of steel tape approximately 0·008 cm. in thickness, 0·4 cm. in width and 5 cm. in diameter. Using a single mirror in conjunction with a telescope and a scale at a distance of 2 metres, a force of 1 gm. wt. gave a change in reading of approximately 4 cm., while the scale could be read to one-tenth of a millimetre.

All grease was removed from the steel spheres by washing three times in ether (B.P.). In some of the experiments the glass spheres were prepared in the same way. In other cases they were cleaned in concentrated nitric acid, washed in many changes of distilled water, and finally allowed to dry under cover to prevent contamination by dust. Redistilled mercury, filtered to give a clean new surface at the beginning of each set of observations, was contained in a square glass trough of side 7 cm., sufficiently large, that is, to give a truly plane surface. By means of three similar calibrated screws, the mercury surface was brought up into contact with the lowest point of the sphere, then slowly raised in steps of about 0·01 cm. so as to immerse about half of the sphere, and subsequently lowered until contact was again broken. The time taken for a total motion of a few millimetres was rather more than an hour. The height y of the centre of the sphere above the plane surface of the mercury throughout this procedure was determined from the rotation of the screws and the small change in the absolute position of the sphere as the ring balance was deflected.

The variation of the quantity U/U_1 with the ratio y/a during the raising and lowering of the mercury is shown by the full curves in figure 3 for the case of a steel sphere of radius 0·635 cm. On the same diagram the thin curve represents the variation, with the ratio y/a, of the quantity U_0/U_1, as calculated from equation (2). The points of intersection of the experimental and theoretical curves give the values of y/a when the mercury surface is horizontal right up to the surface of the sphere. The angles of contact are then given by the equation

$$-\cos\theta = \cos\phi = y/a.$$

Clearly the method is capable of considerable precision.

It will be observed that, on first making contact ($y/a = 1$), the mercury rises a short distance up the curved surface, as shown in figure 2 (*a*), and so exerts a downward force on the sphere, the second and third terms in equation (1) being negative and together greater than the first. This adhesion of the mercury to the solid is only observed with really clean surfaces. Adhesion takes place similarly when the mercury is falling, but now, the angle of contact being smaller, quite a pronounced neck develops (figure 2 (*d*)). The downward pull on the sphere passes through a maximum value, as in Ferguson's experiments (1913), after which contact is broken, and a minute drop of mercury remains at the lowest point of the sphere, which may now be as much as a millimetre above the level surface of the mercury.

§ 3. RESULTS

The table shows the measured angles of contact for a number of different spheres. Although in any given case the angles of contact may be measured quite accurately, the angles themselves are not exactly reproducible, even when scrupulous cleanliness is observed. It will be noticed, however, that the receding

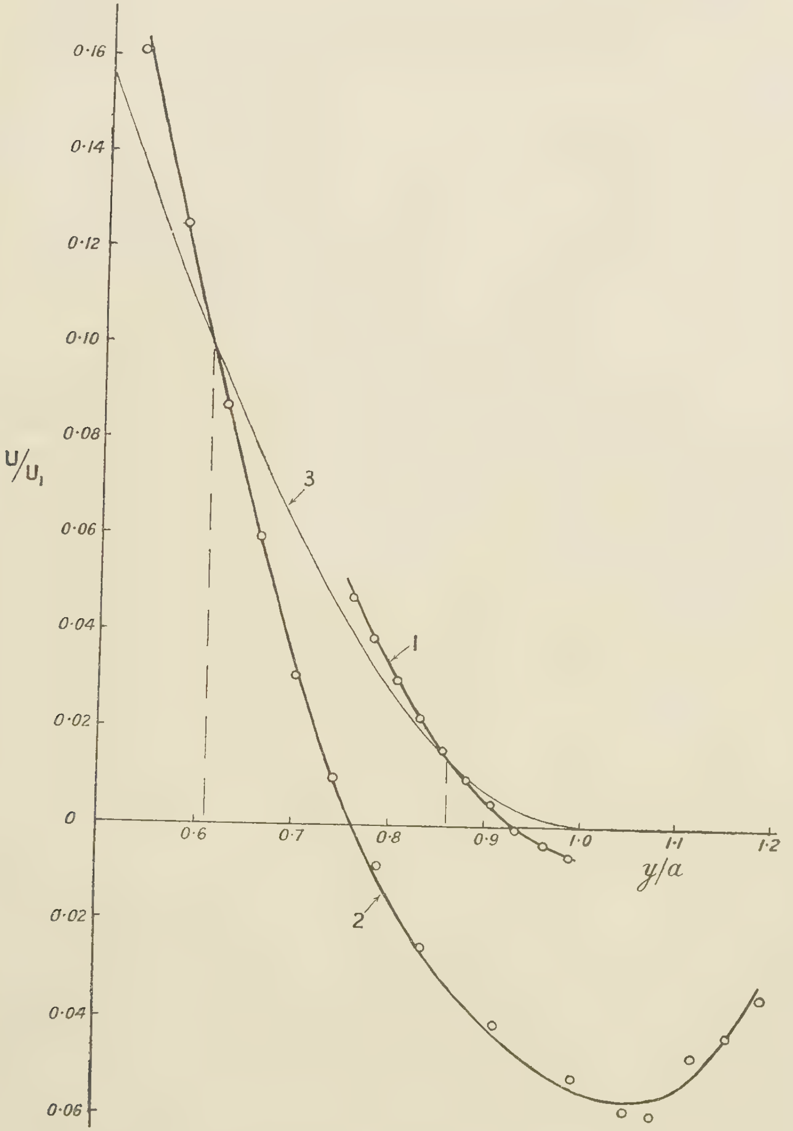

Figure 3. Force on steel sphere. $a = 0{\cdot}635$ cm.
1. Mercury rising. 2. Mercury falling. 3. U_0/U_1 (calculated).

ngles all lie in a comparatively narrow range, while the advancing angles vary nuch more widely. The difference between the two angles is greater when the lass spheres are washed in ether than when they are washed in nitric acid and listilled water. No trace of residue, however, was visible on evaporating several cubic centimetres of ether in a watch-glass. In no case, however, is the difference between the cosines of the angles of contact as great as the difference observed for a mercury index travelling in a glass tube at a velocity of 3 cm. per sec. or faster (Yarnold, 1938). The first group of steel spheres gives angles of contact hardly different from those observed with glass spheres cleaned in the same way. It must not be inferred, however, that this result is due to the presence of a film left by the ether, which forms the true surface in each case, since two other steel spheres, obtained from a different source, give much higher advancing angles.

Following Adam and Jessop (1925), it is usual to ascribe the hysteresis of the angle of contact of a liquid to a frictional force F per unit length acting at right angles to the line of contact. The force F is tacitly assumed to be the same whether the liquid is advancing or receding over the surface of the solid, and, as a consequence, the cosine of the true equilibrium angle of contact is taken to be the mean of the cosines of the advancing and receding angles. The introduction of the force F, however, is equivalent to the statement that part of the work expended in the formation of fresh surface is irreversible. The assumption that the magnitude of F is independent of the direction of motion of the line of contact is therefore equivalent to the assumption that the irreversible work expended in the formation of unit area of the solid-air interface is the same as the irreversible work expended in the formation of unit area of the solid-liquid interface.

Material	Radius (cm.)	Remarks	$-\cos\theta$		θ (degrees)	
			Advancing	Receding	Advancing	Receding
Glass	0·574	Washed in nitric acid and distilled water	0·723	0·600	136·5	127·0
,,	0·522		0·780	0·596	141·0	126·5
Glass	0·574	Stored in alcohol and washed in ether	0·831	0·648	146·0	130·5
,,	0·522		0·848	0·600	148·0	127·0
Steel	0·635	Washed in ether	0·860	0·610	149·5	127·5
,,	0·357		0·806	0·575	144·0	125·0
,,	0·318		0·857	0·648	149·0	130·5
Steel	0·556	Washed in ether	0·930	0·624	158·5	128·5
,,	0·437		0·967	0·640	165·0	130·0

Stated in this form, the assumption hardly appears to be justified, though the error may not be serious when the two angles of contact differ only slightly. Nor does it appear to be supported by the measurements of the angles of contact of mercury. The approximate constancy of the receding angle, together with the remarkable adhesion of the mercury to the solid surface, suggests that a solid-liquid interface of more or less constant energy is formed in all cases, and that more or less the same quantity of irreversible work is expended per unit area in its destruction. On the other hand, the wide variation in the advancing angle suggests that the irreversible work involved in the destruction of the solid-air interface and its replacement by the solid-liquid interface may be extremely variable.

REFERENCES

Adam, N. K. and Jessop, G., 1925. *J. Chem. Soc.* **127,** 1863.
Ferguson, A., 1913. *Phil. Mag.* **26,** 925 ; 1914. *Ibid.* **28,** 149.
Sucksmith, W., 1929. *Phil. Mag.* **8,** 158.
Yarnold, G. D., 1938. *Proc. Phys. Soc.* **50,** 540 ; 1940. *Ibid.* **52,** 191.

ADDRESS

DELIVERED AT THE OPENING OF THE THIRTIETH EXHIBITION OF SCIENTIFIC INSTRUMENTS AND APPARATUS, 1 JANUARY 1946, BY

The Right Hon. Sir STAFFORD CRIPPS, P.C., M.P.

THE Physical Society is much to be congratulated upon its enterprise in organizing an exhibition of scientific instruments, thus giving an opportunity to British scientific instrument makers to demonstrate once again the excellence and ingenuity of their workmanship.

During the years of war we have of necessity become more self-reliant for our research and development in all branches of science and technology upon our own native manufactures. And judging by the outstanding results which we have achieved during the last six years there can be no doubt at all that our scientific instrument makers have served us well. Many of them have turned their efforts to the direct production of instruments for aircraft, tanks or ships of all kinds and have thus entered the field of semi-mass production or even of mass production itself, but this has not prevented them from continuing with the development and production of those many scientific instruments of extreme accuracy upon which so much of our present research and industrial technique is based.

Indeed, instead of debasing their standards by introducing volume production they have carried into that mass production the skill and accuracy which they had long cultivated in their specialized and small quantity productions.

In the result the war should have put us into a position to expand our scientific instrument production upon a large scale, preserving all the excellencies for which our leading firms have so justly been famed in the past.

And the present moment is a most appropriate one in which to demonstrate this fact not merely to our own users of these instruments but also to the potential customers for them from all parts of the world.

As in the first world war, so in this last one, we have learnt how backward we have been in our research efforts during times of peace. Research is easily and widely recognized as the sole basis for rapid progress and superiority in wartime; so much so that every effort is made by the State to entrain every scientist available in one line of research or investigation or in another. The scientist is the blue-eyed boy called in to help the solution of every problem and to force the pace of progress in a never-ending duel of wits and intelligence with the enemy.

And the scientist must be duly and properly equipped for his work. Great research establishments are improvised regardless of cost and filled with the most up-to-date instruments and machinery—which, incidentally, put to shame the accommodation and facilities of our peacetime universities and other research centres.

Nothing is regarded as wasted that may contribute to the superiority over the enemy in any field. Tens of thousands of research man-hours are gladly sacrificed to the merest chance of some new development which will give us advantage over the foe.

But as we experienced between the two wars, the atmosphere is apt to change when the crucial danger of war is past. We then weigh up the £ *s*. *d*. and evaluate whether this or that expenditure is worth our while. And in that calculation we tend to become shorter and shorter sighted. We are liable to forget that progress and superiority in peace are as much based upon research as they are in war. The tempo of our drive forward on the scientific front slows down and we fail to educate and train a sufficiency of highly skilled staff to maintain the intensity of our research.

That at least was the experience after the last war, and it is a folly that we must at all cost avoid repeating after this war.

Research is the life-blood of our industrial progress, and industrial progress is the basis for our continuing prosperity as a great exporting nation.

To attain the degree of research activity which is essential to our future as a great inventive industrial nation four things are required.

First we must have the men and women adequately trained and in sufficient numbers. That is a matter of more and better educational facilities of all kinds and a free access to those facilities for the intelligent youth wherever they may be and whatever kind of homes they come from.

Second we must raise the status of our scientists. Too long they have been regarded as rather superior craftsmen definitely inferior to the leaders of industry or the principal administrators. The Classical Tradition in education still claims a superiority which is out of date, and the scientist is still looked upon by many as of a lower grade. Whether we look at the salaries they are offered or the position to which they are relegated in the hierarchy of industry or of the State Service, we see that they are kept down in a position of inferiority.

I am not one of those who claim that the scientists should rule in all spheres, nor am I a believer in technocracy, but I am firmly convinced that both scientists and technicians are worthy, and have amply proved themselves worthy, of a position equal to that of any other section of the community.

But until we gain the recognition of this fact by the country as a whole we shall not get the best out of our scientists, nor shall we make the headway that we should in applying the results of our research to our every-day needs.

The scientist must not be regarded as an individual to be called in to assist in an emergency when matters have got into a hopeless position—like the plumber with a burst water-pipe—rather he should be looked upon as a valuable and equal co-operator in every phase of the solution of our problems of living.

Third, we require proper accommodation and facilities for our research. It is not necessary that every research institution should be a palace with chromiumplated ware, nor do I believe that string and sealing wax provide the essential setting for all that is of value in research. There is a happy mean in which men and women can do their best work, provided with the most up-to-date instruments that they require.

A good many of our research establishments today fall far below that mean in standard both as regards space—and adequate space is vital to good research—and as regards equipment.

I hope that full advantage will be taken of wartime surpluses to see that all our universities and other research establishments are fully equipped with adequate machinery and instruments.

Finally, there is the all-important matter with which this exhibition is concerned. We cannot afford to be dependent upon others for the instruments necessary for our education of scientists or for the research work which they do, nor, indeed, for all those many testing instruments which are today part and parcel of every up-to-date industrial concern. It is essential that we should have and maintain in this country a pre-eminent scientific instrument manufacture both for our own use and to help to supply those many other countries who cannot themselves afford to set up such manufactures.

I believe that if we could insist upon these four points we could lay the permanent and solid foundation of a live, active and vigorous research in our country which would enable us to keep in the van of the great industrial countries of the world.

It is because I believe that this exhibition will help along the lines that I have sketched that I am so delighted to have the honour today of declaring this exhibition open.

REVIEWS OF BOOKS

Elementary Wave Mechanics, by W. Heitler. Pp. viii + 136. (Oxford and London : Sir Humphrey Milford, at the Oxford University Press, 1945.) 7*s*. 6*d*.

In this little book, Professor Heitler gives the substance of a course of lectures which he delivered in Dublin. It is truly elementary, both in the demands which it makes on the previous knowledge and mathematical ability of the reader, and also in that it deals only with the *elements* of wave mechanics. There is here no metaphysics, but a plain introduction to the physical arguments which led de Broglie and Schrödinger to the wave equation. The uncertainty principle is introduced as a demonstrable theorem, and not as a vaguely supported principle, and is indeed at first named the uncertainty relation, a change in nomenclature which might be advantageous if generally adopted.

The wave equation is used to investigate the hydrogen atom, the Zeeman effect and the two-electron problem in a manner which is not now unfamiliar in elementary texts. The Pauli exclusion principle is introduced in the last-named chapter.

The best part of the book, however, is in the last three of the nine chapters, where the periodic system, the theory of the homopolar chemical bond and the general problem of valency are taken up. In conformity with the plan of the book, these matters are treated in part in qualitative fashion, with guidance from the theory of simple cases, but the treatment is so lucid that these chapters must be of value to all who are concerned with the problems of chemical combination. The explanation of how it comes about that valencies can become saturated after a limited number of atoms have combined, or of how the carbon atom lends itself to the multitudinous compounds in which it is found, are of more value for a clear picture than would be many pages of detailed algebra working out a more complete theory.

In reviewing the same author's *Quantum Theory of Radiation*, the view was expressed that the author would do a service if he wrote a more elementary introduction to the subject. Can he now put all students in his debt by writing a book intermediate in standard and difficulty between this very elementary treatment of the simplest wave mechanics and that very difficult work in which the whole range of quantum mechanics is called on ? Such an intermediate treatment would, presumably, deal fairly exhaustively with the mechanics of particles and would have some introduction to the subject (untouched in the elementary book) of the interaction between matter and radiation, but without attempting an exhaustive treatment of this more difficult topic. J. H. A.

Questions Actuelles de Géophysique Théoretique et Appliquée, par EDMOND ROTHÉ. (Paris : Gauthier-Villars, 1943.) 275 Fr.

Written and published during the German occupation of France, this book has only recently reached Great Britain. It covers a very broad field, and from the data that have been obtained in the realms of gravity observations, radioactivity of the earth's crust, volcanology, seismology and terrestrial magnetism an effort is made to present a unified picture of the modern conception of the earth's constitution. Isostatic compensation is discussed in the light of gravity observations, and is supported by some detail of the work of the Swedish geologist de Geer on varved clays and the retreat of the ice-sheet, leading to the subsequent elevation of the land masses due to the removal of the ice-load. The two following chapters on radioactivity and volcanic action are broadly discussed in relation to isostasy, so that these branches are integrated into a self-consistent whole.

In view of the unity up to this point, it is rather surprising to find the section on seismology so short, and in particular the importance of near earthquakes, and the information revealed by them on the sequence and thickness of layers in the crust, so closely allied to the previous aspects, is scarcely mentioned. The chapter on terrestrial magnetism is also disappointing and does not appear to fit the main theme established in the early part. After a brief description of the earth's field, and ending with the diurnal and annual variations, the main part is devoted to a speculative theory, due to Haalek, on the cause of the earth's magnetism. The work on isopors and its possible implications is ignored. At the end of each chapter a short section describes some of the practical applications to geophysical prospecting, and here the contents supplement a previous publication, devoted to these aspects, by the same author.

A number of numerical errors occur in the text ; but in the majority of cases they are obvious, and will, no doubt, be corrected in later editions. Some of the illustrations leave much to be desired, the reproduction is poor and a few are not easy to follow. In figure 67, for example, the axes are not labelled, but the fortunate inclusion of a table, giving the same data, allows them to be disentangled. In spite of these defects the book is a good review of the present ideas on the subjects treated. J. M. B.

The Mathematics of Ultra-high Frequencies in Radio, by L. N. BRILLOUIN. Pp. vi+210. (Brown University, Providence, R.I., 1943.) Price not stated.

The theoretical background to micro-wave radio has become of increasing importance during recent years, and the present book, which is a record of a course of lectures given at Brown University in 1943, is a welcome addition to the few existing works dealing with the theory. It provides a unified account both of the physical concepts associated with wave propagation and the mathematical methods used in analysing the electromagnetic field. It is readable by the physicist and engineer as well as the mathematician ; and by seriously studying the book, the student and the research worker will avoid the necessity of consulting a large number of the original papers which lie scattered throughout the scientific literature of the past decade.

The book begins at an elementary level. Tuning circuits with lumped or with distributed constants are discussed, and the usual introduction to phase and group velocity is given. Transmission lines and co-axial cables are studied and there is a section on the various types and relationships of units. Acoustic waves are studied preparatory to electromagnetic waves in pipes.

Then the mathematics proper is introduced. The author assumes slight initial knowledge on the part of the reader and begins with a discussion of vector algebra, scalar and vector fields and the expression in curvilinear co-ordinates of various vector functions. Maxwell's equations are set up and solved by the method of the retarded potential. The expression of these equations in tensor form (fundamental from the relativistic point of view) is given, and the Hertz potential and Poynting vector are discussed. A short chapter is devoted to the skin effect.

The propagation of waves along a cylinder of arbitrary cross-section is studied mathematically in some detail ; the treatment is general at first, but particular cases discussed include tubes of rectangular, circular or elliptical cross-section and co-axial cables. All these cases lend themselves readily to a mathematical analysis, and the various types of possible waves are classified.

The last chapter is given to cavity resonators. It is a pity that the treatment is not more comprehensive, and while attenuation, damping and the distribution of the higher modes are discussed, no mention is made of some of the practical problems in resonator theory, such as the calculation of resonant frequencies and losses in a compound resonator by the (numerical) relaxation method, or, in special cases, by the Hahn method of matching solutions. Similarly, in the chapter on wave guides no mention is made of discontinuities in the cross-section, although this has been the subject of discussion in several papers appearing in recent literature. It is disappointing to find no mention of antenna theory (except the reciprocity theorem). But here again recent work by the author on this subject may be found in the literature.

The lecture notes are well presented and the student should not find it difficult to read them. It is gratifying to note the enterprise of Brown University in making available, in mimeographed form, the results of the Advanced Instruction and Research in Mathematics.

L. S. GODDARD.

Science in Progress. Fourth Series. Pp. 331. (Yale : University Press ; London : Sir Humphrey Milford, at the Oxford University Press, 1945.) $3.00.

This delightful set of essays is made up of contributions from eleven very distinguished specialists in various branches of knowledge, edited by George A. Baitsell and with a foreword by L. L. Woodruff. In his thoughtful foreword Mr. Woodruff says :—" The accumulation of knowledge during the millennia since man's emergence from a condition of complete dependence on his environment to the relatively masterful position that he now holds is, except in its broad sweep, beyond the compass of one mind, however talented. The polyhistor has been succeeded by the specialist." This is indeed true, and for this reason the reviewer feels quite unable to do much more than give a broad picture in bold outline of the various subjects presented.

The contributions are mainly the substance of national lectures delivered under the auspices of the organization known as " The Society of the Sigma XI ", which is devoted to the encouragement of research in science, and the book represents the fourth series of such lectures.

The collection is intended to provide scientific men with general outlines, although accurate ones, of fields of research in which, while not actually working, they may be interested. From this point of view the purpose in view has been excellently achieved.

Each author has provided a most excellent series of references attached to his chapter, and it is flattering to national vanity to see that so many Englishmen are mentioned as having pioneered or followed the exciting hunts for the new knowledge which goes to the making of the various chapters.

A striking war-time chapter is the first, by Professor Miles of Yale. The importance of the psychological approach to certain problems in military aviation has been proved to be of paramount importance, and the interested reader will learn how an aviation cadet is examined from all points of view so as to ensure not only that he possesses the personal qualities so essential for an airman's success, but also that he receives the training to develop fully these qualities.

In the second chapter Professor Bronk of the University of Pennsylvania speaks also of war-time interests in the combined fields of Physics and Biology. He gives attention to the subject of sensory impulses from a pressure-sensitive nerve ending, and there is much interesting matter belonging to past history and the live present in regard to those rhythmic oscillations of potential in nerve fibres which are so important in impulse propagation along nerves.

Professor Hecht of Harvard follows with an extraordinarily interesting account of the amount of energy required in the process of vision. He explains the experiments which have led to the remarkable result that for a normal individual to perceive a faint flash of light on the threshold of visibility the minimum energy lies between 5 and 8 quanta.

Professor Loewi of New York University, formerly of Gratz, gives a fascinating account of the discovery of the chemical transmission of nerve impulses. It is, indeed, remarkable that the nervous system produces so many of its effects through the liberation of chemical substances.

From the pen of the late Professor Birkhoff comes a masterly historical account of some aspects of mathematical physics garnished with personal recollection and luminous with individuality—it makes excellent reading.

Professor Debye of Cornell gives, as is to be expected, a first-rate résumé of modern methods of obtaining very low temperatures and some of the problems to which these methods have provided a key. The subject of his choice is clearly not a closed book, for he points out the possibility of extending the experimentally accessible range towards the absolute zero by removing the disorder which may exist in the nucleus itself and connected with nuclear magnetism, just as the methods he described have nearly removed all the disorder associated with atoms and their motion.

Professor Eyring of Princeton contributes a valuable article on physical chemistry, including a consideration of the distribution of energy in a molecular system, rates of reaction, and luminescence inhibition.

Professor Rabi of Columbia discourses on molecular beams and "radio-frequency spectroscopy".

Dr. Hickman, who is Director of Research of the Distillation Products Company, and is an Englishman, produces a valuable chapter on vacuum chemistry—in particular molecular stills and their applications, for example in the vitamin A industry. The new substance kitol, which is the mirror image in properties of β-carotin, itself the normal precursor of vitamin A, was discovered with the use of the vacuum still.

Professor Elvehjem of Wisconsin gives a detailed and convincing account of the vitamin B complex. The formulae of the various substances, about a dozen, are discussed where possible and the dietary factors explained—altogether a most illuminating article.

Professor Cohn of Harvard University, in this last chapter, gives a most interesting account of work on which he and his colleagues have been engaged during the war on the chemistry of proteins, particularly in the chemical interactions and the separation of the protein components in protein solutions—researches which involved the proteins of blood plasma, so important in the alleviation of human suffering. A great deal of information appears to be concentrated in a few pages, from the relative dimensions of various proteins through the chemical fractionation of the components of plasma to details in connection with the regulation of bodily function by hormones and enzymes.

The impression gathered from reading through this remarkable collection of masterly essays is one of immense satisfaction at being privileged in one small volume to read such clearly presented accounts of current research in so many widely separated fields. The references at the end of the book will be valuable to anyone whose curiosity is aroused sufficiently to follow up particular points ; the excellent diagrams and photographs are fully illustrative and give the impression of great accuracy. If one may intrude a word of friendly envy, it is to say what a rare pleasure it is to handle a book produced so lavishly and so perfectly on such beautiful paper. If it can be bought in this country, it is magnificent value for three dollars.

R. WHIDDINGTON.

Chemical Crystallography, an introduction to optical and X*-ray methods*, by C. W. Bunn. Pp. xii+422 and 13 plates. (Oxford : Clarendon Press, 1945.) 25*s.*

The book is addressed to " students of chemistry who wish to acquire some knowledge of crystallographic methods and research workers who wish to make practical use of such methods ". It is divided into two sections, the first dealing with the identification of solid substances by physical methods and the second with the determination of crystal structures. After an introductory survey, the author begins with a chapter entitled *The Shapes of Crystals*, which gives an introduction to crystal morphology and the relation between shape and structure. He approaches the subject of crystal symmetry through the phenomena of crystal growth and achieves a simplified treatment of elementary crystallography, e.g. indices of crystal planes by means of the unit cell rather than in terms of axial ratios. This is followed by an account of crystal optics and the properties of crystals observed in the polarizing microscope, leading up to the procedure which is then given for the identification of transparent crystals by microscopic methods. The last chapter of section one introduces the elementary theory of diffraction of X rays and is concerned with the practical details of taking X-ray powder photographs for identification.

Over half the book is devoted mainly to the determination of the arrangements of atoms in crystals. This second section opens with an account of the single-crystal techniques, how unit cell dimensions are measured and how this knowledge is applied, amongst other things, to identification and determination of molecular weight. Succeeding chapters give a masterly treatment of the principles involved in the determination of crystal structures by trial and error, and numerous examples of both organic and inorganic compounds are worked out in detail. A chapter on electron density maps and vector maps includes an account of Fourier series methods, of the use of optical methods in place of calculations and the scope of vector methods. The author also discusses the evidence on crystal structure given by optical, magnetic and other physical properties, and concludes with a brief account of broadened X-ray reflections and diffuse spots.

The well-balanced review of progress in method and technique since the publication of *The Crystalline State*, by W. L. Bragg, makes this an indispensable companion to that volume. Formal physical and mathematical treatment are avoided, but the book has a discipline of its own and demands careful reading. The author assumes more than a passing interest in both the organic and inorganic compounds, thus revealing the range of his own contributions to the subject. He has not hesitated to adopt an unorthodox development in order to reflect the course of his own experience in applying crystallographic methods to chemical problems.

The text is profusely illustrated and provided with useful appendices and excellent indexes. Both author and publisher are to be congratulated on producing so fine a book under war conditions at a reasonable price. F. A. B.

Polarographic and Spectrographic Analysis of High Purity Zinc and Zinc Alloys for Die Casting, by various authors. Pp. 117. (H.M. Stationery Office, 1945.) 5*s.*

An account is presented of researches, carried out under a British Standard Institution Panel, to investigate the use of physico-chemical methods for the analysis of high-purity zinc and zinc alloys for die-casting.

The work concerned has proved the basis for a British Standard Method on the same subject, and the present publication is in the nature of a detailed discussion of alternative techniques, rather than a working manual for use in the laboratory. Such being the case, its primary appeal is to the specialist and to the spectrographer in particular, but the body of evidence presented is sufficient to warrant consideration by all interested in analysis in the wider sense. In view of the emphasis in modern spectrographic research on the investigation of different excitation methods, two papers giving considerable detail of variations on simple condensed sparks and an intermittent A.C. arc technique are of considerable interest. In a further section an arc technique is described in which the sample is placed on a suitable electrode in the form of oxide. This procedure allows of the preparation of standards of known composition, enabling the spectrographer to be independent of chemical analysis. In this paper methods of plate calibration are discussed in some detail, but at the same time it is agreeable to find the results presented in such a manner as to be readily intelligible to a non-specialist reader.

The description of an alternative method of attack by the polarograph will be of interest to laboratories without spectrographic equipment, and also as providing an independent result by an entirely different technique. It is shown that results of considerable precision can be achieved by modifications in chemical pre-treatment, suitable to the particular problem in hand.

In fact, the standard deviations of the results by all the methods discussed agree very closely and provide important additional evidence, not in vague generalizations but in a precise and concrete manner, of the value of physical methods to the critical analyst. Finally, it may not be out of place to mention that the amount of information presented for a modest sum compares exceedingly favourably with the usual scientific text-book.

H. G. SHORT.

Radiocristallographie, by ANDRÉ GUINIER. Pp. ix + 294, with 15 plates. (Paris: Dunod, 1945.) Price not stated.

This can be recommended as a really excellent book, the sort of book that has been badly needed for several years. It is written specifically for those who wish to use the study of crystals by x-ray methods as a means to some further end. It is not meant for specialists in crystal-structure determination. Yet all will benefit by reading it, especially those who lightly play with structure factor tables, Fourier series and calculating machines, without ever troubling to understand the foundations upon which the subject is built. True, it dismisses gas tubes in a contemptuous seven lines and gives 1 in 10,000 as a desirable limit for precision work with powder cameras. But it introduces the reciprocal lattice where it ought to be introduced—right at the beginning ; it relegates all tiresome but necessary mathematical proofs to appendices ; it show the *raison d'être* of some of those mysterious tables in the *International Tables for Crystal Structure Determination* that we ourselves never seem to need ; and it lays proper emphasis on the study of crystal texture and imperfection. Every theorem is ilustrated by practical and interesting examples ; and numerous useful hints about apparatus and methods are given from the author's own wide experience.

Yet the book gives a bad first impression. The pages are uncut and the title is not clear to an English technical reader. It sounds as if it might have something to do with wireless receiving sets, but the prospective buyer is left to guess. After all, x rays are not entitled to a corner in the expression " radio ". The cover is of thin paper of a bilious shade of yellow (or is the reviewer perhaps jaundiced through having read the book during an attack of gastric influenza ?). The paper is of extremely poor quality and bad colour ; the type is crowded and difficult to read. There is a table of contents, but no subject or author index, and the references are not up to date (for instance, the reader is referred to the 1932, instead of the 1940, edition of Clark's *Applied X-Rays* "). Finally, and most unkindest cut of all, the present writer's name is misspelt. It was Robert Louis Stevenson who, when some American publisher (*before* the days of lease-lend) had pirated one of his books, said that it was not the theft that angered him so much as the mis-spelling of his name. " I saw my book advertised as the work of R. L. Stephenson ", he says, " and I own I boiled. It is so easy to know the name of a man whose book you have stolen, for there it is, full length, on the title-page of your booty. But, no, damn him, not he ! He calls me Stephenson ".

But in this case the author and publisher must be forgiven. The book is a revelation, not only of the difficulties of writing and producing in occupied France, but of the indomitable spirit that would undertake such a work at such a time and under such conditions. And, with all its faults, it is certainly a book that will be referred to again and again. The pity is that it will fall to pieces in the process ; but surely we may soon expect a more worthily produced second edition, with references brought up to date and a modernization of the text where necessary ? Or cannot some British or American publishing firm negotiate for the translation rights and produce an agreed English text in a better setting ? The book deserves it.

K. LONSDALE.

**ELECTRICAL MEASURING
INSTRUMENTS
OF THE HIGHER GRADES**

TURNER

**ERNEST TURNER
ELECTRICAL INSTRUMENTS
Limited**
CHILTERN WORKS
HIGH WYCOMBE
BUCKS.

**Telephone : High Wycombe 1301/2
Telegrams : Gorgeous, High Wycombe**

DIFFERENTIAL COMPRESSION

(A NEW DEVELOPMENT IN HEARING AID TECHNIQUE.)

We believe that we have made considerable advances in understanding the most complicated problem of fitting deaf people with hearing aids with a performance most suitable to their needs. In the past a great deal has been written and said of taking an audiometric curve of a patient and adjusting the hearing aid to the curve with the same certainty as an optician deals with a prescription for lenses.

Those familiar with the subject know that the problem is actually of great complexity, and it is possible for two people with identical audiometric curves to react quite differently to a particular type of hearing aid. We have given the name of "Differential Compression" to the type of amplification in which the relative amplification of the higher speech frequencies and the rest of the scale is a function of the total sound level handled by the amplifier. This it is believed will make it much easier to fit difficult inner ear deaf cases with hearing aids, and be of benefit to children in special schools for the deaf. We have incorporated this feature in some of our wearable instruments as well as in new group hearing aid installations for schools.

MULTITONE ELECTRIC Co. Ltd.
223-227 ST. JOHN STREET, CLERKENWELL, E.C.1.